University of Rome "La Sapienza"

Ph. D. in Chemical Sciences

XVII cycle

Chemistry of biological systems and macromolecules

"Influence of cardiolipin on the functionality of the Q_A site of photosynthetic bacterial Reaction Centre"

MAIN SUPERVISOR
Prof. Marcello Giomini

CANDIDATE
Dr. Ivan Husu

OTHER SUPERVISORS
Prof. Francesco Castelli
Dr. Mauro Giustini

General index

OUTLINE AND MOTIVATION.

The photosynthetic process, as well as the other reactions involved in the energetic metabolism of a living organism, always requires at least a boundary membrane and, together with it, one or more integral proteins - often several - and liposoluble cofactors.

In the cell energetic machinery the function of the membranes is not only to give rise to well delimited compartments and to support the metabolic processes, but also to assist these processes since specific relationships exist among all the cell membrane constituents.

From the pioneer work of Singer and Nicholson dated back in 1972, that led to the famous fluid mosaic model of the biological membranes (a lipidic matrix which adsorbes and inserts proteins), our knowledges and therefore opinions of their structure and function are appreciably changed. It is today well assessed that the lipidic portion is not only a mere mechanical support to the protein fraction of the membrane: on the contrary it enters in a more active role into the functioning of the whole system. A membrane is now seen as a microcosm where intense and specific relationships bind the lipidic and proteic components building up well defined domains within the bilayer itself.

It is well known that the energetic apparatus of an eukaryotic cell is confined in specific, membrane-delimited, functionally distinct units (*organellae*). In a prokaryotic cell, instead, is the plasma membrane itself that hosts functionally distinct domains arising just from the mutual relationships between proteins and phospholipids.

The aim of this Ph.D. thesis is to provide some experimental evidences of specific and functionally important interactions between a particular phospholipid molecule (cardiolipin, CL) and an integral bacterial protein (the photosynthetic Reaction Centre, RC), mainly by kinetic Vis-NIR spectroscopy studies carried out on artificial supramolecular systems as phospholipid vesicles, in which the RC is reconstituted.

Rising prices and sporadic shortages of fossil fuels in the 1970's gave the impetus for a worldwide effort directed to the research of renewable energetic sources. Among these it is known that the exploitation of solar energy can represent an especially

attractive option, since this resource is very abundant, environmentally clean, and embargo-proof (hoping that no new wars will be waged for the search of a “sunlight place”!). Referring to its features the solar energy then seems to be completely antithetical to the most fashionable and often “politically correct” hydrocarbon resources, which appear to be in an already stored and “ready to use” shape, but well limited and, above all, polluting if employed in a so huge scale as it happens today.

However, because of the difficulties encountered in the concentration of the solar radiation (low power per unit area) and of its intermittent availability, some effective method of storage must be found in order that energy can be saved when it is plentiful, for use at a later time when demand exceeds supply.

In this scenario, one of the first direction investigated by scientists was the light to chemical energy conversion performed by green plants, algae and some prokaryotic organisms, where the solution to the storage problem is intrinsic to the process called photosynthesis.

Therefore, research on this topic sped up and in 1980's the first X-ray high resolution structure of a membrane protein was deposited in the protein data bank. That protein was the bacterial RC (purified from the bacterium *Rhodopseudomonas viridis*). From this moment bacterial RC became the archetype of all the integral proteins since it constitutes the minimal functional unit able to convert the energy carried by the electromagnetic radiation into chemical energy (in the form of specific reduced molecules and of electric potential across the bacterial membrane). After thirty years RCs are still among the most studied integral proteins, in the elucidation of their properties being concentrated the efforts of biologist, chemists and physicist.

The refinement of the investigation techniques made possible to show the presence of specific phospholipid molecules associated to the purified RCs of practically all the photosynthetic prokaryotic organisms (and it can be safely assumed that similar associations exists also in the superior photosynthetic organisms, though the lacking of high resolution X-ray structures of many photosynthetic complexes allows only reasonable assumption to be made).

In particular, it has recently been shown by high resolution X-ray diffractometry that the RC purified from *Rhodobacter sphaeroides* contains a close associated cardiolipin (CL) molecule (in a 1:1 mole ratio): in this Ph.D. thesis it will be shown how

the presence of CL molecules is fundamental for the right functioning of the RC by means of a kinetic study performed *in vitro* both in detergent solution and in vesicles. The choice of working also with proteoliposomes is due to the necessity of exploring the protein behaviour in a system closely mimicking the natural environment of the RC.

As often it happens in science, a deepen understanding about bacterial RC behaviour, even in membranes (their native environment) could surely represent a preferential starting point in the approach to more complex proteins as the green plants Photosystems, whose crystallization has been recently performed.

Concluding, few words will be dedicated to how this thesis is organized.

In the first chapter it will be offered to the reader a general review of what is presently known about the subject protein-lipid relationship (and related matters), with particular emphasis given to the RC structure and function. Apart of being exhaustive on this huge topic, the literature cited at the end of the chapter will provide to the interested readers guidelines to deepen their knowledge on particular aspects of the subject.

The second chapter will deal with the more practical aspects of the topic discussed in the thesis. The methods used to isolate and purify the protein, to prepare the samples and to study them will be described in detail together with the techniques used to characterize the system and to analyze the acquired experimental data.

The core of the thesis is the third chapter, where the experimental results will be presented and discussed and where the originality of the scientific contribution represented by this Ph. D. thesis will arise.

It has to be underlined that the main laboratory instrument by which the results have been achieved during the Ph. D. period and reviewed in this thesis is an experimental result itself. In fact, a large part of the work carried out was dedicated just in building up a kinetic spectrophotometer working in the microseconds timescale, equipped with a temperature-controlled cell holder and with a digital data acquisition system, whose detailed description is given in a dedicated section within the second chapter.

CHAPTER 1

INTRODUCTION. LIPID-PROTEIN INTERACTIONS: THE CASE OF THE REACTION CENTRE FROM *RHODOBACTER SPHAEROIDES*

1.1. The photosynthetic process.

The physical definition of energy as the “ability of a system to carry out a material work” is strictly related to natural phenomena and to human intuition: so science, which starts its pathway just from the observation of the nature, is based on the concept of energy as a quantity variable in shape and subject to continual transformations.

Heat, electromagnetic radiation, chemical bonds and intermolecular interactions, nuclear and electrostatic forces, gravity force and so on, are all forms of energy that can be interconverted according to precise physical and chemical equations. Heat should be considered the most degraded of these forms: energy indeed cannot be completely converted into work, or, in other words, every energy transformation produces some not utilizable amount of heat.

Life and its complex processes are born as a result of one or more of these conversions. As a consequence, in the early stages of evolution living cells became highly ordered systems just to satisfy their energetic requirements; on the other side, their correct functioning in this sense, that is obtaining energy from the external environment, made possible to maintain the above mentioned order. It is just the organization of the photosynthetic apparatus of green plants and of certain bacterial strains - these last in particular - that we are going to examine further.

For both kind of organisms, the primary energy source is the sunlight, which through well defined biochemical pathways is converted into chemical energy stored in some specific organic molecules.

The oxidation of such organic molecules supplies then the photosynthetic organisms (as well as those using bacteria and plants as food) with the energy they need to grow. The oxidation process is long, gradual and under the control of a well-tuned enzymatic machinery. This complex series of enzyme-catalyzed metabolic reactions is coupled with the synthesis of ATP (adenosine triphosphate nucleotide) and is named cell respiration.

As a matter of fact ATP is the molecule regulating any energy exchange in biochemistry: it is necessary for every process requiring energy to go on. The key of this role stands in its strong oxygen-phosphorus chemical bonds, whose hydrolysis releases

a great amount of free energy (more than 7 Kcal*mol^{-1} in standard conditions and at pH 7[1]). This is an example of energy conversion from that hold in chemical bonds to that of metabolic type available for the organisms. Of course, also the reverse process is possible: the storage of metabolic energy received from environmental resources by means of building suitable chemical bonds (otherwise the benefit in using the ATP molecule would be inadequate). In other words biochemistry, as well as economy, teaches that universal exchange currencies are always strictly related to energy needs...

In all living organisms every process involving energy conversion and accumulation takes place in suitable structures, all sharing a similar building architecture: they are constituted by many enzymes supported on the cell membrane. In eukaryotes - animal, plants, algae and microrganisms such as fungi and yeasts - these apparata are held in well distinguishable compartments (organellae), separated from the rest of the cell by membranes. In prokaryotic organisms such as bacteria instead, the cell plasmic membrane itself folds in a suitable way in order to reach an optimal efficiency for energy production.

The common feature of both these membrane systems is the tendency to develop structures characterized by an high surface-to-volume ratio. So chloroplasts (eukaryotic cell organellae in which the green plants photosynthesis takes place) and mitochondria (eukaryotic cell organellae in which the cell respiration takes place) display a large amount of folded internal membranes.

The knowledge of energy production and conversion mechanisms allows to understand both this tendency to a specific morphology and the central role played by membranes in these processes. Among the products of both photosynthesis and cell respiration, in fact, there is an electrochemical gradient which of course could not exist in the absence of any physical separation between contiguous compartments.

Such a gradient is the result of a difference in proton concentration between the two sides of a membrane: it will be utilised by a membrane enzyme, the ATPase complex, for the synthesis of ATP, according to the cell needs. By this way the ATPase plays a fundamental role in the cell energetics: with almost the same amino acidic sequence it has been found in every eukaryotic and prokaryotic organism (respectively with the name CF_0-CF_1 in chloroplasts and F_0-F_1 in bacteria and mitochondria)[2].

In order to produce the necessary energy to generate the proton gradient,

mitochondria, chloroplasts and bacteria developed a “trick” named chemiosmotic coupling, whose functioning will be explained in relation to photosynthesis[1, 3, 4] (scheme 1.1).

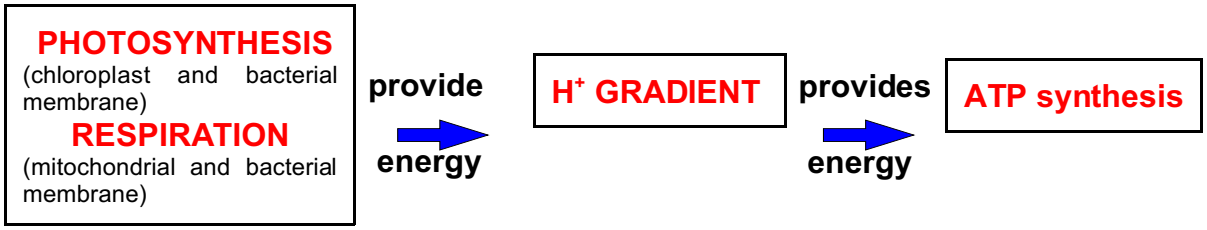

Scheme 1.1.

In both prokaryotic and eukaryotic photosynthesis of course everything starts with the absorption of sunlight, whose wavelength falls in the UV-visible-NIR portion of the electromagnetic spectrum. Photosynthetic organisms have developed various and efficient apparatus for harvesting light by means of the same suitable organic molecules, called pigments (mainly chlorophylls and carotenoids)[5].

The absorption peak of these pigments lies in the visible part of the electromagnetic spectrum: chlorophylls at wavelengths below 500 nm and above 640 nm (their extinction coefficient, ε, higher than 10^5, is one of the highest in nature), carotenoid in the almost complementary region 400 ÷ 530 nm (fig. 1.1). After the absorption of solar radiation some of their electrons are promoted to excited states

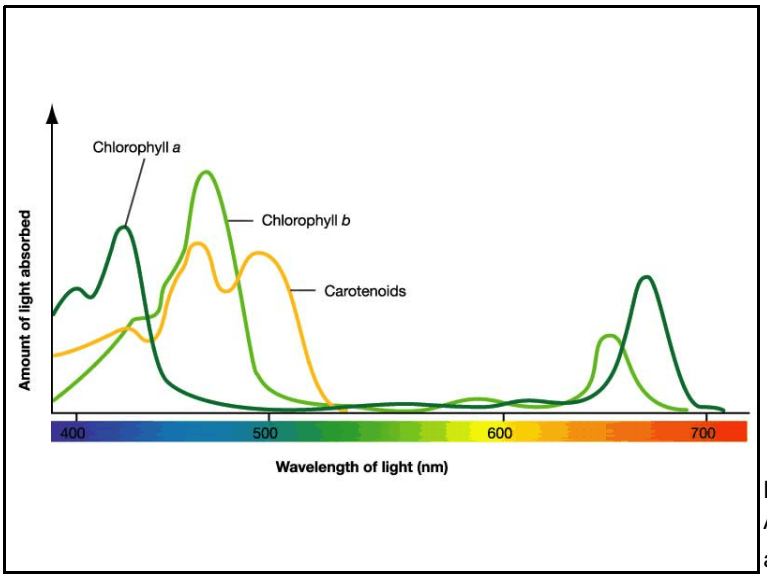

Figure 1.1.
Absorbance spectra of chlorophyll (*a* and *b* types) and carothenoid pigments.

characterized by an higher energy content. In the cell respiration instead, energy arises from the oxidation of reduced substrates and it is released to specific oxidized molecules.

In both cases the process goes on by an electron transfer from donor molecules to final acceptors which are therefore reduced. The transfer involve many electron carriers, each of them supported on or inserted within an ion-impermeable membrane, with electrons falling down on lower and lower energy levels. A portion of the released energy is used just to pump protons from a side of the membrane to another, thus generating the above mentioned electrochemical gradient. In this way the light-induced electron transfer is coupled with the generation of a proton concentration gradient (*i.e.*: a chemical gradient, which is the basis of any osmotic pressure, hence the term "chemiosmotic").

In this general overview of the photosynthetic process some attention must be dedicated to the role played by another class of molecules that will be met in this thesis, the quinones. They are hydrophobic molecules, then liposoluble, acting within the energetic machinery as mobile carriers of both electrons and protons. Such a role derives from their capability to undergo to reversible redox changes: each quinone can reversibly traslocate a maximum of two electrons and two protons. In the field of bioenergetics the prokaryotic protein Reaction Centre (RC) can be considered the reference model for the study of the interactions between quinones and proteins.

Apart of being classified as prokaryots and eukaryots (with all that it means in terms of their internal organization) living organisms can also be classified depending on the source of their methabolic energy. Such criteria, as we will examine, are very significant in order to understand the background of the photosynthesis itself[3, 4].

From the metabolic energy balance point of view, living beings can be mainly referred to two different classes: organisms which depend on chemical substances as energy supply (named *chemiotrophs*) and others whose energy source is light (named *phototrophs*).

Animals (men included) and some microrganisms belong to the former class: substances they utilize are organic, so they are called *chemio-organotrophs*. On the contrary some prokaryotes, defined as *chemio-lithotrophs*, use only inorganic chemical

compounds as energy supply (scheme 1.2).

Phototrophs include both green plants and several microorganisms, either prokaryotic or eukaryotic: they all convert light energy into chemical (in the form of ATP and some reduced organic molecules) during the metabolic process called photosynthesis.

Organisms utilizing inorganic substances or light as energy source are often able to grow even in complete absence of organic compounds, being carbon dioxide their only carbon source (CO_2 is considered an inorganic source). It gives rise to another practical classification in biology, based on the carbon source adopted by organisms (having nothing in relation with energy).

Autotrophs are those organisms who need only carbon dioxide to grow (plants and other prokaryotes and eukaryotes). They may synthesize organic material from inorganic one, and for this reason they are essential to the survival of the other class of organisms, the *heterotrophs*, which depend instead on organic carbon substances for their life (scheme 1.2).

So organisms are often referred to these classifications in order to explain some of their properties: for example it will be mentioned later that different types of purple bacteria may have either a photoautotrophic or a photoheterotrophic metabolism.

Scheme 1.2. Distinction among biological organisms on the basis of their energy and carbon sources.

<table>
<tr><th colspan="2">ENERGY SOURCE</th><th colspan="2">CARBON SOURCE</th></tr>
<tr><td rowspan="2">PHOTOTROPHIC
(LIGHT)</td><td>CHEMIO-LITHOTROPHIC
(inorganic C)</td><td rowspan="2">AUTOTROPHIC
(CO_2)</td><td rowspan="2">HETEROTROPHIC
(organic C)</td></tr>
<tr><td>CHEMIO-ORGANOTROPHIC
(organic C)</td></tr>
</table>

In next paragraphs will be examined first the green plants photosynthesis (par. 1.1.1), then - more in detail - the bacterial photosynthesis (par. 1.1.2). Later it will be the moment to illustrate the structure and functions of cell membranes, already many times mentioned (par. 1.2). In such a way it will be possible to subsequently approach the subject of lipid-protein interactions in the membrane environment (par. 1.3), central in this thesis.

After that, there will be an examination on how the photosynthetic apparatus of bacteria chosen for our studies (*Rhodobacter sphaeroides*) is organized and on structure and functions of the extracted protein Reaction Centre (RC, par. 1.4). A review of the available literature data on recently discovered molecular contacts between the RC and its lipidic native matrix (par. 1.5) will then introduce to the new challenges opened in the understanding of membrane proteins.

1.1.1. The green plants photosynthesis.

1.1.1.1. Localization.

Among several analogies, two main differences distinguish the photosynthesis of green plants and that of some microorganisms, prokaryotic (e.g. cyanobacteria) and eukaryotic (e.g. other algae), from the bacterial one. These are: the localization, well defined (in plants) or generically situated within plasmic membranes (in bacteria); the organization of the whole process, following an open (in plants) or rather a cyclic path (in bacteria).

The first difference has been already discussed: in eukaryotic organisms the photosynthetic apparatus is represented by chloroplasts, special cell organellae which contain membrane-made closed structures (*thylakoids*) tightly leant one on the other to form piles, named grana (fig. 1.2).

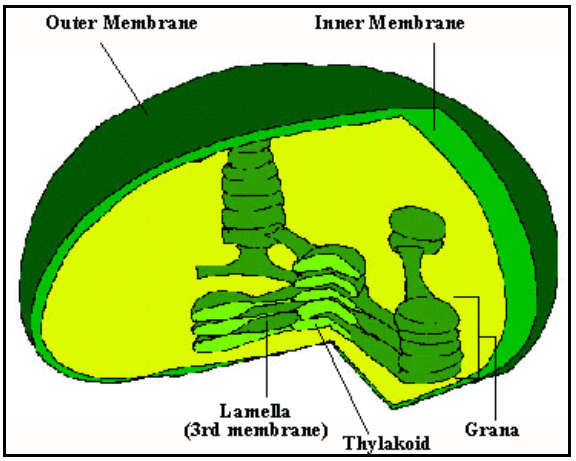

Figure 1.2.
Cross-section representation of a chloroplast.

Thylakoids divide chloroplasts in two regions: the liquid matrix surrounding them and an internal space (named lumen). This arrangement makes possible to produce a light-induced pH gradient which in turn will be utilized for the ATP synthesis.

Within thylakoid membranes the chlorophyll is associated in complexes containing up to 250 molecules, among which only very few are directly involved in the photochemical reactions producing ATP (these are called “Reaction Centre chlorophylls”), most of them instead serving only as light-harvesting antennae. The function of these latter is just to collect and funnel light to the already mentioned special and rare ones[1, 3, 4, 5].

Such functional aggregates of a specific photosynthetic protein - as Photosystem II (PS-II) for green plants - together with light harvesting complexes containing many chlorophyll and carotenoids molecules[1] are defined as photosynthetic units (PSU): a wealth of experimental evidences actually proves that their organization is universal in both higher plants and photosynthetic bacteria[6].

1.1.1.2. Metabolic reactions.

About the second main difference between green plants and bacteria - the organization of the photosynthetic apparatus - this is arranged in two photosystems in series, named Photosystem I (PS-I) and II, (PS-II, scheme 1.3). They are an ensemble of several proteins and pigment-protein complexes working in concert building up functional units of methabolic importance.

As it will be seen also for prokaryotes (par. 1.1.2.3), the final results of the interaction with the electromagnetic

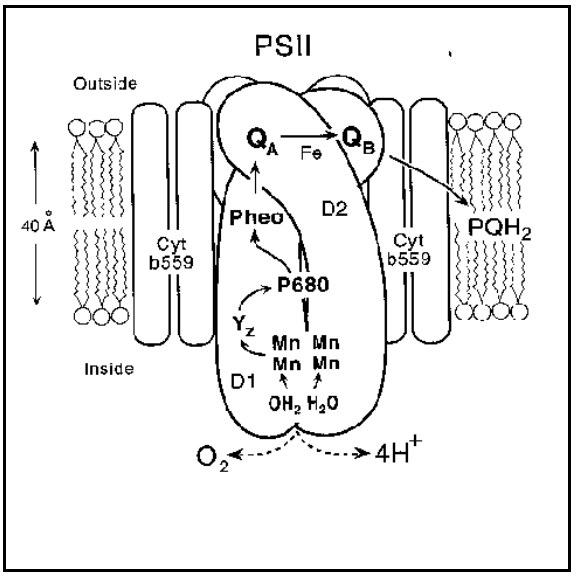

Figure 1.3.
Structure of the Photosystem II of the green plants.

1. Besides the already mentioned pigments, in green plants are often present also other molecules, such as phycobilins and several different xanthophylls.

radiation are: (1) the generation of a transmembrane proton gradient necessary to the ATP synthesis; (2) the production of the reducing power necessary to the NADPH biosynthesis[1, 3].

The radiation absorbed by chlorophylls belonging to the light-harvesting complex of PS-II (represented as green coins in scheme 1.3) is transferred to the pigment P680, made of two chlorophyll molecules arranged in such a way to form an excitonic dimer (the so-called "special pair") and located at the interface between two similar subunits. These form the nucleus of the dimeric reaction centre (fig. 1.3). Because of the homology in the primary structure and functions (e.g. for the sensitivity of both RC and PS-II to triazine herbicides), the whole PS-II is considered the "eukaryotic analogous" of the bacterial photosynthetic RC[1], whose properties will be discussed later.

Hence, thanks to the energy "jump" provided by the absorption of the electromagnetic radiation, the excited electrons possess now enough energy to reduce the pheophytin cofactor (green in the scheme 1.3) and then two plastoquinone molecules (PQ) bound to both Q_A and Q_B sites (fig. 1.3); the binding of two protons leads to the complete plastoquinone reduction (PQH_2).

The photooxided P680 dimer is then reduced by the electrons recovered from the oxidation of water to molecular oxygen operated by a Mn-containing complex bound to the reaction centre (fig. 1.3). Then the global reaction catalyzed by PS-II is the light-induced electron transfer from water - with the concomitant release of O_2 - to the second plastoquinone, together with the production of a transmembrane proton gradient.

Subsequently electrons coming from PS-II arrive to the Photosystem I (PS-I) through the transmembrane cytochrome *bf* complex (indicated generically as

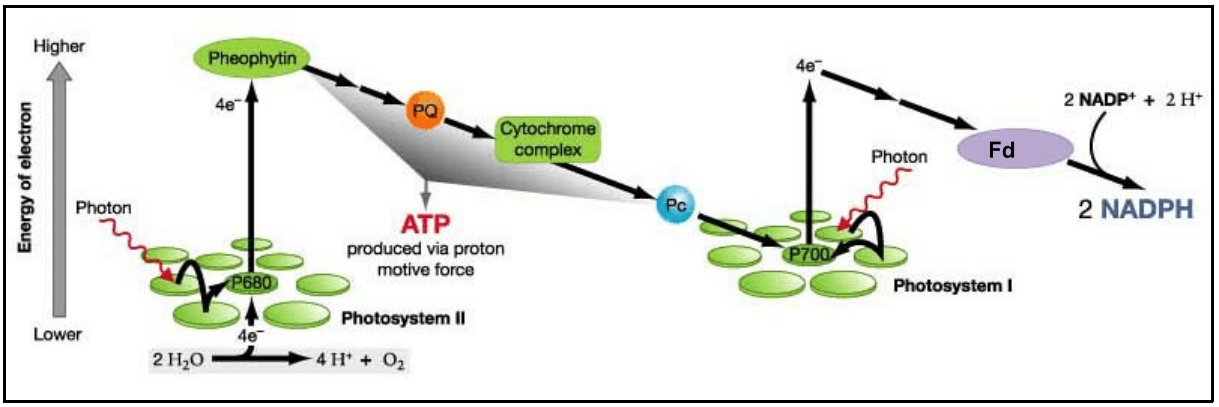

Scheme 1.3.
Energy diagram of the green plant photosynthesis (see text for details and explanation of the symbols).

cytochrome complex in scheme 1.3). It moves protons inside the thylakoid space (the space internal to thylakoid membranes of the grana) when electrons are transferred from PQH_2 to plastocyanine (Pc, blue in the scheme 1.3), a water soluble protein. Now the thermodynamic driving force of the electron transfer is definitely exhausted: it is necessary a second photosystem, PS-I, to promote a light-induced electron transfer from Pc through the pigment P700 (at the interface between identical subunits of the PS I) and then, through chlorophyll molecules, to ferredoxine (Fd, violet in the scheme 1.3), a strong reducing agent.

Hence the ferredoxine-$NADP^+$ reductase, a flavoprotein located on the stromal side of the membrane, will catalyze the NADPH synthesis. By this way the connection between PS-II and PS-I allows the electron transfer from H_2O to NADPH to proceed and, moreover, it leads to the formation of a proton gradient necessary for the ATP synthesis.

The global reaction of the passage through PS-II, Cyt *bf* and PS-I is[1]:

$$2\,NADP^+ + 2\,H_2O \xrightarrow{light} 2\,NADPH + 2\,H^+ + O_2 \qquad \textbf{(1)}$$

Alternatively, electrons can be transferred from Fd to PS-I through the cytochrome *bf* complex, instead of going to $NADP^+$: this cyclic photophosphorilation leads to production of the proton gradient without NADPH synthesis (as in bacteria with NADH, par. 1.1.2.3). This biochemical shunt is active when no $NADP^+$ is available: following this pathway PS-II is not involved in the photosynthetic process and therefore no oxygen production is observed.

Subsequently ATP and NADPH so formed in the light-driven phase of photosynthesis are partly consumed to convert CO_2 in monosaccharides and other organic compounds, through the “dark phase” of the same process, the so-called Calvin-Benson cycle, whose global reaction is[1]:

$$CO_2 + 2\,H_2O + 3\,ATP + 2\,NADPH \longrightarrow (CHOH) + 3\,ADP + 3\,P_i^- + 2\,NADP^+ + H^+ \qquad \textbf{(2)}$$

By the sum of the eqns. (1) and (2) and keeping into account the ATP synthesis reaction - from ADP and phosphate P_i - it is obtained the basic equation of the oxygenic

photosynthesis (where CHOH is a carbohydrate unit), very simple only at a first glance:

$$CO_2 + H_2O \xrightarrow{light} (CHOH) + O_2 \qquad (3)$$

1.1.2. The bacterial photosynthesis

1.1.2.1. Purple bacteria.

Purple bacteria are unicellular prokariotes[2]: they are phototrophic since they are able to use solar energy to oxidize reduced substrates, being carbon dioxide the final acceptor of the electrons. Their colour depends on their complement of carotenoids, and varies from red to brown; some mutants are green. They can be divided into two groups[7]:

- *Thiorhodaceae* or *Chromatiaceae* (purple sulphur bacteria);
- *Athiorhodaceae* or *Rhodospirillaceae* (purple non-sulphur bacteria)

depending on whether they use sulphur compounds as reducing agents for photosynthetic carbon dioxide fixation (instead of water as in green plants, see below).

All the *Chromatiaceae* are obligate anaerobes, and oxygen is toxic to them (as for green sulphur bacteria); they typically use hydrogen sulphide to reduce carbon dioxide by the pentose cycle, in a classical photoautotrophic metabolism (most purple bacteria can also use molecular hydrogen as an alternative reducing agent). Moreover it may be noted that the means by which some purple photosynthetic bacteria utilize inorganic substances (H_2S and other reduced sulphur compounds, or H_2) as donors in the electron transport chain are not at all specific to phototrophic organisms: in fact they are able to grow chemio-litho-autotrophically in the dark, that is using inorganic

2. Many unicellular organisms, prokaryotes and eukaryotes, are responsible for most of the photosynthetic activity carried out on Earth, taking place in aqueous environment.

compounds as energy source and CO_2 as the only carbon source.

Rhodospirillaceae are better differentiated: many of them are facultative anaerobes, but lose most of their photosynthetic pigmented proteins when they are grown aerobically (which may be in the dark or not). In the presence of oxygen, the cells of the *Rhodospirillaceae* carry out respiration, behaving like eukaryote's mitochondria. They constitute the largest group of photosynthetic bacteria and account for 8 genera and 30 species identified up to now. To this group belongs *Rhodobacter (Rb.) sphaeroides*, rod-like bacterium provided with flagella.

They normally use organic materials[3] which are elaborated as required using light energy: in other words they live by means of a light-driven reverse version of fermentation (photoheterotropic metabolism); some of the *Rhodospirillaceae* can also use hydrogen sulphide (but only at low concentration). This latter feature is a clear sign of a high methabolic flexibility that induces to suppose that any distinction between *Rhodospirillaceae* and *Chromatiaceae* is difficult and often arbitrary[7].

Contrary to green plants, algae and cyanobacteria (par. 1.1.1), purple bacteria carry out a photosynthetic process called anoxygenic, that is without producing oxygen: it allows to some types of these microrganisms (obviously not to anaerobic ones) often to grow in aerobic environments with strong reducing properties, as pond muds and pond depths, and to create there a privileged ecological niche without competition with any other photosynthetic organism. They are able to utilize either the products of the anaerobic metabolism of the sea depths (hydrogen sulfide, hydrogen gas, carbon dioxide) or the product of the anaerobic fermentations and of the partial oxidations taking place in the intermediate layers of the stagnant waters (lakes, pounds, lagoons).

The metabolic choices of these bacteria highly contributed to their success in evolution, since they are well differentiated according to their natural habitats: the *Rhodospirillaceae* family, facultative anaerobic and photoheterotrophic, is able to grow even in the dark, aerobically oxidizing the reduced carbon compounds, even though their optimal oxygen tolerated concentration is low. For this reason their native environment is limited to the water layers closer to the surface, at the border between oxygen-containing and oxygen-free waters, where the oxygen concentration is low.

---

3. The organic material available may be more reduced or more oxidised than the average of the cell component , then hydrogen gas or carbon dioxide are produced to correct the balance (hence the bubbles from pond mud).

Moreover, their impossibility to decompose organic macromolecules requires the presence of aerobic microrganisms able to do it since simple organic molecules are necessary in the dark metabolism of the *Rhodospirillaceae*.

To complete this short description of the bacterial family of *Rb. sphaeroides* (facultative photoheterotrophic), it can be finally added that *Rhodospirillaceae* are free of moving, so they can look for the best conditions of light, carbon dioxide, oxygen and organic substances[7].

1.1.2.2. The role of the bacterial pigments.

In order to survive in native environments the photosynthetic efficiency of purple bacteria primarily depends on the presence and nature of pigment molecules able to highly absorb solar radiation: bacteriochlorophylls (similar to chlorophylls except for slight differences shifting the light absorption peak in the near IR zone, NIR) and carotenoids. Thanks to these pigments purple bacteria absorb light in a spectral region complementary to that of plants and algae: the main wavelengths are about 500 nm through carotenoids and above 800 nm through bacteriochlorophylls[4] (fig. 1.1), two regions different from the typical peaks of the *a* and *b* chlorophylls. This right evolutionary choice made them adjusted to a habitat below plants and among algae.

The primary pigments are bacteriochlorophylls, whose structures as well as that of chlorophylls - can be divided in two main parts (fig. 1.4):

- a polycyclic and hydrophylic moiety porphyrin-like composed by a substituted tetrapyrrole, whose nitrogen atoms coordinate a magnesium atom (head);
- a 25 carbon atoms long hydrophobic alcoholic chain (tail) bound through a ester linkage to the polycyclic head, named phytyl.

Because of the presence of this hydrocarbon tail the bacteriochlorophyll is able to interact with lipids and with the hydrophobic moieties of the photosynthetic membrane proteins.

The wide electronic delocalization of the bacteriochlorophyll molecules makes

4. In the bacterial RC the bacteriochlorophyll dimer shows the following absorption peaks: 870 nm in that from *Rb. sphaeroides*, 960 nm in that from *Rps. viridis*.

them able to absorb light in the visible range of the electromagnetic spectrum, mainly below 500 nm and above 700 nm, presenting very high molar extinction coefficient (10^5 $M^{-1}cm^{-1}$ and even more, together with chlorophylls some of the highest values observed in nature). Moreover, according to the chemical identity of the substituent groups, different bacteriochlorophyll molecules may show typical absorbance spectra ranging from blue wavelengths to the near infrared zone.

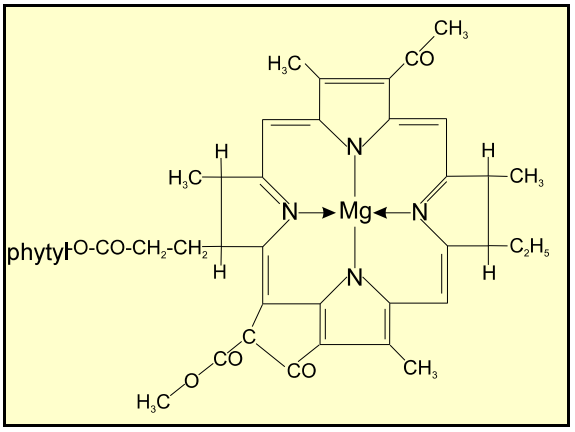

Figure 1.4.
Molecular structure of the *a*-bacteriochlorophyll, the only present in *Rb. sphaeroides* [7].

The apparatus of photosynthetic bacteria - as well as that of plants - holds also accessory pigments: carotenoids and xanthophylls (fig. 1.5). Since the electronic spectra of carotenoids show absorption peaks in a spectral region where the bacteriochlorophyll does not absorbe, their presence/absence in an organism deeply influence their colouration (purple bacteria represent a classical example). Carotenoids are also able to exchange excitation energy with bacteriochlorophylls: hence the definition of accessory pigments; their main metabolic function seems to be photoprotection[7].

The bacteriochlorophyll excited state usually has a very short lifetime, then it is quite immune from the attack of potential oxidizing agents such as oxygen. With small but finite probability, because of light the normal singlet excited state (^{1}BChl* in scheme 1.4, the excited electron generally keeps the same spin state of the ground level) may change into a triplet one, having a longer lifetime (^{3}BChl* in scheme 1.4). Hence photoexcitation leads to a spin inversion. This triplet can transfer the excitation energy to common triplet oxygen molecules (O_2 in scheme 1.4) forming the singlet oxygen species $^1O_2$ (reported in the spectroscopic notation $^1\Delta_g O_2^*$ in scheme 1.4), which in turn- because of its electronic rearrangement - may be reduced to the very reactive doublet superoxide anion O_2^-.

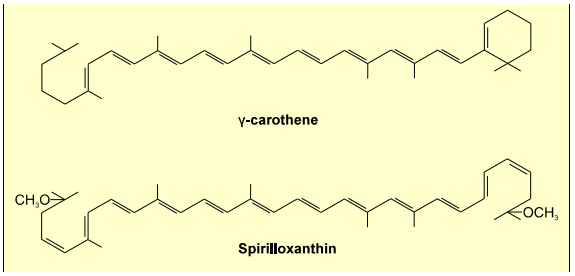

Figure 1.5.
Molecular structure of two typical accessory pigments very common in purple bacteria: carothene and xanthophylls.

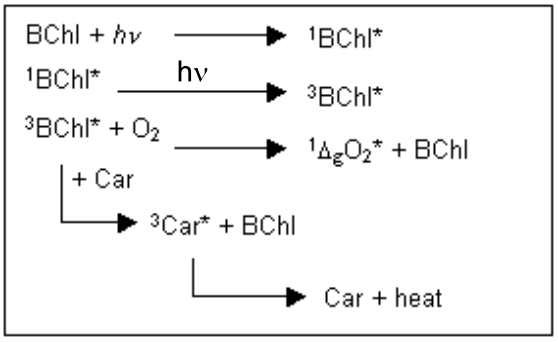

Scheme 1.4.
Illustration of the photoprotection mechanism exerted by carothene molecules (Car). Asterisk refers to excited states. ^{3}BChl and Bchl (or ^{1}Bchl) indicate respectively triplet and singlet states of bacteriochlorophyll, while O_2 and $^1\Delta_g O_2^*$ indicate respectively the same for molecular oxygen species (singlet O_2 is reported in spectroscopic notation).

Carotenoids act as deactivating agents of the excited triplet bacteriochlorophylls (*quenchers*) since they can dissipate the excess energy as heat and because they can react with O_2^- in a sacrifice-like mechanism[4, 7] (not reported in scheme 1.4).

In native photosynthetic membranes both primary and accessory pigments are associated to protein molecules. The reasons and therefore the advantage obtained by such a coupling are twofold. In order to reach an efficient transfer of the light excitation energy, both distance and mutual orientation between the excited molecule and the transfer destination one must be extremely well defined. Moreover the association with proteins provides every pigment molecule with a chemical environment able to alter and to tune their absorption spectrum. This last effect allows the same pigment to show an almost continuous absorption spectrum depending on the protein moieties associated with it, thus extending the wavelength range capable of initiating the photosynthetic process.

1.1.2.3. Metabolic reactions.

As already specified, the anoxygenic photosynthesis of purple bacteria is different from the oxygenic one of green plants, both in localization and organization (par. 1.1.1.1).

In prokaryotes there are no chloroplasts and the photosynthetic pigments are localized just on the plasmic membrane organized in structures deriving from its extensive folding. In *Rb. sphaeroides,* for example, the extent of membrane invagination depends inversely on the light level because of the tendency to maximize the photosynthesis efficiency: after having been grown in low light on breakage the cells yield a high proportion of sealed vesicles (chromatophores, par. 2.1); after high-light growth instead this yield is much lower[7].

Also in the purple bacteria, as already mentioned for green plants, the heart of the photosynthetic process is a molecular machinery called Photosynthetic Unit (PSU). It is formed by two main integral-membrane enzymes, the Light Harvesting Complex (LHC), harvesting the electromagnetic radiation, and only one RC, that utilizes the light absorbed (only one compared to the two of the green plants, one for each photosystem).

A single RC molecule is made of up to 25÷30 bacteriochlorophyll molecules, although only very few of them are directly involved in the photochemical reactions leading to the ATP synthesis (most of them are associated with specific polypeptides to form the so-called light-harvesting complexes[5]).

Photosynthetic bacteria lack the water photo-oxidation mechanism and thus of the oxygen production. They need for their growth other reduced substances, organic or inorganic, that may be oxidized for the biosynthesis. Hence the global and general reaction of the bacterial photosynthesis - in analogy with the equation (3) - is[1, 3]:

$$CO_2 + 2H_2A \xrightarrow{\text{light}} (CHOH) + 2A + H_2O \qquad \textbf{(4)}$$

where H_2A and A are two suitable but not specified substances, respectively in the reduced and oxidized form (according to the available environmental sources and to the bacterial type they can be H_2S and S, or H_2); CO_2 is the final acceptor of the electrons and (CHOH) is a carbohydrate unit.

The above chemical equation should be interpreted in a schematic and global sense: during the intermediate metabolism CO_2 is reduced in a series of light independent reactions, the Calvin-Benson cycle, utilizing as reducing agents the NADPH (for higher plants, par. 1.1.1.2) or the NADH coenzyme (for cyanobacteria and other photosynthetic bacteria), besides ATP for energetic needs.

The NAD^+ reduction to NADH is performed by the NADH dehydrogenase, operating in an opposite direction in relation to that of the cell respiration: the electrons are extracted from the reduced substrates (H_2A) and it represents the conclusions of the light-dependent part of the bacterial photosynthesis, whose complete reaction - in analogy with the equation (1) - is:

$$2\,NAD^+ + 2\,H_2A \xrightarrow{\text{light}} 2\,NADH + 2A + 2H^+ \qquad \textbf{(5)}$$

(NADH is necessary for every reductive reaction of the bacterial metabolism).

The prokaryotic photosynthesis is carried out by a unique photosystem composed of three multimeric membrane protein complexes: they carry out a cyclic photophosphorylation, similar in every bacterial type, though with few exceptions[7].

The light, harvested by antenna proteins (LHC, one of the three membrane complexes), is funnelled to the RC primary photoinduced electron donor (a bacteriochlorophyll dimer), the RC being another of the three complexes. An electron is therefore raised to an energy level suitable to initiate the electron transfer that, through a series of intermediate acceptors, reaches the final acceptor, usually a ubiquinone molecule (par. 1.4). Once fully reduced - *i.e.*: after taking up two electrons as well as two protons from the cell cytoplasm - the ubiquinol can leave the RC exchanging with a pool of ubiquinone molecules present in the core of the bacterial membrane (fig. 1.6). The reduction of a single ubiquinone molecule requires, therefore, the absorption of two photons by the RC.

This means that at the end of the first turn of the photocycle (leading to the formation of a semiquinone radical), the photooxidized bacteriochlorophyll dimer needs to be reduced. This task is accomplished *in vivo* by the soluble cytochrome c_2.

To close the cycle the cytochrome (cyt) bc_1 - the last of the three complexes of the photosystem - oxidizes the ubiquinol just arrived from the membrane quinone pool, with the concomitant release of two protons in the periplasm. As a consequence, the net

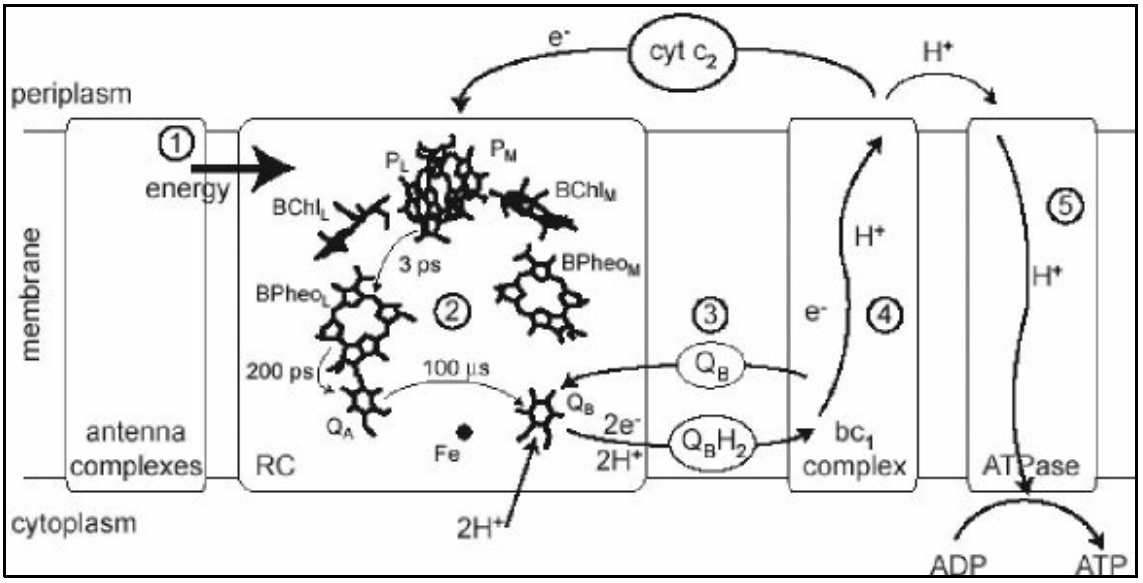

Figure 1.6.
Scheme of the photosynthetic apparatus of the *Rb. sphaeroides* bacteria.

result of the absorption of two photons is the traslocation of two protons from the cytoplasmic to the periplasmic side of the bacterial cell[5]. Within this perspective, RC can be assimilated to a light driven pump producing the proton gradient required for the right function of both the ATP synthase - the third photosynthetic membrane complex - and the NAD^+-reductase. A detailed description of the photosynthetic apparatus of *Rb. sphaeroides* will be reviewed in par. 1.4.

By this way, when the activation energy barrier of the direct electron transfer between the primary donor and the final acceptor is overcome using light excitation (they have an unfavourable energy difference of about 0.5 eV; see fig. 1.32, par. 1.4), then the process may go on since it has become thermodynamically favoured and it doesn't need the intervention of a second photosystem.

Purple bacteria are also able to vary their proportions of light-harvesting to RC complexes in response to changes in the level of light[7] - as it happens for the extent of membrane invagination (see above) -: to lower lights correspond higher bacteriochlorophyll/RC ratios in order to maximize the photosynthesis efficiency even in not optimal conditions. In the high-light conditions, moreover, have been found higher amounts of quinone (electron acceptor), of cyt bc_1 complex (electron transporter), and of ATPase particles, always in relation to RC proteins: in these conditions the arrangement of the antenna complexes in the membranes is modified, smaller units would be more efficient and the RC turns over more often, allowing faster electron transfer within the photosystem. The mechanism of this control is not understood, although it has been established that the genes for both RC and LHC polypeptides are cotranscribed (it is possible that even the supply of carotenoid has its own role)[7].

Finally, while size and efficiency of the photosystem are regulated by light intensity, the synthesis of the whole photosynthetic apparatus has been found to be controlled by oxygen at a transcriptional level[7].

---

5. The space between the plasmatic membrane and the cell wall is called *periplasm*, while the space enclosed by the cell membrane is called *cytoplasm.*

1.2. Structure and function of the cell membranes.

1.2.1. Lipids of biological importance.

The word “lipids” refers to a wide class of organic and biological compounds whose features are quite different from that of other biomolecules: many of them are known since long time in the history of the mankind, with more familiar names as fats, waxes, etc., if they appear solid, oils if they appear liquid.

As a consequence of their chemical structure, lipids are molecules insoluble in water but well soluble in organic solvents such as chloroform and ethanol. In particular natural lipids (commonly called biological lipids) are generally amphiphilic compounds: their chemical behaviour is a direct consequence of the structural separation between a very limited polar region ("head”) and a predominant apolar one (“tail”). The head region is responsible for their affinity for polar solvents, such as water (generally low), while the tail justifies their large solubility in apolar solvents.

The amphiphilic nature of lipids is the starting point to explain their tendency in aqueous media to arrange as oriented monolayers at the air-water interface (“oils spread on water”) or rather to organize themselves in hydrophobic domains as micelles and bilayers, where lipid chains are directed inward and only polar headgroups are exposed to water (par. 1.2.2). Although this behaviour seems to find its origin only in the intermolecular interactions water-lipid polar headgroups and among lipid apolar moieties, this interpretation is not completely correct and requires further considerations.

The unique intermolecular force acting among hydrocarbon chains is the weak Van der Waals attraction, rapidly vanishing to zero when particles are few angstroms apart. The driving force for lipid self-assembly cannot be therefore just the cohesion among chains, but it has to be searched within the so-called “hydrophobic effect”.

The “hydrophobic effect” is basically entropic in nature and arises from the hydrogen bonded structure of water: this latter is not disrupted but is undoubtedly distorted when an apolar molecule has to be dispersed in this medium (we may represent this situation as the transfer of such a molecule from a pure hydrocarbon phase to water). The formation of a clathrate-type structure around the hydrophobic molecule, so as to preserve the hydrogen bonding, causes an ordering of the water

molecules and a consequent loss of configurational entropy (negative $S_{transfer}$ variation for the hydrophobic to aqueous phase transfer[6]). On the other side enthalpic variations coming from newly formed intermolecular interactions are very small: among the heterologous interactions, lipid-water ones are negligible (even between polar lipid headgrups), as well as the homologous lipid-lipid in any new assembly. The enthalpic contribution coming from hydrogen bonding changes (water-water interactions) is also little in comparison with the entropic one because the bonds, although distorted, are not broken: the $H_{transfer}$ can be positive or negative but smaller than $T S_{transfer}$ value, at room temperature. Since by this way the $G_{transfer}$ (free energy difference) value would be always positive, lipid molecules are forced to adopt the only remaining strategy: assemblying together as a monolayer (oil molecules with polar moieties towards water and apolar regions air-faced) or as more complex structures like micelles and bilayers, according the polarity distribution of their structures[8, 9].

The variety of the supramolecular aggregates formed by the dispersion of biological lipids in water will be examined in the next paragraph.

Lipids participate to several biological functions: metabolically they act as fuel and concentrate energy reserve molecules (most times as triacylglycerols, reduced carbon compounds similar to hydrocarbons, so the task analogy becomes not so surprising!), as signalling molecules and as cell membrane building blocks. In our perspective the latter function is the most prominent: biological lipids involved are phospholipids, glycolipids and cholesterol.

Because they establish the permeability barriers for cells and cell organelles and provide the matrix for the assembly and function of a wide diversity of catalytic processes, the phospholipids obviously need a flexible variety in their structures.

They are the most abundant lipids in the biological membranes: this is attributable to their ability to form bilayer vesicles spontaneously, when dispersed in water. This was also the origin of the great interest they always raised in chemistry and biology. They are divided in two classes, glycerophospholipids and sphingophospholipids.

The glycerophospholipids, the predominant phospholipids in biological

---

6. $S_{transfer} = S_w^\circ - S_H^\circ$; S_w°, S_H° are the standard molar entropies of the lipid in the aqueous and hydrophobic phase, respectively.

membranes, are made of two fatty acid chains - equal or different, either saturated or with one or more unsaturations - and a phosphate group, all the three elements esterified to the three hydroxyls of a glycerol backbone. To complete the description, on the opposite side to the glycerol the phosphate is bound to another molecule. This latter, according to its chemical nature and to its electrical charge, provides different properties to the corresponding phospholipid and represents its polar head. The chemical unit of the glycerophospholipid without the characterizing molecule is called phosphatidic acid.

So, according to the nature of this molecule, there can be several phosphatidyl derivatives: as examples, if the molecule is an amino alcohol we can have phosphatidylcholine (PC) and phosphatidylethanolamine (PE), both zwitterionic; if it is an amino acid we can have phosphatidylserine (PS); if a alcohol we'll have phosphatidylglycerol (PG); if it is a monosaccharide we can have phosphatidylinositol (PI). Di-phosphatidylglycerol (or cardiolipin, CL) instead can be almost considered a PG dimer since a phosphatidic acid is esterified to a PG molecule. Except PC and PE, the mentioned glycerophospholipids are all negatively charged, CL being the only with double charge (some structures are reported in fig. 1.7). The zwitterionic glycerophospholipids PC, in higher amount, and PE together represent the major components of the membranes of eukaryotic cells and bacteria[10].

Moreover, glycerophospholipids have an asymmetric carbon atom: in biological membranes they are all derivatives of the L-stereoisomer, the so-called *sn*-glycero-3-phosphatidic acid.

Finally, a given natural (not synthetic) phospholipid type, for example PC, is always

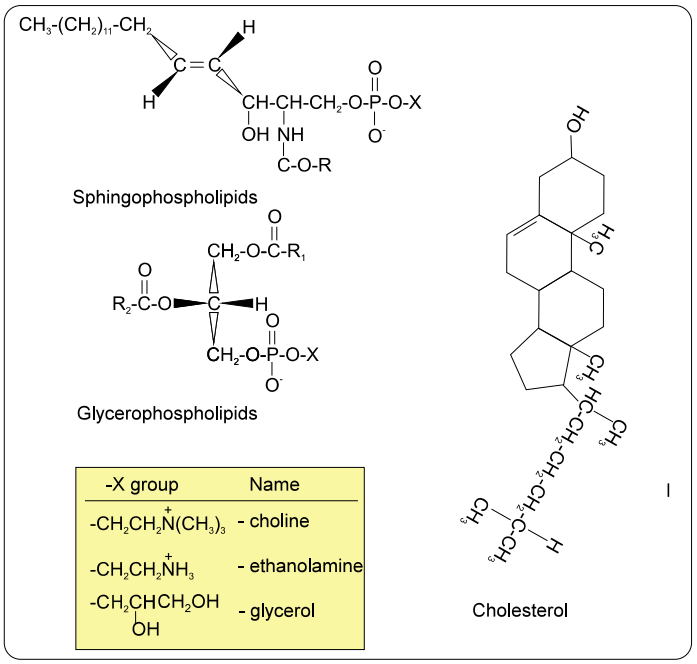

Figure 1.7.
Structure formulae of some lipids (out of scale). In the yellow box there are structure formulae of some substituents of the phosphate group of glycerophospholipids and sphingophospholipids.

a mixture of many different species depending on the fatty acid chain composition of the lipid source (par. 1.2.4 and 2.1 for the fatty acid composition of the membrane polar lipids of *Rb. sphaeroides* and of the PC used in our experiments, respectively). The 16 or 18 carbon atom chains are usually the most common, many times with a single unsaturation.

The sphingophospholipids have sphingosine as the alcohol to which the phosphate is esterified, and the second fatty acid chain is linked to the amino group: within this lipid class sphingomyelin is the sole phospholipid example in membranes (fig. 1.7).

Other variants on phospholipid structure include glycerophospholipids with ether-linked chains (glyceryl ethers), with one vinyl ether and one acyl chain (plasmalogens), and with a single acyl chain instead of two (lysophospholipids)[11].

Cholesterol (structure in fig. 1.7) is neutral and exists only in the eukaryotic membranes with a important regulating role (par. 1.2.3).

Glycolipids, as substituted lipids with oligosaccharide residues, can be neutral or negatively charged; they are generally located on the external side of the plasmic membrane, their function being to help proteins in the cell recognition mechanisms or to make the structural cohesion of protein complexes stronger[12] (for this reason glycolipids - and lipids in general - are becoming important crystallization reagents). Examples can be glucosylgalactosyl-, mono- and digalactosyl diacylglycerol (neutral glycerol derivatives).

It is worth noticing that positively charged natural lipids do not exist[13].

Anionic lipids, thanks to their charge or even to their greater specificity of both charge and structure, seem to be the most suitable to strongly interact with the other biomolecules present in the membranes, the proteins, which show generally non-zero surface charges. Moreover they provide membranes with assembly sites for multisubunit protein complexes. Because of these properties and since this thesis is dedicated to the effects of cardiolipin binding to the bacterial Reaction Centre (RC), our attention will be focused essentially on negatively charged phopholipids.

Anionic phospholipids such as PG and CL are found in virtually all prokaryotic and eukaryotic membranes (in the latter case largely confined to mitochondria), both

contributing to the physical properties of the lipidic phase and interacting with proteins (par. 1.3 and 1.5). In fact they are located especially in electron transporting membranes, providing the immediate environment for the hydrophobic proteins that catalyze photosynthesis and cell respiration[14] (respectively taking place in bacterial or in chloroplast membranes and in the inner mitochondrial membrane).

In the photosynthesis field, structural and mutagenesis studies on lipid-protein interactions are relatively recent, but they already provided several examples on how lipids - especially anionic - are crucial to the correct assembly, function and long range order of photosynthetic proteins, as well as being important for the formation of highly ordered crystals. It has been discovered that bacteriochlorophyll-containing proteins from purple bacteria, such as the RC, preferentially associate with negatively charged lipids (mainly CL)[15], that the presence of anionic lipids in an artificial membrane bilayer (liposomes) strongly influences measurable properties of the bacterial RC (if compared with that observed in neutral membranes)[16, 17]. Moreover, recent investigations on bacteriorhodopsin from purple membranes[18] have shown a precise role of anionic lipids in the activity and structural cohesion of the enzyme, while the LHC-II antenna protein from chloroplasts, the cyanobacterial Photosystem I and the Photosystem II have been found to retain their structural cohesion only if associated with PG[19]. Even cytoplasmic proteins from *E. coli* showed specific requirements for PG and CL in membrane association and activation processes; their lack do not compromise membrane integrity and then cell viability, but only limit cell growth as a consequence of the slowing down of other functions as the synthesis of other membrane constituents (lipoproteins, etc.).

CL is one of the biologically most significant anionic lipids. It has a polar headgroup composed of three glycerol molecules connected by two phosphodiester linkages, with four acyl chains connected to the primary and secondary hydroxyl groups of the terminal glycerol moieties; it has a small headgroup in relation to the size of the acyl chain region (fig. 1.8).

Almost all the CL of the eukaryotic cells is located in the inner mitochondrial membranes (about 20 % of the total lipids); moreover, CL is also a minor component of the periplasmic bilayer of many purple bacteria (about 25 % of the total lipids, see par.1.2.4). Its intensely hydrophobic character is crucial in order to give the

membranes a coherent structure and a determined permeability, particularly in biomembranes which have coupled phosphorylation and electron transport (bacterial plasma membranes, chromatophores[7], chloroplasts and mitochondria).

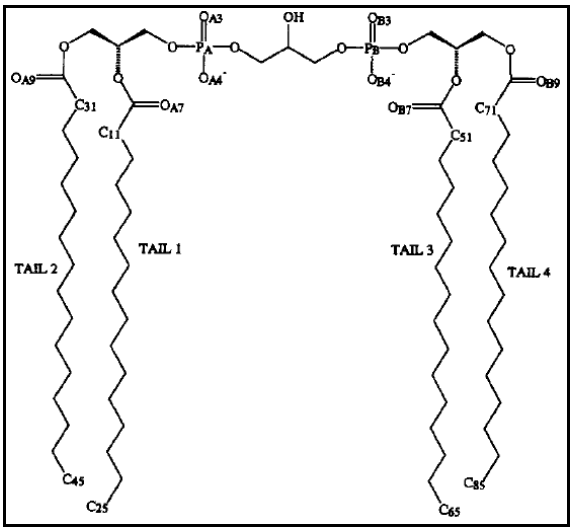

Figure 1.8.
Molecular structure of the cardiolipin (diphosphatidyl glycerol) with four acyl chains, each with 16 carbons

This lipid has been shown to be a fundamental factor in the maintenance of structural cohesion and/or optimal activity of several major integral membrane proteins, both from prokaryotic and eukaryotic organisms, though by mechanisms still not entirely defined. Among a wide number there are: NADH dehydrogenase (or NADH-Q reductase), cytochrome bc_1 complex (or cytochrome reductase), cytochrome *c* oxidase[20] and ATP synthase, all of mitochondrial origin; formate dehydrogenase[21] (mediating interactions between monomers in multimeric structures); Reaction Centres (RCs) from purple bacteria and some cytoplasmic proteins from *E. coli*[10]; transporter proteins as the ADP/ATP and the phosphate carriers (both form mitochondria)[14] .

In particular the need of CL displayed by cytochrome *c* oxidase (the terminal enzyme in the oxidative phosphorylation process) is one of the best known: even after extensive purification the enzyme contains at least one tightly bound CL molecule that cannot be removed without destroying enzyme activity[22]; moreover an X-ray crystal structure of this protein places the CL molecule at the interface between monomers in a dimer[23]. Similarly, when bacterial RC/Light Harvesting I core complexes in intracytoplasmic membranes of *Rhodopseudomonas (Rps.) viridis*[8] were depleted of lipids by extraction with Triton X-100, CL was found to be the most abundant of the

---

7. This term indicates the subcellular fractions of the cell membrane containing most of the photosynthetic enzymes.

8. It has been proposed that *Rhodopseudomonas viridis* should be renamed *Blastochloris viridis* [A. Hiraishi, *Int. J. Syst. Bacteriol.* 47 (1997), 217]. As the former name has permeated the literature on the bacterial Reaction Centre for almost 20 years , and it is still in widespread use, it will be used throughout this Thesis.

remaining lipids, probably reflecting a high affinity of cardiolipin for the proteins of the membrane[24] (par. 1.5 will be dedicated just to the CL affinity for the RC from *Rb. sphaeroides*).

Since it has two acidic and protonatable sites on two negatively charged phosphoryl oxygen atoms (fig. 1.8), CL, as well as other anionic phospholipids, has been proposed to be involved also in the mechanism of lateral conduction of protons through the bilayer surfaces, that would go on just along the surface of anionic phospholipid headgroups (especially in mitochondria)[14]. To strengthen this hypothesis it can be considered that the anionic headgroups of lipids in biomembranes should conduct protons 10^5-fold faster than water does[25]; CL and PG are often the only anionic presences in bilayers; the CL phosphoryl groups are well extended and rigidly fixed in their positions; finally, the oxygen atoms equipped with electron lone pairs and the charged ones, as well as the ester carbonyl group, can contribute to the stability of an intra- and intermolecular, tridimensional hydrogen-bonded network, making easier the proton transport.

In this connection, recently the location of a structurally important CL molecule at the entrance of a proton delivery pathway on the yeast cytochrome bc_1 protein surface, besides stabilizing the assembly of the complex, suggested a "proton transfer role" both for this molecule and for the CL similarly bound to the RC from *Rb. sphaeroides*[26, 27] (par. 1.5).

1.2.2. Phospholipid properties and self-assembly in supramolecular aggregates.

Biological lipids - and also synthetic detergents and other chemical species - are members of the big family of the tensioactives (also called surfactants), amphiphilic chemical compounds able to decrease the surface tension value of a liquid when suitably solved in it as solutes.

Tensioactive molecules are large enough to allow to distinguish between two regions - although their dimensions are well limited on a macromolecular scale -: an apolar hydrophobic moiety (commonly named “tail”), usually made of one or more hydrocarbon chains of variable length, and a polar hydrophilic moiety (named “head”), with or without net electrical charge. This paragraph will be focused essentially on two types of tensioactives, glycerophospholipids and biological detergents: the former because they are the most abundant lipids in biological membranes, natural environment of the bacterial Reaction Centre (RC) subject of our studies; the latter since they have been used to solubilize phospholipids for the RC’s environment reconstitution in liposomes (par. 2.2).

From pure geometrical considerations it is useful to define the packing parameter P (dimensionless). Each surfactant molecule at the oil-water interface of a dispersion[9] (or solution) has its own characteristic parameter P, given by

$$P = \frac{V}{A^* L} \qquad \textbf{(6)}$$

where V represents the volume of the hydrophobic tail (L nanometers long) and A is the polar headgroup area.

According to the P value it is possible to reasonably forecast which kind of packing shape and supramolecular aggregate the surfactant molecules will adopt[8]:

When P is well below 1, the surfactant will preferentially form *direct micelles*, that is globular aggregates with polar heads on the surface and hydrocarbon tails located inside, having an highly positive curvature of the interface (fig. 1.9); this is the usual behaviour of detergents (e. g. biliar salts)[28].

In particular, *spherical micelles* (bottom row of fig. 1.10) can be formed only for those lipids for which $P \leq 1/3$, mainly fatty acid salts or single-chained phospholipids (lysophospholipids) with large headgroup areas. *Long cylindrical micelles* instead are

9. The term *dispersion* (or *suspension*) defines a not completely homogenous liquid mixture tensioactive-solvent (as small unilamellar vesicles of lipids in water, e.g. 100 nm in size), while the concept of *solution* requires a complete homogeneity in every part (as direct micelles of detergent in water, usually few nanometers large). This distinction is related to the old Graham’s classification: solution particles (*solutes*) pass through parchment filters (dimensions smaller than few nm), while real dispersion particles don’t pass (dimensions larger 200 nm). Lipid and detergent aggregation particles can show both and even intermediate cases (from few to 200 nm dimensions).

formed when 1/3 ≤ P ≤ 1/2, for example for single-chained phospholipids with small headgroup areas.

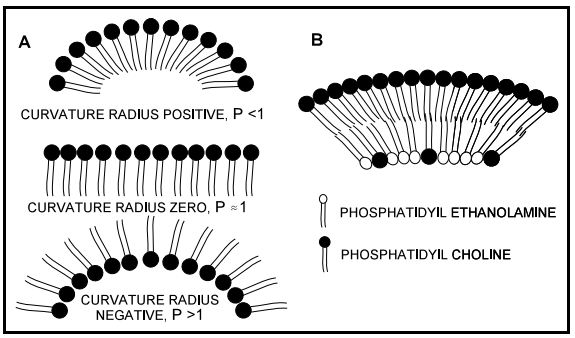

Figure 1.9.
Illustration scheme reporting: (**A**) the interface curvature radius of some aggregates of tensioactive molecules; (**B**) the asymmetrical distribution of the phospholipids in a typical positive curvature bilayer.

This behaviour arises from the requirement that all the internal volume of the micelle (spherical or cylindrical) is filled by the hydrocarbon chains of the surfactant molecules: it leads to the condition that the characteristic half-thickness of the hydrophobic region of the aggregate (the radius R in both types of micelles) cannot be greater than the molecule chain length L (R ≤ L). Of course L in turn cannot be greater than the length of a fully extended, all-trans chain[10]. The whole thickness of the hydrophobic region is then covered by two facing hydrocarbon chains of the surfactant molecule; its polar moieties are instead exposed to the aggregate external surface (considerations in par. 1.2.1 showed that there is no alternative to this assembly).

When 1/2 ≤ P ≤ 1 (as for double-chained lipids with bulky or charged headgroups and with fluid chains) the preferred aggregates will be slightly curved, flexible bilayers making up liposomes, which are aqueous compartments enclosed by a lipid bilayer and dispersed in aqueous environment (intermediate row of fig. 1.10)[11].

For P values approaching to 1 (as for PC and many double-chained phospholipids with intermediate headgroup areas) the spontaneous aggregate curvature reduces to zero. In this case the most stable supramolecular organization is represented by planar and lamellar-like bilayers, few nanometers thick and extended even for millimeters in two dimensions. This is the key motif of the biological membranes; for structural reasons it has the tendency to be bidimensionally extended and closed, that is without hydrophobic chains exposed to water and without any functionally motivated holes, energetically very unfavoured (see fig. 1.9, where it is shown a single layer of a

---

10. For spherical micelles of radius R the aggregation number is N= 4 R / 3V = 4 R^2/A (V, A being above defined, as well as L). It gives R= 3V / A; but it should be R ≤ L, so *P* ≤1/3 is obtained. For long cylindrical micelles: N= R^3/ V = 2 R^2/ A (R_{MAX}= L); it gives R= 2V / A, hence *P* ≤1/2.

11. In this case the lipid molecule is roughly cylindrical and the half-thickness of the hydrophobic aggregate would be R= d / 2 = V / A (d is the bilayer thickness); from it and R ≤ L, P ≤1 arises.

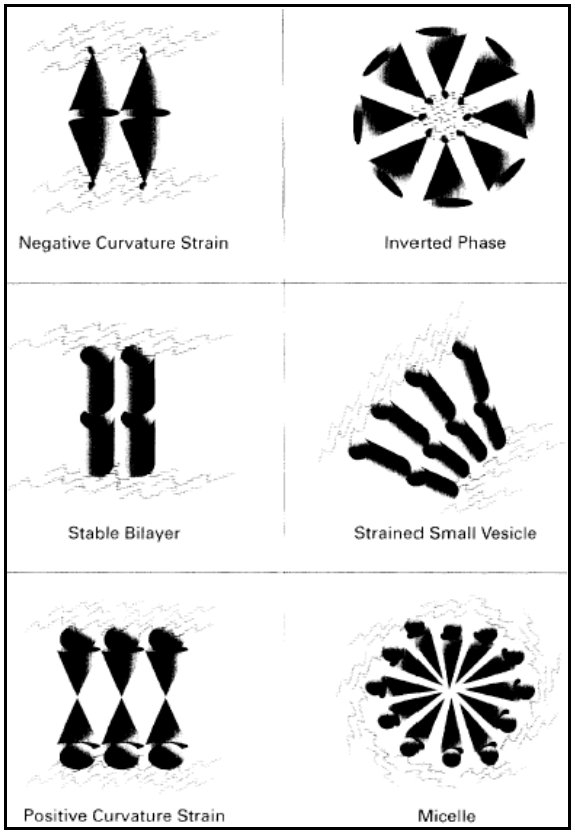

Figure 1.10.
Furher examination of the topics presented in fig. 1.9. In the left-hand column are schematically represented three alternative bilayer motifs. The right-hand panels indicate the types of curved structures that the corresponding types of phospholipids can form; wavy lines show the location of the water. The representations of the shapes of the lipids have been exaggereted in order to emphasize the consequences of packing into flat structure phospholipids that have an effectively small headgroup (negative curvature strain), a headgroup of size comparable to the cross-section of the acyl chains (stable bilayer) or a phospholipid with a large headgroup (positive curvature strain).

double one, and the intermediate row of fig. 1.10); for the membrane structure it is necessary to wait for next paragraph.

P >1 instead is found with double-chain phospholipids with small, uncharged headgroup (e.g. phosphatidylethanolamine, PE): they will give rise to negative curvature systems, named also inverted structures (fig. 1.9), as reverse micelles in apolar organic solvents solutions containing small amounts of water (top row of fig. 1.10 and below) and inverted hexagonal phases (see below).

For phospholipids with highly fluid hydrocarbon chains - that is those for which there are no further steric restrictions between chains at high curvature, apart from the already mentioned geometrical constraints - the smallest aggregates respecting these criteria will result the thermodynamically stable ones. There is significant coexistence of two different packing systems only in borderline cases[8].

Since every biological bilayer presents some parts with non-zero curvature, in order to obtain stable membranes or small vesicles two monolayers with opposite curvature are required: the inner leaflet, having a slightly negative curvature, will be populated by phospholipids sharing a packing parameter greater than one (e.g. PE, PS) while the outer one, with a slightly positive curvature, will contain $P \approx 1$ phospholipids (such as PC and sphingomyelin, see fig. 1.9 and 1.11).

Therefore a large variety of supramolecular organizations results from the spatial delimitation of the hydrophobic and aqueous compartments in surfactant - water

mixtures (surfactants are both phospholipids and biological detergents), as dispersions or solutions: they are all examples of topologically disconnected hydrophobic domains, then showing in detailed studies many typical drawbacks of the heterogeneous phase systems. However the versatile behaviour exhibited by surfactants is referred as *polymorphism:* later phospholipid polymorphism will be examined in some detail, although an extensive treatment of this topic is well beyond the scope of this introduction.

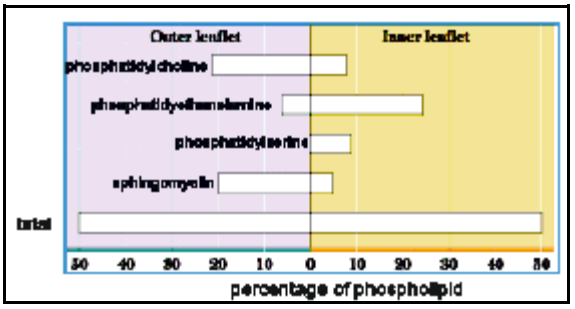

Figure 1.11.
Distribution of different phospholipid molecules between the inner and the outer leaflet of the bilayer.

Up to now detergents have been only mentioned as a class of tensioactive molecules, without adding anything about them: this lack of attention becomes particularly embarassing if it is considered that they represent a very important class of chemical substances - even in common life - and that they have been widely used throughout our experimental work.

Detergents are water-soluble surfactant molecules necessary to solubilize lipids in aqueous environments; solubilization occurs thanks to the association between detergent molecules and lipids, the former with their hydrophobic moieties exerting a shielding effect towards water on the latter.

They can be natural or biological (e. g. biliar salts such as sodium cholate, NaC - used by us, see par. 1.2.5.2 -, are of steroidic origin); otherwise they can be synthetic (e. g. alkylsulphosuccinates, tetraalkylammonium salts, polyoxyethylene-ethers, etc.). They can be divided in three classes in relation to their chemical structure: ionic (anionic, as all the biological detergents, or cationic), amphoteric and non-ionic.

After lipid solubilization in aqueous media detergents should be removed in order to obtain diluted and almost pure lipid aggregates such as liposomes (par. 1.2.5 and 2.2). It is just the difference in water solubility between lipids and detergents that allows separation in their mixtures; structural differences between them are in turn responsible for their limited miscibilities and phase separation. Such and other details can be evidenced in ternary or bidimensional experimental phase diagrams of two partially miscible constituents in water. This is the case of the samples we prepared: mixed

micelles and liposomes both containing the Reaction Centre protein and made respectively of detergent DDAO (dodecyl dimethyl amine oxide) and phosphatidylcholine.

In particular when micellar- and lamellar-forming surfactants are mixed together - corresponding respectively to pure detergent and pure phospholipid systems -, depending on their proportions they give rise to various types of structures ranging from punctiform to three-dimensional ones, respectively in relation to highly curved interfaces (spherical micelles made of detergent) or to very compact aggregates as pure lipid cubic phases (see below).

As always observed in phase diagrams, when one of the two partner molecules is in a much larger proportion than the other, the aggregate structure of this main constituent is adopted, the minor one only acting as an impurity and only contributing in slightly modifying it. When the proportion of the minor constituent increase, the changes that its insertion induces may be compatible with the aggregate or not, leading in the latter case to the formation of a new structure. This will feel the effect of the proportions between the component molecules, exhibiting intermediate curvature radii between extreme structures, being possible several packing combinations.

Detergent-phospholipid mixtures (e. g. NaC-PC) richer in detergent than in lipids usually give rise to spherical mixed micelles, as pure detergents do; they gradually transform into long and mixed cylindrical ones when detergent starts to be removed. Still removing it, at a critical point, named “micelle-to-vesicle phase transition”, mixed vesicles appear and, losing further amount of detergent, they progressively replace the previous aggregates. This phenomenon will be better clarified when it will be again mentioned within the Experimental Section (par. 2.2.2).

It is necessary to stress that micelles, pure or mixed, and liposomes are morphologically very different. Besides their different composition - the former being made of pure detergent or detergent and lipids, while the latter are (almost) pure in lipids-, micelles are thermodynamically stable and optically isotropic[12]. Vesicles, on the contrary, scatter light (i.e. they are optically anisotropic) and are often metastable, that is in time they tend to transform to some other aggregate more stable, by sedimentation,

12. Isotropic materials show equal properties in every direction in relation to a determined phenomenon (here the light propagation).

membrane fusion processes, etc.[28].

There is also a difference in size between these two aggregates, but it is not the main point: the minimum diameter of spherical micelles is roughly the double of the hydrocarbon chain length of a detergent molecule, the maximum being generally well below 20 nm[13]; liposome diameter can vary instead from about 20 ÷ 30 nm (maximum curvature limit) to several micrometers (giant vesicles)[29] (par. 1.2.5).

It is important to highlight that not only the molecular structure of the surfactants and the composition of their possible mixtures, but also "external factors" as ionic strength and pH, for instance, are well recognized to have a direct influence on the interface organization[28].

The lamellar bilayer is the most frequently adopted structure by double-chain phospholipids with sufficiently large headgroups in conditions of high water content (full hydration) and room temperature, but it is not the only one.

Pure phospholipids composed of a small polar headgroup and a large hydrophobic domain ("cone shape", P >1), in specific conditions among which low water contents and temperatures higher than room temperature, may prefer to assume a so-called "non-bilayer" (or non-lamellar) phase or they may spontaneously undergo a phase transition from bilayer-like to a non-bilayer assembly[30] : they can be CL in the presence of divalent cations, PE[10], the synthetic lipid monoolein (glycerol monoester of the cis-9-octadecenoic acid)[31], monogalactosyl/monoglucosyl diacylglycerols (MGDG)[10], etc.. Among alternative non-lamellar phases of pure phospholipids with P >1 the main are[30,32]:

- *inverted hexagonal phases* (named H_{II}, the "II" indicating inverted phases), generally consisting in hexagonally packed cylinders with the polar headgroups facing toward an interior aqueous core (not in rapid exchange with bulk water); due to structural reasons its role in biological systems is probably very limited; the transition to H_{II} phases can be induced by cholesterol owing to its cone shape[10];

- *inverted cubic phases* have been suggested to be present in biological systems; there are two types, the micellar cubic phase and the bicontinous cubic phase;

a typical structure consists of two interpenetrating networks of oriented cylinders with an aqueous core[32] (fig. 1.12); cubic phases can facilitate and influence the crystallization process of membrane proteins[32] (see in par. 1.5.3 the example of the lipid monolein, forming a cubic phase and promoting the crystallization of the Reaction Centre from *Rb. sphaeroides*).

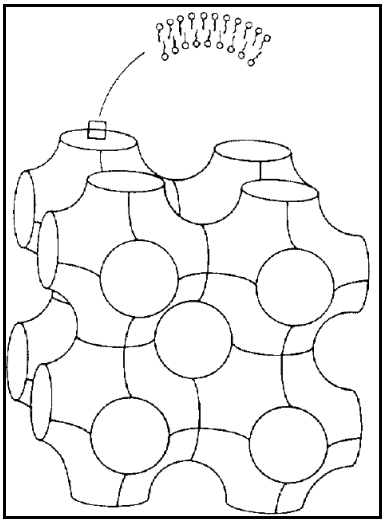

Figure 1.12.
Representation of the bicontinuous cubic phases in terms of a pair of 3D networks of rods which are mutaually intertwined and interconnected.

These are the favoured aggregation phases at low water contents and in the absence of apolar solvents which solubilize lipids. On the contrary, in apolar organic solvents containing small amounts of water suitable mixture of phospholipids form reverse micelles[33]. Such aggregates can be described as consisting of water droplets surrounded by the polar heads of the phospholipid molecules facing toward the interior of the micelle (hydrophilic core), while the hydrocarbon chains are directed towards the bulk, continuous organic phase. Contrary to the case of the water-solved aggregates of direct micelles and liposomes, here the aqueous phase is made of topologically disconnected domains, while the hydrophobic phase is continuous.

By their packing shape non-lamellar-forming lipids often play important roles in determining the physical properties of membranes, mainly about curvature strain (par. 1.2.3). Non-bilayer phases, as every lipid aggregation state (par. 1.5), affect the assembly and the activity of membrane proteins and peptides[29].

Indeed bilayer and non-bilayer lipids present different intrinsic curvature radii: this feature is very useful to stabilize curved parts of membranes, where therefore their common presence is required. Nevertheless, dramatic changes in the proportion of these two lipid classes will result in changes of the collective physical properties of a membrane, even compromising their barrier function.

All biological membranes contain one non-bilayer-forming lipid component at least: then lipid polymorphism in these cases is the rule, not the exception.

Though cardiolipin (CL) may form liposomes being the unique component[34] (par.

2.2.2), it would give rise also to non-bilayer structures[8], if in the presence of divalent cations (with higher affinity for Ca^{2+} than for Mg^{2+}). These structures may alter the local hydrophobic environment and induce conformational changes in the membrane proteins embedded in the lipid phase[10].

Zwitterionic phospholipids, such as PC and PE, in spite of their structural similarity (fig. 1.7), result to be not interchangeable in relation to their properties. PC ($P \approx 1$) has more desirable physical properties, easily forming vesicles and bilayers in solution; it only forms non-bilayer structures under extreme conditions or in the presence of non-bilayer-forming lipids. For these reasons it is by far the most used phospholipid in the majority of the in vitro studies. PE ($P > 1$) instead has a smaller headgroup and has the unique property, shared with divalent cation-CL complexes, of undergoing a bilayer to non-bilayer physical transition, influenced by its fatty acid content and the temperature. Both PC and PE possess a dipole moment across their respective headgroups (as also other phospholipids do) that can be oriented according to the electrochemical potential of the membrane in which they are located, affected in turn by the surrounding medium. So it becomes clear that PC and PE are also not functionally exchangeable in supporting biological processes: by different ways they are both required for many membrane protein structural cohesion and function[10] (par. 1.3.1).

The conditions for the formation of non-bilayer phases - taking place more readily with unsaturated lipids - can be broadly explained in terms of the lipid molecular shape and of the concept of an equilibrium area/molecule at the polar-apolar interface arising from the hydrophobic effect; moreover several factors affect the lamellar-to-non-lamellar thermotropic phase transitions. Nevertheless these topics are well beyond the purposes of this work.

The space here dedicated to the lipid polymorphism is justified by:

- the importance of understanding changes in the bilayer physico-chemical properties introduced by non-lamellar phospholipids, rather than trying to explain the actual formation of non-bilayer phases, very limited in biological environments;

- the finding that collective physical properties of membrane strongly influence processes as diverse as confomational changes in enzymes and cell division[10].

In addition to the ability to organize themselves in different supramolecular aggregates, among several properties phospholipids show another physico-chemical feature particularly interesting for the subjects treated in this Thesis. Fully hydrated bilayers composed of a single phospholipid species undergo a well-defined thermotropic phase transition in which the lipid chains change from an ordered and regularly arranged state (named *gel* and conventionally designated L) to a fluid or liquid crystalline state (named *sol* and designated L), with a larger conformational mobility for the chains. An intermediate phase P ', in which the bilayer is rippled, is found in the gel phase of certain phospholipids.

The transition temperature (indicated often as T_{tr}), also called melting temperature, increases with the phospholipid acyl chain length, while decreases upon increasing the double bond content in the acyl chains; both these factors deeply influence in turn the membrane bilayer fluidity (as it will mentioned in par. 1.2.3), playing a very significant role also in determining the lipid aggregation structure in addition to packing considerations already mentioned. As an example, small bilayer vesicles with small radii of curvature (such as those produced by sonication), although favoured according to packing parameters and to the entropic point of view, may suffer additional packing constraints deriving from lipid fluidity and thus may not be the equilibrium structure, but rather a metastable state[11].

Finally, it is well demonstrated that the physical state of the lipids, that is their phase, actively influences membrane protein function[11, 30]: when Reaction Centres or bacteriorhodopsin are reconstituted in proteoliposomes made of phospholipids with transition temperature ranging around room temperature (e. g. dielaidoyl-PC, T_{tr}= 9.5˚C[35]; dimiristoyl-PC, T_{tr} = 24˚C; dipalmitoyl-PC T_{tr}= 41.4˚C[13, 11]), a clear change in the protein behaviour is always detectable at that temperature [35, 36, 37, 38].

13. The listed compounds are all phosphatidylcholines with different couples of acyl chains: the first has both oleyl monounsaturated chains with trans configuration (18:1tΔ^9); the second has both 14:1 chains; the third has both 16:1.

1.2.3. Cell membranes and membrane proteins.

1.2.3.1. Cell membrane structure and features.

A cell can be essentially described as an aqueous region solubilizing or dispersing chemical species of different nature, charged or neutral, delimited by a hydrophobic closed interface - the membrane bilayer - that separates it from the surrounding aqueous medium. The outer cell membrane, also defined as plasmic membrane, determines the composition of the inner environment of the cell by regulating the inward and outward passing of substances and acting as a barrier of permeability for ions and polar molecules[14]. Its function of selective barrier is confirmed by the sharp dielectric gradient existing between the aqueous environment at both membrane sides and the bilayer interior, having respectively dielectric constants of about 80 (water value) and 2[39] (adimensional figures). Nevertheless biological membranes are not just inert physical boundaries, they are metabolically well active.

It has been demonstrated that several cell activities are strictly related to the proteins embedded into - or bound to - the plasmic membrane: respiration and photosynthesis, signal transduction (as hormone detection, antigenic reactions, synaptic nerve transmission and stimula responses), solute transport, DNA replication, protein targeting and trafficking, hormone secretion, cell-cell interactions, motility, etc.[40, 41].

As already mentioned in par. 1.1, in the eukaryotes besides the plasmic membrane there are a lot of inner membranes organized to form close systems that act as structurally and functionally indipendent units (cell organelles). In the prokaryotes, instead, is the plasmic membrane itself that is organized in functionally distinguished structures, that act as support for the metabolic processes of respiration, cell movement and, in the case of photosynthetic prokaryotes, even for the photosyntesis (besides, obviously, regulating the substance exchange with the outside).

The huge versatility of membranes in cell metabolism can induce to suppose that their structure would be extremely variable according to the functions performed, while, on the contrary, their basic structure can be referred to a unique scheme for all the

14. The permeability coefficients of the small molecules through bilayers are directly related to the their solubility in apolar solvents [13].

living organisms. Besides several micro-components among which hydration water and carbohydrates, it is made up of two main classes of chemical species, proteins and lipids, in simple form or as derivatives, on an average in all membranes present in equal weight proportions (50 %), kept together without covalent bonds but rather by non-covalent cooperative interactions[13].

Such a simplicity is only apparent: it will be shown that between the lipidic and protein components exist strong interactions that are at the basis of the extreme versatility displayed by membranes, both on the structural and on the functional level. Moreover, according to the task a membrane is called to perform, the ratio among the two building species can vary considerably[15], as well as the lipid composition itself; of course the composition and activity of the membrane is always at least adequate, if not optimized through continual evolution, for the particular function being performed.

The protein component (simple membrane proteins, glycoproteins, lipoproteins) is commonly considered the most “intelligent” part of the system since it determines the typical functions of membranes, acting for example as ion pumps, solute channels, receptors, energy transducers and enzymes; these are nearly all embedded within the lipid bilayer, their most suitable environment. Membrane protein will be examined below.

The lipidic component, essentially made up of phospholipids (besides glycolipids, cholesterol and other small molecules), acts mainly as a viscous, semi-permeable barrier between the inside and the outside of a cell, through which or on which are inserted or adsorbed membrane proteins and other possible components, in different ways. Phospholipids do not play a static role in cell processes but are active partecipants: among several functions they strongly affect the properties of the proteins associated with the membrane and they serve as precursors to important cellular components[16].

In most membranes the balance of phospholipids favours the zwitterionic ones (or uncharged diacylglycerol glycolipids), because usually less than 30 mol% of them

---

15. The more active in the cell metabolism are the membranes the higher is their protein content: e. g. from 18 % w/w of the myelin insulating membrane to about 75 % of the prokaryotic bacterial purple membrane embedding bacteriorhodopsin[41] and of mitochondria and chloroplast eukaryotic inner membranes [13].

16. Since phospholipids have no inherent catalytic activity, one of the major challenges in biochemistry now is to develop approaches (in vitro and in vivo) in order to investigate the specific role of these lipids in the cell functions.

are anionic[10], although there is evidence from a broad range of organism that anionic phospholipid headgroups are well involved in the association with many membrane and cytoplasmic proteins[10] (as reported in par. 1.2.2).

The general organization of membranes has been described in a careful manner only with the advent of the X-ray diffraction methods and electron microscopy (EM), because the membrane thickness is much smaller than the resolution of an optical microscope. EM has shown that membranes are made up of two leaflets opaque to the electrons separated by a brighter and transparent one; the whole bilayer thickness varies in the range of 6 ÷ 10 nm for the majority of the membranes[13] (many of them being less or equal to 7.5 nm thick[42]). These microscopy data, together with further experimental informations collected during several years, allowed Singer and Nicholson[43] in 1972 to propose a new model for the membrane structure, defined as "fluid mosaic".

In this model, today yet valuable as general guidelines though well extended, phospholipid molecules are organized to form a bilayer with their polar headgroups facing the internal and external aqueous medium and the apolar moieties turned toward the inside of the membrane. Both these domains are involved in the interactions with integral and peripheral membrane proteins (fig.1.13 and par. 1.2.3.2). The structure of the phospholipid polar headgroup, together with the electrostatic field created by its electric dipole, gives also to these species the possibility of recognizing the different substances that come in contact with the cell membranes and of selecting them with

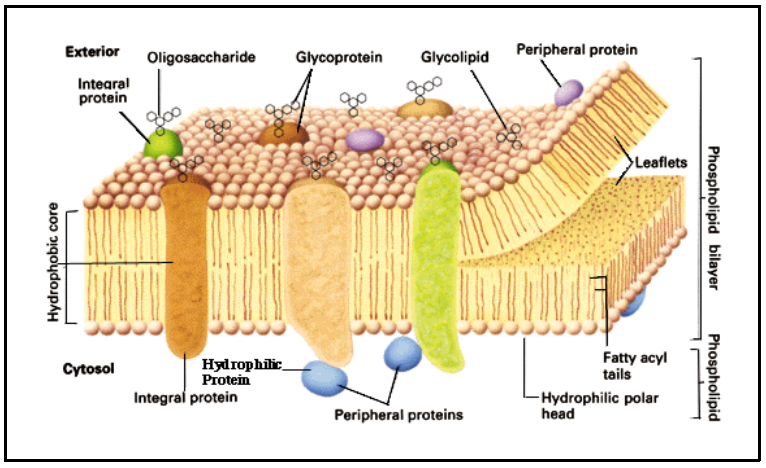

Figure 1.13.
Fluid mosaic model of the cell membrane as proposed in 1972 by Singer and Nicholson.

mechanisms complementary to that carried out by proteins.

Taking into account the dynamic phenomena that occur in its interior, by molecular dynamics studies[11] the cross section of the bilayer can be virtually divided in four different zones (fig. 1.14):

(**I**) from outside a first one composed by the water in contact with the membrane surface;

(**II**) a second one made up of polar headgroups of lipids, tightly bound water molecules and the nearby acyl chain portion;

(**III**) a third zone composed by hydrophobic acyl chains arranged in ordered segments;

(**IV**) the inner one, representing the hydrophobic core of the membrane, holds the terminal portions of the acyl chains, the most free of moving (in that comparable to liquid decane, having a dielectric constant ε of about 2).

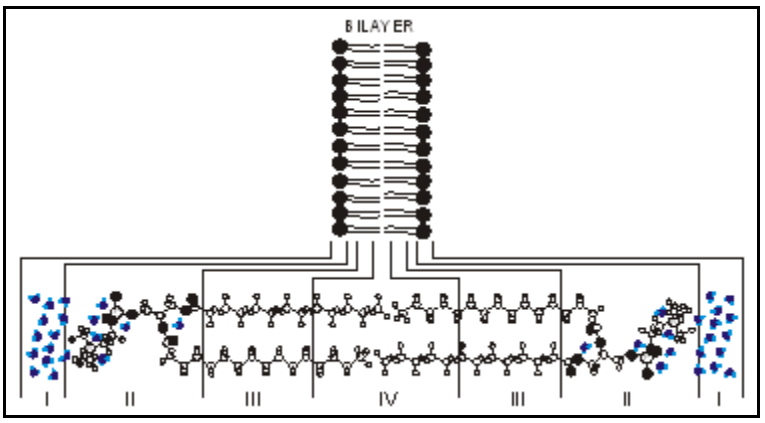

Figure 1.14.
The different regions composing a typical phospholipid bilayer.

From this scheme it is clear that membranes are fluid structures: experimental studies revealed that phospholipid molecules shift rapidly in the surface plane (*lateral diffusion*), as well as many membrane proteins[17] - if not anchored by specific interactions-; movements through the bilayer, passing from side to side, called also *flip-*

17. The majority of phospholipid molecules show diffusion coefficients about 1 $\mu m^2 * s^{-1}$ (2 μm covered every second, leading to a medium viscosity similar to olive oil). Membrane proteins show a larger variety ranging from a lateral mobility similar to lipids to a nearly null mobility [13].

flop movement or *transverse diffusion* are instead very slow in the case of lipids[18] (null for glycolipids, see below) and absolutely forbidden in the case of membrane proteins.

Membrane proteins in fact have a specific orientation since they are synthesized and inserted in membranes in an asymmmetrical way; during the cell life they maintain this orientation because flip-flop diffusion is impossible and because new bilayers always grow on the basis of previously existing bilayers. Hence membranes can be considered as bidimensional solutions of oriented lipid and protein molecules, well maintaining their protein and phospholipid asymmmetry[13].

With regard to the lipid composition, especially referring to non-zero curvature regions, biological membranes were already described as necessarily asymmetrical on the pure basis of the packing constraints mentioned in par. 1.2.2. Nevertheless, in order to satisfy their metabolic requirements[19] all the known membranes were found asymmetrical also in protein composition - as just explained - and even at a carbohydrate content level (representing usually 2 ÷ 10 % w/w of eukaryotic cells). When there are oligosaccharide residues bound to lipids (glycolipids) or proteins (glycoproteins) , they are always placed on the outer layer, acting as important signal molecules for the protein insertion in the membranes and being involved in the intercellular recognition processes.

This multiple structural asymmetry is ubiquitous in every prokaryotic and eukaryotic plasma membrane since it allows to maintain a permanent potential difference (named “membrane potential at rest”) between the cytoplasmic and periplasmic environments: this electrical polarization is basic for the membrane mechanical stability and for many cell functions as substance transport, energy conversion, excitability processes, etc[20, 44]; the inner side is negatively polarized (typically - 60 mV)[13].

The physical properties of membranes obviously modulate their function.

There are an high number of physical properties to be considered, including

---

18. Transverse diffusion coefficients are about 10^9 times smaller than lateral ones [13].

19. The lipidic asymmetry of membranes is also a consequence of the lipid biosynthesis.

20. In many eukaryotic cells the disruption of the lipid asymmetry is a trigger signal for macrophage recognition of apoptotic cells; moreover at least three distinct enzymes are involved in the regulation of the right membrane lipid asymmetry [44].

fluidity, bilayer and hydrophobic thickness (par. 1.3.2.1), curvature strain - measured as lateral pressure profile and free volume -, interfacial polarity, membrane charge and lateral organization (in membranes composed of more than one lipid): each membrane function will have its own sensitivity to different properties; some of them are even affected by the presence of non-lamellar-forming lipids[28].

The *fluidity* is strongly dependent on the phospholipid fatty acid chain composition: in prokaryotes it will decrease only decreasing the acyl chain length or incrementing the number of unsaturations; in eukaryotic organisms also the cholesterol has a complex role in relation to its concentration, variable according to environmental conditions (as temperature) and metabolic requirements[13]. In fact many membrane proteins require "fluidity windows" and precise degrees of molecular motions within the bilayer for biochemical activity to take place[45].

The *hydrophobic thickness* of a membrane is the thickness of the apolar region of the bilayer, polar headgroups excluded; it can vary according to the membrane type and to the membrane protein embedded into; it has been estimated to be in the range 20 ÷ 40 Å just from high-resolution structures of membrane proteins (being about 28 Å for the Reaction Centre protein from *Rhodobacter sphaeroides*[41]*)*. In fact every biological membrane shows a strong tendency to closely match its hydrophobic thickness and that of the protein itself in order to minimize destabilizing energy contribution coming from unfavourable interactions and from bilayer compression or stretching strains[46] (fig.1.15).

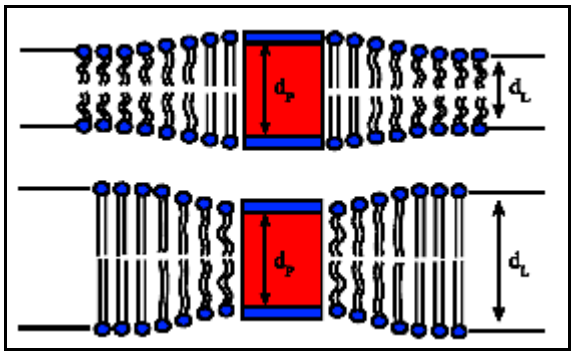

Figure 1.15.
Schematic illustration of hydrophobic matching of a integral membrane protein that is embedded in a thin (top) and a thick (bottom) membrane. d_P and d_L are the hydrophobic thicknesses of protein and lipid bilayer, respectively.

The *lateral pressure profile* of the bilayer is a direct measure of the curvature strain: for example if both the monolayers are symmetrically composed of phospholipids with packing parameter P larger than 1 or "cone shape" (the hydrophobic tail is more bulky than the polar head, see par. 1.2.2) an increased negative curvature strain will lead them to curve away from each other and to an increase in the lateral pressure in the centre of the

membrane, in a very unfavourable stress situation. Hence, the less uniform is the lateral pressure profile, the more packing defects there will be in a membrane, creating increased *free volume* within the bilayer, which can be filled only with suitable shape phospholipids and that can be measured as an increase in the motional properties of a membrane-embedded fluorescent probe (par. 1.3.2.3). On the contrary, if the lipids are all “cylinder shape” (packing parameter P about 1) they will have a uniform lateral pressure throughout the bilayer and they will have also little free volume and low negative curvature strain (fig. 1.16).

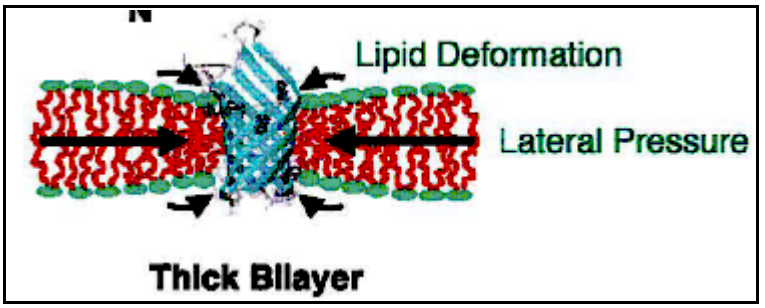

Figure 1.16.
A schematic illustration of the lateral pressure acting on an integral membrane protein inserted in a relatively thick bilayer.

For the same reasons, if the bilayer suffer from negative curvature stress, then the membrane interface is likely to be more hydrophobic: this other physical property related with curvature is the *interfacial polarity*.

About *membrane charge* it is interesting to mention that cationic peptides and cationic surface proteins have been found to interact with membranes containing anionic lipids: the resulting charge neutralization allows the headgroup region of the bilayer to be compressed and to increase the negative curvature tendency.

In relation to the *lateral organization* of membranes, in the last few years a very topical question emerged in biochemistry whether membrane lipids mix uniformly or are arranged and segregated in discrete microdomains (named “patches” or “rafts”): here lipid conglomerates would be associated with specific membrane proteins assuming possible functional roles (in the transport of lipids and proteins, signal transduction, etc.[47]).

Although every fluid native membrane bilayer contains more than one class of lipids, the lateral organization rarely results in the segregation of some of them as a

consequence of the lipid molecular shape. Nevertheless some lateral phase separation and formation of lipid rafts - always maintaining bilayer assembly - has been observed in the presence of cationic peptides bound to anionic membrane regions[29], then having functional tasks. However it is not clear whether these islands of anionic phospholipids form independently in membranes or rather they are induced only by association of positively charged domains of membrane proteins. It is certain instead that segregation of lipid negative charges would provide membrane proteins (always partecipating to rafts, when there are, since rafts exist for functional purposes) a more attractive binding site than segregation of zwitterionic phospholipids[10].

The “raft hypothesis” in fact states that separation of discrete liquid-ordered, the rafts, and liquid-disordered phase domains, non-rafts, occurs in phospholipid model membranes containing sufficient amount of sphingolipids and steroid-like lipids as cholesterol (fig. 1.17). The experimental confirmation of this hypothesis came from the partitioning of fluorescent lipid probes into either raft or non-raft domains (fluorescence quenching assays)[47]. This distinction between different domains has been incorrectly compared to the existence of gel-ordered and fluid-liquid crystalline phases for phospholipids (par. 1.2.2): the raft and non-raft domains exist together at the same temperature in different membrane regions, contrary to phases alternating in the same place at different temperatures.

If, for instance, the amount of cholesterol in binary mixtures phospholipids-

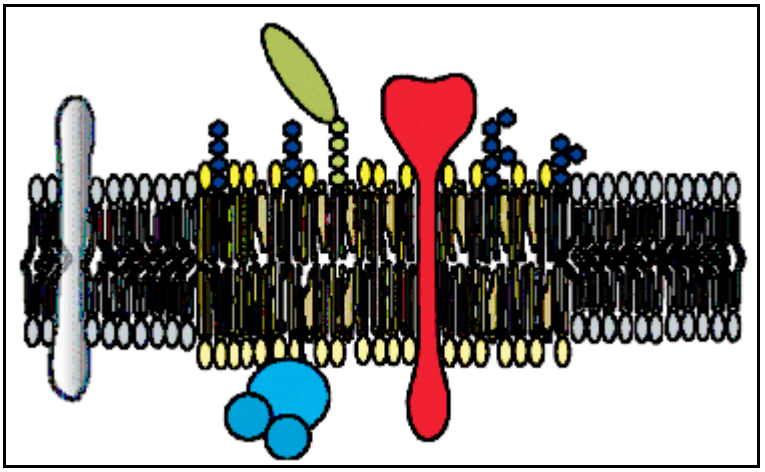

Figure 1.17.
Schematic illustration of a membrane raft, consisting of a lipid patchenriched in sphingolipids, glycolipids, and cholesterol to which certain proteins are attached.

cholesterol - similar in composition to many eukaryotic membranes - is increased, the formation of cholesterol-rich liquid-ordered phases - in coexistence with liquid-disordered domains, composed primarily of phospholipids - is obtained. When present, sphingophospholipids form an ordered state in conjunction with cholesterol (fig. 1.17): so rafts can be considered cholesterol-dependent.

An important feature of rafts is their general insolubility in detergent solutions used to solubilize lipid membranes, resulting from the tight packing of raft lipids, whereas the non-rafts domains result completely solubilized.

Much of the evidences obtained so far about raft existence referred to models of complex membranes artificially reconstituted: though it is difficult to relate these results to living cells, several approaches suggest that cell membranes do contain rafts as independent and clustered patches of proteins and lipids on the cell surface, ranging in size from tenths of nanometers to microns, certainly showing a higher degree of complexity than model membranes[47].

During life evolution the first microrganisms presenting lipid bilayer membranes as we know today were eubacteria (prokaryotes): but while in prokaryotes the number of lipid species remained small, with poor versatility, instead the eukaryotic cell membranes, developed much later in the evolution ladder, show more than 2000 species of lipid molecules, including sphingolipids and sterols[48].

Sterols - among which cholesterol is the main mammalian membrane-active and the most studied - are the major means by which eukaryotic cells modulate and refine membrane properties (e. g. controlling permeability by reducing average fluidity and free volume)[48]: since photosynthetic bacteria - our main subject of interest - don’t possess them, the existence of rafts, though well scientifically attracting but not documented in prokaryotes, will not receive further attention.

1.2.3.2. Membrane proteins.

Membrane proteins are hydrophobic, insoluble in aqueous solutions. They may be simple proteins or glycoproteins and lipoproteins if a saccharidic or lipidic moiety, respectively, is covalently bound to the aminoacidic backbone.

Although these proteins represent the 20÷35 % of the proteins encoded in the genome[49], our knowledge about them is yet rather poor, even at structural level: at this moment (september 2005) high resolution structures have been obtained only for 96 membrane proteins[21, 50], while water-soluble protein structures were already more than 20,000 in 2004 [H. Palsdottir *et al.*, *Biochim. Biophys. Acta* 1666 (2004), 2] (fig. 1.18 shows how their numbers are growing).

This lack of knowledge severely limits, among other relevant topics, especially

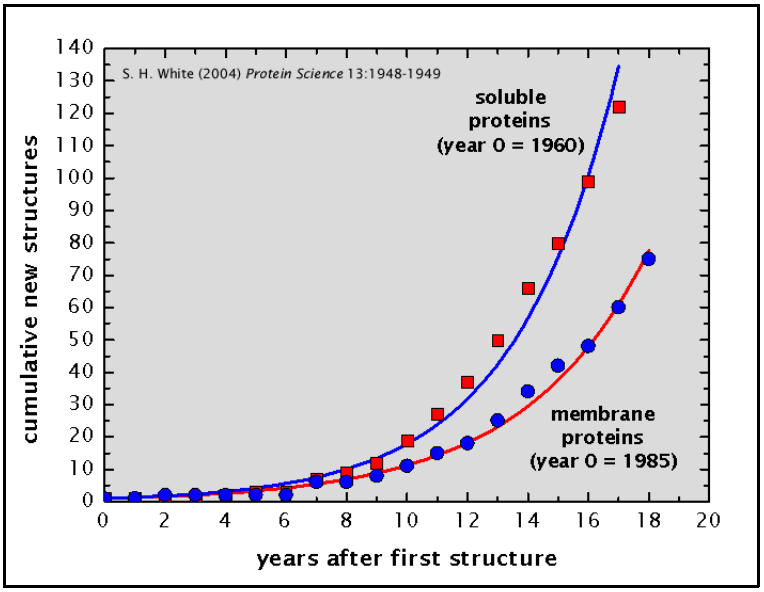

Figure 1.18.
Growth rate of the number of new protein structures, either water soluble or membrane proteins.

21. This number refers to so-called "unique" membrane proteins: structures of the same type but coming from different species (e.g. Reaction Centre from *Rb. sphaeroides* and *Rps. viridis)* are included in the database and then counted. On the contrary, structures of mutagenized versions of proteins already in the database or structures that differ only by substrate bound or by physiological state are excluded as unique and then not counted in this database.

our understanding about the influence of the lipid environment on protein functions.

Fig. 1.19 shows all the categories of membrane proteins. Everyone of them has a specific arrangement in the bilayer; some of them are examined as follows.

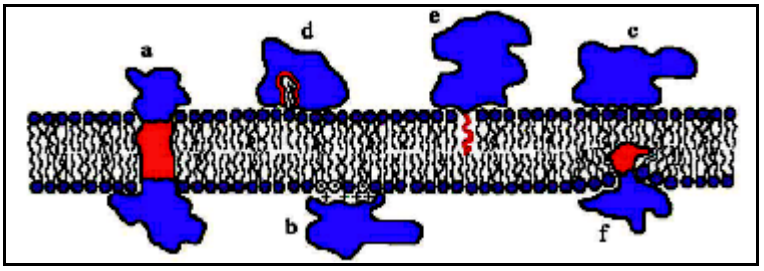

Figure 1.19.
Schematic illustration of integral membrane proteins that spans the bilayer (indicated by **a**, class 2 in the text), compared to five modes of binding of peripheral protein to a membrane surface: (**b**) electrostatic binding (class 1a in the text); (**c**) nonspecific binding by weak physical forces; (**d**) anchoring via a lipid extended conformation; (**e**) anchoring by an acylchain anchor attached to the protein (class 1b in the text); (**f**) amphiphilic protein partially penetrating the bilayer.

1) Peripheral membrane proteins.

1a) Some of them are anchored to the membrane by hydrogen bonds and by ionic interactions between residues with positively charged side chains and anionic lipid headgroups, since biological membranes tend to have a net negative charge (natural cationic lipids don't exist).

1b) Other proteins, water-soluble, are bound to the bilayer through an hydrophobic anchor generally formed by covalent bond post-synthetic attachment of fatty acids (myristoyl, palmitoyl) or prenoid units (farnesyl or geranyl-geranyl). Both types of membrane proteins (1a and 1b) are defined *peripheral* or *monotopic* because they don't penetrate the membrane surface and are thoroughly located in a unique aqueous extramembrane domain; they have contacts with water, ions and hydrophylic molecules, membrane polar headgroups, and possibly also with water-soluble proteins and integral membrane proteins (external moieties). Hence peripheral proteins can be released from the membrane simply by increasing the ionic strength or changing the pH of the solution.

Some examples of peripheral membrane proteins are: the cyclic GMP-phosphodiesterase (cGMP-PDE) involved in the transduction signal process following the visual excitation; the G stimulatory protein involved in the signal transduction

triggered by many hormones (among which adrenaline); the C lipoprotein subunit of the bacterial Reaction Centre from *Rps. viridis*, anchored to the membrane by a diacylglycerol moiety.

2) Integral (or transmembrane or polytopic) membrane proteins.

They are instead thoroughly embedded within the membrane: part of their surface is exposed to the aqueous phase on one or both sides of the membrane (depending on whether the protein spans or not the whole bilayer); the remainder of their surface is exposed to the membrane, either both the mainly hydrophylic interface regions made of phospholipid headgroups (usually 15÷20 Å thick[51]), or the hydrophobic core of the bilayer (often 30÷35 Å thick[51]). Hence these proteins can be released from membranes only if the bilayer is disrupted by detergents (par. 1.2.5 and 2.1).

Bacteriorhodopsin, most receptors, β-barrel proteins (multimeric such as porins, or mono- and dimeric), channel proteins, transporters, photosynthetic Reaction Centres, Light-Harvesting complexes, Photosystems, cytochrome bc_1 complexes, ATPase proteins, respiratory proteins[41, 50]: these and many others are all examples of polytopic transmembrane helical proteins with small, variable extramembrane regions according to the function they carry out. Rather than being a membrane-anchor, the orientation and alignement of the transmembrane helices are thought to mediate protein function.

Membrane proteins play a fundamental role in many prokaryotic and eukaryotic cell processes, such as selective molecular transport across membranes and energy transduction in photosynthesis and respiration. *In vivo* they inhabit a heterogeneous cell environment that consists of lipids, water, numerous small molecules and solutes, other proteins: of course their biophysical and biochemical properties (such as assembly, stability and many functions), so different from the properties of cytosolic water-soluble proteins, result to be critically determined by the lipid environment (par. 1.3).

In fact, rather than a homogeneous aqueous solvent, the native “solvent” of an integral membrane protein, for example, consists of the aqueous region outside the membrane, the ionic region of the membrane surface and of the lipid headgroups (these being the zones I and II of the membrane section scheme of fig. 1.14) and the oily region of the membrane interior (regions III and IV). These differing dielectric environments represent a severe constraint to the structure of membrane proteins: in

particular, length and magnitude of the *dielectric gradient* through the bilayer thickness have a important role in determining the protein arrangement.

The change in the dielectric constants (ε_r) between the ionic headgroups and the hydrophobic interior of a transmembrane protein is very large (for the Reaction Centre from *Rb. sphaeroides* ε_r varies between 20 and 4[52]) and occurs over a distance always smaller than 10 nm[13] (for the RC it is estimated to be about 4.5 nm[52]). It makes highly unfavourable to bury a charge (about 80 kJ*mol^{-1}) or to leave an unsatified hydrogen bond within the apolar moiety of the membrane (about 20 kJ*mol^{-1})[41].

Always referring to integral membrane proteins, it is the *membrane thickness* that determines the dielectric gradient intensity, influencing in turn the molecular contacts between the bilayer and the protein interior and exterior (that is the interface protein-membrane); in addition, the bilayer thickness may also stabilize certain conformational states of the protein.

Another important structural detail is the already mentioned necessary *matching* between the hydrophobic thickness of the bilayer and that of the transmembrane proteins embedded (par. 1.3.2.1). Mismatching can lead proteins to aggregate in an effort to minimize unfavourable interactions.

Also the right *packing* of the transmembrane protein backbone and side chains may stabilize and favour certain membrane protein structures. Since hydrophobic lipid chains find energetically favourable to align with each other to maximize Van der Waals interactions, they will prefer - as guests - protein species which do not greatly disrupt their architecture: proteins with a cylindrical shape meet this requirement, this minimizing the perturbations and the area exposed to the bilayer.

Many membrane proteins structurally related within families are also functionally related: as examples the family of the growth factor receptors, usually monomeric; the family of the seven transmembrane helices receptors (the most abundant class in mammalian cells) and the family of carrier proteins, often very large and multimeric.

Generally speaking, integral membrane proteins are much more difficult to study than water-soluble ones for the following reasons:

- their solubilization, purification and crystallization involves the substitution of the membrane phospholipids with suitable detergent molecules[53]; dealing with

water-insoluble proteins, the study of their reactivity in vitro needs the use of topologically disconnected hydrophobic domains (such as direct micelles and liposomes), making every experimental step more complicated;

- recombinant membrane proteins are difficult to obtain[54] because of their need to be targeted and inserted into membranes; even molecular engineering techniques required are non-standard;
- crystallization step, already critical for every protein, become in this case more laborious: pure protein and detergent phase behaviours are superimposed in protein-detergent complexes, with reciprocal influences[55];
- the presence of a large number of lipid (or detergent) molecules around the protein is an heavy constraint to molecular dynamics investigations (par. 1.3.2.4);
- thermodynamical stability studies about water-soluble proteins use to examine the energetics of the reversible folding/unfolding process induced by heat or denaturants; this approach is not applicable to membrane proteins which resist denaturation until the process becomes irreversible, because of the great stability of transmembrane domains[56];

Consequently, the number of high-resolution structures obtained so far from membrane proteins is quite limited, though recently, despite all the above mentioned drawbacks, the knowledge about this topic is fastly growing[57].

The best resolved structures up till now are those from photosynthetic bacterial Reaction Centers (RCs), for which many of the experimental problems above listed have been already solved; moreover they have been the first structures obtained for membrane proteins about 20 years ago (see par. 1.4.1 for further details and refs.). In many crystals detergent molecules were positioned to accommodate extended regions of electron density found on the protein surface: as the quality of X-ray diffraction data improved some of these molecules were better identified as bound lipids (par. 1.5).

Other details concerning membrane proteins and structural data useful to understand the molecular basis of the lipid-protein interaction will be discussed in dedicated paragraphs (1.3 and 1.5).

1.2.4. The membranes of *Rhodobacter sphaeroides* bacteria.

The microenvironment surrounding the integral membrane protein Reaction Centre (RC), subject of our studies, is represented by the membranes of *Rhodobacter (Rb.) sphaeroides* bacteria. Since it has been already mentioned in previous paragraphs the possible structural and functional roles of many lipids for the nearby protein activity and being the cardiolipin-RC the main topic of the present work, it is easy to understand why the knowledge of the lipid nature and fatty acid distribution in these photosynthetic membranes can have so large importance. In particular, the fatty acid chain composition is related to the membrane fluidity, which in turn is recognized to be one of the factors affecting protein functioning (par. 1.2.3).

In the cell membranes of the R-26 carotenoidless strain of the purple non-sulfur bacterium *Rb. sphaeroides* (the strain used in the whole experimental work described in this thesis, conventionally referred as wild-type since no mutations are present in the protein sequence, see par. 1.4) the major phospholipids have been found to be PC, PE, PG and CL - as in many other photosynthetic bacteria -, with the small contribution of two glycolipids (sulfoquinovosyl diacylglycerol and glucosylgalactosyl diacylglycerol)[58].

From another recent work performed on the same bacterial strain, grown photoheterotrophically (that is in the light) under anaerobic conditions[17], the intracytoplasmic membranes (ICM) resulted to have the following percentage composition in polar lipids: PC 26 %, PE 27 %, PG 20 % and CL 26 %; the unidentified components are less than 1÷2 % of the total[22].

For wild-type Y strain *Rb. sphaeroides* grown anaerobically in the light the phospholipid composition is qualitatively the same, but the relative amounts are significantly modified since the bacterial strain is different and the composition is known to be related to the medium and to other experimental conditions (that of course can be quite variable): PC 22 %, PE 38.7 %, PG 34.7 % and CL 4.6 %[34].

Cardiolipin (CL) is central in our interests: in fact it is a component of the cytoplasmic membrane in a wide variety of photosynthetic bacteria, including many species of the *Rhodospirillaceae, Chromatiaceae*, and *Ectothiorhodospiraceae*; but it

---

22. For the sake of comparison, the phospholipid content of the chromatophore membranes from *Rhodospirillum rubrum* bacteria have been found to be PG 22 %, PE 65 %, CL 13 % [M. Snozzi and R. Bachofen, *Biochim. Biophys. Acta* 546 (1979), 236].

is also worth noticing that, though important, however CL is not ubiquitous[59].

The relative amounts of phospholipids composing the *Rb. sphaeroides* membranes vary significantly depending on specific growth conditions (particularly the oxygen level); nevertheless the most common fatty acid chains are always 18 carbon atoms long with only one unsaturation (18:1); there are minor contributions from 18:0 and 16:0 (saturated), 16:1, and also trace amounts of shorter chains[60]. The relative percentage composition of the ICM and the saturated/unsaturated ratio of fatty acids among total and polar lipids, separately, are summarized in table 1.1[17, 61].

The lipid composition, as the lipid nature and fatty acid distribution, is already known to critically determine the morphology of the cell membranes (par. 1.2.3). An interesting and outstanding question is whether and how certain lipids may affect the energy conversion mechanisms in photosynthetic membranes and, specifically, the charge recombination process in bacterial Reaction Centres (RCs, par. 1.4 and 1.5.2). Within this PhD thesis, a possible way to find an answer in the case of RCs of *Rb. sphaeroides* reconstituted into vesicles of different composition will be presented.

Table 1.1. Distribution of the hydrocarbon chains of the total lipid and polar lipid components and the ratio of saturated/unsaturated lipids from *Rb. Spheroides R-26* Reaction Centres.

Fatty acid	Total lipids(%)	Polar lipids(%)	Fatty acid	Total lipids(%)	Polar lipids(%)
C 12:0	0.788	9.45	C 18:1 n-9	69.7	57.7
C 13:0	2.64	2.46	C 18:2 n-6	not available	1.41
C 14:0	0.72	305	C 18:3 n-3	not available	3.24
C 16:0	7.26	7.76	C 20:2	not available	0.78
C 16:1 n-9	1.9	2.26	Others	3.4	0.4
C 16:2	0.549	1.6	**Total satd.**	21	30.7
C 16:3	2.74	1.87	**Total unsatd.**	75	68.9
C 18:0	10.3	7.99	**Satd. / Unsatd.**	0.28	0.44

1.2.5. Membrane-mimetic systems: the protein environment reconstitution.

The complexity of most biological membranes makes the study of its individual components *in situ* difficult.

In order to mimic the native environment of many biologically interesting membrane proteins (par. 1.2.3), closed artificial phospholipid vesicles incorporating purified proteins (proteoliposomes) provide a better approximation of membranes than may do lipid-detergent-protein mixed micelles or lipid-protein reverse micelles[23] (par. 1.2.2). This is quite obvious being the membrane morphology much closer to a liposome bilayer - though with approximations and with not negligible curvature strains -rather than to another heterogeneous phase system (mixed micelles) or to an homogeneous hydrophobic domain (reverse micelles), whose existence in native membranes remains a topic of research and discussion[33]. Moreover the value of proteoliposomes as membrane model systems derives also from the fact that they can be prepared with the desired lipid mixtures, to obtain bilayer compositions in principle identical to native cell membranes.

The “liposome approach” allows to control experimental parameters otherwise inaccessible or highly variable in the native membranes and to elucidate structural and functional aspects of membrane associated enzymes: it has been applied with success to different classes of membrane proteins as receptors, transport and photosynthetic proteins[62, 63]. Very often the functions and properties of many membrane proteins has been found to be approximately the same in proteoliposomes and in native membranes, a clear indication of an optimal reconstitution: this is the case of the bacterial RC[] and rhodopsin[38, 41]. On the contrary, in other cases, as for channel proteins, some of the most important functional properties are correctly expressed only in native membranes[13].

Despite the extensive use and the manyfold applications of liposomes proposed since 1965 - when Bangham first described artificial vesicles made of phospholipids - the mechanism of their formation is surprsingly ill-defined. The reason consists in the interest shown by most of the researchers more for the development of reconstitution

23. These latter two aggregates correspond to the same lipid-detergent direct micelles and lipid reverse micelles dealt with in par. 1.2.2 with the only addition of a membrane protein located in the hydrophobic phase.

methods that “work for their proteins” rather than in the physico-chemical parameters involved in the proteoliposome preparation[63]. This is not our case, since, before to start working on RC proteoliposomes, we carried out a detailed characterization of the proteinless liposomes made of phosphatidylcholine (PC), in order to know some physico-chemical features of these systems (data not shown). It is well known, in fact, that many features of the lipid host-system can strongly affect the experimental behaviour of the guest-protein[41]: RC also shows several examples of such an interplay[33].

Nevertheless this is not at all the main subject of this thesis. Consequently the present paragraph will contain only: a short explanation of the process leading to liposomes (vesiculation); a list of the possible ways to insert membrane proteins into lipid bilayers (proteoliposomes); a more detailed description of the detergent-mediated reconstitution methods for the lipid environment surrounding membrane proteins.

1.2.5.1. Phospholipid lamellae and vesicles.

Even though the aggregation of phospholipid molecules dispersed in water is a thermodynamically favoured process driven by the hydrophobic effect (par. 1.2.1), the system needs however some amount of energy in order to give rise to liposomes since it is necessary to overcome an activation energy barrier: the vesiculation process is under kinetic rather than thermodinamic control[8].

When hydrated at the solid state, over their gel-sol phase transition temperature, phospholipids - especially referring to PC, named also lecithin - exist as overlapped and bidimensionally hydrated lamellae, well extended in relation both to the single molecule size and to the bilayer thickness.

In aqueous environment such an arrangement tend to swell because of the penetration of solvent molecules between adjacent bilayers (fig. 1.20); so the hydrophobic moiety of the bilayer composing the perimeter of each lamella is exposed to the aqueous solvent, causing a sharp increase in the internal energy of the system, which however remains thermodynamically stable until the hydrophylic lamellar surface (made of phospholipid headgroups) is much larger than the unfavoured perimeter area.

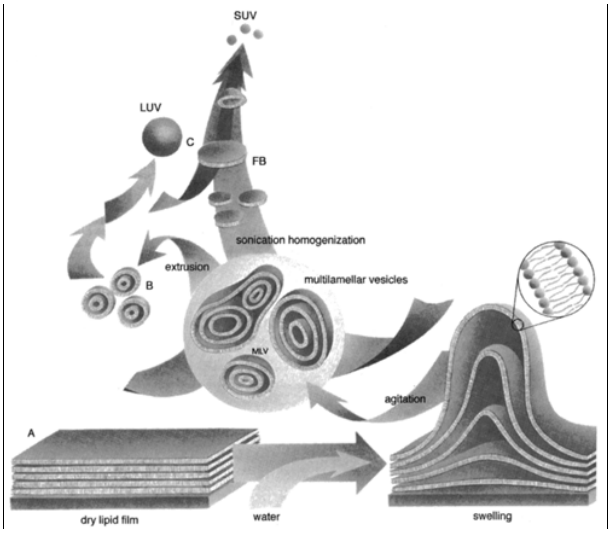

Figura 1.20.
Schematic representation of some of the processes most commonly employed for the proteoliposome preparation (in the scheme are omitted the detergent-mediated preparation methods, widely described in the text and in par. 2.2.2).

Mechanical means make the formation of individual vesicles (liposomes) more favoured than the existence of lamellae. If the extensive lamellae are mechanically broken by stirring then the hydrophobic perimeter energy contribution to destabilization cannot be any more neglected, leading the lamella fragments to fold and progressively rearrange giving rise to closed bilayer vesicles[64]. Of course the first product of this fragmentation are the larger lamella portions, whose subsequent reaggregation lead to multilamellar "onion-like" vesicles (MLVs, 100 nm ÷ several μm in size). Higher energy mechanical stirring would lead instead to large unilamellar vesicles (LUVs, 100 nm ÷ 1 μm in size) and small unilamellar ones (SUVs, less than 100 nm in size): the latter require even higher mechanical energies for their preparation[65].

1.2.5.2. Methods for proteoliposome preparation.

Four main technical methods can be outlined, all derived from the strategies used to prepare pure phospholipid vesicles[63].

A. Mechanical means. They are also called "physical methods" for membrane protein environment reconstitution, indicating the procedures adopted in order to fragment hydrated and extensive lamellae; they differ from one another essentially in the method by which the mechanical energy is transferred to the sample.

A-1) *Manual stirring*: this is the easiest method to fragment lamellae, but the lipid aggregates formed result to be extremely heterogeneous in relation both to their nature and size: a mixture of MLVs and SUVs is obtained, ranging in size from 50 nm to

several micrometers (μm). Moreover this method is scarcely reproducible, since it depends on several experimental not controllable factors.

A-2) *Ultrasound sonication* (that is using high energy ultrasounds): performed on MLVs or directly on the hydrated phospholipid film, it produces instead SUVs having diameters even smaller than 100 nm and moderate size polydispersity; unfortunately this technique is potentially destructive for many guest species of biological origin (proteins, DNA, etc.).

A-3) *French Press extrusion*: potential damage to membrane proteins incorporated into the bilayer is shown also by another way to prepare SUVs. It uses an instrument called "French Press", which forces an aqueous dispersion of lipids to pass through a microscopic hole. The passage creates an intense shear stress on adjacent liquid layers leading to the fragmentation of the lamellae, which are forced to rearrange in smaller size aggregates. The treatment can be repeated, but the final size polydispersity remains however quite high.

The extrusion of already prepared MLVs through polycarbonate (or similar materials) filters of the appropriate diameter is an effective method by which one can obtain, in less severe conditions, proteoliposomes of the desired size and with low polydispersity.

A-4) *Freezing/thawing - sonication:* for proteins sensitive to long sonications or to detergents (see below) it has been proposed a combined method of reconstitution freezing/thawing - sonication: the former, applied to lipid suspensions containing the solubilized protein, produces MLVs some micrometer in size (giant proteoliposomes); then a brief sonication restores smaller diameters (20÷200 nm) but however polydisperse. It has been used successfully for a glucose transporting protein[63].

B. Direct incorporation into preformed liposomes. Spontaneous incorporation of membrane proteins into preformed LUVs or SUVs can happen if catalyzed by low concentrations of detergents or phospholipids, preferentially into liposomes of small diameters (the smallest available are about 20 nm, being a curvature limit) in order to make more tolerable the bilayer curvature stress. Probably direct incorporation occurs as fusion of the membrane protein lipid envelope, named "lipid annulus" (par 1.3.1), with liposomes.

The main advantage of this strategy is that in all cases where it has been checked[56], the protein was found unidirectionally oriented in the proteoliposome membranes. Nevertheless the vesicle size distribution is wide and the protein results to be heterogeneously distributed among the vesicles.

The last two reconstitution methods (C and D) can be indicated as "chemical methods", since they utilize chemical properties as the immiscibility of organic solvents and aqueous phases (C) or the ability of suitable detergents to solubilize lipid and proteins in water (D), in order to prepare proteoliposomes.

C. Organic solvent-mediated reconstitutions. Organic solvents have been widely used to prepare liposomes (ethanol injection, ether infusion, reverse-phase evaporation methods), but the usefulness of such strategies for studies of membrane proteins is limited because it requires exposure to solvents often harmful for biological molecules.

C-1) *Protein extraction- evaporation- hydration:* one method to reassemble membrane proteins into large vesicles is to extract a protein-lipid complex into apolar solvents and after solvent removal to rehydrate the dryed films, forming giant liposomes (5 ÷ 300 μm) with highly inhomogeneous size distribution and high proportion of useless MLVs. This technique has been applied to some membrane proteins such as rhodopsin, cytochrome *c* oxydase, reaction centres and acetylcholine receptors[66].

C-2) *Reverse phase evaporation*: this is the most suitable method reported in organic solvent-mediated reconstitution of membrane proteins. Rhodopsin[67] and bacteriorhodopsin[68] have been efficiently incorporated into LUVs by this strategy.

Due to their packing parameter, suitable phospholipids dispersed in a water/oil mixture lead to the formation of water-in-oil microemulsions, characterized by a negative curvature of the interphase (also called reverse micelles, thus the name of the whole procedure). Once the organic solvent solubilizing the lipids is evaporated under high vacuum, the water droplets coalesce resulting in a viscous gel; such a gel, once diluted with water (or directly with solution of the membrane protein to insert into the bilayer) and mechanically disrupted, finally produces a suspension of LUVs and SUVs.

Some proteoliposomes prepared by this technique were found to possess important experimental properties such as homogeneous protein distribution and good

unidirectional orientation of protein in the membrane[68]. Unfortunately, both the presence of biologically incompatible organic solvents and the lack of general procedures to transfer relatively hydrophilic membrane proteins in active form into apolar solvents have precluded the general use of this method.

D. Detergent-mediated reconstitutions. Detergent are amphiphilic species with packing parameter smaller than one, having tendency to form in water direct micelles (par. 1.2.2). The detergent-mediated is the most successful and employed strategy to prepare proteoliposomes since most of the membrane proteins are isolated and purified just in the presence of detergents; moreover it is applicable even to prepare liposomes embedding easily denaturable biological species (DNA, proteins, etc.).

In the standard procedure - utilized also in our case, see par. 2.2.2 - membrane proteins are first cosolubilized with phospholipids in water by an appropriate detergent, in order to give rise to an isotropic aqueous solution of lipid-protein-detergent and lipid-detergent mixed micelles. Then the detergent is removed or diluted (see below) resulting in the spontaneous formation of bilayer vesicles with incorporated protein.

D-1) *Selective detergent removal*: several are the methods for detergent removal; the choice of the "right one" depends mainly on the critical micelle concentration (CMC)[24], the most important physico-chemical property of detergents.

D-1A) Detergents with high CMC are easily removed by *dialysis* since the removal acts on the detergent monomers (eqn. 7): examples are biliar salts such as cholate, octylglucoside, etc.; drawbacks are the slowness of the method (many hours) and the non-reproducible size-distribution profile.

D-1B) Detergent with low CMC are neither readily removed by *gel permeation chromatography* (GPC) nor by dialysis. Efficient removal of these detergents, which include Triton-X100 and $C_{12}E_8$, can be achieved only through *adsorption on hydrophobic resins*; this type of removal however is efficient for all kinds of detergents.

---

24. The cmc is the minimum detergent concentration (in distilled water and at room temperature) at which detergent monomers form direct micellar aggregates: below this value there are only monomer species. For the same detergent this parameter considerably changes with temperature, ionic strength, pH, etc..

D-1C) Detergents with any CMC can be easily removed by GPC passing the preformed mixed micelle solution through a suitable resin-packed column. Detergent-phospholipid-protein mixed micelles are excluded from the resin pores and elute in the void volume (*i.e.* out of the pores), while the detergent monomers penetrate the gel network and then are slowed down and selectively removed from the whole solution, acting on the equilibrium existing betwen the two form of detergent (eqn. 7).

Dialysis, GPC and any other detergent removal method acts in the same way on the partition equilibrium of the detergent between the dispersed phase (mixed micelles) and the bulk-continuous phase (aqueous phase containing detergent monomers):

$$detergent_{\,mixed\ micelles} \rightleftarrows detergent_{\,monomers} \qquad \textbf{(7)}$$

Progressively depriving the bulk phase of detergent molecules these strategies shift the equilibrium in the right direction; then, in order to restore equilibrium values, during the elution mixed micelles lose detergent and enrich in phospholipids, so finally they coalesce and give rise to proteoliposomes.

This is the fastest detergent removal method (less than 1 hour): it has been used also in the preparation of our phospholipid proteoliposomes mediated by sodium cholate (NaC), allowing to obtain approximately spherical particles about 50 ÷ 120 nm in diameter, with low size polydispersity.

D-1D, E, F) In order to remove the detergent other methods may be applied: enzymatic transformation of detergent molecules in species devoid of tensioactive properties (D); precipitation of the detergent (E); selective extraction of the detergent (F); the last two methods employ organic solvents.

D-2) *Dilution*: this is another procedure to form proteoliposomes from micellar solutions, alternative to detergent removal. It consists in diluting the reconstitution mixture, lowering then the detergent concentration below its CMC, so as proteoliposomes form spontaneously. The usefulness of the method is limited to detergent with high CMC, whose residual amount, not negligible and destabilizing for liposomes, has to be removed by previously described procedures. Hence the method is not suitable for preparative purposes.

1.2.5.3. The proteoliposome formation during detergent removal.

Because of their complexity, the molecular mechanisms for the formation of proteoliposomes upon detergent removal from detergent-lipid-protein micellar solutions are only partly known. Their understanding relies on a model proposed by Lasic for the generation of pure phospholipid vesicles[69], well consistent with many results reported in the literature.

According to the model, the vesiculation process can be divided into three steps:

(1) micellar equilibration in a mixed micellar domain;

(2) vesiculation in a micelle-vesicle coexistence domain;

(3) postvesiculation size transformations in a vesicle domain variable in detergent content.

Step 1. When detergent molecules are removed, a series of micelle-micelle interactions is initiated in order to minimize the unfavourable energy contribution resulting from the possible exposure of lipid and protein hydrophobic regions to the aqueous medium. According to recently confirmed observations this situation results in extended, worm-like mixed micelles[70] (described also as mixed bent cylindrical micelles[28]), especially favoured for bile salt detergents (e. g. sodium cholate, NaC), which are composed of two opposite faces with polar and apolar character[25, 29]; the edges of these structures are coated by detergent.

Step 2. When these particles have grown reaching a critical micellar size, a subsequent and further bending occurs -since they might be already slightly curved -: if the amplitude of the bending is sufficient to cause bilayer closure, vesicles start forming. Liposomes are kinetically stable aggregates, contrary to detergent-lipid and detergent pure micelles[28].

Step 3. At the end these initially formed vesicles still undergo size transformation processes as long as the level of residual detergent remains high.

Other models are based on the idea that reassociation of lipids upon selective removal of detergent from detergent-lipid-protein mixtures is the mirror image of the

---

25. According to recent theories [29], other detergents showing a more linear partition of the polar and apolar moieties, as alkyl glycosides, would give rise preferably to discoidal or ellipsoidal mixed micelles.

corresponding solubilization process[71], then it has been decided to study this latter, reaching the same general conclusions as those previously mentioned.

It has been demonstrated[72] that the detergent used in reconstitution procedures is not only important regarding the protein integrity and activity but also crucial for the mechanisms of protein incorporation into the vesicle bilayer, the key step of the whole reconstitution. As a consequence, the choice of the detergent and of the removal method greatly influences the products in terms, for example, of homogeneity of the protein distribution and orientation and in terms of the protein incorporation rate (besides obviously influencing proteoliposome size)[28].

In fact three classes of detergents exist with respect to the protein incorporation mechanisms[28]: those like octyl glucoside, those like Triton-X-100 and those like sodium-cholate (NaC).

The latters are different from the others: they allow protein incorporation only from totally solubilized material, that is coalesced protein-free and protein-containing micelles[63] (for informations about other detergents see refs. therein). The peculiar behaviour of NaC may derive from its steroidic structure, thus having a rigid backbone, very different from aliphatic chain detergents with a polar headgroup (fig. 1.21). This structure maybe is responsible also for the ability of NaC to solubilize lipid membranes by “chunks” and not by progressive rearrangement of the lipid organization.

Comparing cytochrome *c* oxidase incorporation carried out by different detergent-mediated procedures, Eytan[71] suggested that the rate of detergent removal is crucial in proteoliposome formation. The author suggested two alternative mechanisms:

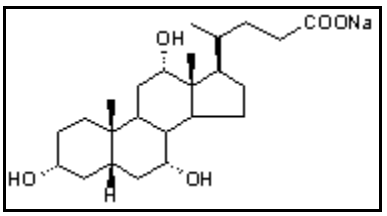

Figure 1.21.
Structure of the biliar salt sodium cholate.

(a) *if the detergent removal is slow*, vesicle formation might precede the protein insertion into the bilayer (little amounts of detergent are long time available for protein solubilization in lipid-protein-detergent micelles);

(b) *if the detergent removal is rapid*, soon the unshielded protein (lipid-detergent-protein mixed micelles deprived of detergent) partecipates to the vesiculation process corresponding to the micellar-lamellar phase transition (par. 1.2.2).

The rate of detergent removal was found to strongly influence both the homogeneity of protein distribution (from studies about rhodopsin) and the final orientation of proteins in the reconstituted vesicles[73]: rapid detergent removal caused coalescence of lipid-detergent and protein-lipid-detergent micelles leading to more homogeneous protein distributions and random orientations; gradual removal instead allowed micelles to assembly at different stages, in a situation similar to a protein incorporation into preformed pure liposomes, giving rise to more heterogeneous proteoliposome populations and almost unidirectional protein insertions.

Another example is provided by the detergent employed in our reconstitution of the bacterial Reaction Centre (RC) into vesicles (par. 2.2.2), sodium cholate, removed by GPC. following this procedure.

On the basis of general observations reported in the literature on several membrane proteins[28], about NaC removal it is possible to deduce with reasonable accuracy that:

- NaC is fastly removed (GPC cannot be considered a thermodynamical equilibrium-driven process);
- the protein incorporation is homogeneous (we did not check it, but results from bR protein were clear);
- the inserted protein results randomly oriented within the bilayer, as found also in the case of bacteriorhodopsin (bR) with the same detergent[28];
- phospholipid-NaC and phospholipid-NaC-RC protein micelles coalesce during NaC removal (as confirmed by the bR study) and RCs partecipate to vesiculation from the beginning.

The high plausibility of these deductions is an indirect confirmation of the general conclusions above reported; moreover, an agreement similar to that shown by bacteriorhodopsin reconstitution was found also with many other membrane proteins inserted in liposomes through the sodium cholate mediation[74].

Up to now no mention has been done about quantitative ratios between lipids, detergents and proteins to reconstitute: the detergent to lipid molar ratio is important only from the point of view of the lipid solubilization, while dealing with the lipid/protein

molar ratio can allow some more relevant consideration, since lipids and proteins are often the main inhabitant species to remain in the reconstituted system.

In native membranes the lipid/protein ratio is usually of the order of a few hundreds[28]. Phospholipid (PC and/or CL) proteoliposome samples described in this thesis instead show ratios variable in the range 2000 ÷ 10000, being about the same quantity mentioned in many literature examples (3000 ÷ 5000)[28]. This means that in the starting micellar solution lipids are in great excess over the protein, and that almost all of the detergent interacts with lipids and very little with the protein. Hence the amount of detergent bound to solubilized proteins is small enough to have a negligible effect on the micelle to vesicle transition: thus the transition is not significantly influenced by the detergent interacting with the protein.

In this conditions the use of two different detergents is possible, as it has been the case of our samples: one for the protein isolation and solubilization, in smaller amount in the starting solution for protein reconstitution (DDAO in our case) and a second one for lipid solubilization, in larger amount in that solution (sodium cholate NaC in our case).

Many experimental factors are responsible in producing proteoliposomes different in size, size and protein distribution, composition, etc. through each of the reconstitution methods illustrated before: the detergent and protein chemical nature, the lipid composition, the ionic strength, pH and protein solubilization conditions, the typical pure liposome size and polydispersity[63].

Just because of this it is important to be careful in the choice of the appropriate protein insertion method, since no one procedure serves equally well for the reconstitution of all membrane proteins.

In addition it is useful to point out that a wide characterization of the liposomes and proteoliposomes obtained with a specific method can greatly help in understanding the detailed mechanisms of vesiculation and protein reconstitution.

1.3. Lipid-protein interactions in biological membranes.

Lipid and proteins are the main constituents of membranes. In their native environment they can give rise to two types of intermolecular relationships:

- the *interactions between adjacent proteins*, which will be examined in par. 1.4 only for the case of *Rhodobacter (Rb.) sphaeroides* photosynthetic apparatus;

- the *lipid-protein interactions*, examined in detail and from a general point of view in this paragraph; specific reference to the *Rb. sphaeroides* Reaction Centre (RC) will be discussed instead in par. 1.5.

1.3.1. General background

There has long been an interest in how proteins interact with the lipid molecules surrounding them in biological membranes: of course these interactions are of great importance for the assembly, stability and function of membrane proteins. Nevertheless, from this point of view the membrane-mimicking systems (par. 1.2.5) and, even more, the complex environment of cell membranes at present are still poorly understood.

Lipid-protein interactions are at the heart of many different and scientifically attracting biological processes, among which lipolysis, blood coagulation and the mode of action of polypeptide toxins[75].

The history of this basic topic in biochemistry starts in 1972, when Singer and Nicholson had coherently placed mobile trans-membrane proteins in their fluid mosaic model of the membrane (par. 1.2.3); from 1977 then Israelachvili[76], in his refinements of that model, had anticipated that lipids and proteins interact via the structural and morphological properties of the lipid bilayer. Two decades ago, in 1984, E. Sackmann[77] suggested that the functions of integral membrane proteins may be strongly affected by the lipid-bilayer properties, anticipating the possibility that the local lipid environment

around such proteins may have quite different properties from those that characterize the average, global state of the membrane, e.g. in terms of varying molecular composition, curvature, or hydrophobic thickness.

After the first years of lively activity about lipid-protein interactions, during the subsequent decade - because of a seeming lack of progress - there has nearly been a drop out of this subject from mainstream science, rather concentrated on genome research successes. Nevertheless, fortunately, in recent years this topic has become fashionable again and rapidly expanding. Hence, after decades of focus on genes and proteins, lipids are “back on the scene”[46, 78].

In fact a conventional molecular biology approach to the most difficult problems in membrane and cell biology has to be necessarily supplemented by biophysical techniques able to reveal the macromolecular organization of the membrane. Complete knowledge of a genome does not permit predictions about the supramolecular organization and functioning of a complex biological system: for this purpose biophysics principles are called for.

How do membrane proteins perturbate and influence lipid bilayers, and how do lipids affect proteins? The answer implies that the system of lipids and proteins is considered as a complex macromolecular aggregate, and the clarity of the answer will ultimately rely on our understanding of the physical interactions within the combined system[46].

Several present circumstances induce to forecast new developments in the field of lipid–protein interactions[46]:

- a major result of the genome projects has been the finding that about 30 % of the genome codes for membrane proteins, shifting the attention toward them;
- the advent of more powerful experimental and theoretical approaches together with recent findings, as the discovery of both the presence and the central role of lipids in the crystallized membrane proteins, stimulated investigations on the nanometer and submicron scales (e. g. atomic force microscopy and fluorescence microscopy);
- molecular biology techniques are now able to routinely express many membrane proteins and produce them in such large amounts as to permit quantitative physical studies;

- the latest progresses focussing on membrane structure and functions in terms of so-called “rafts” (par. 1.2.3) have renewed the interest on crucial subjects in membrane biology such as the lateral molecular organization in the plane of the membrane and the importance of this organization for lipid-protein interactions.

Speaking in an evolutional sense, lipids and proteins must obviously have coevolved to allow membrane proteins to function in the environment provided by the lipid bilayer and to allow membrane proteins to be inserted into the bilayer without disrupting it.

Therefore the complexity of the lipid-protein molecular interactions makes the model of Singer and Nicholson more dynamic and subtle than it could look at a first glance: the bilayer acts not as a passive support or as a structureless embedding solvent for proteins, but it takes a structural and functional role in the ordered incorporation, transfer and assembly processes of the membrane with the protein component, also showing particular dynamics in lateral organization[78].

In order to emphasize that membranes have a characteristic molecular profile in both the perpendicular (fig. 1.23, shown in par.1.3.2.1., and fig. 1.14) and longitudinal direction (fig. 1.13) in relation to its surface, it should be noticed that often groups of lipids and proteins preferably form separate domains form the rest of the bilayer, leading then to high micro-heterogeneity in the planar dimension of the membrane[46] (fig. 1.13). This refers to the concept of lateral segregation of lipids and proteins in bilayers, already introduced as “raft hypothesis”: till now this has been satisfactorily demonstrated only for eukaryotic membranes (par. 1.2.3).

A tight interaction between membrane proteins and phospholipid bilayer is primarily required to maintain the diffusion barrier represented by the membrane and keep it electrochemically sealed: the lipid bilayer exerts a real “lateral pressure” on embedded membrane proteins, preserving also their structural integrity. This is especially important, as many membrane proteins undergo conformational changes that take place in or affect the transmembrane regions and may be essential for catalytic activity or necessary for regulatory purposes, as observed for bacteriorhodopsin, ATP synthase and cytochrome bc_1 complex of the respiratory chain[79]. The mobile lipid molecules are excellent candidates for maintaining this sealing function as they can

adhere to the surface of integral membrane proteins and flexibly adjust to a changing environment.

Three types of protein-interacting lipids can be distinguished on the basis of their binding sites[79].

1. So-called *annular shell lipids* are arranged around the intramembraneous protein surface, resembling the bilayer structure and mediating between membrane proteins and bulk bilayer phospholipids. They are presumably important for vertical positioning of proteins into the bilayer and for their correct folding[79]. Their identification in protein structures (never the whole annulus because of the detergent purification), together with further informations from the protein surface amino acid composition, allows to determine the position and thickness of the bilayer originally associated with the protein (fig. 1.22 shows the example of the RC embedded in the bilayer).

Such lipids cover the roughness of the protein surface (hollow grooves and protrusions) and provide the tight sealing function necessary for membranes. Their number can be deduced from ESR spin-labeling studies, as lipid motionally restricted by the membrane proteins (par. 1.3.2.2); in addition if the structure of the membrane protein is available, it can be approximately calculated from the surface area of the membrane-spanning region (for the RC see par. 1.5.1).

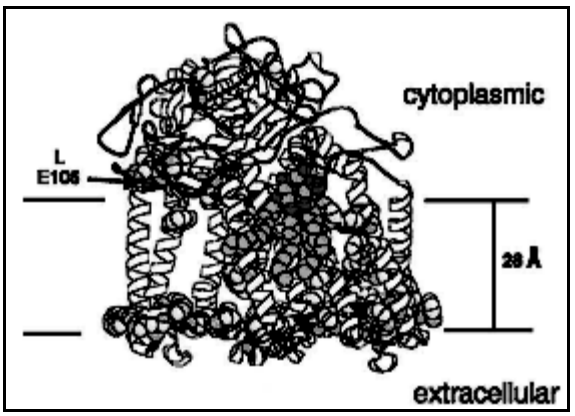

Figure 1.22.
The RC of *Rb. sphaeroides* showing the bound cardiolipin molecule. Trp residues are shown in space-fill representation. The glycerol backbone region of the cardiolipin molecule - also shown in space-fill representation- defines the cytoplasmic surface of the bilayer, together with the position of the residue Glu L106. The extracellular surface is well defined by the girdle of Trp residues, giving a hydrophobic thickness of about 28 Å for the bilayer.

2. *Non-annular lipids* (or other hydrophobic molecules[41]), immersed in cavities and clefts of the transmembrane protein surface, are instead frequently observed in structures obtained from multisubunit complexes and multimeric assemblies: they are typically located at the interface between subunits or oligomers, participating to their assembly and/or association. In this positions lipids are likely to be strongly motionally

restricted, so they can be more readily detected by crystallography and ESR measurements (par. 1.3.2.2).

3. *Few integral protein lipids* are located within membrane proteins (not on the surface) and in unusual positions, e.g. among α-helices of a monomer and/or non-perpendicularly to the bilayer surface, or moreover having head groups below the membrane plane[79]. Sometimes they are indicated also as *non-annular lipids* but such a classification seems to lead to confusion[41].

Evident examples of these three lipid classes are[79]:

(1) a cardiolipin (CL) and a phosphatidylethanolamine (PE) molecules for the yeast cytochrome bc_1 complex, oppositely oriented in the annular shell and then allowing determination of the bilayer position and tickness;

(2) phosphatidyglycerol located between adjacent monomers of the homotetrameric potassium channel KcsA;

(3) three PG and one glycolipid tightly bound close to the central core of the cyanobacterial Photosystem I, not on the surface exposed side.

Apart from their conventional role, lipids directly interacting with integral proteins show very different biological functions. All the three classes result to be well-distinguished from the lipid bulk phase. Their “order of interaction-strength” cannot be easily related to their class of origin. The first two classes of lipids are involved in intramembraneous surface interactions, so they both contribute to a tight and sealed protein integration into the membrane.

Moreover, since naked charges (without counter-ions) are highly unfavoured to be buried within low dielectric constant environments, as transmembrane regions, the presence there of possible annular and non-annular anionic lipids is related to the existence of positively charged amino acid residue on the same surface[79]. This opportunity can be checked through surface potential maps of proteins, as it will be showed for the RC in fig. 1.29 (par. 1.4). Such couplings are recently suggested to guide membrane insertion and topology of proteins[80].

The above mentioned binding sites at present stimulate researchers to elucidate

their possible functions, by diverse approaches (e. g. structure-based mutagenesis). Every binding site is generally characterized by multiple non-covalent interactions between polar or charged moieties - as amide bond and side chains of polar amino acids for the protein and the lipid head group - and between hydrophobic regions - as apolar protein residues and hydrophobic tails of lipids -. The former are electrostatic and hydrogen bond interactions, in membranes usually involving relatively limited and hydrophilic regions, while the latter are weak van der Waals forces taking place over larger areas.

It has been observed that generally a harsh delipidation of many membrane proteins results in loss of biological activity[10]. In fact, a high number of lipids - mostly phospholipids - has been found in protein structures through different investigation techniques (par. 1.3.2).

Lipids are identified in experimental difference electron-density maps by typical "hairpin"-shaped or elongated features, adhering to the transmembrane domains and most often perpendicular to the membrane plane. In most cases these structurally resolved lipids are endogenous: they have been extracted and co-purified with the membrane proteins. In particular, the more the same lipids are reproducibly detected in different structures of the same protein - regardless of different experimental purification and crystallization conditions -, the stronger and the more highly specific are their binding, and more details about them are available. Frequently, however, lipid head groups are not clearly resolved in the structures, even at high-resolution: this is usually interpreted as either low affinity or unspecific binding of the head group. In many cases such a difficulty has been overcome verifying the lipid presence by high-sensitive mass spectrometric analysis[79] (e. g. MALDI, par.1.5.1).

Through many studies it has been established that the correct assembly, stability and functioning of several membrane proteins from a wide range of origins may strongly depend on the presence of particular tightly bound phospholipids - often anionic - with whom they form distinct bidimensional complexes. Some involved proteins are: cytochrome *c*-oxidase, respiratory cytochrome bc_1[41], the Photosystems I and II[12], the ADP/ATP carrier[10] and NADH dehydrogenase[14] (eukaryotic from mitochondria), bacteriorhodopsin[41], the bacterial Reaction Centre and some photosynthetic antenna complexes from prokaryotic organisms[12], the lactose permease of *E. Coli*[81] (see par.

1.2 and table 1.2 for further examples).

The bound phospholipids are able to affect many cell functions by simply influencing the behaviour of the membrane proteins catalyzing these processes.

The following table will try to summarize some of the present knowledges about lipid molecules found in the diffraction models of many membrane proteins.

Table 1.2. Some examples of lipid molecules found in membrane protein structures.

Membrane protein	**Protein native environment**	**Number and identity of bound lipids per protein unit**	**Supposed lipid role** / **Lipid class**: annular (**A**), non-annular (**NA**), integral (**I**)	**References**
Bacterio-rhodopsin	Purple membrane of *Halobact. salinarum*	~30 glycerol ether lipids resolved / trimer	Structural cohesion between monomers (**NA**)	[41]
Bacterial Reaction Centre	*Rb. sphaeroides* membrane	3 (2 lipids +1 glycolipid) resolved: CL, PC, GGDG	CL stabilizes structure (**NA**); PC (**I**?) and GGDG (**A**) also may have functional roles	[12, 41, 51, 82]
Bacterial Reaction Centre	*Tch. tepidum* membrane	1 lipid resolved: PE	Enhanced thermal stability (?) (**NA**)	[82]
Formate dehydrogenase-N	*E. Coli* membranes for nitrate respiration	3 CL / trimer (resolved)	Structural cohesion between monomers (**NA**)	[41]
Light Harvesting Complex II	Chloroplast membrane of spinachs	6 lipids resolved / trimer: 3 glycolipid (DGDG) + 3 PG	2 DGDG at each surface contact between trimers (**NA**); 3 PG every 3 monomers (**NA**)	[12]
Photosystem I	Chloroplast membrane of Cyanobacterium *Synecoccus elongatus* (trimeric protein)	4 lipids resolved/ monomer: 3 PG + 1 glycolipid (MGDG)	PG, MGDG buried within the protein (**I**), with possible role in the electron transfer. Others: PG (**A**); PG (**NA**) (?)	[12, 41, [83]]
Photosystem II	Chloroplast membrane of Cyanobacterium *Syn. elongatus* and others	Several among which PG and SQDG (**not** resolved)	Protein activity and structural organization (?) : lipid presence estimated only qualitatively.	[12]
Cyt b_6f complex	*Chlamydomonas reinhardtii* algae membrane	2 glycolipids resolved: MGDG	Structural role	[12]
Cytochrome *c* oxidase	Bovine heart mitochondrial membrane *Paracoccus denitrificans* membrane	Many lipids among which 8 resolved as PE and PG; CL molecules found by assays, not resolved 2 lipids resolved: PC	Structural role (?) CL essential for protein activity, buried inside (**I**) Structural role (**NA**, **I**) (?)	[41] [41]
Cyt bc_1 complex	Yeast *Saccharomyces cerevisiae* mitochondrial membrane	5 lipids resolved / monomer: CL, PI, 2 PE, PC	One PE, PC, PI bound in clefts at the dimer interface (**NA**);CL, PE bound to the transmembrane surface (**A**); CL essential for protein activity	[41, 78,79]
ADP/ATP carrier	Mitochondrial membrane (most abundant protein), from rat or beef heart, liver...	Several lipids: - CL (some mols. tightly bound, other loosely), PC - possible PE (?)	Tight binding to Lys; other CLs loosely bound. CL essential for protein activity (**A**); PC (**A**)	[14, 41, [84]]

Key of the table 1.2 acronyms and symbols.

Phospholipids acronyms: CL, cardiolipin; PC, phosphatidylcholine; PE, phosphatidylethanolamine; PG, phosphatidylglycerol; PI, phosphatidylinositol. Bold acronyms indicate anionic phospholipids.

Glycolipids acronyms: GGDG, glucosylgalactosyl diacylglycerol; DGDG, digalactosyl diacylglycerol; MGDG, monogalactosyl diacylglycerol; SQDG, sulfoquinovosyl diacylglycerol.

(?) symbol indicates experimental hypothesis yet not thoroughly proved.

In addition to these examples, several other can be given about the importance of lipids, mainly anionic ones, in a large variety of biochemical membrane-involving processes[16, 85].

In table 1.2 the ADP/ATP carrier shows a very high specificity of binding for cardiolipin (CL): it can be explained as an interaction between the major components of the mitochondrial membranes. In fact ADP/ATP carrier is the most abundant protein in that enviroment where almost all the CL of the eukaryotic cells is located (20 % of the total lipids, par. 1.2.4). Likewise, changes in the CL content of the membrane will lead to changes in the activity of major proteins as cytochrome *c* oxidase, involved in the eukaryotic cell respiration process[86].

As it is easily predictable, the majority of the identified lipids is bound on the negatively-polarized side of the membrane[79] (many of these lipids are anionic), always being the cytoplasmic or inner one (par. 1.2.3). Of course, in order to respect the electrostatic neutrality, this membrane potential asymmetry should match with an asymmetrical charge distribution on the integral membrane protein surface: in fact protein regions facing the negative side of the membrane are generally enriched in arginine and lysine residues and then positively polarized, whereas transmembrane regions are largely devoid of them. Therefore on the cytoplasmic side of membrane proteins strong stabilization of bound lipids comes from ion pairs such as basic side chain residues-acidic lipid head groups (see the case of the RC in par. 1.5): the corresponding sites should be considered of high-affinity binding. On the contrary the periplasmic side frequently lacks such stabilizing interactions.

This is especially true for anionic lipids (CL, PG), but not only. The zwitterionic PC requires a lower number of positively charged amino acids in direct vicinity, probably as a consequence of the bulky, triple methylated and cationic choline headgroup[79].

Lipid-protein interactions depend on several factors regarding phospholipids: their

headgroup nature and fatty acyl chain length, their physical phase (affecting the fluidity), possible hydrophobic mismatch phenomena, and so on[45]. In particular, the hydrophobic mismatch is defined as the difference between the hydrophobic thickness values of the protein and bilayer[26]: it strongly influences the organization of both the integral membrane protein and lipids, but the precise consequences depend on the individual properties of the "mismatching partners"[46, 87].

Still about factors affecting lipid-protein interactions, it is common that a fluidity range (or "window") is required within the bilayer for the proteins to satisfy requisite rates and degrees of molecular motions around the active site for its correct biochemical activity. In fact large molecular rearrangements are not possible in a solid matrix. It is the lipid component of such bilayers that provide the fluidity window, and therefore any change in this component will reflect on protein activities[45].

Lipid-protein interactions in turn generally affect the behaviour of both the partner components.

Proteins with longer hydrophobic thicknesses result in the stabilization of the bilayer gel phase in which they are embedded, having the same effect of longer chain lipids, because they force to bilayer to match their hydrophobic thickness; shorter values favour instead the bilayer fluid phase, as shorter chain lipids. An example of the opposite effect of lipids on the protein component is given by the RC reconstituted in phospholipid liposomes that undergo a phase transition: passing through the corresponding transition temperature an evident discontinuity in the protein behaviour occurs[36].

Unfortunately, because of the experimental troubles encountered in crystallizing membrane proteins, few are the structures containing bound lipids (tab. 1.2). Yet more striking, some researchers last year (2004) wrote that "exact measurement for the binding affinity of individual structurally resolved lipids are not available"[79]. So, within the Results Section (chapt. 3) it will be explained how this thesis would try to shed some little light on this dark.

As more high resolution structures of membrane proteins appear, more examples of lipid-protein interactions are expected to be observed - as it effectively happened for

---

26. It does not imply: (a) that in the same membrane cannot well coexist protein with different hydrophobic thicknesses and (b) that membrane proteins with the same hydrophobic thickness cannot be encountered in bilayers differently thick[87].

the RC (par. 1.5.1) -.

Moreover, from the growing number of available data it is becoming possible to establish general short amino acidic sequences (2÷5 residues) responsible for the direct interaction of the phosphodiester groups of tightly bound lipids with membrane protein structures. By definition, these binding motifs are nonlinearly distributed along the protein sequence: even residues from different subunits may contribute.

Such sequences resulted to be made of “primary ligand” amino acids associated with additional so-called “stabilizing ligand” residues, at least one of each type. For tightly bound lipids (except PC) the primary ligands are often positively charged, while stabilizing ligands are only polar, not charged (e. g. aromatic as tyrosine or triptophan). A preliminary and specific motif for tightly interacting CLs has been proposed to be made of three residues: XXY, where X is a positively charged and Y a polar residue.

Similar classification attempts are maybe premature because of the too limited database and of the still hypothetic, not certain, assignment of many head groups. Indeed, despite progresses in this crucial biochemical area, the problem of discriminating electron density due to bound lipids from that arising from detergent molecules still remains very difficult[79].

1.3.2. Investigation techniques for the study of lipid-protein interactions.

The use of versatile experimental and theoretical-simulating techniques allows to improve the knowledge about the nature and extent of the interactions between membrane lipids and proteins.

In this paragraph the results obtained up to now by some of the major techniques will be briefly illustrated, without concentrating on the detecting techniques theirselves - that would be an excessive and not relevant pretension - but only on the important implications following from their application to membranes.

The study of protein-lipid interactions in membranes consists usually in the

identification and description at the molecular level of the structural relationships between the two components in order to explain, in the ideal case, the functional consequences of this mutual interaction.

On the basis of the data produced, the most important experimental techniques to approach this topic are the high-resolution diffraction crystallography[79], electron microscopy[88] (par. 1.3.2.1) and the electron spin resonance (ESR) spectroscopy[41, 89] (par. 1.3.2.2). These investigation methods are employed since many years for the study of lipid-protein interactions in membrane systems: consequenly they have provided a huge amount of fundamental informations about this subject, so they deserve a “special treatment” in the above indicated paragraphs.

Other relevant experimental techniques are some *fluorescence spectroscopies* - as those called fluorescence quenching and steady-state fluorescence anisotropy - and *solid-state NMR spectroscopy*. At present their application to this topic is quite common, but certainly less developed than X-ray crystallography and ESR[79]; this is especially true in the case of the NMR approach, which does not have the same long history in this area as other methods instead do[45].

Therefore here only few words will be spent on the contributions that some “secondary” techniques have given to the knowledge of the lipid-protein relations.

As a consequence of what above mentioned, the number of membrane systems studied by solid-state NMR is smaller than by other methods, not least because of the more complex and specialized instrumentation employed and the larger amount (mM) of sample necessary. Moreover the time scales of the more readily accessible NMR parameters for membrane systems (quadrupolar anisotropy averaging, chemical shift anisotropy, about $10^{-5} \div 10^{-2}$ s) is less appropriate to the faster molecular motions of lipid chains and protein residues when compared with spin-label ESR and fluorescence, something which can be an advantage or an obstacle to the interpretation of lipid-protein interactions[89].

Fluorescence quenching experiments contributed to distinguish the annular and non-annular sites[41].

The steady-state fluorescence anisotropy allowed instead to examine important physico-chemical aspects of lipid-protein interactions[17]. On the basis of the re-orientation of the absorption and emission dipoles of the fluorophore-probe (an external

molecule inserted in the membrane) during the lifetime of the excited state, defining an anisotropy parameter[27, [90]], this technique obtained informations on the structural rigidity of the probe environment[91]. Of course this may be represented also by portions of the lipid bilayer in contact with membrane proteins.

In recent years also computer simulations are rapidly becoming a standard tool to study the structure and dynamics of lipids and membrane proteins. With the increasing number of high-resolution structures of membrane proteins, which also enables homology modelling of more structures, a wide range of membrane proteins can now be simulated over time spans that capture essential biological processes[92].

In particular, molecular dynamics simulations of lipid-protein systems are now able to predict the effects of the insertion of a membrane protein into a lipid bilayer of given composition: the effects are generally restricted to the layer of lipid molecules immediately around the protein, consistent with the idea of lipid annulus, as it will be shown also in the next paragraphs by crystallography and ESR data. The total interaction energy between the phospholipid bilayer and the membrane protein can be obtained as a sum of many electrostatic and weak van der Waals contributions fluctuating widely with time around an average value: there would be no single deep energy minimum corresponding to a single favoured conformation adopted by the phospholipid molecules on the protein surface[41].

It will be interesting now to compare some of the concepts already emerged during this fast overview on few minor techniques with informations available from diffraction and ESR spectroscopy techniques.

1.3.2.1. X-ray and neutron diffraction, electron microscopy.

As structural studies performed so far on water-soluble proteins (e. g. haemoglobin, lysozyme, chimotripsin, etc.) provided informations about structural folding, binding with small molecules and possible reactions catalyzed by these proteins, in the same way it is more and more necessary to have high-resolution images of membrane proteins in order to better understand their biological functions.

---

27. An higher anisotropy value will correspond to a more ordered membrane structure.

In recent years structural techniques such as X-ray crystallography, neutron scattering (named also neutron crystallography) and electron microscopy have been used to examine the whole membrane protein environment, particolarly focussing on lipid-protein specific interactions.

These diffraction methods are able to resolve the structural details of crystals by a sensitivity (resolution) strongly dependent on the wavelength of the electromagnetic radiation used, comprised in the range 0.7÷1.5 Å for both X-rays and neutrons. They however differ for the object of their sensitivity: the electrons for X-rays and the nuclei for neutrons. Therefore X-rays are very sensitive only to heavy atoms, while the latters feel only slightly the effect of relative molecular masses, but they show little scattering and are very expensive to produce. A resolution limit of 1 Å, related to the wavelength of the diffraction beam, has been seldom attained for proteins[93] and never for membrane proteins[50].

Crystals for structure determination can be prepared by various approaches: conventional and most common means as detergent-solubilization methods, or methods based on two-dimensional (bicellar) and cubic lipidic phase (3-D) crystallization; these latter exploit the ability of particular lipids (as the synthetic monoolein, see par. 1.5.3) to form liquid crystalline networks in which a membrane protein can be embedded[31].

Till now only a relatively limited number of high-resolution X-ray structures of membrane proteins is available (96 at september 2005[50]). Moreover, concerning lipid-protein interactions within these structures few lipid molecules have been resolved, corresponding to those highly ordered and motionally restricted (par. 1.3.2.2), certainly not being the bulk lipid molecules typically surrounding proteins in membranes.

The fact that lipids are hindered in their motion raises the possibility to detect them by crystallography, provided that the detergent purification procedure doesn't alter the protein surface. Nevertheless it is necessary that the restriction in motion extends to a sufficient fraction of the lipid molecules, so as they can be well resolved in the diffraction pattern.

In the crystallization of membrane proteins by detergent solubilization (as the case of our Reaction Centre) lipid-protein molecular contacts are replaced by protein-detergent interactions: then obviously the crystals obtained contain less lipid molecules per protein molecule than the native membrane. Consequently lipid molecules

remaining in the crystal could well correspond to tightly bound molecules, but not necessarily reproducing the conformations adopted in the native conditions (the detergent purification may introduce some alterations).

Observations of membrane protein crystal structures are usually compatible with the general idea already reported (and obtained from the cooperation among different approaches) of an external *annular shell* of lipid molecules around proteins: they interact at non-specific binding sites. On the contrary, non-annular binding sites are found to be specific for a small number of "special" lipids (or other hydrophobic molecules), probably involved in the structural cohesion mechanisms adopted by proteins[41].

Because of their specificity in binding, such lipids could be considered almost as protein "cofactors". Phosphatidylinositol-4-phosphate, anionic, and cholesterol, non-ionic, are two examples of non-annular lipids strongly affecting the Ca^{2+}-ATPase activity[94].

Unfortunately, no high-resolution structure available shows a complete annular shell of lipid molecules around a membrane protein, so the nature and role of both annular and non-annular lipids needs yet to be clarified; rather, many diffraction models of proteins deposited in the Protein Data Bank (PDB) exhibit micelle-like girdles of disordered detergent molecules as the mixed micelles RC-DDAO.

In this cases detergent "clusters" cover the whole hydrophobic transmembrane region of the protein[12, 95], mimicking the lipid environment of the native complex. Their dimensions and number vary considerably between different X-ray structures, suggesting a possible variability not only with the data collection method but also with the protein crystallization procedure.

Also the structure of a typical bilayer in the liquid crystalline phase and at relatively low hydration level can be determined by a combination of X-ray and neutron diffraction data. The results of this operation are very useful to define an important parameter for lipid bilayers and embedded membrane proteins, the so-called (and already introduced in par. 1.2.3) hydrophobic thickness[79].

The bilayer can be represented by a number of lipidic fragments, whose presence is described by a distribution of probability. The peak position defines the most probable location of the fragment in the direction normal to the bilayer surface, while the width of the Gaussian curve provides an estimate of the range of thermal motion for it

(fig. 1.23). The narrowest region is that corresponding to the glycerol backbone of the lipid molecule, then the most rigid part of the structure; molecular mobility increase with increasing distance from the backbone, moving both inward and outward from the bilayer core.

The hydrocarbon core of a membrane is delimited by lines in fig. 1.23 and it has an average thickness of 32 Å at low hydration conditions (somewhat less when the bilayer is fully hydrated). It is made up of the phospholipid fatty acyl chains, beginning with the C-2 carbons; its boundaries correspond closely with the positions of the lipid ester carbonyl groups[41]. The concept of hydrocarbon core is essential in order to define the transmembrane part of the -helices belonging to a protein inserted in the bilayer (named “hydrophobic thickness” of the protein itself). The ends of these -helices are usually not noticeable even by high resolution X-ray data.

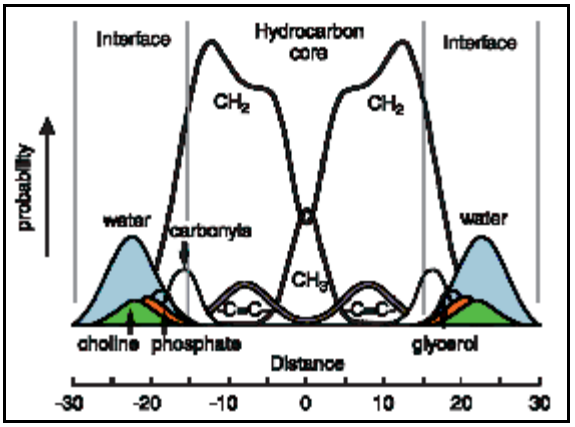

Figure 1.23.
The structure of a bilayer made of di(C18:1)PC, at 23 °C and low hydration. The figure shows projections onto the bilayer normal of the time-averaged transbilayer distributions of the principal structural groups. The hydrocarbon core of the bilayer contains the acyl chains beginning with the C2 carbons, and corresponds closely to the position of the carbonyl groups.

About lipid-protein interactions it should be stressed that transmembrane -helices not only have to match their hydrophobic thickness with the hydrocarbon core thickness of the bilayer, but also that if the helices are longer than the bilayer they have to find hydrogen bonding partners for the “unsatisfied” -NH and -C=O at their ends. The partners may be intramolecular polar side chains of aminoacids (as Proline and Asparagine of the protein itself) or the glycerole backbone and headgroup regions of the lipid bilayer.

So in most cases identifying the ends of transmembrane -helices in crystal structures of membrane proteins is the right way to know their hydrophobic thicknesses and the position of the native proteins in the hydrocarbon core of the bilayer. This is a very important information both on the structural and functional level, though, of course, it is not directly available from membrane proteins solubilized in detergent micelles.

Two relatively amphipathic aminoacids, Triptophan (Trp) and Tyrosine (Tyr), are often found at the ends of the hydrophobic regions of transmembrane -helices, close to the glycerol backbone region of the bilayer: so they act as "floats" at the polar-apolar interface in order to fix the helices within the membrane. It occurs by hydrogen bonds between polar regions and Van der Waals interactions between apolar moieties. The large Trp residue has a side chain volume smaller - but comparable - to that of the phosphatidylcholine headgroup[41].

Also helpful in identifying the ends of transmembrane -helices are any unpaired charged residues close to the hydrophobic regions of membrane protein crystal structures: e.g. Arginine (Arg) and Lysine (Lys) contain long, flexible side chains consisting of a hydrophobic segment linked to a terminal charged group. Since burying charged residues within the hydrocarbon core of the lipid bilayer has a very high energetic cost (about 37 $kJ*mol^{-1}$ for a Lys residue[96]), Arg and Lys are likely to be located within the hydrophobic core of a lipid bilayer "snorkelling" up to the membrane surface to expose the charge in the headgroup region of the bilayer. Here it can be paired by hydrogen bond to a lipid charge or polar group (e.g. to a phosphate or to an ester oxygen), involving often also water molecules.

Interactions of the type mentioned are important in locking a transmembrane -helix into the bilayer, leading to the disruption in packing and to a decrease in mobility of the lipid bilayer molecules. The effect of a membrane protein on the mobility of the lipid bilayer molecules will be illustrated in detail in the next paragraph dedicated to the ESR measures.

Not least, a detailed understanding of the lipid-protein interactions is particularly useful also in relation to the future purpose of forming two-dimensional (2-D) lipid-protein membrane crystals amenable for structural analysis. In fact for membrane proteins it is easier and faster to grow 2-D crystals than large well-ordered 3-D ones[88] (see par. 1.5.3 for an example involving the RC from *Rb. sphaeroides*).

Indeed, if suitable and large lipidic 2-D crystals containing hydrophobic proteins in the membrane plane are available, a structural analysis alternative to complex crystallography techniques is the electron microscopy (EM).

EM on protein samples has been performed the first time in 1975, with a resolution of 7 Å, on the purple membranes of *Halobacterium halobium* (a halophylic

bacterium) containing bacteriorhodopsin - which converts light energy in a transmembrane proton gradient necessary to the ATP synthesis - [97].

Of course the energy of the electrons used to obtain micrographs should be carefully controlled in order to avoid radiation damages. EM is carried out on concentrated samples and with different angles of incidence, the final procedure consisting in the collection of all the data by the Fourier method. Besides the example of bacteriorhodopsin, EM provided also images of the membrane protein receptor channel for acetylcholine - partecipating to nerve impulse transmissions - and of gap junctions, named also intercellular channels[13].

Since then X-ray crystallography progressively became the main high-resolution analysis technique for proteins (until now with about 2 Å resolution). In fact EM has been generally unable to provide comparable high-resolution data.

In recent years the resolution gap between these two techniques decreased: EM has finally proved a powerful alternative to X-ray crystallography to investigate the structure and organization of membrane proteins even at near-atomic resolution: it remains the condition that 2-D crystals should be available.

In case of low degree of crystallinity of 2-D crystals, whereas the classical crystallography fails (because it requires high quality 3-D crystals), the use of EM revealed to be particularly advantageous[88].

1.3.2.2. Electron spin resonance spectroscopy.

Among various spectroscopic techniques, spin-label ESR (named also electronic paramagnetic resonance, EPR) has proved to be one of the most useful in the study of the lipid-protein interactions within the membranes, because its dynamic sensitivity is perfectly matched to the typical time scale of the room temperature rotational motions of lipids in that environment. In fact the time scale sensitivity (represented by the correlation times) of the ESR spectroscopy is about 10^{-8} s, in frequency being $10^{7} \div 10^{8}$ Hz; also the exchange rate between annular and bulk lipids at the protein intramembranous surface (see below), at room temperature, has a value of $10^{7} \div 10^{8}$

Hz[28], (variable until 10^4 Hz depending on the lipid-protein interaction and experimental conditions[79]), but it becomes slower at lower temperatures.

Both these frequency ranges are very close to the intrinsic translational diffusion rate in fluid lipid membranes, at room temperature[41].

In spite of their exchange, the lipids located at the protein interface may however be distinguished spectrally from bulk fluid lipids, since the rotational motions of the lipids are different for the two populations[41].

The two-component nature of the ESR spectra for membrane lipids in the presence of embedded proteins can be explained in the following way[89].

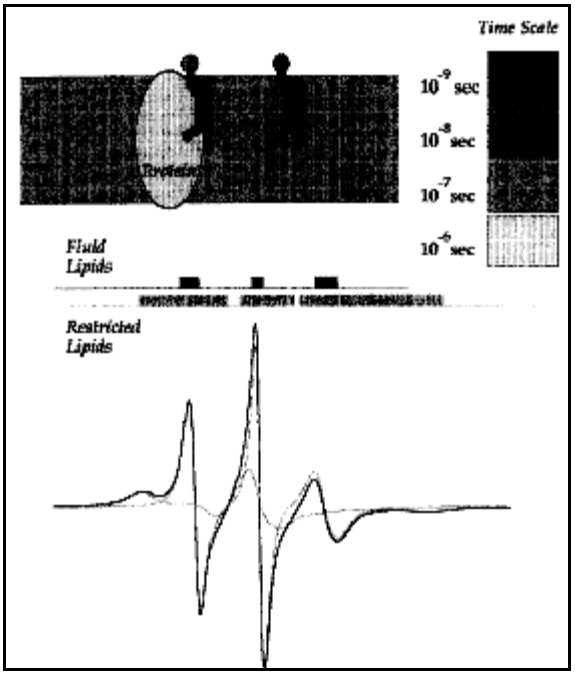

Figure 1.24 .
Upper: schematic indication of the rotational mobility of the lipid and protein components in membranes. The grey scale represents the rotational correlation times of the different components. Lower: ESR spectrum of a lipid spin-labelled on the C-14-atom of the chain in a lipid-protein membrane (full line). The single spectral components arising from the protein-interacting and fluid bilayer lipids are shown by dashed and thin lines. These two components are identified by the corresponding spectral ranges, coded by the overhanging grey scale.

Simple ESR spectra for fluid membranes lacking of proteins and composed of spin-labelled lipids - e. g. nitroxide on a chain methyl end- show relatively narrow peaks (the sharp peaks with thin and dashed lines in fig. 1.24). The reason is that fast rotational motions about C-C bonds of the acyl chains give rise to large-amplitude angular fluctuations (rotations) averaging the orientational anisotropies and resulting in a unique lipid class (*time averaging*).

The ESR spectrum shows changes following the dynamic state of the spin-labelled biomolecule. Indeed protein-containing bilayers exhibit instead broader peaks and side-wings in their spectra. These new elements represent a lipid subpopulation hindered in the rotational chain motion: it arises from interactions of

28. Many lipid and protein molecular motions and lipid exchange phenomena are instead too fast in relation to typical NMR frequencies ($10^2 \div 10^5$ Hz)[45]. Then NMR spectroscopy would not allow to resolve properly the two different lipid populations from one another.

lipids with the intramembranous surface of the protein (fig. 1.24).

Increased relative intensities of the side-wing peaks in relation to the others therefore implies a larger role and selectivity for the lipid-protein interaction.

So by this technique spin-labelled lipids incorporated into membranes may provide information about the rates and amplitudes of motion of the fatty acyl chains (the labelled portions) and about their resulting molecular order.

ESR spectra of native membranes (protein-containing) or reconstituted lipid-protein systems always show the presence of a population of highly immobilized spin labels, not present in protein-free membranes, besides the usual signal of bulk lipids.

This population is the made of so-called boundary or annular lipids, not as well oriented as bulk ones[41]: the surface roughness of the protein cause the phospholipid chains to become essentially fixed in disordered conformations and gives rise to a broad distribution of orientations, not amenable to average in a unique lipid class. Without tilting of the lipid fatty acyl chains in order to match the rigid protein surface the permeability barrier effectiveness of the membrane would be compromised - situation that should be maximally avoided -.

Therefore ESR spectra of lipid-protein systems allows to distinguish between annular and bulk phospholipids, these latter not interacting with membrane proteins.The relative proportions of the two classes display a systematic dependence on the lipid/protein ratio and on factors expected to affect the selectivity of the lipid-protein interaction: internal factors, as the molecular features of the interacting species, or external factors as local microviscosity changes, temperature, steric hindrance, other interactions, etc.[89]. More difficult instead is to distinguish by ESR other classes of molecules (not only lipids but even hydrophobic molecules) different from bulk lipids and interacting with membrane proteins: this could be the case of non-annular or integral lipids, as defined in par. 1.3.1.

ESR spectroscopy is able also to estimate the number of lipid molecules bound to the surface of a membrane protein (that is “motionally restricted lipids”): this number, according to studies[89], fits reasonably well to the expected circumference of the transmembrane region of the protein, giving a strong evidence for the presence of a distinct lipid annular shell around the protein. Bound lipid stoichiometry and selectivity of binding - measured in terms of relative association constants of individual lipids - are

directly related to the nature of the intramembranous secondary domains and to the degree of oligomerization of the integral protein. It gives the chance to study the structure and the state of assembly of membrane proteins by ESR[89].

The selectivity of the interaction with anionic phospholipids (e.g. cardiolipin) is determined, at least in part, by the presence of basic amino acid side chains in the vicinity of the lipid headgroups - as it was easily predictable -, while the thermodynamic specificity of the binding controls the composition of the lipid population associated with the protein.

The binding stoichiometry is related first to the size and structure of the transmembrane domains of proteins[79]. In addition the stoichiometry of first-shell lipids refers to different equations depending on the protein subunit assembly: the protein can be mono- or multimeric, it can be made of α-helix assemblies more or less numerous or compact, it can be composed by β-sheets, etc.[89].

Since ESR lineshapes may be modified by the finite rate of exchange between bulk and protein-interacting annular lipids, ESR spectra allow also to measure the length of time that a lipid molecule remains in the annular shell, by obtaining the on and off rate constants of the lipid exchange phenomena between the two phases. The former is diffusion controlled, while the latter reflects any selectivity in binding.

In fact the lipid off rate constant is lower for annular lipids ($1 \div 2 * 10^7$ s^{-1} at 30˚C) than for bulk ones (about $8 * 10^7$ s^{-1} at 30˚C), demonstrating that lipid-protein interactions are stronger than lipid-lipid interactions. Nevertheless the small differences suggest that lipid and protein do not interact so strongly and that the effects of a protein insertion into a membrane are generally restricted to the shell of lipids immediately around the protein (annulus)[41], as already anticipated by molecular dynamics considerations.

Being a very powerful technique, ESR spectroscopy can provide informations also about the configuration and rotational dynamics of the protein-associated lipid chains; these topics however are well out of our purposes.

Finally, it is important to point out that lipid-protein interactions, as well as their association constants, depend both on structural or internal factors (as the lipid polar headgroup and backbone nature, the acyl chain length, the lipid phase, the protein structure and possible “hydrophobic mismatches”) and on environmental or external factors (as ionic strength, pH, etc.)[79].

1.4. Organization and functions of the photosynthetic apparatus of *Rhodobacter sphaeroides.*

In spite of the wealth of informations on individual membrane proteins making up the photosynthetic apparatus of many purple bacteria, the organization of the different complexes within the membranes has not been so deeply examined till now.

Most of the data collected about this topic have been obtained by both X-ray crystallography and electron microscopy, the latter even performed on *in vivo* membranes[88].

• *The photosynthetic apparatus of Rb. sphaeroides*.

In its native conditions the Reaction Centre (RC) from *Rhodobacter (Rb.) sphaeroides* inhabits a complex membrane environment where the photosynthesis takes place and where it carries out its functions, undergoing many interactions with several molecules on either side of the membrane and inside the bilayer itself. This environment consists of a mixture of lipids and other integral membrane proteins. The interactions of the RC with membrane lipids will be extensively examined in par. 1.5.

From the point of view of the protein-protein interactions, during the last twenty years a combination of X-ray crystallography, electron microscopy, spectroscopy, mutagenesis and modeling techniques has revealed the detailed structure and overall architecture of the photosynthetic apparatus of purple bacteria (par. 1.1.2). In order to obtain transfomation of light into metabolic chemical energy, the RC is organized as an amazing hierarchical aggregate of proteins and pigments utilizing elegant and efficient mechanisms for primary light absorption and transfer of electronic excitation.

The majority of the apparatus of the purple bacterium *Rb. sphaeroides*, available at atomic resolution[98] as well as that of *Rhodopseudomonas (Rps.) viridis*[99], is located in invaginations of the plasma membrane formed during the bacterial photosynthetic growth in half-anaerobic conditions. It is made of three multimeric membrane protein complexes: the light harvesting complexes (LHCs), the Reaction Centre (RC) - which provides a docking site for the water-soluble cytochrome (cyt) c_2 - and the cytochrome (cyt) bc_1 (fig. 1.25)[5].

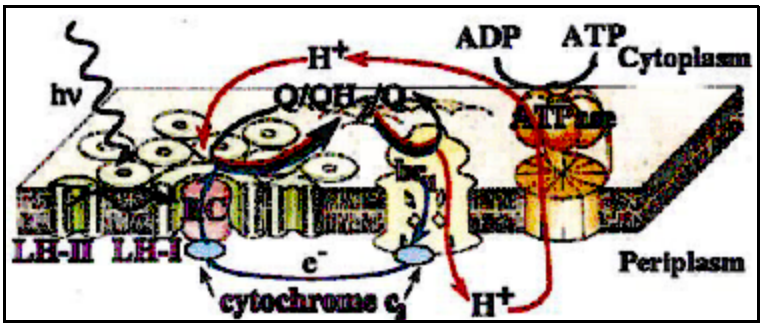

Figure 1.25.
Schematic representation of the photosynthetic apparatus in the intracytoplasmic membrane of purple bacteria. The RC (red) is surrounded by the light-harvesting complex I (LH-I, green) to form the LH-I–RC complex, which is surrounded by multiple light-harvesting complexes LH-II (green), forming altogether the PSU.

Particularly the bacterial RC, in addition to being used as a model system for examining the primary mechanisms of light energy transduction, has also played an important role in the study of general principles of membrane protein design, protein dynamics and biological electron transfer. In fact the light-induced proton transport across cytoplasmic membranes of photosynthetic bacteria results just from proton-coupled electron transfer reactions starting within the RC.

As already shortly mentioned in par. 1.1.2.3, light absorbed by antenna complexes is conveyed to the RC. Here it initiates the transfer of a single electron from a donor, a special pair of bacteriochlorophyll molecules (named P), through a series of acceptors up to a primary electron acceptor (a ubiquinone molecule - Q_{10} - located in a relatively apolar pocket within the protein, named Q_A site), and then to a secondary ubiquinone Q_{10} acceptor (located in a relatively polar domain of the RC, named Q_B site).

This topic will be illustrated in detail in par. 1.4.2.

Only when the photo-oxidized donor P^+ (called also D^+) has been reduced by the cyt c_2, a second photon captured by the RC triggers a second electron transfer (par. 1.4.3.3) leading to the complete reduction of the Q_B ubiquinone to ubiquinol (Q_BH_2), once two protons have been taken up from the cytoplasm (*quinone photoreductase activity*). The light-driven Q_B reduction can therefore be summarized by this equation:

$$Q_B + 2e^- + 2\,H^+ \Rightarrow Q_BH_2 \qquad \textbf{(8)}$$

The ubiquinol exchanges then with a pool of quinone Q_{10} molecules present in the hydrophobic core of the bacterial membrane. The cyt bc_1 will then perform the

oxidation of quinol back to quinone, releasing two protons in the periplasmic space, while the two electrons are used to reduce the cyt c_2, therefore closing a cycle (*ferrocytochrome c_2 photooxidase activity*). A whole photochemical cycle is then completed in a time estimated as 1 ms for every transferred electron[5].

For every two absorbed photons a net translocation of two protons is accomplished: it gives rise to a transmembrane proton gradient of four protons utilized for the ATP synthesis and the NAD^+ reduction, respectively by means of the ATP synthase complex and the NAD^+-reductase.

The system RC-cyt bc_1- cyt c_2 can thus be assimilated to a light-activated proton pump.

• *The photosynthetic unit of Rb. sphaeroides*.

In most purple bacteria, as *Rb. sphaeroides,* the photosynthetic membranes contain only two types of light antenna complexes (LHCs): LH-I and LH-II. LH-I surrounds directly the RCs, whereas LH-II is not in direct contact with the RC but transfers energy to the RC through LH-I.

A 1:1 stoichiometry exists between the RC and the LH-I: together they compose the so-called RC/LH-I complex, where the RC is located at the centre of the ring made by the LH-I subunits (fig. 1.26). The number of LH-IIs instead varies according to growth conditions such as light intensity, temperature, oxygen partial pressure, etc.: in *Rb. sphaeroides* they are usually about ten for each RC.

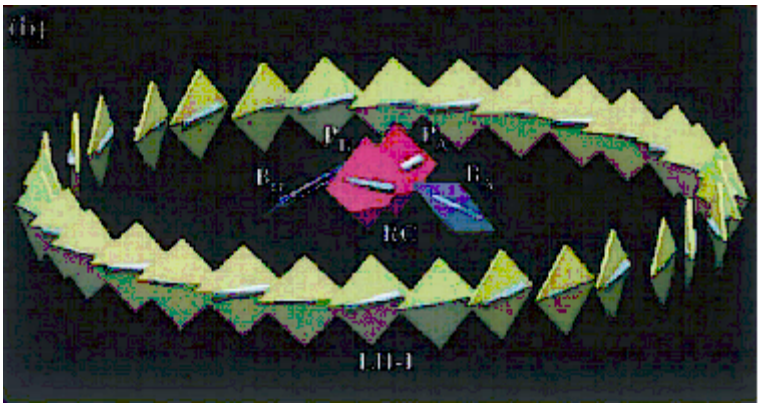

Figure 1.26.
Structure of the LH-I–RC complex.Arrangement of BChls in the LH-I–RC complex. The BChls are represented as squares with B875 BChls of LH-I in green, and the special pair (P_A and P_B) and the accessory BChls (B_A and B_B) of the RC in red and blue, respectively; cyan bars represent Qy transition moments of BChls.

Within the photosynthetic apparatus of purple bacteria an ensemble of an RC with associated one LH-I and many LH-II, containing up to 250 bacteriochlorophyll molecules, constitutes a photosynthetic unit (PSU, par. 1.1.2): the array of LHCs captures light and

transfers the excitation energy to the RC.

A pronounced energetic hierarchy exists in the light-harvesting systems of the PSUs. The carotenoids absorb light at 500 nm, then very rapidly and with nearly 100 % efficiency[29] they transfer the excitation energy to the bacteriochlorophylls of the LH-II complex, with absorption peaks at 800 and 850 nm (named B800 and B850); the last acceptors of the energy, the LH-I bacteriochlorophylls, instead absorb radiation of lower energy, at 875 nm (named B875). The variation in the absorption maximum shown by the same chromophore is explained by the different environment shared by different bacteriochlorophyll molecules.

The electron transfer may be intracomplex and intercomplex, respectively defined as processes within each pigment-protein complex and between them; intracomplex transfers are usually faster than intercomplex (even shorter than 1 ps).

Therefore the flow of the electronic excitation follows the direction of an energy cascade (i.e. decreasing energy)[5]:

carotenoids (500 nm) $\xrightarrow{\text{0.2 ps}}$ **B800 (LH-II)** $\xrightarrow{\text{0.7 ps}}$ **B850(LH-II)** $\xrightarrow{\text{3-5 ps}}$ **LH-I** $\xrightarrow{\text{35 ps}}$ **RC**.

The whole process occurs in about 40 ps and with very high efficiency (95 %). Interestingly, it has been established that Mg-Mg distances must be of the order of 20 Å or shorter in order to have an energy transfer between bacteriochlorophylls on a picosecond time scale[5].

From structural data[5], LH-I complexes of *Rb. sphaeroides* has been modelled as a circular hexadecamer of αβ-heterodimers, having a mean diameter of ~ 90 Å[88]. Each of these αβ-heterodimers contains a pair of short peptides (called α- and β-apoproteins) non-covalently binding one or two spheroidene (a specific type of carotenoid) and two bacteriochlorophyll-*a* (Bchl-*a*) molecules. Two concentric cylinders of α-helices, with the α-apoproteins inside and the β apoproteins outside, form a scaffold for BChls and carotenoids.

The bacteriochlorophylls are organized in a ring of 32 molecules, showed in fig. 1.26 together with the RC special pair (P_A and P_B) and the so-called RC accessory

29. Usually the efficiency of a light excitation transfer is measured by the *quantum yield*, i.e. the number of photons actually transferred per number of photons absorbed.

BChls (B_A and B_B, par. 1.4.1).

Further investigations on this topic suggested that LHCs only partially surround the RC, which would ensure an efficient shuttling of quinones between the RC and the cyt bc_1 complex[100]. In addition, it has been shown recently that the LH-I complexes take the form of two C-shaped structures of more than 100 Å in external diameter, facing each other on the open side and enclosing two Rcs. The shape organization itself would favour an efficient exchange of quinone/quinol between the RC and the cyt *bc1*[101].

In addition, the RC/LH-I complex contains one or two copies of a membrane polypeptide called PufX. It has been suggested that PufX may substitute one or more αβ-heterodimers of LH-I to open up the circular ring showed in fig. 1.26 and to facilitate thereby the flow of quinones (Q_B / Q_BH_2) between the RC, inside the ring, and the cyt bc_1, outside the ring[5]. The fact that in the absence of PufX no photosynthetic growth is observed would confirm this hypothesis[88].

Fig. 1.27 presents a model of the PSU for *Rb. sphaeroides*: for the sake of simplicity only three LH-IIs are shown, although the PSU can contain up to about 10 LH-IIs around each LH-I; electron microscopy[5] and X-ray crystallography[102] observations prove that LH-II from *Rb. sphaeroides* is made of nine αβ-heterodimers; moreover its assembly depends on defined phospholipid and glycolipid species, involved in structural lipid-protein interactions.

The multimeric architecture of LH-I and LH-II complexes is necessary to provide a large enough scaffold for the high number of chromophores or pigments (BChls and carotenoids) employed in light harvesting.

Two essential features of the pigment organization in the PSU are[5]:

- the ring-like aggregates of coupled bacteriochlorophylls within LH-I and LH-II; the chromophores are closer and more tightly coupled at the level of the intracomplex arrangement, more

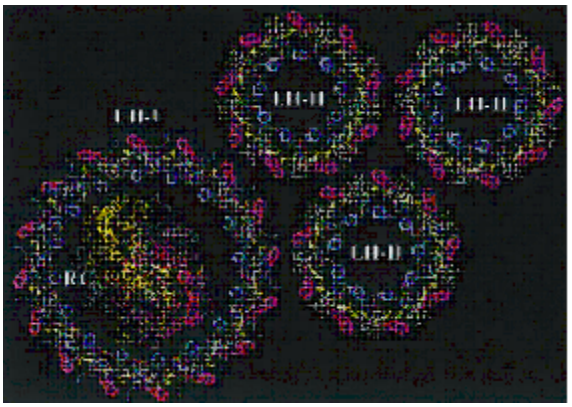

Figure 1.27.
Arrangement of pigment–protein complexes in the modeled bacterial PSU of Rb. sphaeroides. The a-helices are represented as Ca-tracing tubes with a-apoproteins of both LH-I and LH-II in blue and b-apoproteins in magenta, and the L, M, and H subunits of RC in yellow, red, and gray, respectively. All the BChls are in green, and carotenoids are in yellow.

loosely coupled at the level of the intercomplex organization;

- the coplanar arrangement of these bacteriochlorophylls and of those making up the RC dimer; the bacteriochlorophylls of LH-I and LH-II, even if non-covalently bound to the α- and β- apoproteins of the αβ-heterodimers, are held by the protein backbone in a rigid orientation; the planar organization of the bacteriochlorophylls is optimal for the transfer of electronic excitation to the RC.

About the electron transfer it is interesting to note that the *transition dipole moment* of the Q_y excitations (par. 1.4.3) referred to the BChls of LH-I and LH-II are all oriented in the two-dimensional plane that encompasses the ring-like aggregates of the light harvesting complexes and the RC special pair (fig. 1.26 and 1.28).

Recently it has been suggested a role for the accessory bacteriochlorophylls of the RC as mediators in the excitation transfer from LH-I to the RC dimer: in their absence the time of transfer becomes an order of magnitude longer. These BChls represent for excitation transfer a path that bridges and reduces the large distance of ~42 Å (or even more) between the LH-I BChls and those of the RC special pair[5].

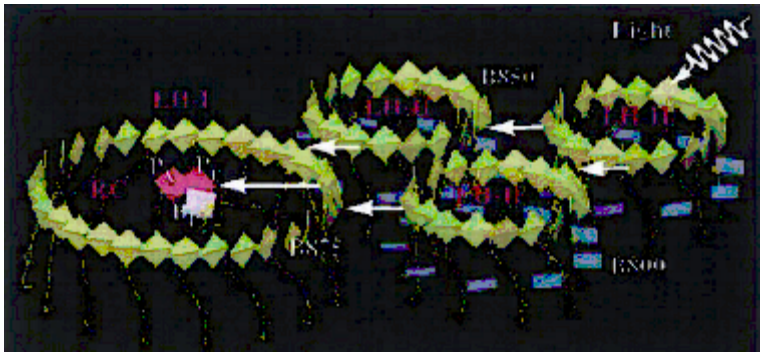

Figure 1.28.
Excitation transfer in the bacterial photosynthetic unit. LH-II contains two types of BChls, commonly referred to as B800 (dark blue) and B850 (green), which absorb at 800 nm and 850 nm, respectively. BChls in LH-I absorb at 875 nm and are labeled B875 (green).

• <u>*Other protein-protein interactions in the apparatus of Rb. sphaeroides*</u>.

Another protein interacting with the RC within the photosynthetic apparatus of *Rb. sphaeroides* is cytochrome c_2 (cyt c_2): this water-soluble protein acts as an electron donor to the photo-oxidized RC, their transient interaction taking place on the periplasmic side of the membrane.

Cyt c_2 and RC from *Rb. sphaeroides* have been successfully co-crystallized[103]:

in the diffraction structure the cytochrome makes contacts with both the L and M subunits (par. 1.4.1) at the periplasmic surface of the RC, although these contacts have not been described yet in fine detail.

The fact that in the co-crystals the rate of electron transfer from cyt c_2 to the RC was found to be extremely similar to solution[103] suggests that the relative modelled orientation of the two proteins in the crystal could be the same as that adopted *in vivo*, although not necessarily. Questions about the analogies between the *in vitro* and *in vivo* organization of the protein complexes are still open also in the case of the above mentioned RC/LH-I complex[5, 88].

Moreover, the fact that many individual structures of purified bacterial photosynthetic proteins have been obtained from different organisms makes more difficult to produce a coherent model of a whole photosystem. In spite of this, the wealth of data available about *Rb. sphaeroides* however seems to confirm this species as the best model system for an integrated study of prokaryotic photosynthesis[88].

Among the three complexes making up the photosynthetic apparatus of *Rb. sphaeroides* only the RC will be examined in detail in next paragraphs since the main subject of this thesis is the study of a specific lipid-protein interaction within this protein.

1.4.1. The structure of the Reaction Centre.

The RC of the purple bacteria is a protein-pigments complex which can be isolated from the photosynthetic membranes without any loss in activity only using suitable detergents (par. 2.1).

Most bacterial RCs contain four protein subunits, referred to as H, M, L[30], and C (a tetraheme cytochrome *c*); some, however, such as the RCs of *Rhodobacter (Rb.) sphaeroide*s, *Rb. Capsulatus*, *Rhodospirillum (Rs.) rubrum*, contain only the first three subunits[104].

---

30. The letters H, M, L come from the apparent molecular weights of these subunits as first identified by SDS gel electrophoresis: Heavy (28 kD), Medium (24 kD) and Light (21 kD). On the contrary, these last are larger than H and almost equivalent in weight (see below in the text).

Photosynthetic bacterial Reaction Centres hold a place of honour within the field of membrane protein structural biology: in fact in 1984 the X-ray structure of the RC from *Rhodopseudomonas (Rps.) viridis*[105] represented the first integral membrane protein to be reported with a high resolution; it was followed shortly afterwards (1987) by that from *Rhodobacter (Rb.) sphaeroides*[106, 107].

Since the RC contains large hydrophobic domains the X-ray structures have been obtained from crystals grown in a suitable detergent solution (in most cases dodecyl dimethyl amino oxide, DDAO, besides other crystallizing agents such as 1,2,3-heptanetriol and phosphate or citrate salts[15, 56, 60]).

Subsequently a number of X-ray structures from bacterial photosynthetic RCs - as well as in complexes with cytochrome c_2 [108] - have been reported using detergent-based crystallization protocols, reaching a gradual improvement in the resolution and quality of the obtained diffraction data (until the present resolution limit of 1.9 Å[109]). So actually a great deal is known about the structure and function of this protein.

Three kind of well-diffracting crystals have been obtained by different procedures from *Rb. sphaeroides* RC: orthorombic, trigonal (considered one of the best crystal set) and tetragonal. Moreover, the fact that *Rb. sphaeroides* bacteria can be grown under non-photosynthetic (aerobic and anaerobic) conditions, being able to fully express its photosynthetic apparatus in anaerobic conditions, allows site-directed mutagenesis to be carried out straightforward[31]. So many RC functions were easily studied by X-ray crystallography through the use of mutants, e.g. changing many amino acids considered important for pigment binding or electron transfer[104].

Apart from the large number of X-ray structures available up till now about this protein[109], the major reason why the purple bacterial RC (not only that from *Rb. sphaeroide*s) has become the "hydrogen atom of the protein electron transfer"[110] - that is a "pioneer" protein in the study of the biological electron transfer - is the richness of its characterization, e. g. by optical absorption, ESR, FTIR, fluorescence[111, 112]. In fact long before the X-ray structure was known, some particular features of the RC complex were already suggested, based on previous different observations[104].

---

31. Site-directed mutagenesis of the structurally best characterized RC from *Rps. viridis* is possible but more difficult because *Rps. viridis* can grow only under photosynthetic conditions: under slightly aerobic conditions the photosynthetic apparatus is not correctly expressed.

The architecture of the RCs from the purple bacteria *Rps. viridis* and *Rb. sphaeroides* is constructed on a common principle, since they present several analogies[113, 114]. Both these RCs are structurally considered the prokaryotic correspondent of the eukaryotic Photosystem II (PS-II) of green plants. In fact there exist some similarities between the LM core of the bacterial RCs and the D1 and D2 subunits of the PS-II, which compose the dimeric green plant reaction centre (fig. 1.3 shown in par. 1.1.1.2)[1, 104].

This is the reason why purple bacterial RCs during many years have served and still serve as bases for models involving PS-II, even now that good resolution structures of this latter are becoming available[115, 116]. E.g., since bacterial RCs - particularly those purified from *Rb. sphaeroide*s R-26 strain - are easily isolated and well characterized, studies of the herbicide binding at the Q_B site for these RCs led to a greater understanding of the herbicide action mechanisms also in eukaryotic photosynthesis.

In the same way the green plant Photosystem I (PS-I) has been found to possess structural analogies with the RC from green sulphur bacteria, though PS-I (and PS-II also) have integral light harvesting pigments directly associated with them[5], differently from bacterial photosynthetic apparatus (see the introduction of par. 1.4).

In addition, recent structural results from PS-I and PS-II of the thermophilic cyanobacterium *Synecocchus elongatus,* which - within conserved regions - shows a distribution of cofactors very similar to the bacterial RCs, add weight to the suggestion that a common evolutionary origin is shared by all Reaction Centres[117].

Analogous to the RCs, also bacteriorhodopsin (bR) is another light-driven proton pump: this heptahelical retinal-binding protein was really the first integral membrane protein from whom any structural information was gleaned[98] (1975), although by electron microscopy. Then it took a further fifteen years (1990) until a high-resolution X-ray diffraction structure was reported[118].

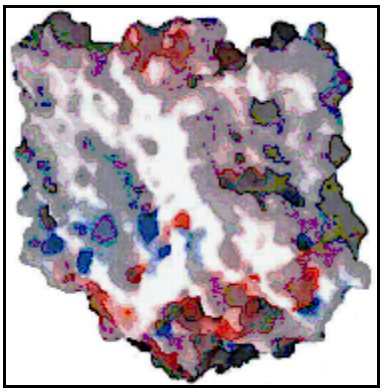

Figure 1.29.
View of the reaction centre as a solid object, with the surface coloured according to surface potential (blue—positive; red—negative; white— neutral).

In terms of design the RC from *Rb. sphaeroides* shows the classic features of an α-helical membrane-spanning protein. A surface potential map (fig. 1.29)

shows that most of the protein exposed on either side of the membrane is coated with hydrophilic residues, presented as regions of positive (blue) or negative (red) potential[51].

In marked contrast, the intra-membrane surface of the protein is distinguished by wide band of neutral surface potential: in this region the protein consists of a bundle of tightly packed membrane-spanning α-helices having hydrophobic residues on the surfaces exposed to the membrane interior. When the protein is purified this hydrophobic surface is shielded from the aqueous phase by detergent micelles (par. 2.1, Experimental Section). Neutron diffraction experiments have shown the structure of these micelles in RC crystals[94].

The RC from *Rb. sphaeroides* contains three subunits called L (32 kD), M (34 kD) and H (28 kD)[32] (called sometimes polypeptides). The L and M subunits contain each five α-helices traversing the membrane perpendicularly to its plane; together they contain pigments and cofactors and provide the connection site for the cytochrome c_2 on the periplasmic (external) side. The H subunit, more globular in shape, is anchored to the bilayer by a single transmembrane α-helix, attached to the LM core: the major part of the polypeptide is located on the cytoplasmic (internal) side of the RC surface, over the quinone-binding region (fig. 1.30).

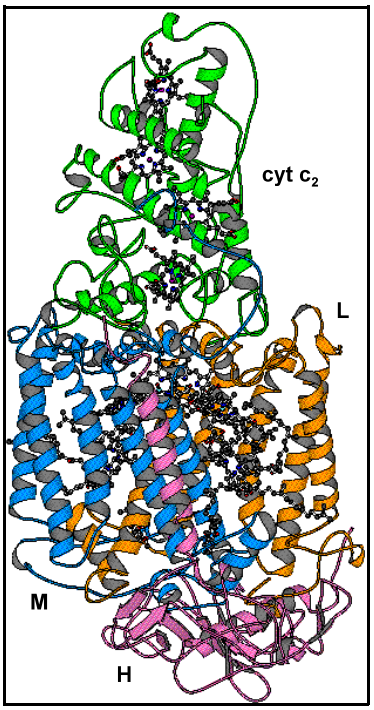

Figure 1.30.
Schematic structure of the RC: the M, H and L subunits are respectively indicated as blue, magenta and orange. In green, the *cyt* c_2 identifies the periplasmic side of the protein.

These 11 transmembrane α-helices form a cylindrical core, whose elliptical section has axes of 70 and 40 Å; as a whole the apolar region of the protein extends for 25 ÷ 30 Å[109].

The high-resolution X-ray diffraction structure of the RC allowed to obtain not only the tridimensional organization of the protein backbone but also the space arrangement of the cofactors. They are all firmly embedded within the protein scaffold, without covalent

32. L, M and H subunits are encoded by the *pufL, pufM* and *puh*A genes, respectively. The labels L, M and H (Light, Medium and Heavy) were assigned on the basis of their apparent mobilities on SDS gel: only subsequent analyses revealed the actual molecular weights.

bonds with the subunits, though they strongly interact with many amino acids. They are divided in two branches spanning the membrane, labeled A and B.

For the RCs from *Rb. sphaeroides* the cofactors are ten: four Mg-containing bacteriochlorophylls (*a* type, made of a conjugated tetrapyrrol ring called bacteriochlorin and a central Mg atom, as reported in fig. 1.4), two composing a dimer (P_A and P_B) and two as monomers (labeled B_A and B_B); two bacteriopheophytins (indicated usually as Φ, or H as in fig. 1.31, *a* type); two equal ubiquinone-10 molecules (Q_{10}, made of a redox active head group and a hydrophobic side chain ten isoprenic units long), usually distinguished as Q_A and Q_B from the name of the branch - and then of the site - in which they are located[33]; a non-heme high spin iron-II (Fe^{2+}); a carotenoid molecule (spheroidene, absent in the R-26 bacterial strain always used in our RC preparations, indicated as Crt in fig. 1.31), playing a role in photoprotection[34, [104]].

The bacteriochlorophyll dimer (indicated either as P for primary donor - as conventionally it will be done in this Thesis except for few figures and schemes - or D for dimer) is located on the periplasmic side of the RC, near the membrane surface (fig. 1.31).

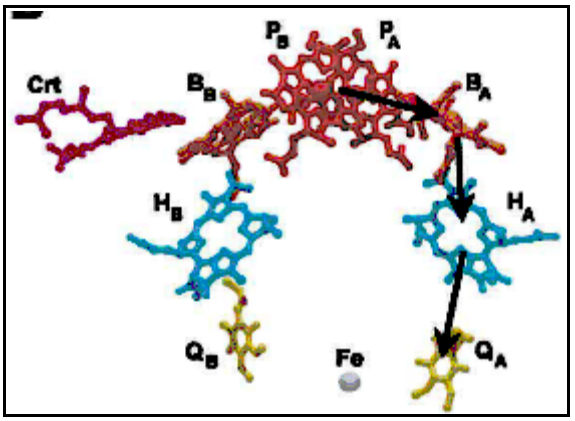

Figure 1.31.
The arrangement of the reaction centre cofactors, shown in stick format. The symmetry axis runs from the pair of bacteriochlorophylls on one side of the membrane (P_A and P_B, red) to the non-heme iron on the opposite side of the membrane (Fe, grey sphere). The accessory bacteriochlorophylls (B_A and B_B, sienna), bacteriopheophytins (H_A and H_B, cyan, elsewhere usually indicated as Φ_A and Φ_B) and ubiquinones (Q_A and Q_B, yellow) are arranged in two membrane-spanning branches. Only the A branch is active in transmembrane electron transfer, indicated by the arrows.

As it is evident from fig. 1.30, between L and M subunits there is a considerable sequence identity and a very similar protein folding: the A and B branches (respectively associated with the L and M subunits) are almost symmetrical in relation to a non-crystallographic binary axis passing through the Fe^{2+} ion and the dimer

33. Since a dissociable quinone molecule is the terminal electron acceptor, the bacterial RC from *Rb. sphaeroides* belongs to the family of type II Reaction Centres.

34. For the sake of comparison in the RCs from *Rps. viridis* , already mentioned, the cofactors are: four bacteriochlorophylls *b* type, two bacteriopheophytins *b* type, two different quinones as menaquinone-9 and ubiquinone-9, the non-heme iron II and the carotenoid 1,2-dihydroneurosporene.

P (a 180° rotation of one of the two subunits about this axis superimposes approximately 2/3 of its C-α carbon atoms on the corresponding ones of the other subunit). In other words, after the optimization of the rotation axis relating equivalent cofactors between the two branches, the root of the mean square deviation between equivalent atoms has been found to be about 1 Å[119]. The unique carotenoid molecule is itself an element disrupting the symmetry.

In spite of the high symmetry the primary light-induced electron transfer occurs at least 20 times faster along the A branch than along B. Small deviations in the orientation of the cofactors in relation to the binary simmetry axis, slight differences in geometry and in rigidity, differences in the amino acid composition of the L and M subunits have been suggested to contribute to the unidirectionality of the electron transfer[104]. The latter aspect was specified by the theoretical identification of a large electrostatic field favouring the charge separation along the A branch[120].

It is important to notice that the crystallographic temperature factors obtained for the diffraction images of *Rb. sphaeroides* RCs, measuring the rigidity of the structure, are considerably higher along the B-branch than along the A-branch[104], confirming that an efficient electron flow through cofactors is often related to their suitable molecular adaptations, induced also by the chemical environment itself. In par. 1.5 it will be shown for RC that even bound lipids may be responsible for a differentiation in electron transfer kinetics between A and B branches. The function of the B-side cofactors in the *Rb. sphaeroides* RC is yet unknown, though the high level of their conservation among several structures implies that one must exist[121].

The two bacteriochlorophyll molecules making the dimer (P_A and P_B) are overlapped regarding the position of the ring I; the distance between the centres of the rings is 7 Å, in the direction perpendicular to the simmetry axis (being approximately the direction of the plane of the membrane in which the RC is embedded); the average distance between the planes of the rings I in the two molecules is instead about 3.5 Å.

The electron transfer along the A branch proceeds from P, acting as primary electron donor, through B_A, Φ_A (indicated as H_A in fig. 1.31), the primary quinone Q_A, to the secondary dissociable quinone, Q_B (see par. 1.4.2 for further details).

Near the dimer P, along both the branches, the two bacteriochlorophyll monomers (B_A and B_B) are potentially involved in the stabilization of the electron

transfer from the primary donor to the bacteriopheophytin molecules Φ_A and Φ_B - though actually only the A branch is active in the electron transfer -.

The Mg atom in each of all the four bacteriochlorophyll molecules (BChls) is non-covalently coordinated to a histidine (His) residue of either the L or M polypeptide, besides the binding with four ligands provided by the bacteriochlorin ring nitrogen atoms: the pair of BChls making up P are bound to His L173 and M 202, while the monomer BChls to His L153 and M182. The Mg atoms are thereby all penta-coordinated.

In order to continue the electron transfer chain the Q_A ubiquinone is located near the Φ_A molecule and it is fixed in its position (see also par. 1.4.3), while the Q_B quinone is mobile and dissociable from its site, so it may be partially lost during the RC purification and it may be considered more as a substrate than as a cofactor.

The Fe^{+2} ion instead is located between the two quinones Q_A and Q_B, separated by a distance of 15 Å (edge to edge) and both located about 15 Å far from the cytoplasmic surface. Here the two quinone molecules are linked by H-bonds through a [histidine-Fe^{+2}-histidine] complex. The iron atom is six-coordinated and lies near the cytoplasmic edge of the RC hydrophobic region: four coordination sites are His residues, two from the L and two from the M subunit (His M219, M266, L190, L230), while other two sites are offered by a glutamic acid (Glu M234) acting as a bidentate ligand. It results a distorted octahedron, with the centre of coordination slightly closer to the secondary acceptor Q_B.

This structure contributes to the stability of the transmembrane core of the RC, further stabilization being provided by the H subunit interacting with both L and M subunits. Indeed experimental evidences showed that in absence of the H subunit the electron transfer between the primary acceptor Q_A and the secondary one is blocked[104].

It has been found also that the non-heme iron of *Rb. sphaeroides* RCs may be removed and replaced with Mn^{2+}, Co^{2+}, Ni^{2+}, Cu^{2+} and Zn^{2+}, without any loss of biological activity[104]. Neither Fe^{+2} nor any other divalent cation is required for rapid electron transfer from Q_A^- (semiquinone species, see below) to Q_B, though the presence of a metal ion in the iron site seems instead to be necessary to establish the characteristic electron transfer properties of the Q_A site[122].

In addition to the site for Fe^{2+} another metal-binding site has been identified by X-ray crystallography: it is located on the cytoplasmic surface of the RC and it has been

found to stoichiometrically and reversibly bind Zn^{2+} (or Cd^{2+})[104, 123]. This binding site for divalent cations involves two His and one Asp residue at the cytoplasmic surface of the H-subunit. The Asp residue (H124) forms the end of a short hydrogen bond network that connects the surface of the protein with the Q_B binding site[35]: the network involves three water molecules and residues Ser L223, Asp L213, Asp M17 and Asp L210[124]. Further informations about water molecule assembled in networks and clusters are reported also in par. 1.4.3.2.

It has been demonstrated also that Cu^{2+} has an effect similar to Zn^{2+} on the rate of electron transfer from the Q_A^- to Q_B ubiquinone, and it has been proposed that RC has also a Cu^{2+} binding site that involves four His residues located at the cytoplasmic surface of the protein, in a region of close contact between the H-, L- and M-subunits[125].

Besides metal-binding sites recent crystallographic studies showed the presence of several water molecules inside the RC, some of them organized in clusters at distances suitable to allow to interact by intermolecular hydrogen bonds (distances lower than 5 Å). Many of these molecules are located in the protein regions out of the membrane and at the interface protein/membrane; on the contrary, the majority of the water molecules grouped in clusters are in the protein interior or near the H subunit.

Three large clusters are located near the Q_A and Q_B sites[26]:

1) The water molecules of the cluster near the Q_A site do not interact with the quinone by hydrogen bonds since the distance is always larger than 5 Å. This group is close to the RC cytoplasmic surface, in contact with three polar amino acids (two glutamic acid and one arginine): it constitutes an interface between the external medium and the hydrophobic moiety of the protein buried in the phospholipid bilayer.

2-3) The two clusters close to the Q_B site contain the water molecules most strongly interacting with the protein: one of them is in contact with the residue Glu L212, the other with Asp L213;

2) The “cluster Glu L212" shows an almost linear structure and it is oriented perpendicularly to the membrane plane; it is composed of two groups of water

35. This can be the basis of the hypothesis that the binding of Zn^{2+} or Cd^{2+} to RC would influence both the charge recombination process from the Q_B site and the electron transfer rate from Q_A to Q_B ubiquinone.

molecules (4 and 8), in the middle of that there is a space of 4 Å not occupied by the protein neither by the cofactors, which may contain two mobile water molecules not revealed by X-rays;

3) The “cluster Asp L213" presents a branched structure and is approximately oriented parallel to the membrane plane. The network of water molecules involved in the Zn^{2+} binding site, above mentioned, is made of a branch of this cluster.

The most probable role of these water clusters is to make easier the proton transport toward the interior of the protein[26, 27]: it will be better examined in par. 1.4.3.

1.4.2. Photosynthesis primary events.

The RC catalyzes an energetically uphill reaction, the reduction of the ubiquinone at the Q_B site by cytochrome c_2. To achieve this goal, light energy is used to initiate the transmembrane electron transfer and is converted into electrochemical energy with a high quantum yield.

The photosynthetic process starts when a UV-Vis photon captured by the antenna complexes is conveyed to the dimer P - located in the RC region close to the periplasmic side of the membrane - having the effect of exciting it to the P* state. The P to P* energy gap is 1380 meV in *Rb. sphaeroides* RCs[104] (fig. 1.32, where D symbol is used instead of P).

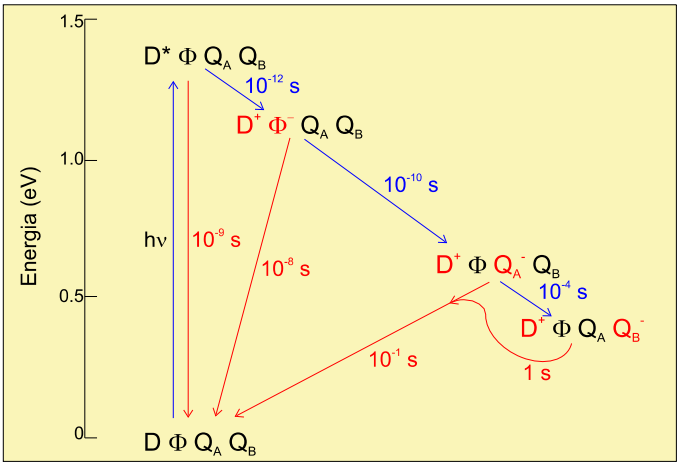

Figure 1.32.
Energy diagram of the electron transfer reactions within the RC (in red are labeled the species involved at each step in the charge transfer). Arrows blue and red respectively indicate the direct and reverse process performed by the electron with the corresponding necessary times (approximated at the closest magnitude order). For the dimer, D symbol is used instead of P.

The next step is the basis for

the subsequent highly efficient energy conversion: one electron is transferred to the bacteriopheophytin on a very fast time scale (reaction halftime of about 4 ps), originating an electrical charge separation between P and ϕ_A, indicated as the $P^+\Phi_A^-$ radical pair state. This high rate of electron transfer does not match well with the relatively long distance separating the two cofactors (~17 Å): hence several mechanisms have been proposed in order to justify this experimental evidence.

One of these involves the bacteriochlorophyll monomer B_A in a charge translocation process made of two sequential steps; another mechanism assumes the partecipation of other species such as the tyrosine (Tyr) M210. In fact, due to its spatial position it may establish Van der Waals interactions either with the phytyl chain of one of the chlorophyll of the dimer (called P_L or P_A) or with the tetrapyrrole ring of Φ_A.

The subsequent electron transfer between Φ_A^- and Q_A occurs in about 200 ps and the rate of this transfer has been found to be indipendent of the temperature. This latter finding can be explained considering that the aromatic ring of the triptophan (Trp) M252 is approximately parallel to the ring plane of the ubiquinone at the Q_A site, making possible for the electron transfer a “superexchange” mechanism in which Trp acts as a mediator between Φ_A^- and the Q_A quinone. A confirmation comes from the fact that the substitution (by site specific mutagenesis) of the Trp M252 with a valine (Val) dramatically reduces the photosynthetic growth of the bacteria.

The last electron transfer between Q_A^- and Q_B requires times in the range 10÷200 μs. Since in RCs from *Rb. sphaeroides* both Q_A and Q_B sites are occupied by identical ubiquinones a one-way electron transfer may be explained only referring to a different chemical environment for the two molecules: in comparison to the Q_A site, the Q_B site is surrounded by a larger number of polar amino acids, many of them with protonatable residues, and it is also closer to the Fe^{2+} ion. Both these factors contribute to decrease the energy content of Q_B^- in comparison to Q_A^-, since in the former case more electrostatical interactions can be established with the surrounding chemical environment[126] (par. 1.4.4.1). Moreover, by this way the Q_B site, contrary to Q_A, results to be sensitive to changes of environmental factors such as pH, ionic strength and even protein-protein and lipid-protein interactions[127].

Triazine herbicides block the electron transfer from Q_A to Q_B. In absence of H the LM subunits - besides containing all the cofactors - retain the main photochemical

activities, but the rate of electron transfer from Q_A to Q_B is altered.

Finally, it is worth mentioning that the processes of direct electron transfer from P to Q_B (employing about 100 μs) are much faster than the subsequent proton uptake, occurring in the millisecond time scale[126], as it will be reported in par. 1.4.3.3.

It may be interesting now to briefly explain how it has been possible to understand with such a precision the mechanisms following the absorption of a quantum of light by the RC, especially since many intermediate steps have very short lifetimes. The next paragraph will pursue this aim.

1.4.3. Electronic structure, arrangement and functions of the cofactors.

1.4.3.1. Electronic structure of cofactors.

The electronic structure of the cofactors of the purified RC protein has been explored so far using several experimental techniques, each of them sensitive to the strong modifications that the interaction with the electromagnetic radiation induces in the cofactors.

Among them, the most important are the ESR spectroscopy (Electron Spin Resonance, already met in par. 1.3.2.2, though about different topics) and the UV-Vis spectroscopy[128].

The first is sensitive only to paramagnetic species, while the second is strongly affected by the electronic distribution on the chromophore groups (e. g. those molecular moieties interacting with the electromagnetic radiation). Further details about the application of the UV-Vis spectroscopy to the study of kinetic phenomena - as the electron transfers internal to the RC showed up till now - will be given in par. 2.3, since this technique has been employed to collect all the data reported in this thesis.

In fig. 1.33 are shown the UV-Vis absorption spectra of an RC in TLE buffer (Tris-HCl, LDAO or DDAO, EDTA) in the dark and after light illumination able to produce a

charge-separated state. In addition, table 1.3 reports all the visible and near-infrared (NIR) absorbance bands of the RC[104].

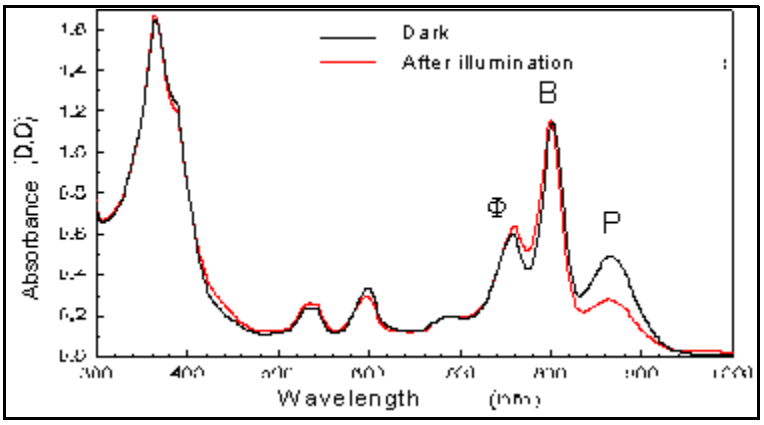

Figure 1.33.
UV-visible spectrum of the RC in the dark and after illumination.

Table 1.3 . Assignement of the room temperature visible and NIR absorbance bands for RCs from *Rb. Sphaeroides*; the cofactor acronyms correspond to those used in the text.

λ **(nm)**	ε ($mM^{-1}cm^{-1}$)	Band type	Assignment	Comments
535		Q_X	Φ_B	
545		Q_X	Φ_A	10 nm shift due to H-bonds with an amino acid
600		Q_X	P, B_A, B_B	
760		Q_y	Φ_A , Φ_B	
800	288	Q_y	P, B_A, B_B	Higher energy transition of P; transition of B_A, B_B
865	128	Q_y	P	Lower energy exciton transition of P
1016		Q_y	B_A^-	B_A in the charge separated state $P^+B_A^-$
1260		Q_y	P^+	P photo-oxidized (charge separated state P^+Q^-)

The UV-Vis absorption spectrum of the RC from the *Rb. sphaeroides* is characterized by the presence of three well-distinguished peaks in the region over 700 nm: at 760, 800 and 865 nm, attributable respectively to the bacteriopheophytin (Φ), the bacteriochlorophyll monomer (B) and the dimer (P). Other important bands are: the absorption peak at 545 nm (attributable to Φ) and that at 600 nm (attributable to B).

Following light absorption the spectrum is widely modified: the absorption band of P at 865 nm is greatly reduced because of its photo-oxidation to P^+; the 800 nm peak of B shifts about 5 nanometers towards the blue, showing a phenomenon associated

with the presence in the RC of a charge-separated state (*electrochromism*). The absorbance at 760 nm increases due to the illumination, indicating that also one of the two molecules of bacteriopheophytin (Φ_A) is involved in the electron transfer.

Similar spectral changes due to illumination are found also in other regions of the spectrum: slight modifications in the absorbance value at 600 and 545 nm; little increases and decreases, respectively at about 440 and 380 nm, represent instead the formation of the semiquinone radical (see below).

Finally, the intense absorption band in the region of the near UV is due to both the aromatic amino acidic residues of the protein backbone and the ubiquinone molecules (e. g. the semiquinone at 380 nm).

Also the near-infrared region of the spectrum (not shown) is very interesting for the RC: at 1260 nm the P oxidation to P^+ cause the rising of an absorption band which, in the same way as other in the UV-Vis, can be employed to monitor the formation of the P^+ species.

Since the light-induced spectral changes reflect the redox equilibria in which the different RC cofactors are involved, their time evolution will reflect the average lifetime of each of them. Therefore if the RC is excited by a short and saturating light pulse (this latter means that light pulse does not leave RC moleciles unexcited), it is possible to record the evolution with time of different absorption bands illustrating the redox state of their corresponding cofactors.

In order to measure, for instance, the rate of decay of the charge separated state $P^+Q_A^-$ - that we are interested in - it is necessary to satisfy two general conditions:

1) the excitation light pulse has to be much shorter than time necessary for an electron to recombine from Q_A^- to P;
2) the time response of both detector and whole apparatus should be fast enough to properly record absorbance variations related to the life time of the state $P^+Q_A^-$.

In other words, both these experimental parameters should have duration negligible in comparison to kinetic phenomena which have to be measured. This is easily satisfied for the $P^+Q_A^-$ recombination, since it is a very slow type of electron transfer ($k_{AP} \sim 10\ s^{-1}$). Besides more suitable lasers, every flash lamp with pulse width shorter than hundreds of microseconds may be used as excitation beam.

From fig.1.32 it is evident that going ahead during the electron chain transfer of

cofactors the time needed for every step increases, then the required experimental condition just mentioned becomes less and less restrictive. Nevertheless every step in the electron transfer from primary donor P to final acceptor Q_B is thermodynamically well favoured.

1.4.3.2. Some details on the arrangement of the Q_A and Q_B sites.

Based on structural data, the RC cofactors - Q_A site included - are not directly exposed to the surface of the protein: they are well shielded in the protein interior by hydrophobic amino acid side-chains.

Moreover all the cofactors fit the electron density of the protein crystal structure very well except for the ubiquinone at the Q_B binding site: this is the most difficult feature of the RC to establish by X-ray crystallography[60]. As found in several diffraction models, low density is due to the fact that this quinone is dissociable, contrary to that at the Q_A site. In other words, the secondary ubiquinone Q_B is the free substrate on which the "RC enzyme" works, then it results loosely bound to the active site. In fact crystallography structural details appear well defined only if the molecular target of the X-ray beam is strongly fixed, as usually crystals do.

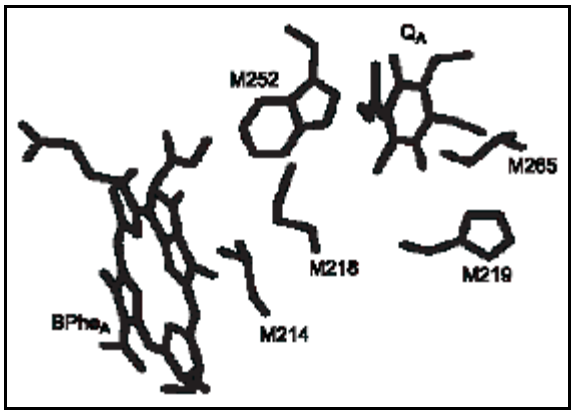

Figure 1.34.
View of the Q_A binding region showing the position of methionine M218 relative to Q_A and BPh_A. Residues shown are: M214 (leucine), M218 (methionine), M219 (histidine), M252 (tryptophan), M265 (isoleucine).

As a comparison to Q_B site, fig. 1.34 shows the Q_A ubiquinone in its native site[109]: it lies close to the bacteriopheophytin of the L subunit (Φ_A), though it is surrounded mainly by amino acid residues of the M subunit. The quinone oxygen, located proximally to Fe^{2+}, is hydrogen bonded to the side chain of His M219, while the distal oxygen forms a hydrogen bond to the backbone nitrogen of

Ala M260 (not shown). In the structure presented the Q_A head group is located symmetrically between the hydrogen bonded residues, both distances amounting to 2.75 Å in the neutral (dark adapted) as well as in the charge-separated state (light adapted), in both cases Q_A itself being not charged.

The Arg M267 residue forms a salt bridge with Glu M263 over the apolar Ile M265 (fig. 1.34) that probably contributes to stabilize the top of the transmembrane helix E belonging to the M subunit. Helices MD and ME are the anchor points for the Q_A binding loop motif.

Several different structures for Q_B by different research groups have been reported: the most recent and qualified are those proposed by the teams of Feher and Michel[104, 126]: both these RC structures describe an ubiquinone loosely interacting by hydrogen bonds with a protein region out of its real Q_B binding site.

Based on structural analysis refinements, the usual Q_B occupancy was estimated to be less than 40 %[60]: possible reasons for this low occupancy include the fact that in its pocket the quinone Q_B may be positioned in two alternative conformations.

A confirmation of this hypothesis arrived when Stowell et al. obtained different Q_B site structures from RCs frozen under illumination (i.e. in the charge-separated state $P^+Q_AQ_B^-$, see below) and from dark adapted samples (PQ_AQ_B state)[124]. Following light excitation the ubiquinone shifts by approximately 5 Å undergoing a 180° twisting movement of its headgroup (fig. 1.35), displacing also some water molecules[104].

In the light-induced position, Q_B is hydrogen bonded to His L190 and Ser L223 and to the amide proton of the peptide bond between Ile L224 and Gly L225 (this last interaction is conserved from the dark adapted state); also a rather weak hydrogen bond between Thr L226 and Q_B quinone has been observed in the light adapted structure. A strong interaction between Q_B and His L190 facilitates the electron transfer from Q_A^- to Q_B because His L190 is coupled to Fe^{2+}, which in turn is

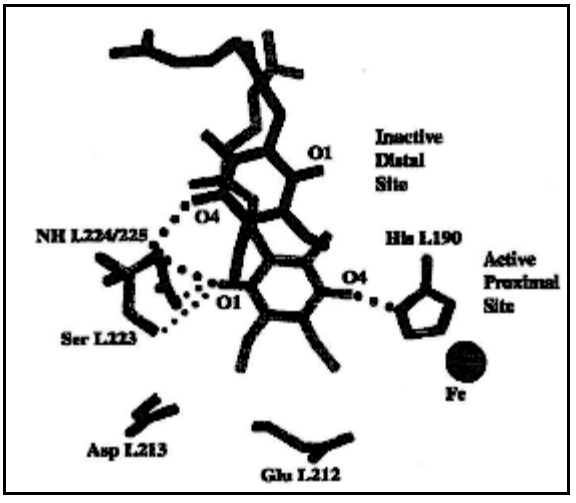

Figure 1.35.
Structure of the RC from Rb. sphaeroides showing the position of Q_B in the RC before (black) and after (gray) electron transfer.

connected to Q_A through another His residue. The arrangement of the amino acids in the charge-separated state however does not allow any other orientation[124].

The shift of Q_B in the charge separated state represents a transition from an inactive position of the site (distal) to an active one (proximal) and accounts for a conformational gating mechanism of the first electron transfer[126] (see below). The distal is the position in which the neutral Q_B quinone accepts a first electron from Q_A^-.

Finally, it should be added that the distribution of the Q_B ubiquinone between the two states is somewhat statistical: in the neutral state 55 % of the quinone is located distally and 45 % proximally to the cytoplasmic side; after excitation by light, instead, at least 90 % of the quinone is found at the proximal position[128].

Though the last results seem to evidence the opposite, the position of the Q_B cofactor does not solely depend on the oxidation of state of Q_B (light/dark), but it is affected even by the chemical environment: in the RC mutant L209PY the Q_B quinone is located proximally even in the dark state, leading to think that the residue Proline (Pro, P) L209 should have a role in destabilizing the charge-separated state (maybe by steric hindrance)[129].

Another important feature of the Q_B binding site is the close presence of polar and acidic residues and water molecules, whose function seems to make pathways for the transfer into the Q_B site of the protons necessary to the ubiquinone reduction (as already reported in par. 1.4.1). The water molecules are grouped in two distinguished clusters: the most involved amino acidic residues include Ser L223, Asp L213, Glu L212, Asp L210; these residues have been studied by site directed mutagenesis.

In addition, recent X-ray crystal structures with improved resolution have shown chains of water molecules connecting the region near Q_B to the protein surface, generally proposed as possible pathways for proton transfer[98, 124]. The longest pathway (P1) connects Q_B with the surface through a long chain of 10÷12 water molecules; the P2 chain is relatively short and connected to a pool of water molecules; P3, the shortest pathway, passes through a cluster of acidic residues and in the *Rb. sphaeroides* RC it seems to be the most probable way for a proton transfer to Q_B site[27].

1.4.3.3. Electron and proton transfer reactions of quinones.

• *Quinone chemistry*.

Quinones are well suitable species for coupling electron and proton transfer reactions, since different redox states, between them reversible, show different affinity for protons. Quinones (Q), semiquinones (Q^-) and quinols or dihydroquinones (QH_2)[130] are shown in fig. 1.36, with attention only to their polar head, the most important part in determining the redox properties of the molecule.

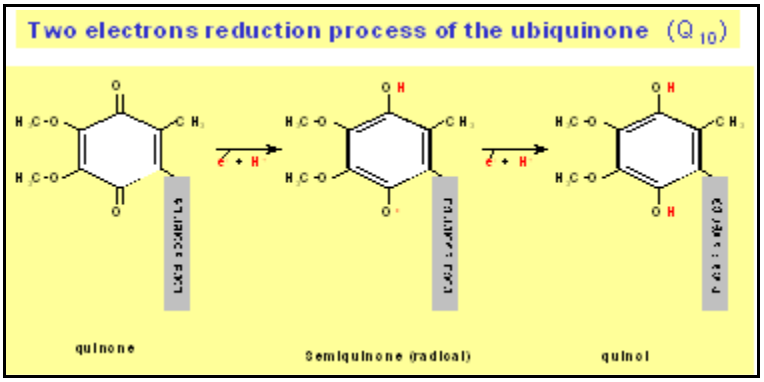

Figure 1.36.
Redox and protonation equilibria involving the cofactor ubiquinone Q_{10}.

It is important to stress that the quinone properties in the RC (and also in other proteins) are strongly modified by the protein environment, usually in order to accommodate their functions in the energy conversion process.

Indeed the primary ubiquinone Q_A, situated in a hydrophobic environment, following light-induced charge separation accepts in 200 ps only one electron each time and it acts as the electron donor to the Q_B quinone. The midpoint potential (E_m) for the Q_A reduction is $E_m(Q_A/Q_A^-)$= -45 mV[131]; further reduction of Q_A is normally not observed, probably because of the inaccessibility of Q_A site to protons which are needed to stabilize the semiquinone and then the quinol state.

It is interesting to notice that the redox potential of Q_A is higher in the *Rb. sphaeroides* RC than in *Rps. viridis* RC - being *Rps. viridis* probably the member of the family of purple bacteria with the RC most similar to that of *Rb. sphaeroides*[104] -: the reason is the different chemical nature of the quinones at the Q_A site, ubiquinone-10 (Q_{10}) vs. menaquinone-9 respectively, while the Q_B site contains ubiquinones in both cases, but differing for the number of isoprenic units of the hydrocarbon tail (Q_{10} vs. Q_9).

The secondary quinone Q_B, situated in a relatively polar environment, undergoes full reduction to the quinol in two electron reduction steps. The first and second electron reduction steps occur at the following potentials: $E_m^{(1)}(Q_B/Q_B^-)$ = +20 mV and $E_m^{(2)}(Q_B^-/Q_BH_2)$ = +100 mV [132]. These potentials are reasonably close to each other (compared to the large difference in solution of about 400 mV[126]) and well matched to the potential of Q_A in order to reach an efficient electron transfer.

Since the RC from *Rb. sphaeroides* has two identical Q_{10} molecules at the Q_A and Q_B sites, their difference in the redox potentials for the first reduction (65 mV) is necessarily determined by the interactions of the cofactors with the protein environment. As reported in the previous paragraph, many polar and charged amino acids and water molecules are present at the Q_B site and partecipate to several hydrogen bonds stabilizing Q_B^- and increasing the $E_m^{(1)}(Q_B/Q_B^-)$ value (fig. 1.35). Some aspects of this topic have been emphasized in recent literature (see also par. 1.4.2 and 1.4.4.1):

- the role of peptide dipoles which stabilize negative charges on Q_B^- and neighboring acid groups; thereby it facilitates also the proton transfer and the Q_B^- protonation to Q_BH_2[120], increasing the $E_m^{(1)}(Q_B/Q_B^-)$ and $E_m^{(2)}(Q_B^-/Q_BH_2)$ values;
- the importance of protein flexibility in the vicinity of the Q_B site[133].

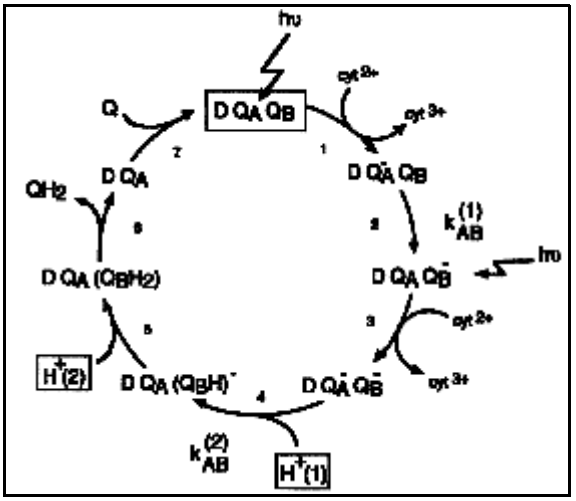

Figure 1.37.
The quinone reduction cycle in bacterial RCs. Q_B is reduced in two one-electron reactions, $k^{(1)}_{AB}$ and $k^{(2)}_{AB}$, and binds two protons, $H^+(1)$ and $H^+(2)$. The reduced QH2 leaves the RC and is replaced by an exogenous quinone, thereby resetting the cycle.

• *Quinone reduction cycle*.

The RC cycle of reactions involving electron and proton transfer to quinones is shown in fig. 1.37 (where for the dimer D symbol is used instead of the usual P)[126]. Each step in the cycle represents a change in the state of Q_A or Q_B due to electron transfer or proton binding. The initial state PQ_AQ_B is shown at the top of the cycle.

The *step 1* is the photochemical reduction of Q_A, forming the state $PQ_A^-Q_B$. This step represents a combination of several electron transfer steps: the light-

induced electron transfer from the primary donor, through some intermediates (BChl, BPh), to form $P^+Q_A^-Q_B$, followed by reduction of P^+ by the cytochrome (cyt) c_2 (in the RC from *Rps. viridis* this role is carried out by a tightly bound tetraheme-cytochrome *c* subunit).

This reduction occur by a biphasic reaction: the fast phase of about 1 μs is attributed to the intermolecular electron transfer, while the slow phase of ~ 100 μs is limited by the docking and reorientation of the cyt c_2-RC complex[104].

The *step 2* is the electron transfer from Q_A^- to Q_B with rate $k^{(1)}_{AB}$, forming the photochemically active $PQ_AQ_B^-$ state. Further hydrogen bonds (e. g. an additional one given by the Ser L223 side chain) lead to a tighter binding of the negatively charged semiquinone Q_B^- compared to the neutral Q_B. Rearrangements of hydrogen bonds as that of Ser L223 seem to be necessary to make Q_B reduction more favourable than Q_A reduction[104].

The *step 3* represents the photoinduced second electron transfer forming a new charge separated state $P^+Q_A^-Q_B^-$, followed by the cyt c_2 reduction (at the same rate of the first one) giving rise to $PQ_A^-Q_B^-$.

The *step 4* is the proton-coupled second electron transfer reaction producing the doubly reduced $PQ_AQ_BH^-$ state: it results from the sequential protonation of the semiquinone Q_B^- formed in the previous step ($H^+(1)$) and subsequent electron transfer from Q_A^- (with rate $k^{(2)}_{AB}$).

The *step 5* is the binding of the second proton ($H^+(2)$), giving rise to the dihydroquinone $PQ_AQ_BH_2$.

The *step 6* is the dissociation of $Q_{(B)}H_2$, followed by the *step 7*, in which a new quinone Q is bound to form the initial state PQ_AQ_B.

• <u>*Examination of the electron transfer reactions*</u>.

The most important reactions in the quinone reduction cycle are the two electron transfer steps in the reduction of Q_B.

The first electron transfer between quinones occurs with rate $k^{(1)}_{AB} \approx 10^4\ s^{-1}$ (pH

7), the decay time[36] of the starting state being the reciprocal 1/ $k^{(1)}_{AB} = \tau^{(1)}_{AB} = 10^{-4}$ s; it has been shown to be rate limited by conformational gating[134], consistent with the observations of Stowell et al. of different conformations of Q_B before and after illumination (above mentioned). This step which involves the transfer of an electron from Q_A^- to Q_B can be monitored by measuring either electrochromic shifts of pigment bands[135], changes in the semiquinone optical[134], or infrared spectra[136]. The stable product in this reaction is the anionic semiquinone Q_B^-.

The second electron transfer occurs with decay time $\tau^{(2)}_{AB} \approx 10^{-3}$ s = 1 ms (pH 7) and is coupled to the uptake of the first proton, faster than the former: $\tau^{(1)}_{H} \leq 10^{-3}$ s; the proton is transferred probably via a transient protonated Ser L223-OH_2^+ [104]. Therefore the rate-limiting step is represented by the electron transfer.

Then the second proton binding occurs with a decay time $\tau^{(2)}_{H} \gg 10^{-3}$ s (pH 7), and it is generally not resolved from the previous second electron transfer. Since this reaction involves the disproportionation of the two semiquinones Q_A^- and Q_B^- to form a fully oxidized (Q_A) and a fully reduced quinone (Q_BH_2), the reaction may be monitored by measuring the decay of the semiquinone by transient optical absorption spectroscopy[134].

Structural studies on a *Rps. viridis* RC binding the antibiotic stigmatellin found that this inhibitor of the Q_B site shows additional hydrogen bonds with the protein in comparison to the native quinone[137]: this result, which can be extended also to the RC from *Rb. sphaeroides,* indicates clearly that the Q_B site is not optimized for quinone binding, but rather for its reduction to quinol, being this a more important and meaningful function in the bacterial metabolism.

In view of the detailed functional and structural informations gained in the last decades, the quinone acceptor system of bacterial RCs has become a reference model in the study of the interactions of quinones with electron transfer complexes[33].

36. The decay time is the time necessary to see the observed amplitude of the phenomenon decrease by a factor of 1/e.

1.4.4. The charge recombination process.

The electron transfer internal to the RC from *Rb. sphaeroides* needs an electron donor - e. g. *in vitro* the cytochrome *c* from horse heart, or *in vivo* the cyt c_2 - to re-reduce the primary donor P^+ oxidized after a light pulse and to continue the photochemical cycle illustrated in par. 1.4.3.3.

In the absence of any reducing donor the electron arrived on Q_B, or on Q_A (if the Q_B site is empty), recombines with the hole on P^+, giving rise to the so-called "charge recombination". This occurs in a slow time scale (0.1 ÷ some seconds) compared to the usual time scale of the direct charge transfer (~10 μs) or to the time necessary for a whole photocycle (~1 ms).

This phenomenon occurs with different time scales depending on which is the charge-separated state. It is worth noticing that charge recombination from every state, being a reverse electron transfer and having not a precise physiological function, always occurs with times at least 100 times longer than the corresponding direct electron transfers, which are the most favoured processes in biological conditions (fig. 1.31 and 1.32).

If there is ubiquinone Q_{10} bound to the RC - that is if RC is not totally depleted of the mobile cofactor quinone - the charge recombination consists in a simple "reverse" electron transfer (*back reaction*) from the state $P^+Q_A^-$, in the case of Q_B site empty, or from $P^+Q_AQ_B^-$ up to PQ_AQ_B (ground state). On the contrary, if no Q_{10} is available the recombination should proceed from the last possible charge-separated state along the electron transfer pathway, i.e. $P^+\Phi_A^-$. In this case the time scale of the process is too short (10^{-8} s) to be studied by a millisecond-resolved laser photolysis apparatus such as that we have built.

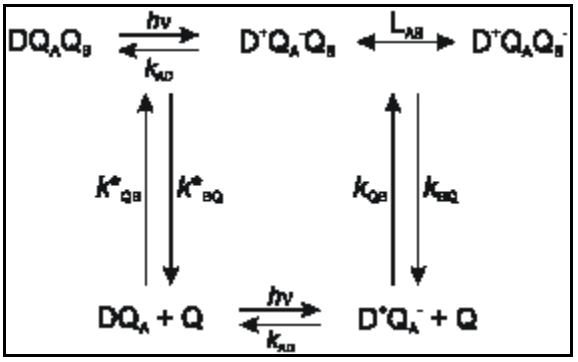

Scheme 1.5.
Kinetic scheme summarizing the equilibria occurring to the RC in the dark and after a light pulse.
Here k_{AD} and k_{BD} (elsewhere usually indicated as k_{AP} and k_{BP}) are the kinetic constant for the charge recombination from $D^+Q_A^-$ and $D^+Q_AQ_B^-$ respectively (elsewhere usually indicated as $P^+Q_A^-$ and $P^+Q_AQ_B^-$). k^*_{QB} and k^*_{BQ} are the kinetic constants for the binding and release, respectively, of the ubiquinone at the Q_B site of the RC, before the interaction with the electromagnetic radiation (hv), while k_{QB} and k_{BQ} are the same constants after light absorption. L_{AB} is the equilibrium constant for the $Q_A^-Q_B$ to $Q_AQ_B^-$ single-electron transfer ($L_{AB}= k_{AB}/k_{BA}$).

Since the recombination from $P^+Q_AQ_B^-$ passes through the repopulation of the thermally activated state $P^+Q_A^-Q_B$ (dotted arrow in scheme 1.5, where for the kinetic constants k_{AD} and k_{BD}), the rate of the $P^+Q_A^- \rightarrow PQ_A$ reaction, (represented by k_{AP}) is approximately two magnitude orders larger than that from $P^+Q_AQ_B^-$ (represented by k_{BP}): their ratio is $k_{AP}/k_{BP} \approx 10$ (although the k_{BP} value is strongly dependent on the environment surrounding the RC[33]). The value of k_{AP} is about 10 s^{-1} for *Rb. sphaeroides* RCs (decay time $\tau_{AP} \approx 0.1$ s)[33].

Kinetic studies carried out by means of suitable experimental apparatus measuring the time evolution of a generic $P^+Q_i^-$ charge-separated state (par. 2.3) - which may be both $P^+Q_A^-$ and $P^+Q_AQ_B^-$ - represent a very useful way to examine the functional properties of the acceptor quinone complex, made of the Q_A and Q_B sites. Both the recombination rates from $P^+Q_A^-$ and $P^+Q_AQ_B^-$ are measurable from non-linear *fitting* operations[37] performed on the kinetic traces of the decay of generic $P^+Q_i^-$ species (par. 2.4).

Indeed real RC samples can show the following type of charge recombination traces (the equations for the first two cases are reported in par. 2.4):

a) traces well fitted by a *unique $P^+Q_A^-$ exponential decay* - then monoexponential with rate constant k_{AP} -, as in the case of our measures recently accepted for publication[138];

b) traces well deconvoluted by the *sum of the decays* from $P^+Q_A^-$ and $P^+Q_AQ_B^-$ - then biexponential with two rate constants, k_{AP} (fast decay) and k_{BP} (slow decay) -, as in several literature reports[33];

c) traces that need more complex recombination models - as for example cumulant analysis[139] - in order to understand the experimental phenomena occurring.

The chemical environment in which the RCs are reconstituted - though

37. The *fitting* is a mathematical operation performed on experimental points in order to research the best matching between them and a chosen equation supposed to describe all the experimental data.

representing an external factor in relation to the RC sample - is undoubtely very significant in determining the type of charge recombination of the sample measured. Supramolecular aggregates made of lipids such as normal and reverse phospholipid micelles, as well as liposomes - par. 1.2.2 -, have strong effects as host-systems for the protein. In fact they affect both the concentration and distribution of the mobile quinone cofactor[33], or directly influence some RC's electron transfer by specific lipid-protein interactions (par. 1.5).

It is useful to remember that the charge separation process should be considered a substantial perturbation of the protein that results in conformational changes affecting in turn several electron transfer rates, as has been noted in some studies[140]. These changes can be studied conveniently in the RC, because the reaction, initiated by light, can be followed spectroscopically and is usually completed on the milliseconds time scale[141]. Therefore conformational changes can be probed and investigated through their effect on the electron transfer kinetics.

The recombination process from $P^+Q_A^-$ to the ground state would occur by *quantum-mechanical tunneling*[38] through a distance of about 25 Å from Q_A^- to P^+. At a molecular level this is such a long distance that it leads to weak coupling between donor and acceptor electronic states (according to the Marcus theory for the electron transfer[142]). The "tunnel effect" has been evoked from quantum mechanics in order to explain the "strange" experimental increase of the kinetic constant value for the P^+Q_A recombination (k_{AP}) following temperature decreases. In fact k_{AP}, as kinetic constant referred to a (reverse) electron transfer, can be described by the famous Marcus equation for electron transfers (reported as eqn. 3-30 in the Third Chapter).

The trend of k_{AP} is opposite to that typical of kinetic rate constants corresponding to thermally activated reactions: this has been already detected by several authors in previous studies on detergent micelles[141] (for further references see the third chapter). Nevertheless it does not strictly imply that electron back reaction occurs by quantum

38. Physical phenomenon which cannot be explained on the basis of the classical physics rules and which is a strong evidence in support of the undulatory interpretation of the quantum mechanics. It consists in the passage of an *E* energy-possessing particle (e. g. an electron) through a *potential barrier*, that is a limited space region where the only potential energy *U* is higher than *E*. According to the classical physics the barrier should elastically repel the particle. The more the *E* energy is close to the *U* value and the thinner is the barrier thickness, the probability of a *tunnel effect* increases.

tunneling - since this would be independent on the temperature - but rather in last years it induced many researchers to reason about complex and alternative electron transfer mechanisms (the third chapter will show our results and our interpretation also about this topic).

In real RC samples fast recombination may occur just in Q_B quinone-depleted proteins, that is at very low Q_{10} concentrations (as in our measures shown in the third chapter), or in the presence of high amounts of inhibitors of the Q_A^- to Q_B electron transfer (e. g. herbicides).

On the contrary, the $P^+Q_AQ_B^- \Rightarrow PQ_AQ_B$ recombination depends on the temperature since it is a real chemical equilibrium involving the charge transfer from Q_B^- to Q_A, described by the thermodynamical constant L_{AB} (scheme 1.5 and equations below). This explains why charge recombination from $P^+Q_AQ_B^-$ generally provides a wider range of informations about the RC behaviour.

Nevertheless, a data fit treatment based on almost pure recombination from $P^+Q_AQ_B^-$ is meaningful only if the total Q_{10} concentration is at least five times higher than the RC concentration ($[Q_{10}] > 5*[RC]$). Otherwise, in lipidic systems as proteoliposomes for example, further parameters regarding the polydispersity of the quinone concentration should be considered, since the hydrophobic quinone freely redistribute itself in the bilayer[139].

The larger stabilization of the charge on Q_B^- rather than on Q_A - the reasons will be explained in the following paragraph - allows that, in absence of inhibitors of the electron transfer $P^+Q_A^- \Rightarrow P^+Q_AQ_B^-$, the kinetics of the recombination involving the Q_B ubiquinone is influenced by some parameters regulating the ubiquinone exchange at the Q_B site. For these reasons the kinetics of the process results to be dependent on the quinone binding equilibrium, not only for the time scale following the light absorption inducing the charge separation but even for the time scale before the light pulse, in terms of Q_B site occupancy when the first photon arrives. Such a dependence can be rationalized by the previous scheme1.5[139].

On the basis of the above reported scheme it is possible to define the binding constants to the Q_B site both for the light-adapted ($K_{bind} = k_{QB}/k_{BQ}$) and for the dark-adapted states ($K^*_{bind} = k^*_{QB}/k^*_{BQ}$).

In order to precisely relate our experimental measurements of charge

recombination to the kinetic scheme above mentioned it is necessary to remember that they have been performed to determine:

1) the thermodynamic parameters of the Q_A ubiquinone binding in RC-containing liposomes (par. 3.1);
2) the thermodynamic parameters of the cardiolipin binding to RCs reconstituted in micelles and proteoliposomes (par. 3.2).

Every RC used was depleted of the majority of the Q_{10} content; consequently only some quinones strongly bound to the Q_A site are present. Hence the experimental traces could be fitted by monoexponential curves (RC micelles) or biexponential with predominant fast decay (k_{AP}), since even at low contents the quinone may redistribute itself into the liposome bilayer.

1.4.4.1. The Q_B^- state stabilization.

The secondary quinone plays a central role in exporting reducing equivalents from the RC. The Q_B binding pocket and its function in electron and proton transfer are very sensitive targets of structural modifications, both of internal and external origin.

Then the energetics of the Q_B site can be modulated either by (slight) internal structural perturbations as site-directed mutations or by factors affecting the protein environment, that is the lipid bilayer. The following discussion will focus only on the first topic, the second being postponed to the dedicated par. 1.5.

Although the primary and secondary quinones are located at approximately equal distances from the membrane surface (~15 Å), and are chemically identical in *Rb. sphaeroides,* it has already been stressed in previous paragraphs that their properties are quite different, certainly due to the microenvironment existing within the protein.

While Q_A works on one-electron chemistry, Q_B can be reduced by two electrons as well. Moreover, the highly polarizable environment shifts the redox potential of Q_B to more positive values[143, 144] and makes the cofactor configuration $Q_AQ_B^-$ more stable than $Q_A^-Q_B$. In contrast to Q_A, the ubiquinone Q_B keeps dynamic cooperation with the

photosynthetic membrane and the aqueous bulk phase: it takes up protons from the cytoplasm and exchanges QH_2 for Q in the membrane.

The optimal two-electron gate functioning of Q_B is set by several factors such as large thermodynamical equilibrium constants for the $Q_A^-Q_B$ to $Q_AQ_B^-$ electron transfer (L_{AB}), large equilibrium constants for the Q_B quinone dissociation (K_Q), saturating Q_B concentration in the quinone pool ($[Q_B]$), intact proton delivery pathways, and fast quinone/quinol turnover. Any of these parameters can be modified by mutation of the relevant amino acids (besides that by specific lipid-protein interactions, see par. 1.5.2). As an example, the mutation of the Ile L229 to Met displaces the quinone ring at the Q_B binding site and alters the orientation of the substituents as well: the sigma backbone branching of Ile allows a more favourable energetic stabilization of the Q_B ubiquinone than that of Met.

Moreover, electrostatic and mutational effects can be propagated over large distances through salt bridges of acidic and basic residues of amino acids, probably with the contribution of water molecules, as it has been already proposed[145]. Similar interactions between distant sites can lead to the rearrangement of residues in contact with the Q_B site, and also to the relocation of the charges around Q_B, therefore modulating the energetics of charge stabilization for the $P^+Q_AQ_B^-$ state.

Therefore the energy stabilization of the flash-induced electron on Q_B is critical for an efficient electron transfer through the RC. Consequently, the energetics of the $Q_AQ_B^-$ state can be determined from the kinetic analysis of the $P^+(Q_AQ_B)^- \rightarrow PQ_AQ_B$ charge recombination.

1.5. Lipid-protein interactions for the Reaction Centre.

1.5.1. Structural details of the lipid-RC interactions.

In this paragraph the specific lipid-protein interactions in the bacterial Reaction Centre (RC) membrane protein will be examined in detail.

Although RC is structurally well characterized (par. 1.4), being one of the most actively studied integral membrane proteins, little is known in detailed structural terms about the problem of the protein interactions with its lipid bilayer environment. This is also the case for other integral membrane proteins that have been found to possess bound lipids and for which high-resolution X-ray structures are now available: many channel proteins and porins, electron-transporters, light-harvesting antenna complexes, bacteriorhodopsin, Ca^{2+}-ATPase[12, 41, 94].

Surprisingly, the first report of a lipid molecule strongly bound to the RC crystals from *Rb. sphaeroides*[15] (1999) occurred more than ten years after the first description of the protein high-resolution structure[106, 107] (1987).

In order to understand why it happened and to clarify the route leading to the discovery of lipids in protein structures it is useful to remember that in RC crystals both from wild-type and mutant strains of *Rb. sphaeroides* some surface electron density was firstly attributed to erroneous non-proteic fragments. These were detergent (DDAO), buffer and salt (phosphate and/or sulphate ions) or crystallization agent molecules[124,146], modelled in X-ray structural maps in such a way to cover the area that subsequently has been attributed - after further analyses and with no doubts - to the lipid cardiolipin.

By this way, as the quality of the diffraction data collection improved this experimental misunderstanding was solved.

In 1999 an X-ray structure of an Ala to Trp (AM260W) mutant[39] of the photosynthetic RC from *Rhodobacter sphaeroides* was discovered to contain a lipid

---

39. A keto oxygen of the head group of the ubiquinone at the Q_A site forms a hydrogen bond with the backbone amide nitrogen of residue Ala M260: the reason why this residue was mutated to Trp is to cause exclusion of the Q_A ubiquinone from its pocket and to prevent electron transfer up to the Q_A site, blocking it at the $P^+\Phi^-$ state. X-ray data confirmed that AM260W RC lacks the Q_A quinone and that changes in structure were confined only to the vicinity of the mutated residue.

molecule bound to the hydrophobic intramembrane surface of the protein[40,[15]](fig. 1.38). It was the only feature not attributable to the protein in the electron density map and very reliably it could be modeled as a diphosphatidylglycerol (or cardiolipin, CL, whose structure is reported in fig. 1.8) molecule - better than other lipid or detergent structures -, since the lipid headgroup and adjacent parts of the four acyl chains were clearly resolved (fig. 1.22).

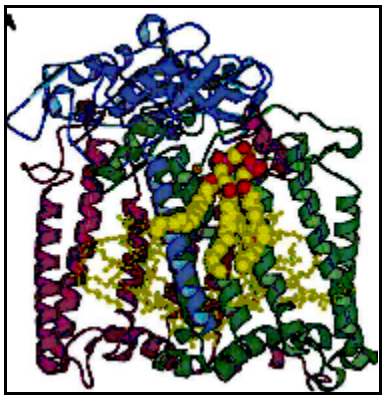

Figure 1.38.
The *Rb. sphaeroides* AM260W mutant RC containing one bound CL molecule (*up*, cytoplasmic domain; *down*, periplasmic domain).

The diffraction data collected over the resolution range 30.0 - 2.1 Å showed that the lipid-protein binding involves:

- a combination of ionic and hydrogen bonding interactions between the RC polar moieties (charged and polar side chains of many amino acids, the protein backbone and bound water molecules) and the CL headgroup;
- Van der Waals interactions between the lipid tails and the electroneutral intramembrane surface of the protein.

The CL molecule occupies a depression in the intramembrane surface of the RC[15]: it is located between the single -helix of the H subunit and the transmembrane -helices C and D (or 3 and 5 respectively[41]) of the M subunit (green ribbons in fig. 1.39), on the cytoplasmic face and in a region of positive potential of the protein (fig. 1.29). At the periplasmic side of the membrane these α-helices are in Van der Waals contact with one another; on the contrary at the cytoplasmic side, in the region that binds the lipid head group, the C and D helices splay apart due to interdigitation of the E α-helix of the L-subunit (magenta ribbon in fig.1.39), which prevents direct interactions between them. The E α-helix of the L-subunit forms an overhang below which the CL binds: by this way, though indirectly, CL is in contact with all the three subunits L, M and H.

40. As an example, when the RC/ LH-I complex of *Rps. viridis* was solubilized from membranes by Triton X-100, CL was found to be the most abundant of the remaining lipids, reflecting a high affinity of CL for the proteins of the membrane.

The CL headgroup is approximately 15 Å far from both Q_A and Q_B sites, being a little closer to the Q_A site[56].

Three direct interactions were observed between phosphate oxygens of the CL headgroup and: a) side chains of Histidine (His) M145 (E helix of the M-subunit) and Arginine (Arg) M267 (D helix of the M-subunit); b) the backbone amide of Lysine (Lys) M144 (E helix of the M-subunit)[15]. The former two amino acids are located at a distance of 2.8÷3.5 Å from the counterpart, the P_A phosphate; the third instead is slightly farther from the P_B phosphate.

CL phosphate groups show also indirect interactions (mediated by four crystallographically-defined water molecules) with:

- Lys M144 and Trp M148 (P_B phosphate), via two water molecules;
- residues Arg M267, Trp M271, Tyr H30 (P_A phosphate), by means of two additional water molecules.

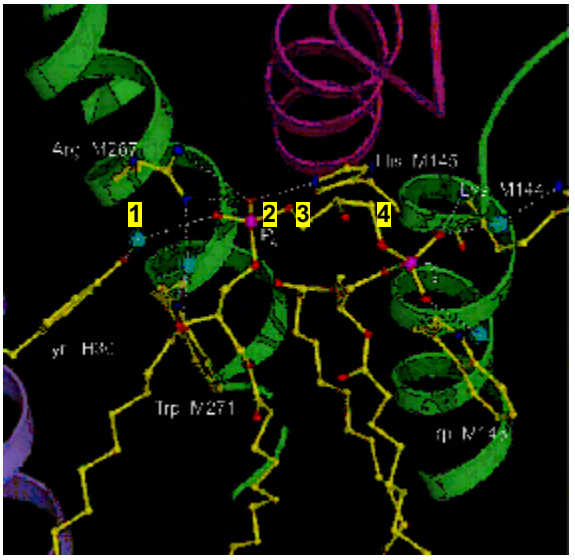

Figure 1.39.
View of the bonding interactions between the cardiolipin head-group and the surrounding protein, as revealed by the structural model of the AM260W Reaction Centre. Cardiolipin (CL) and bound amino acid residues are shown in stick format (cpk colours: blue for nitrogen, red for oxygen and violet for phosphorus atoms), while crystallographically defined water molecules are shown as blue spheres. CL connects the D and E membrane-spanning helices of the M-subunit (green ribbons, left and right respectively) at the point where they are separated by the C membrane-spanning helix of the L-subunit (magenta ribbon, top centre). The acyl chain numbers for CL (black on yellow background) are the same as in fig. 1.8.

The lipid fatty acid chains sit along largely hydrophobic grooves in the irregular transmembrane surface of the protein, interacting over a wide area, with the strongest contacts occurring at the top of the chains 3 and 4 and toward the middle of the chains 1, 2 and 4 (fig. 1.39). The result is that the lipid headgroup and the upper parts of the chains are immobile, and consequently well resolved in the electron density maps, whereas the end of the chains are mobile and disordered and do not appear in the X-ray structure. By this way, from the above descriptions the bound CL could be well considered and counted as a non-annular surface lipid[79] (par. 1.3) playing critical roles in the structural cohesion and in several functional processes (par. 1.5.2).

The specificity of the binding site for CL presumably follows from its unusual four-chain structure and from its small head group. In spite of such a restriction also other hydrophobic molecules can bind to this site since other crystal structures of the *Rb. sphaeroides* RC show detergent molecules in this groove, precisely in the location corresponding to the deeply buried fourth chain of CL.

Contrary to *Rb. sphaeroides*, the published X-ray structures of the *Rps. viridis* RCs did not include a modeled CL. Several of these however supposed the presence of a modeled sulphate ion in a position approximately equivalent to that of the P_A phosphate group of CL in the AM260W structure of *Rb. sphaeroides*: in the perspective of recent literature data however this hypothesis has been demonstrated to be wrong. In addition some models include also water molecules closely matching the CL head group position on the AM260W structure[147, 148, 149]. However, no detergent molecules have been modeled in the region where the acyl chains of CL might be expected to be located[150].

In *Rb. sphaeroides* RCs the acyl chains of CL can vary in length and in degree of unsaturation[151]; also environmental changes can alter their composition[40]. The most common acyl chain has 18 carbon atoms and a single unsaturated bond (18:1), but about 20 % of the total acyl chains are fully saturated (par. 1.2.4). The methyl ends of the four acyl chains are not resolved in the X-ray electron density (then they were modelled only for the first 9 ÷ 15 carbon atoms), since they are mobile in the crystals and therefore disordered; also double bond positions cannot be determined from the electron density with sufficient certainty[15].

The same crystallographic data attributed to CL have been found also in other structures published subsequently, derived both from mutant and wild-type *Rb. sphaeroides*[152]. Hence it is certain that the detected CL is not present as a consequence of any particular mutation.

There is a large variability in the extent and completeness of the electron density feature from data set to data set . This may be explained by the substoichiometric binding of the lipid to the detergent-purified RC and hence to the differences in the occupancy of the CL binding site[41], though the *Rb. sphaeroides* type selected and the protocols of bacterial cell growth and of protein isolation and purification were essentially the same in each case[82].

A significant factor of variability can be for example the chemical precipitant used for the RC crystallization, though actually on the basis of the experimental conditions adopted, this is considered unlikely by many researchers[15, 82]. Another explanation is that low-resolution diffraction data (up to 30 Å) are particularly employed for the observation of surface features such as bound lipids, favouring by this way those data sets including "rough" terms.

Another intriguing feature that emphasizes the CL role in lipid-protein binding is the strong conservation of the residues interacting with the phosphate lipid head group P_A across many available sequences of purple bacterial reaction centres (discovered by protein sequence alignments)[150]. These residues may therefore constitute a conserved site for the binding of CL on the RC surface.

In the RC from *Rps. viridis,* for example, the amino acids corresponding to those interacting with CL in the RC from *Rb. sphaeroides* (around Arg M267) probably form part of a cluster of 24 residues electrostatically coupled to the Q_A ubiquinone[153]. The CL binding site is not very far from the Q_A site (about 15 Å[56]) in both the RCs: the same feature could be expected also for the *Rb. sphaeroides* RC.

Just in relation to the existing similarities between reaction centres from different bacterial strains, it has been supposed the presence of a lipid binding site for phosphatidylethanolamine (PE) - present in the RC from *Thermochromatium (Tch.) tepidum* - also in the RC from *Rb. sphaeroides*[150], though not yet discovered. In this purpose, extra-protein electron density seen in the RC from *Rps. viridis* and attributed to a sulfate ion and LDAO molecules could well correspond to a lipid such as PE[154].

Only sequence comparison studies can allow comparisons among RC structures from different bacteria: for example they can help to draw interesting parallels on CL binding, whose completeness and extent have been found very variable.

In the RC from *Tch. tepidum* PE occupies a deep groove in the protein surface formed by the H-subunit transmembrane α-helix and the α-helices of the L- and M-polypeptides. The head-group phosphate is bound to the residues Arg H31 and Lys H35; the fatty acyl chains are not located within grooves on the RC surface but, rather, interact with the exposed chains of two bacteriochlorophylls and one quinone molecule. The PE location lies on the opposite side of the H-subunit α-helix in relation to the site occupied by CL in the *Rb. sphaeroides* complex (fig. 1.39).

Interestingly, the basic residues Arg and Lys are not conserved in the *Rb. sphaeroides* RC, where they are Gln and Met, respectively: these substitutions significantly change the potential of the protein surface in the region adjacent to the PE head-group from positive - favourable for the interaction with the lipid phosphate group - to largely electroneutral. In spite of this, some diffraction data sets of *Rb. sphaeroides* RC have shown an elongated and unattributed density feature in a position approximately equivalent to one of the PE acyl chains[82].

Reciprocally, the CL included in models of the *Rb. sphaeroides* RC was not detected in the structure of *Tch. tepidum* complex, but it could be a component of the membrane. One molecule of detergent β-octylglucoside was found in a position which corresponds to the acyl chain 1 of CL in the *Rb. sphaeroides* RC[155], making extensive contacts with the α-helix of the H-subunit[15, 150].

Similarly the residues engaged in bonding interactions with the head-group of CL in the *Rb. sphaeroides* RC are conserved in the *Tch. tepidum* complex, including the main bonding residues Arg M267 and His M145.

Even the enhanced thermal stability of the *Tch. tepidum* RC could be attributed, at least partly, to strong interactions with the surrounding membrane lipids[155]: three arginines residues (L71, L84 and M104, not present in RCs from mesophilic bacteria) on the protein surface are in a suitable position to interact with the headgroups of lipids on the periplasmic side of the membrane.

Few years after the discovery of the CL molecule (2002) another diffraction structure of a non-mutant RC from *Rb. sphaeroides* (at a resolution ranging from 30 to 2.55 Å) showed three lipid molecules well resolved in the electron density maps and lying on the protein surface. They were phosphatidylcoline (PC) and glucosylgalactosyl diacylglycerol (GGDG), a glycolipid, in addition to the already known cardiolipin (fig.1.40 A, B)[60]. The two last discovered lipids were not found in the previous RC mutant structures containing CL[15] presumably because the mutations caused significant changes involving the lipid binding sites.

As already pointed out for the first CL-containing structure, in the earlier models of the RC all the subsequently revealed lipid-including regions have been erroneously identified as arising from bound detergent molecules[98, 124, 146]: this was due to the low

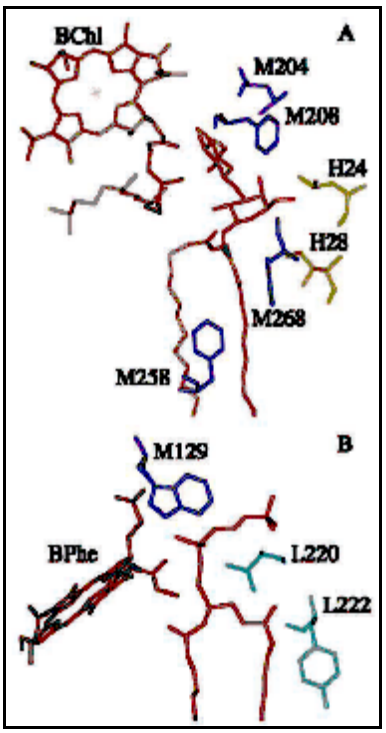

Figure 1.40.
(A) The glycolipid (red) binds near the active bacteriochlorophyll monomer (brown) and nearby amino acid residues of the M subunit (blue) Leu M204, Phe M208, Phe M258, and Trp M268, and the H subunit residues (yellow) Leu H24 and Ile H28. (B) The phospholipid phosphatidylcholine (red) binds near the L subunit residues (light blue) Val L220 and Tyr L222, and the M subunit residue Trp M129 (dark blue), and the inactive bacteriopheophytin (brown).

resolution of the diffraction data. For example, GGDG was previously modeled as arising from three dodecyl dimethylamine oxide (DDAO) molecules; PC was modeled as resulting from only one DDAO molecule, although the interpretation of this region was strongly influenced also by the positioning of the phytyl and isoprenoid chains of the cofactors.

As for the previous RC structure containing CL, the extended features of electron density not attributable to the protein could be well fitted by this newly revealed lipid molecules; the presence of the three lipids was also confirmed by Matrix-Assisted Laser Desorption Ionization (MALDI), a particular type of mass spectrometry (see below). The overall structure of the protein was very similar to previous models of RC from *Rb. spharoides*, with no significant alterations of the cofactor organization or in the interactions between cofactors and protein side chains. The three lipids are located in the hydrophobic region of the protein surface, interacting mostly with apolar amino acids, particularly aromatic ones and leucines. They belong to surface zones partially disordered and consequently weakly resolved in other electron density maps previously obtained.

While the CL polar group is far from any of the RC cofactors (at least 15 Å from Q_A and Q_B sites) the other lipids are in close contact with them (fig. 1.39).

GGDG interacts primarily with the cytoplasmic side of the membrane, between the M subunit and the α-helix of the H subunit: its disaccharide moiety lies at 3.5 Å from the active bacteriochlorophyll monomer (B_A), for which it acts as a shield from the solvent in contrast to a much greater exposure evident in the case of the inactive bacteriochlorophyll monomer B_B (fig. 1.40 A). The rings of the disaccharide moiety are located within 4.5 Å from the esters of the E ring and 5.5 Å from the conjugated macrocycle of B_A; moreover the glycolipid acyl chains make contact with the isoprenoid

tail of the Q_A ubiquinone (not shown in fig.1.40 A) and with Phe M258.

PC is situated toward the cytoplasmic side of the protein, at the interface between L and M subunits, with the phosphate group lying 6.5 Å from the inactive bacteriopheophytin Φ_B (fig. 1.40 B). The ring of the secondary quinone Q_B is located 9.5 Å from the lipid but the isoprenoid chain is in contact with it (not shown in fig. 1.40 B)[60].

Therefore it is clear that both GGDG and PC, as well as CL, have the role of surface non annular lipids, but their locations are very different from the one usually reported for lipid molecules identified in other protein crystal structures[41].

For all the three lipids the fatty acid chains make contacts with predominantly apolar residues. Nevertheless, whereas CL is largely exposed on the protein surface and tightly binds it by means of ionic interactions between the phosphate groups and nearby charged residues (as above mentioned), the interactions involving the other two lipids are mainly hydrophobic since they are more buried in the protein. In particular, GGDG and CL are positioned apart, with a separation of about 30 Å between the CL phosphate and the saccharide moieties.

Moreover, in the structure containing all the three lipids the electron density of CL is notably more extended than that of the other two lipids because of the presence of four acyl chains instead of two, making CL the most easily distinguishable lipid among the three.

Finally, it should be remembered that the electron density for the polar group of each lipid is the best resolved region; on the contrary the resolution is particularly weak for the hydrocarbon chains, which have limited interactions with the protein and then are less hindered in motion, resulting in less fixed and not well distinguishable positions.

Always in relation to the diffraction data, the relatively better resolved lipid tails appear as oleyl chains (16:1) rather than shorter chains, although precise hydrocarbon lengths and chemical identities of the lipid polar heads cannot be uniquely defined.

For example, the electron density near the Q_B site can be modeled as either PC or PE; also the glycolipid is identified at best as a lipid possessing a disaccharide moiety, the remaining experimental deductions are proposed on the basis of other informations such as mass spectrometry (MS) data and the membrane lipid compositions of *Rb. sphaeroides* (par. 1.2.4).

MS data show some weak traces due to dioleyl-PE, in addition to PC well pronounced ones: probably both phospholipids are present at the site, with PC being significantly more abundant.

GGDG and CL are recognizable by laser mass spectrometry. Nevertheless the glycolipid, since it is not charged and then the amplitude of its peak would be intrinsically weak, may be well detected only as sodium-adduct form, for which the peak is higher. Such an experimental measure requires the use of increasing concentrations of sodium iodide and preferably also of a commercial standard as digalactosyl diacylglycerol. The anionic CL instead has a higher molecular weight and therefore is less easily volatile, shows a weak peak. Based on the remaining peaks other lipids may also be present but in much smaller amounts than those already identified[60].

Lipid-associated electrostatic interactions could be well related to electron transfer rates involving the RC cofactors: each lipid in a peculiar way may contribute to the difference in energetics between the two branches of cofactors that is primarily responsible for the asymmetry of electron transfer (par. 1.5.2).

The distance of about 30 Å between the polar groups of CL and GGDG (saccharide groups) is consistent with a bilayer-like organization. It confirms the hypothesis of the presence of an “inner shell” of lipids around membrane proteins critical for membrane functions. In fact, interactions with other proteins aside, the intramembrane surface area of the RC has been evaluated to be such that it could associate with about 30 lipids of the “first shell”[12, 52, 89, 156] (par. 1.3).

Nevertheless, this does not mean that CL, GGDG and PC should be annular lipids - which usually are weakly bound with respect to non-annular ones and then more difficult to detect in crystal structures (par. 1.3.1) -. Simply, most of the times the two lipid classes coexist one close to the other[41].

The knowledge of the position of the bound lipid polar groups on the protein surface is a little but useful step in approaching the exact determination of both the bilayer arrangement and its thickness around the protein itself. Since identifying the ends of the transmembrane -helices in membrane protein structures is often very hard, other right ways to determine the bilayer thickness and position in relation to integral proteins are based on informations such as: the position of amphipatic amino acids (Trp, Tyr) “floating” at the polar/apolar bilayer interface; the position of charged aminoacids

(Lys, Arg), “snorkelling” from the apolar to the polar region with their charge (par. 1.3.2.1)[41].

The photosynthetic RC contains a relatively large number of Trp residues, most of which located in the transmembrane region of the protein (fig. 1.22). They are divided in two girdles exposed to the bilayer lipids: 4 Trp residues are on the cytoplasmic side of the membrane, while 16 are on the periplasmic surface, many of them serving to anchor interhelical loops into the membrane surface. Assuming that the glycerol backbone region of the bound CL molecule defines the cytoplasmic boundary of the bilayer hydrocarbon core, the Trp residues of the cytoplasmic girdle result to be located just within the hydrocarbon core; if this is considered true even for the “periplasmic Trp girdle” it gives a hydrophobic thickness of about 28 Å for the RC, in comparison with an average of 32 Å for a lipid bilayer (par. 1.3.2.1).

In the case of RCs, also the charged Glu-106 residue of the L subunit contributes to define the cytoplasmic surface of the protein (fig. 1.22)[41].

On the basis of these informations and reflections, the RC-bound lipids have been suggested to adopt very unusual orientations in the bilayer: PC lies almost parallel to the membrane surface, while GGDG is buried with its head group close to the centre of the bilayer.

An increased knowledge about the molecular interactions between membrane proteins and specific lipids - this is what we are trying to reach in the case of the CL/RC interaction through the work collected in this thesis - generally stimulates a high number of hypotheses for the lipid role in the structural and functional integrity of proteins *in vivo.* These models need to be challenged by complementary techniques, among which site-directed mutagenesis is one of the most powerful and informative: the use of mutant RCs from *Rb. sphaeroides* allows to examine the effects of individual lipid modification on the protein behaviour.

1.5.1.1. Calorimetric studies carried out on mutated RCs.

A relatively simple experimental way to study the specific molecular interaction between the bound CL and the purple bacterial RC is to disrupt it and then to examine

the structural and functional consequences.

This has been performed by a double and separate site-directed mutagenesis on two basic and highly conserved residues directly involved in the interactions between RC and the lipid headgroup: Arg M267 and His M145, changed respectively to Leucine (Leu, L) and Phenylalanine (Phe, F), obtaining the mutants labelled as RM267L and HM145F[56]. Absorbance spectroscopy is very sensitive to changes in the arrangement of the RC-cofactors matrix; this technique showed that the mutagenesis treatment did not affect neither the rate of photosynthetic membrane growth (in terms of the RC expression level) nor the X-ray crystal structure (determined to a resolution of 2.8 Å) and the typical functional properties of the protein[56].

As a result of the mutations, only the RM267L mutant RC no longer bound detectable amounts of CL at its usual site. At this place there was another electron density feature, too intense to be a water molecule and having a tetrahedral form, modelled hence as a phosphate ion, as in the previously collected and less resolved crystal structures.

In spite of its structural integrity, the thermal stability of the RM267L mutant protein - examined by Differential Scanning Calorimetry (DSC) measurements - was compromised, part of the RC micelle population showing an approximately 5 ˚C decrease in melting temperature, from about 55 to 50°C. This observation suggested that CL binding contributes significantly to the thermal stability of the protein complex, at least when in detergent micelles (the system being the subject of the study)[56].

DSC and Circular Dichroism (CD) studies revealed that the thermal denaturation of membrane proteins, contrary to that of the water-soluble ones, does not involve the unfolding of membrane-spanning α-helices. Rather, the enthalpy change - smaller for membrane proteins of comparable molecular weight[157] - mainly reflects loss of secondary and tertiary structure in extra-membrane domains, including loops that connect α-helices, and perhaps the loss of packing interactions between α-helices[157].

Therefore, in the unfolding processes occurring when membrane proteins are thermally denaturated, CL assumes the structural role of stabilizer for the interactions between adjacent transmembrane α-helices in a surface region where there are no direct protein-protein contacts. In that, CL behaves as many other non-annular lipids located on the surface of proteins[79].

It can be added that the RM267L mutant RC exhibited a higher ease of chromatography purification than the other one (HM145F), suggesting a decrease in the tendency to the association with other photosynthetic proteins[56]. Hence the former mutation further revealed to be the most important in affecting the CL binding between the two. This fact indirectly confirms that CL behaves like a structural "glue", both inside the RC and between different protein complexes, in the latter case through a mechanism still unknown.

Moreover, the RM267L mutant protein shows a single endothermic DSC peak, instead of two overlapping peaks detected for the wild-type and the HM145F mutant, centred in both cases at 47÷48 °C and about 55 °C. In thermograms of membrane proteins two components mean that thermal denaturation involves the unfolding of distinct protein domains with different melting temperature values (T_m), as in the case of cytochrome *c* oxidase[56].

Temperature differences of 7÷8 °C are well consistent with the magnitude of the effects observed in calorimetry experiments in which lipids are added or removed from membrane proteins (e.g. Ca^{2+}/Mg^{2+} ATPase or cytochrome *c* oxidase[56]). It stimulated different hypotheses on the DSC thermograms coming from wild-type and HM145F mutant RCs: the most reliable is that they are made of *two heterogeneous populations* undergoing the same unfolding process, but with different values of T_m. The population becomes unique only after the RM267L mutation.

Possible source of heterogeneity are the partial occupancies of the Q_B binding site for ubiquinone and that for cardiolipin. The former is unlikely to be relevant to these observations since it affects the wild type as well as the two mutant RCs. The latter site occupancy instead, involving only the M267 residue (the HM145F mutant RC retains its CL molecule), would allow to attribute the higher transition temperature - absent for the M267 mutant - to an RC population stabilized by the binding of cardiolipin. On the contrary the lower temperature transition would correspond to RC molecules without cardiolipin bound.

Moreover, DSC thermograms of wild-type RCs in the presence of added cardiolipin produced a narrower peak indicating lower sample heterogeneity and so confirming the above mentioned hypothesis. However, this was only a preliminary result and left open the possibility that the observed behaviour arises from non-specific effects,

such as binding of cardiolipin to sites on the protein surface other than the already described crystallographic one[56]. In relation to it, among the results of this thesis and on the basis of our experimental data, in par. 3.2 will be demonstrated the existence of additional weaker binding sites for CL on the RC surface, in addition to a strong one. This latter holds a single CL molecule and with high probability concides with the site detected by crystallography.

Experimentally the size of the destabilizing effect of the RM267L mutation resulted to be of the same order of magnitude as that seen when the lipid environment of a membrane protein is altered (*direct effect*) or when a change is made that destabilizes part of the protein structure, on the cofactors or on the backbone arrangement (*indirect effect*); this latter effect existing for every protein.

The HM145F mutation, with no evident effects on the DSC traces or on the spectroscopic and biochemical RC properties, presumably does not affect the affinity of CL for its binding site, maintaining a DSC profile characterized by two component, albeit with some small variations in the T_m and ΔH_{cal} measured values[56]. The explanation of such a behaviour may be found in the extent of the bonding interaction between each side-chain specifically mutated and the adjacent CL head group.

In the case of His M145 this binding involves a single hydrogen bond between the nitrogen atom of the His side chain and the oxygen of the lipid P_A phosphoryl group. For the Arg M267 residue instead both the terminal -NH moieties are within hydrogen bond distance from a cardiolipin oxygen of the P_A group (2.8 and 3.2 Å), while one of these -NH is also in contact with a crystallographically defined water molecule. This water is in turn within hydrogen bond distance from two carbonyl oxygen atoms at the top of the lipid acyl chain 1 and 4 (fig. 1.39).

Thus it seems feasible that the loss of a single hydrogen bond donated by His M145 would not weaken the CL binding to the same extent as loss of the complex network of interactions involving Arg M267. So the stabilizing influence of the lipid results to be seriously compromised only for the RM267L mutant RC, not showing any detectable CL amount[56].

1.5.2. Functional consequences of the lipid-RC interactions.

Although “photographed” very precisely at a molecular level, actually the lipids found in the RC structure were not related to any effect on the electron transfers among the protein cofactors. Trying to understand the bound lipid influence on one of these measurable properties of the RC, the charge recombination process (illustrated in par. 1.4.4) has been the major challenge of the experimental work collected in this thesis.

Therefore detailed implications of the lipid CL on the protein functions will be discussed in dedicated paragraphs of the Results Section (see third chapter). Now only brief considerations about experimental consequences of the structural data previously shown will be introduced.

1.5.2.1. Consequences on the electron transfer between cofactors.

In spite of the almost perfect simmetry displayed by the two RC branches of cofactors (par. 1.4.1) only one branch is active in the electron transfer process: extensive characterization of mutagenesis modified RCs has led to the general conclusion that this asymmetry is largely due to differences in the energetics of the two possible pathways[158]. Explanation models have been proposed suggesting a variety of interactions between the cofactors and the protein environment: however, alterations of even a significant fraction of the amino acid residues surrounding the cofactors caused only a limited activation of the second branch[159].

Therefore the asymmetric presence of the lipids on the protein surface suggests that lipid-cofactor interactions may represent the resolutive contribution to the establishment of energetic differences between the two branches[60] (fig. 1.40 A,B).

The bound glycolipid GGDG shields the active branch bacteriochlorophyll (B_A) from water, producing a relatively hydrophobic environment; the inactive one (B_B), in contrast, with no bound lipids, is found to interact with solvent molecules through polar interactions. Then a preferential hydrophobic environment should have a role - maybe slight - in the reduction of B_A; the electron transfer from the bacteriochlorophyll dimer (P) to the bacteriopheophytin (Φ_A) through B_A (par. 1.4.2) should experience some

reorganization energy and so become optimized.

Another contribution to the asymmetry is due to the presence of PC only near the inactive bacteriopheophytin (Φ_B): its negatively charged phosphate could establish an electrostatic interactions resulting in a destabilization of the reduced state Φ_B^- and hence making the electron transfer to this cofactor energetically unfavourable, compared to the active branch.

It seems that a hydrophobic environment near Φ_A has the effect of stabilizing Φ_A^-, maybe in relation to the fact that free charges in low dielectric and apolar environments are very unfavoured, representing then a necessary strategy; on the contrary, polar environments around Φ_B have more complex effects and could be destabilizing for charged cofactors (Φ_B^-).

1.5.2.2. Consequences on the Q_A^- state stabilization and functional linkage Q_A-Q_B.

Based on structural data, no cofactor results to be directly exposed to the protein surface and in particular the Q_A site is known as made of a highly hydrophobic pocket (par.1.4.1). Nevertheless it has been discovered that lipid-protein interactions around the Q_A site - at present essentially represented by the binding of the X-ray detected CL - strongly influence properties of the Q_A ubiquinone such as the mid-point redox potential of the Q_A/Q_A^- couple ($E_m(Q_A/Q_A^-)$)[160].

Since then the role of characteristic phospholipids of native membranes (PC, phosphatidylglycerol, PG, and CL) in the energetics of the acceptor quinone side of *Rb. sphaeroides* RCs was deeply studied by many researchers: it is also the central topic of this thesis.

As an example, in chromatophores (native membrane vesicles containing RCs)[131] and in RCs incorporated in liposomes[161] $E_m(Q_A/Q_A^-)$ was found to be pH-dependent, contrary to RC/detergent micellar solutions[131]. An increased interaction between Q_A^- and its binding pocket was reported in both cases and interpreted as an effect of the small effective dielectric constant[162].

As a consequence, it seems not at all strange that addition of CL to isolated RC micelles from *Rb. sphaeroides* lowers the $E_m(Q_A/Q_A^-)$ value by 30÷40 mV, bringing it

more in line with that measured in chromatophores (- 45 mV[131]). The lowering of the $E_m(Q_A/Q_A^-)$ value was indirectly detected by delayed fluorescence measures as an increased emission yield from the the $P^+Q_A^-$ state.

On the same sample the addition of 100 μM CL caused also two other effects related to the Q_B site, confirming the already known "functional linkage" between Q_A and Q_B sites[163, 164]. It has been suggested that the Q_A pocket residue methionine M218 might have a role in this cooperative inter-site linkage, since it is in contact with the edge of the Q_A head group and could conceivably transmit steric interactions to the Q_B site via histidine M219 and the iron-histidine complex that binds both quinones (fig. 1.34).

The above mentioned CL effects on the Q_B site are the following.

(***a***) A 3-fold slowing of the charge recombination process from $P^+Q_B^-$. Since the major route for recombination is via the $P^+Q_A^-$ state this is indicative of a larger equilibrium constant ($L_{AB,}$ see scheme 1.5) and of a more negative standard free energy difference ($\Delta G^\circ_{AB} = -RT*\ln L_{AB}$, see below) for the first electron transfer $Q_A^-Q_B \rightarrow Q_AQ_B^-$. This slowing may be also related to a CL-induced decrease in the rate of the first electron transfer from Q_A^- to Q_B ($k_{AB}(1)$): significant decreases have been already measured for PC proteoliposomes to which were added increasing amounts of PG[165] - the anionic phospholipid with two acyl chains-analogous of CL (par. 1.2.1) -. At the same concentration of CL, PG had a qualitatively similar effect but with smaller magnitude (slowing less than 2-fold); PC has no effect at all.

(***b***) An increase from 70 % to more than 90 % of the relative amplitude of slow phase of the charge recombination, when experimental traces are fitted with biexponential curves (in par. 1.4.4 this amplitude has been identified as S). This indicates a substantial increase in the occupancy of the Q_B site.

All these consequences can be brought back to a 30÷40 meV destabilizing effect of CL - and of other anionic phospholipids such as PG - on the free energy level of the $P^+Q_A^-$ state, resulting in an increase of the free energy drop from $P^+Q_A^-Q_B$ to $P^+Q_AQ_B^-$[163]. In turn this may be due - at least partly - to the double negative charge of the CL bound to the protein surface, causing an electrostatic repulsion with Q_A^-. This topic will be widely

discussed in par. 3.3.

It is interesting to note that the destabilization effects can be detected and studied also by other experimental techniques such as kinetic spectroscopy, through charge recombination measures. It is just by such an experimental approach (par. 2.3, 2.4) that we collected many data about the influence of the CL binding on the RC: our results will be exposed in the third chapter.

For the sake of completeness and in order to draw more reliable conclusions about energy differences between the Q_A and Q_B ubiquinones, also the lipid effect on the $P^+Q_B^-$ state should be taken into account: it will be done in the next paragraph, but it is useful to anticipate that it is quantitatively smaller than that on $P^+Q_A^-$ [163, 165], also because of the lower absolute free energy content (G°) of the $P^+Q_B^-$ state.

In addition it has been established that CL exerts its influence almost entirely on the Q_A site, the above reported effects on Q_B quinone being mainly "reflexes" of the activity on Q_A rather than real perturbations of the thermodynamic stability of the $P^+Q_B^-$ state. In fact the rate of the recombination from Q_B site and the site occupancy by quinone - as mutually related parameters of the fitting biexponential curve of the back reaction from $P^+Q_B^-$ (fig. 1.4) - are influenced by the CL addition only through the lipid effect on the energy level of the $P^+Q_A^-$ state[163].

The destabilization effect on the energy level of the $P^+Q_A^-$ state - e.g. quantified by the 30÷40 mV lowering in the $E_m(Q_A/Q_A^-)$ potential - is not large, but sufficient to account for a significant part of the larger Q_A^- to Q_B electron transfer free energy change (ΔG°_{AB}) seen in chromatophores and proteoliposomes compared to isolated RC micelles[17]. The fact that the Q_B ubiquinone has a lower free energy content than Q_A makes spontaneous electron transfers from Q_A^- to Q_B; of course the energy difference $\Delta G^\circ_{AB} = G_B^\circ - G_A^\circ$ is negative.

ΔG°_{AB} values strongly depend on the phospholipid environment: their trend appears to be logical if a possible destabilization effect on $P^+Q_A^-$ of CL and PG is considered. ΔG°_{AB} were found to be - 57 meV, -69 meV, -85 meV for wild-type *Rb. sphaeroides* RCs reconstituted respectively in detergent DDAO micelles (pH=8.0), liposomes (made of polar lipids extracted from chromatophores, then containing about 26 % of CL and 20 % of PG, besides PC and PE[17]) and chromatophores[17].

When the amount of polar lipids - and then of CL - of the reconstitution

environment surrounding the protein is increased, ΔG°_{AB} becomes more negative because of the increase of the energy amount of the $P^{+}Q_A^{-}$ state.

Though the destabilizing effect of CL has been widely thought as related to the CL molecule found in the X-ray structures, recent data showed that the effect is not influenced by the RM267L mutation above mentioned (causing the loss of the bound CL molecule), remaining very similar also in the mutant RCs. This suggests that CL may exert its effect on the Q_A site through other means, such as interactions at other specific, but weaker, lipid binding sites and intraprotein hydrogen bonding networks[165].

Moreover, the relatively small magnitude of the $E_m(Q_A/Q_A^{-})$ shift could also indicate a partial effect due to partial occupancy of the binding sites by one or more CL molecules[163]. These and other related topics, very important in this thesis, will be dealt with in the third chapter (par. 3.2 - 3.4).

Finally, it should not be forgotten the contribution to the study about the role of bound lipids given by several site-directed mutations more or less close to the crystallographic CL binding site[56, 165]. Some of these involved residues of the Q_A pocket (Ile M265, Met M218, Trp M252, fig. 1.34) and revealed that the mutation effects were largely localized to the thermodynamic properties of Q_A site, as it was expected, in spite of the concept of "functional linkage" between Q_A and Q_B previously explained[163].

1.5.2.3. Consequences on the Q_B^{-} state stabilization.

Another example of the influence of lipids on the functioning of RC cofactors is the possible presence of specific lipid molecules interacting with the Q_B pocket, facilitating the release of ubiquinol and the insertion of ubiquinone from the surrounding pool (par. 1.4.3).

Recently, the location of a CL molecule at the entrance of a proton delivery pathway on the yeast cytochrome bc_1 protein surface (partecipating to the cell respiration) - besides stabilizing the assembly of the complex - suggested a similar role for the CL bound to the RC from *Rb. sphaeroides*.

RC also has a ubiquinone reductase site (Q_B) implicated in the acquisition of protons from the aqueous phase: here the ubiquinone-10 is doubly reduced and doubly

protonated, forming ubiquinol. This site is connected to the extra-membrane surface of the protein via hydrogen bond networks[26, 27]. However, the CL bound to the RC is located about 15 Å from the Q_B site, so it is remote from the hydrogen bond networks that are proposed to connect the Q_B site to the aqueous phase, and therefore a role for this lipid as a local proton buffer seems unlikely[56].

Since, contrary to the Q_A ubiquinone, the secondary acceptor Q_B is surrounded by polar amino acids (par. 1.4.3) and then its semiquinone form Q_B^- can be better stabilized, the mid-point potential of the Q_B/Q_B^- couple is higher than that of Q_A/Q_A^- [132]. For the same reason only the Q_B site structure is sensitive to changes of environmental factors such as pH, ionic strength and even protein-protein and lipid-protein-interactions[127]: electron transfers[35, 36]- as well as other redox and protonation properties of the Q_B quinone[127]- resulted to be significantly perturbed by protein-protein and lipid-protein interactions when RCs are reconstituted in phospholipid vesicles.

The energetics of the $Q_AQ_B^-$ state can be determined from a kinetic analysis of the $P^+Q_AQ_B^- \rightarrow PQ_AQ_B$ charge recombination. This method has been applied to the study of the effects of bound lipids, such as CL and PG, on the stabilization of the Q_B^- semiquinone in different systems containing the RC. It has been done comparing the results from wild-type (herbicide-sensitive) and suitable mutant RCs, both belonging to the *Rb. sphaeroides* R-26 strain. Ile L229 was mutated to Met (LI229M mutation), creating an herbicide-resistant protein.

The difference in the free energy content of the Q_B^- form between the two RC types (called $\Delta\Delta G^\circ_{AB}$) was evaluated from the free energy variations associated to the $Q_A^-Q_B \rightarrow Q_AQ_B^-$ first electron transfer (ΔG°_{AB}) in the two cases; ΔG°_{AB} in turn derived from the life times associated to the biexponential decomposition of the kinetic traces (see par. 1.4.4 and ref. 17 for further informations).

$\Delta\Delta G^\circ_{AB}$ decreased in the following order: RC in micelles, then RC in vesicles (made of the polar lipid extracted from chromatophores, in proportions reported in the previous paragraph) and finally chromatophores. Since the lipid composition of the native membranes of the two strains is nearly identical[17], it revealed a greater flexibility of the lipidic environments in comparison with detergent micellar solutions in the adaptation to the perturbation represented by a site-specific mutation and in the arrangement of the

Q_B site during the protein reconstitution process. Hence the energetics of the first interquinone electron transfer - as well as that of the second one $Q_A^- Q_B^- \rightarrow Q_A Q_B^{2-}$ [36] - is affected by the lipid environment surrounding the Q_B pocket. The stability of both $P^+Q_A^-$ (see previous paragraph) and $P^+Q_B^-$ states exhibit dependence on the same lipid-protein interactions.

By this way steric and/or electrostatic lipid-protein interactions can modulate the energetics of the charge stabilization on Q_B^- even over large distances. It allows to couple the electron transport in the bacterial membrane to the metabolic processes - e. g. the lipid biosynthesis -, in order to satisfy precise survival requirements.

The same study showed that the dark recombination of the $P^+(Q_A Q_B)^-$ charge pair of RCs embedded in liposomes and in chromatophores was slower than in detergent micellar solutions (as mentioned in the previous paragraph). It indicated a better stabilization of the semiquinone electron on Q_B in vesicles and in native membranes compared to the detergent system. This trend is observed both for the wild-type and for the LI229M mutant, but in the latter case is less pronounced. The larger stabilization of Q_B^- in liposomes and chromatophores is confirmed by a faster second electron transfer $Q_A^- Q_B^- \rightarrow Q_A Q_B^{2-}$ ($k_{AB(2)}$) and by a stronger driving force associated ($\Delta G^\circ_{AB(2)}$) measured in the same environment[17]. This is also interesting because Q_B in RCs serves as a two-electron gate (par. 1.4.3.3).

As a further example of lipid-protein interactions, also glycolipids and squalenes strongly influence the kinetics of the bacteriorhodopsine photocycle in purple membranes, in a way very similar to RC[166].

1.5.2.4. Consequences on the ubiquinone binding at the Q_B site.

Further experiments performed on the same samples above illustrated (wild-type and LI229M mutant RCs) allowed to determine the quinone dissociation equilibrium constant ($K_{D,QB}$, par. 1.4.3.3) for RCs reconstituted in different systems[17]: different systems imply different thermodynamical equilibrium parameters.

$$K_{D,Q_B} = \frac{[RC][Q]}{[RCQ_B]} \qquad \textbf{(9)}$$

$K_{D,QB}$ is small if the RCs are within LDAO micelles, being lower for mutated RCs; the value increases when RC is embedded into phospholipid vesicles, remaining invariable even following the mutation. The lowering of $K_{D,QB}$ in micelles as response to a mutation that modifies the Q_B site environment was expected, because the quinone exchange equilibrium is altered and then less free ubiquinone at the equilibrium ([Q]) will be available. The invariability of the proteoliposome values instead confirms that lipid bilayers possess a greater flexibility than detergent micelles concerning the whole protein reconstitution; this concept is particularly relevant to the Q_B site arrangement when mutation at the Q_B pocket has been introduced.

Therefore the role of lipids in the modulation of the protein structure and function is crucial for the Q_B site, which otherwise results significantly altered in micelles containing mutated Rcs. Environments mimicking *in vivo* conditions assure more favourable energetics of the electron transport to Q_B.

Finally, it is demonstrated that all the living systems have special interests to neutralize the possible consequences of mutations (both artificial or natural, random), which are dangerous for the normal functioning of the organism. This compensation is a quite general mechanism and it can occur at the level of[17]:

(a) the RC protein itself;
(b) the lipid environment (either as reconstituted bilayer or as native membrane);
(c) the metabolic processes of the entire cell.

Up till now only the first two points have been examined since the third one is clearly out of the interests of this thesis.

From the study of lipid-Reaction Centre interactions a general conclusion can be drawn: membrane proteins together with surrounding lipids (annular, non-annular, integral) and other possible substances, form molecular complexes ("quasi-proteins"[60]) with properties very different from those of the bare isolated protein, just as ion-counterion complexes in solution behave differently from bare ions. In a deliberately simple way this concept may be considered as the most advanced development, at present, of the Singer and Nicholson model of "fluid mosaic".

1.5.3. Lipid-protein interactions in a lipidic cubic phase.

Although detergent-based crystallization experiments on membrane proteins (such as bacteriorhodopsin (bR)[167] and RC[106]) have been well promising, rapid and significant improvements in resolution emerged only with the introduction of a novel concept for crystallization in a lipidic cubic phase (par. 1.2.2)[168]. Further interesting results seem also very close to be reached.

An interesting and recent model for the crystallization of bR from the lipidic cubic phase[169] can be extended also to other membrane proteins. The proteins are thought to diffuse from curved lipid bilayers into patches (i.e. “rafts”, see par. 1.2.3) of lower curvature, finally incorporating into planar lattices that in turn associate to form highly ordered three-dimensional lipid crystals.

The generality of the lipidic cubic phase crystallization[170] was further demonstrated by its successful application to the photosynthetic RC from *Rb. sphaeroides,* the first among the RCs from purple bacteria. A very recent report[31] describes a new crystal form grown from RCs embedded in a cubic phase of the lipid monoolein[41] (glycerol monoester of the cis-9-octadecenoic acid).

This three-dimensional crystal - referring to the protein and lipid arrangement together - is the sum of stacked and multilayered bidimensional aggregates parallel to the *ab* plane of the crystal unit cell (fig. 1.41).

Every RC molecule shows the same orientation within each layer and its two-fold symmetry axis makes a fixed angle (11.5°) with respect to the vector normal to the membrane plane[42], that is the short axis of the crystal unit cell (named *c* in fig. 1.41). Within each layer the cubic phase lipids and the RCs are therefore arranged approximately as they would be in a membrane bilayer, whose location and plane can be assigned with confidence because of the crystal packing.

The thickness of the hydrophobic part of the membrane (*hydrophobic thickness*) is 34÷35 Å at room temperature[171], which is in line with that of the cell membranes of

---

41. Monoolein naturally form bilayers with varied curvatures.

42. This tilt angle appears unlikely to influence significantly the uni-directionality of electron flow between the A and B branches of cofactors (par. 1.4.2), since it is already present in RCs crystallized from detergent solutions.

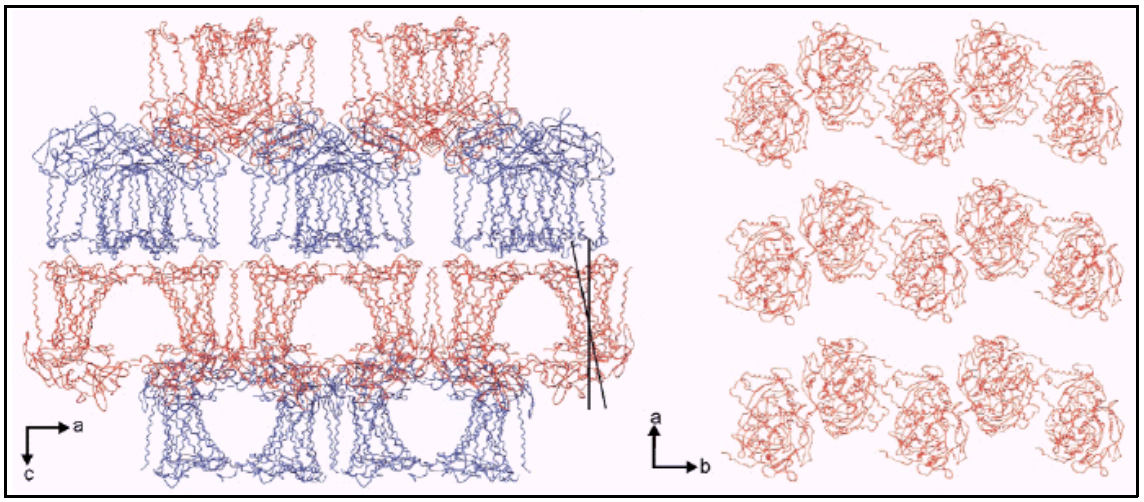

Figure 1.41.
Packing arrangement of the Reaction Centre membrane protein from *Rb. Sphaeroides* bacteria within lipidic cubic phase grown crystals. *Left*: the direction of view is parallel with the ab (membrane) plane. *Right*: the direction of view is parallel with the c-axis.

Rb. sphaeroides excluding the polar head groups (about 28 Å[41]). In fact the cell membranes of *Rb. sphaeroides* contain lipids whose apolar tails are mainly composed of vaccenic acid[172] (*cis*-11-octadecenoic acid), isomer of the oleic acid (*cis*-9-octadecenoic acid) making up the lipid monoolein.

The most important detail of the structural model obtained from these crystals was the presence of a CL molecule whose binding has been widely discussed elsewhere, the so-called “crystallographic cardiolipin” (par. 1.5.1); other lipids could not be observed in the X-ray structure due to static or dynamic disorder (par. 1.3.2.1).

Alternate layers exhibited opposite, antiparallel orientations (in relation to the *c* axis of fig. 1.41): within individual planes RCs appear to be arranged in dimers around an axis of two-fold symmetry; the contact surface between pairs consisted of intramembrane regions of the M- and H- polypeptides and included the CL binding site, whose charged phosphate head group was at the boundary between adjacent layers.

Besides conserving the most important CL-RC molecular contacts (represented by the amino acids Arg M267, HisM145 and Lys M144), new interaction sites were found in this lipid crystal.

The first site discovered was deeply buried within the membrane-spanning region, between the P_B phosphoryl of the tightly bound CL molecule and the Lys L202 belonging to the adjacent symmetry-related RC[31], at the protein-protein interface; here CL acted as a mediator of a salt-bridge contact.

The second was suggested to be a chloride (Cl^-) ion-binding site, located within the transmembrane region but close to the cytoplasmic side of the protein.This site was too small to accommodate a sulphate or a phosphate ion (as reported in the first structures of the RC crystals, grown in detergent solutions, see above) and it was assigned to a Cl^- because the pH of the buffer used was adjusted with hydrochloric acid. The Cl^- ion was located at the centre of an almost perfect tetrahedral of positively charged (two arginines) and neutral residues (two glycines): then it interacted by hydrogen bonds with amino groups both from side-chains (Arg) and backbones (Gly) of amino acids.

In a RC micellar crystal structure from *Rps. viridis* a sulphate ion was observed at a position similar to that of Cl^- in the *Rb. sphaeroides* RC, even though the binding interactions were quite distinct in the two cases. In addition, in many RC micellar structures from *Rb. sphaeroides* variable numbers of water molecules have been modelled in this same place occupied by Cl^- in the lipid crystal structure.

While the mechanistic significance of the Cl^- site is still unclear, it is interesting to note that it lies close to a water channel connecting the mobile quinone (Q_B) binding site with the protein surface. This site results clearly *a priori*-formed in the structures obtained from detergent-grown crystal from which the above water-channel was first identified[4]: in fact two water molecules were modelled into the Cl^- -binding site.

Obviously, partial compensation of two positive charges from Arg residues may be an energetically sufficient reason to explain the Cl^- presence within the low-dielectric medium of the membrane. A more speculative hypothesis is that a cluster of charged side-chains located near the protein surface - but within the transmembrane region - could indicate specific sites for the interaction with other photosynthetic membrane proteins: the Light-Harvesting antenna I, the cytochrome bc_1 complex or the peptide PufX (par. 1.4). The latter possibility receives circumstantial support from the fact that the Cl^- -binding site lies adjacent to the entry/exit channel of the mobile quinone/quinol pocket[173], as above mentioned.

All the new crystallographic data thus give an interesting insight into how CL could facilitate molecular contacts in a dimer of the RC, although the fact that the protein is reconstituted in a lipid cubic phase makes difficult the comparison with native photosynthetic membranes, where the presence of a dimer form remains still to be

proved. Nevertheless dimeric organization of RCs was predicted for a membrane-bound environment on the basis of spectroscopic and biochemical evidence[174]. The peptide PufX is considered mainly responsible for dimerization[173, 175] and the involvement of CL molecules in dimerization was already predicted by modelling studies[150]: both these informations seem to confirm the mentioned crystallographic data.

Also in structures of other membrane proteins determined from cubic phase-grown crystals several lipid molecules have been identified: they act as mediators in the cooperative interactions between monomers, corresponding to the definition of *non-annular* surface lipids or *integral* lipids (par. 1.3, in a role similar to that of the 2,3-diphospho-glycerate molecule for the tetrameric water-soluble haemoglobin[176]). Halorhodopsin and bacteriorhodopsin are the main examples[177].

The last results obtained for RCs grown in a lipid cubic phase provide a unique example of protein-protein crystal contacts directly mediated by a negatively charged lipid head-group[43]. Moreover, in addition to bacteriorhodopsin, the RC represents a second case in which high-resolution X-ray structures both from micellar and lipidic cubic phase-grown crystals may be compared.

According to complex structural analyses there are many indications of a slight compression of the lipid-grown structure towards the centre of the protein, possibly due to its location within a lipid-rich packing. However the surface pressure exerted by the stacked bilayers is believed to have a stabilizing effect on the structural integrity of the entire membrane[178]. In addition, the surface pressure and, consequently, the close packing in multilayered lipidic systems may contribute also to the thermal stability of membrane proteins[179].

The RC transmembrane region most affected by variations between the two crystal structures (micellar and lipidic) is the single transmembrane helix of the H-subunit, which presented also the greatest degree of heterogeneity, even from one detergent structure to another. On the other hand, for L and M subunits the conformational changes are considerably more homogeneous[31].

A rational explanation for it could be that most crystal contacts are made through hydrophilic domains, primarily the H-subunit. Since crystal contacts can vary

43. It would explain the recently entered-in-use addition of charged lipid molecules as crystallization agents.

considerably from one space group to another, also micellar structures show significant heterogeneity in this region. It happens the opposite for the membrane-spanning region, (essentially made of the L and M subunits), relatively unaffected by crystal contacts: rather, it is structurally perturbed by interactions with the surrounding detergent and lipid molecules (e.g. annular shell).

Among the data examined only faint traces of electron density have been found at the locations occupied by PC and by the glycolipid GGDG (see above) in RCs grown in detergent micellar solutions[31]. An explanation for this might be that within a lipid bilayer structure - then in a system that better mimicks to the native membranes - the lateral diffusion of lipid molecules is less restricted than within a detergent micelle in water. So, in micelles the hydrophobic nature of the fatty acid chains is likely to constrain lipid molecules near the protein surface, making them more visible.

With this argument in mind, the head group of CL is strongly bound to the RC surface in lipid cubic phase crystals; the tails instead are tightly confined within small cavities formed between the two symmetry-related protein molecules of the dimer, in an almost “hidden” location and in a relatively ordered arrangement[31].

The crystallographic data discussed above not only illustrate the potential of lipidic cubic phase crystallization for structural studies as those on the RC from *Rb. sphaeroides,* but they also shed light on the influence of the lipid environment on membrane protein structure. Although lipidic crystals of RCs have reached diffraction limits similar to micellar ones (2.1 Å versus 2.0 Å resolution, respectively), the optical properties of lipid-rich crystals may be advantageous for many applications[31].

First, the membrane bilayer can be identified within the crystal structure with a high degree of confidence, contrary to detergent-grown structures, where this attribution is not at all simple[41].

The importance of lipid molecules and specific binding sites in the functions of membrane proteins as well as in forming protein-protein contacts may grow further as more X-ray structures from lipid crystals emerge, as the CL and the chloride-binding site seem to suggest. Finally, also the studies about the surface pressure effects within stacked lipidic bilayers could lead to remarkable improvements in the knowledge of membrane environments.

CHAPTER 2
EXPERIMENTAL SECTION

The aim of this Experimental Section is twofold:

1) to provide the reader precise informations on the experimental work necessary either to obtain the protein RC in a “ready-to-use” form (par. 2.1) or to prepare the samples undergoing the measures described within this thesis (par. 2.2);

2) to introduce the reader to laboratory techniques (par. 2.3) and theoretical elaboration concepts (par. 2.4) used in order to collect the experimental data and to interpret them, respectively.

Introduction.

The procedure illustrated in this paragraph may be considered a paradigm of the common experimental problems to overcome in the isolation and purification of all the membrane proteins. In fact, in order to purify an integral protein without altering its structure and activity, it is necessary to reconstitute in solution a favourable environment, that is to create in vitro conditions similar to those existing in native membranes. The major condition to be satisfied is to protect from the contact with aqueous solvents the hydrophobic moieties of a membrane protein, without altering its function (shielding effect).

This requirement may be met by the use of a particular class of molecules, the detergents (already introduced in par. 1.2.2), whose major and characterizing property is to possess two regions with different polarity.

The first step in the study of a membrane protein (either isolated in a micellar solution or reconstituted in a membrane system) is the choice of the most suitable detergent[180]. An optimal detergent must possess three main features[13]:

(a) it should effectively separate the desired protein from other components in the membrane, being selective and having a low CMC (par. 1.2.5);

(b) it should neither alter the structure or the activity of the protein - most of membrane proteins remain fully active if purified in the presence of a suitable detergent - nor be influenced in its action by the experimental conditions optimal for the protein (pH, temperature, ionic strength, etc.); e.g. SDS, sodium dodecyl sulphate, is highly effective in solubilization but its denaturating power prevents its use;

(c) it should be easy to be removed after purification.

In relation to the purification of membrane proteins the action of detergents is twofold: on one side they solubilize the membrane lipids, extracting all the substances that bilayers can contain; on the other side they provide to membrane proteins a friendly environment.

The action of a detergent on a complex native membrane environment - as that of photosynthetic membranes - generally produces an ensemble of protein-lipid-detergent aggregates such as mixed micelles, often polydisperse in composition because detergents, lipids and also hydrophobic cofactors (e.g. quinones) are non-homogeneously distributed. For instance, in the isolation of a protein an excess of detergent is generally employed: by this way it gives rise to a simpler mixture to deal with and study, made of detergent micelles containing not more than a protein[].

The components of these mixture of proteins, lipids and detergent are then separed one from the other by means of chromatographic and centrifugation methods similar to those employed to purify water-soluble proteins[13].

As an example, the ion-exchange chromatography (par. 2.2.4) is very useful in these cases, when non-ionic (e.g. Triton-X-100) or zwitterionic (DDAO, see below) detergents have been used.

2.1. Isolation and purification of the Reaction Centre.

All the studies have been carried out on the *Rb. Sphaeroides* mutant strain R-26 (carotenoidless), purple non-sulphur photosynthetic bacterium, facultative aerobic (par. 1.1.2.1).

We deliberately decided to avoid a detailed description of the interesting part regarding the cell growth and harvesting, because we did not perform them, taking advantage of the precious work carried by Dr. Antonia Mallardi (Istituto per i Processi Chimico-Fisici, CNR c/o University of Bari).

It is interesting instead to briefly illustrate some of the experimental steps necessary to isolate and purify the *Rb.Sphaeroides* RCs from bacterial membranes. The chosen procedure was a slightly modified version of that proposed by Gray and coworkers[181].

2.1.1. Preparation of chromatophores.

After lysozyme and DNAase treatment of the bacterial cells (in order to decompose the bacterial wall and the bacterial DNA, respectively), the cell membranes were broken by means of a French press. By this way the membrane fragments reorganize themselves forming vesicles containing RCs and other photosynthetic proteins and pigments, named *chromatophores*.

By means of a first ultracentrifugation run ($1.5 \cdot 10^{+4}$ *g*, 15 min, room temp., where *g* is the gravity acceleration), fragments of the cell wall and various cell residues were selectively removed and collected in the form of pellet at the bottom of the centrifugation tubes. The supernatant, instead, contained the chromatophores and, after a second ultracentrifugation run ($1.5 \cdot 10^{+5}$ *g*, 2 h, 4°C), they were collected at the bottom of the tube. This pellet was then resuspended in a Tris-HCl 20 mM buffer (pH= 8.0).

A further mechanical homogenization (by means of a potter) has been necessary in order to have a population of chromatophores small enough to allow a reliable electronic spectrum to be recorded. The presence in the chromatophores of the antenna

proteins (par. 1.4.1) with their cofactors (bacteriochlorophylls), leads to a spectrum characterized by a broad and intense peak centered at $\lambda \approx$ 863 nm which hides the characteristic features of the RC spectrum. Even though the resolution of such a spectrum is so poor, it is extremely useful to correctly dilute the chromatophores dispersion in order to reach a dispersed phase concentration suitable for the other steps of the RC purification (a typical optical density for such a dispersion of chromatophores is around 50[44]).

2.1.2. Extractions with DDAO.

Until this point the isolation procedure consisted essentially in mechanical operations: now the chemical action of the detergent DDAO (N,N-DimethylDodecylAmine-N-Oxide, fig. 2.1) is required. Among different detergents proposed in the course of many years for the RC purification, DDAO is by far the most commonly utilized and it has been employed also in the work described in this thesis.

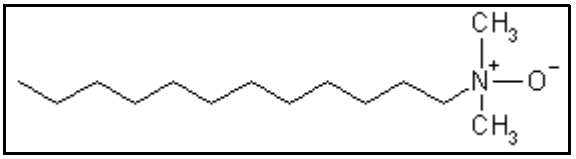

Figure 2.1.
Molecular structure of DDAO.

RC is an integral membrane protein: it can be removed from native membranes only by detergents, differently from peripheral membrane proteins, which are removable also by pH or ionic strength variations (par. 1.2.3).

First extraction. To the resuspended chromatophore volume were added: NaCl 125 mM, PMSF (phenilmethan sulphonylfluoride, a protease inhibitor necessary to avoid the RC digestion by any protease present) 0.5 mM, NaAsc (sodium ascorbate) 1 mM and DDAO 0.25 % w/V (i.e., at a concentration higher than its CMC). The mixture was stirred for 45 min in the dark at room temperature and then ultracentrifugated (90 min at $1.5 \cdot 10^{+5}$ g, 4°C) in order to eliminate the supernatant composed essentially of LH-II

44. It is possible to measure such a high optical density value just taking an aliquot of the chromatophores suspension and conveniently diluting it with buffer until absorbance values fall in the measurement range of the used spectrophotometer (e.g. in our case about 0.001 ÷ 1).

antenna proteins (since the R-26 mutant strain synthesizes almost only LH-II, not LH-I) and cytochrome c_2.

Second extraction. The pellet of the previous centrifugation, containing RC, was resuspended with the usual buffer to its initial concentration (OD_{863}=50). NaCl 125 mM and LDAO 0.35 % w/V were added to the suspension, stirring for 30 min in the dark at room temperature. After this treatment, a last ultracentrifugation run (90 min at $1.5 \cdot 10^{+5}$ g, 4˚C) was performed to obtain the extraction of the RC from the chromatophores and its separation from heavy antenna proteins: therefore the supernatant was kept.

2.1.3. Ion-exchange chromatography.

After the extraction, the fraction containing the RCs was not yet pure but rich enough in protein to allow another purification step, this time based on chromatography.

The RC fraction was passed through a chromatographic column (2.5 cm diameter x 30 cm high) for ion-exchange filled with the cationic resin diethyl amino ethyl (DEAE) cellulose; the resin was previously equilibrated with a buffer made of Tris-HCl 20 mM pH=7.5 and DDAO 0.08%.

Since at pH= 8 the RC molecules exhibit a negative surface charge, they were retained by the cationic DEAE. Once loaded in the column, the RC was electrostatically attached to the resin. The protein could then be washed with buffered NaCl solutions of increasing ionic strength. The aim of these “elution washings” was to remove protein impurities such as various cytochromes, whose global charge is the same (negative) as the RCs, though with lower surface density, allowing the RCs itself to remain more tightly attached to the resin.

The Cl^- ions of the added NaCl competed with the eluted protein fraction for the binding sites on the resin: increasing the salt concentration in subsequent washing steps, they caused the detaching from the resin of the protein having lower surface density, until with NaCl 210 mM the RC itself was eluted out of the column.

At every salt concentration the eluted volume was spectrophotometrically

controlled in order to be sure that RCs were not present.

The first NaCl concentrations used in the elution were 80 mM, then 100 mM: at this concentration can be observed a peak at λ~280 nm corresponding to the aromatic residues of eluted proteins other than RCs (it detaches at higher NaCl concentrations). Other peaks at λ~419 nm and λ~753 nm correspond respectively to the cytochrome bc_1 and to the pheophytin molecule. It was important to check the absence of the λ~860 nm peak - which indicates that RC presence -: it assured that RC was still bound to the resin.

The elution proceeded with buffered solutions (Tris-HCl 20 mM, pH= 8.0 containing DDAO 0.08 %) of NaCl 115, 130, 150, 165, 180, 210 mM. The fractions containing the protein were separately collected and spectrophotometrically checked as indicated in the following paragraph.

Then the whole RC solution was dialyzed overnight at 4˚C in the dark against the same buffer (but without salt), in order to remove residual NaCl; then the purified RC solution was kept frozen at -70 ˚C.

2.1.4. Purity tests.

RC purity and integrity can be verified by means of the UV-Vis spectroscopy. We will refer to the RC spectrum reported in fig. 1.33, p. 106.

The spectral indexes indicating purity and integrity can be summarized as follows:

- the $Abs_{865\ nm}$ / $Abs_{760\ nm}$ ratio in pure RCs should be about 1; this is an integrity index for the P dimer (the degradation of the RC primarily involves the bacteriochlorophyll special pair, converted to bacteriopheophytin, leading to an increase in the 760 nm absorbance and to a simultaneous decrease of the 865 nm absorbance);

- the $Abs_{280\,nm}$/ $Abs_{802\,nm}$ ratio should be equal to 1.2÷1.5; higher values suggest the

presence of other contaminating proteins (the 280 nm peak derives from aromatic amino acids in proteins); the $Abs_{802\ nm}$ value allows to calculate the RC concentration from the eq. 1 both in micelles and liposomes once the correct ε value is used.

In the RC preparation that we used for the experiments discussed in the Third chapter the $Abs_{280\ nm}$ / $Abs_{802\ nm}$ ratio was about 1.2.

2.1.5. Ubiquinone-depletion procedure.

Without further operations the purified RCs show heterogeneous ubiquinone contents (the Q_A site is fully occupated while only the 10÷50 % of the Q_B sites retain their native quinone). Since for the work described in this thesis it was essential that the Q_B site was completely empty and that the exact $[Q_{10}]$/[RC] ratio was well-known, an ubiquinone-depletion procedure was performed on the RCs according to the method proposed by Okamura and coworkers[182].

A small chromatographic column for ion-exchange (1÷2 ml capacity) was filled with ~2 ml of DEAE-cellulose resin equilibrated with a buffer made of Tris-HCl 10 mM pH= 8.0 and DDAO 0.1%.

The whole RC solution obtained at the end of the main step of ion-exchange chromatography (par. 2.1.3) was introduced on the top of the column. The elution washing was performed overnight by passing a Tris-HCl pH=8.0 10 mM, DDAO 4 %, ortho-phenantroline 10 mM (a weak competitor for both the quinone binding sites[183]), and dithiotreitol 1mM (as mild reducing agent for quinone that in the form of quinol are more easily removed from the protein[184]) buffer. The constant flow of the buffer was ensured by a peristaltic pump working at a flux rate of about 250 mL per hour.

At the end another elution was performed with 0.5 L of the same buffer previously used for the column equilibration; in the final step, the use of a buffer containing NaCl

400 mM allowed to collect a concentrate[45] and almost completely (see further) quinone-depleted RC sample. Two days of dialysis (against a Tris-HCl 10 mM pH= 8.0, DDAO 0.1% buffer) are then necessary in order to eliminate the added NaCl.

As already stated, the above described procedure leads to a RC preparation where all the ubiquinone-10 was removed from the Q_B-site while approximately 40% of the Q_A site still retain the native quinone. Since this procedure induces some loss in the protein integrity, it has not been repeated preferring to have a higher amount of active protein though slightly contaminated by quinone at the Q_A site.

The degree of occupancy of Q_A-site has been evaluated by comparing, in micelles, the extent of the laser-induced absorbance changes ($\Delta Abs_{870\ nm}$) before and after the addition of a saturating concentration of the water soluble 2,3-dimethoxy-5-methyl-1,4-benzoquinone. In fact, in the presence of a saturating excitation light, the $\Delta Abs_{870\ nm}$ quantity results to be directly proportional to the concentration of RC having the Q_A site occupied (see eqn. 3-3 in the Third Chapter).

For RC samples maintaining the quinone, the same column employed for the depletion procedure - together with the solvent used for its equilibration with added NaCl 400 mM - may be used to obtain concentrate RC solutions from diluted ones. A subsequent dialysis overnight at 4°C against the same solvent devoid of NaCl is necessary.

45. The elution through the small column has also the effect to concentrate RC samples previously eluted with larger columns, since the dilution produced by small column is reduced if compared with that produced by the larger ones.

2.2. Preparation of the samples: the Reaction Centre in micelles and proteoliposomes.

Cardiolipin (di-phosphatidylglycerol), purified from bovine heart, was from Sigma in the form of lyophilized sodium salt, while terbutryne and dodecyl dimethylamine oxide (DDAO) were from Fluka. Soybean lecithin (1,2-diacyl-*sn*-glycero-3-phosphatidylcholine) was a generous gift from Degussa Bioactives AG (brand Epikuron 200, minimum purity 95 %). All the chemicals have been used without further purification.

Since both cardiolipin (CL) and phosphatidylcholine (PC) are natural products they are composed of a mixture of different fatty acid chains, generally dependent on the source of the lipid (e.g. if vegetable or animal, prokaryotic or eukaryotic, etc.) and influencing in turn their physico-chemical and biological properties[14]. Consequently the molecular weights (MW) of these natural species should be considered averaged on their fatty acid composition: molar concentrations of CL were calculated on the basis of a MW of 1480 Dalton (Da), appropriate for a composition dominated by 18:1 unsaturated chains[163] (par. 1.5.1).

Informations about PC instead have been kindly provided by the supplyer itself: the average (anhydrous) MW was 772 Da, while the fatty acid composition relatively to the total amount is reported in table 2.1. Among impurities there is also water (~2 %), whose content ranges between 0.3 and 1 molecules per PC molecule, depending on the lot and on the storage procedure.

Table 2.1. Fatty acid composition of the PC used in the experiments described in this thesis.

Fatty acid	% composition	Features
C 16:0, C 18:0	16 ÷ 20	Prevailing at the glycerol 1-oxygen
C 18:1-cis (oleic)	8 ÷ 12	Prevailing at the glycerol 1-oxygen
C 18:2-cis (linoleic)	62 ÷ 66	Prevailing at the glycerol 2-oxygen
C 18:3-cis (linolenic)	6 ÷ 8	/

In the calculation of local concentrations, within this thesis indicated also as hydrophobic (par. 3.2), we used the following quantities:

- for the molecular and molar volumes of the PC hydrophobic tails[185] v_{PC} = 1.053 nm^3 and $(v_m)_{PC}$ = 0.634 $L*mol^{-1}$ respectively;
- for the molecular and molar volumes of the CL hydrophobic tails $v_{CL}= 2v_{PC}$, $(v_m)_{CL}= 2 *(v_m)_{PC}$;
- for the DDAO molar volume[186] $(v_m)_{DDAO}$ = 0.2557 $L*mol^{-1}$.

2.2.1. Preparation of RC-DDAO micelles.

After its isolation from bacterial membranes and purification (par. 2.1), the RC was in the form of a concentrate aqueous micellar solution (typically, [RC]= 70÷80 μM)..

Therefore DDAO-RC direct micelles can be prepared simply by diluting and vortex-stirring a suitable volume of this concentrated solution with TL aqueous buffer at pH 8.0 (so called from the initials of its components, Tris-HCl 10 mM, LDAO[46] 0.025 % w/V). Generally, around 35 μl of this concentrated RC solution were diluted to 1 mL with buffer in order to get a final concentration around 2÷2.5 μM. In order to maintain both its water solubility and cofactors integrity, it is important that DDAO is always more or equal than 0.025 % w/V.

The RC concentration in the micellar solutions was easily determined by means of its UV-Vis spectrum. In particular, the absorbance at 802 nm leads to the RC concentration (expressed as micromoles of protein per liter) by means of the classical Beer-Lambert relationship (optical path *l* = 1 cm, $\varepsilon_{802\ nm}$= 0.288 $\mu M^{-1}cm^{-1}$):

$$[RC] = \frac{Abs_{802\,nm}}{\varepsilon_{802\,nm} * l} \qquad \textbf{(2-1)}$$

46. LDAO, lauryl dimethyl amine oxide, is an alternative, traditional name for DDAO: this latter however, because recommended by IUPAC, will be extensively used in this Thesis.

2.2.2. Preparation of PC, CL, PC/CL proteoliposomes.

Much has already been said in the par. 1.2.5 to try to properly introduce the reader to this apparently easy subject, more and more interesting in biochemistry.

In spite of all the efforts necessary to isolate a functionally active membrane protein in micellar solutions, some of their most important properties are expressed only when these proteins are located within the membrane environment or in bilayer-mimicking reconstituted systems such as liposomes. Recently it has been clarified that not only vectorial, directional properties (e.g. transmembrane potentials, pH gradients) - based on the physical separation between compartments - but also generic properties, such as electron transfers in photosynthetic proteins (see third chapter), become fully meaningful only when integral membrane proteins are incorporated into bilayers.

Therefore, after the careful choice of a detergent for protein purification (par. 2.1.1), the second step in the study of a membrane protein is the “back transfer” into a lipid bilayer. The reconstitution of active membrane systems from purified components represents a fundamental approach in order to characterize the multitude of biological processes involving membranes (par. 1.2.3).

Phospholipid vesicles containing RCs (proteoliposomes) of course are not so easy to obtain as micelles, but - together with chromatophores (par. 2.1) - they represent the system most closely mimicking the RC native membranes. Pure PC, pure CL and mixed PC/CL proteoliposomes were prepared by detergent solubilization and subsequent detergent removal, as follows (scheme 2.1).

According to the type of sample, variable amounts of PC and/or CL were weighted (PC 2÷18 mg, CL 4÷16 mg) in polyethylene vials (1.5 or 2.0 mL eppendorf tubes) and dissolved in chloroform. Then they were dried first under N_2 flow (to prevent O_2 oxidation) and finally by vacuum pump, until a dry, thin lipid film at the bottom of the tube was formed. The lipids were then resuspended in 0.4 mL of an aqueous solution of this composition: 0.25 mL of 10 mM imidazole and 100 mM KCl buffer (pH= 7.0), 0.15 mL 10 % Na-cholate solution (pH= 7.0). Subsequent vortex-stirring and a brief sonication (Branson Cell disruptor, cup horn geometry, pulsed power 1/3 of the maximum available) provided transparent solutions of mixed lipid-cholate micelles.

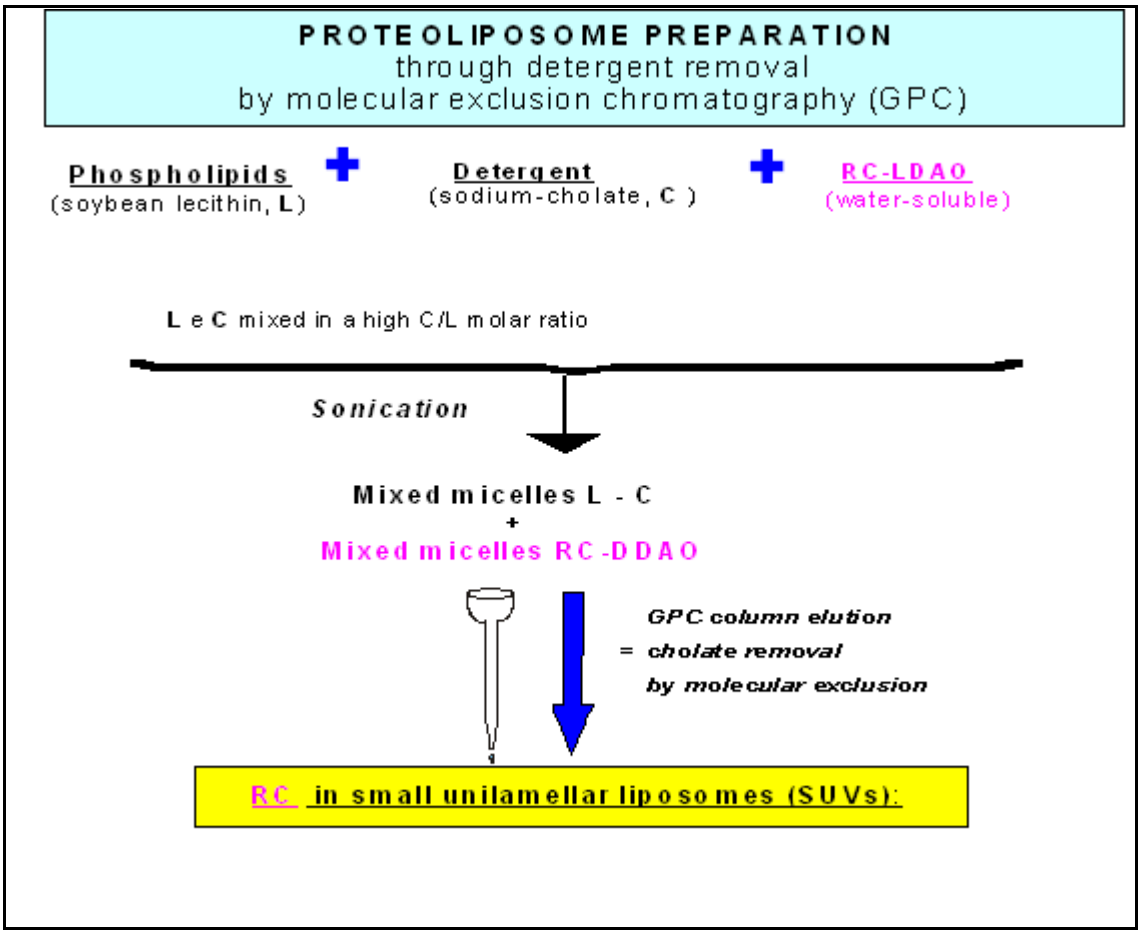

Scheme 2.1.
Experimental procedure for the proteoliposome preparation. In violet are written the reagents necessary to obtain liposomes containing RCs (*proteoliposomes*), instead of simple phospholipid liposomes (in black).

The use of such experimental parameters is motivated. A detergent-to-lipid (cholate /PC) molar ratio higher than 1.3[187] is necessary in order to properly solubilize phospholipids as mixed micelles: these latter represent the right sample to load on the column necessary to remove the detergent and consequently to give rise to vesicles (see below). PC is water-soluble even at low ratios, minimum ~0.5[188], but in form of large multilamellar vesicles (LMVs)[63].

The indicated amount of cholate is well enough to solubilize phospholipids even without sonication but this latter is suggested to make micelle sizes more monodisperse.

Pure concentrate RC - such as that used for RC micelles (70÷80 μM in Tris-HCl 10 mM pH= 8.0, DDAO 0.025%) - was added to the mixed micelles solution, then vortex-stirred.

Subsequent detergent removal was obtained by eluting this suspension through

a glass column (about 18 cm high x 0.5 cm diameter) packed until 2/3 of its height with Sephadex G-50 porous resin (commercial name for dextrane beads, from Pharmacia). 0.4 ml is the optimal sample volume to introduce on the top of the column in order to match the features of the described system. The elution solvent was the same buffer as that of the sample introduced, 10 mM imidazole/100 mM KCl (pH= 7.0). The elution process will be briefly discussed later in this paragraph.

Detergent removal results in RC-containing small unilamellar vesicles[189]: the elution fractions containing proteoliposomes were collected together and diluted with buffer to 1 ml volume. They were well distinguishable because of the mild blue color of the RC and of the milk-like scattering of the whole suspension.

The presence of the RC into the vesicles bilayer is easy to check: a visible absorption spectrum (300÷900 nm) of the suspension should show the typical protein peaks but with a baseline influenced by the liposomes scattering.

The RC concentration in proteoliposomes was determined from the visible spectrum of the sample by drawing the tangent line to the bacteriochlorophyll monomer (B) peak at 802 nm and measuring the absorbance over the tangent basis, as indicated in fig. 2.2. The measured value, with the proper molar absorbivity (for the tangent method $\varepsilon_{802\,nm} = 0.200\ \mu M^{-1}cm^{-1}$), once inserted in the Lambert-Beer relationship (eq. 2-1 and equation in fig. 2.2) gave the RC concentration in the vesicles preparation. Fig. 2.2 shows the spectrum of RCs in vesicles. In addition, alternative undesidered events during the protein reconstitution into liposomes are quite simple to rule out. RCs are highly hydrophobic and as only possibilities they may remain trapped into column in the absence of sufficient DDAO before they incorporate into bilayers: in this case the blue band of the eluting protein

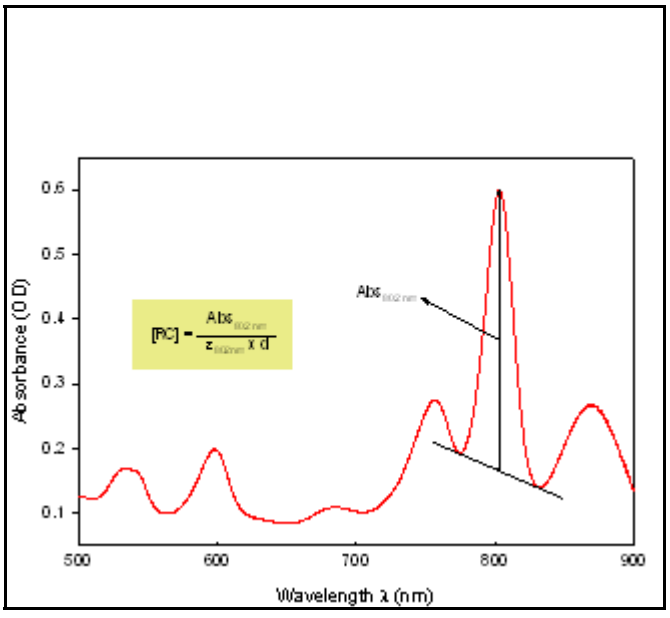

Figure 2.2.
UV-Vis spectrum of RC in liposomes.

will stop. Non-incorporated RC precipitation after the end of the elution would be also suddenly revealed by an heterogeneous blue color of the vesicles suspension.

The detergent removal process will be now briefly examined (par. 1.2.5 point D1).

This method exploits a selective permeation phenomenon through a gel matrix based on the different size of the chemical species present in the mixed micellar solution, containing - as already said - the lipid(s), the protein and the detergent molecules (both DDAO and sodium cholate). By passing through the polydestrane resin (whose network of cross-linking fixes the dimensions of the meshes and, therefore, its size selectivity), smaller molecules are retarded due to their partition in the stationary phase, while larger aggregates are excluded from this process and therefore pass through the column practically without any retard. By this way both detergents, cholate - present in higher amount - and DDAO are selectively removed from the solution. During this process, because of the continuous loss of cholate monomers, micelles progressively enrich in phospholipids, coalesce and increase in size, transforming into vesicles (fig. 2.3).

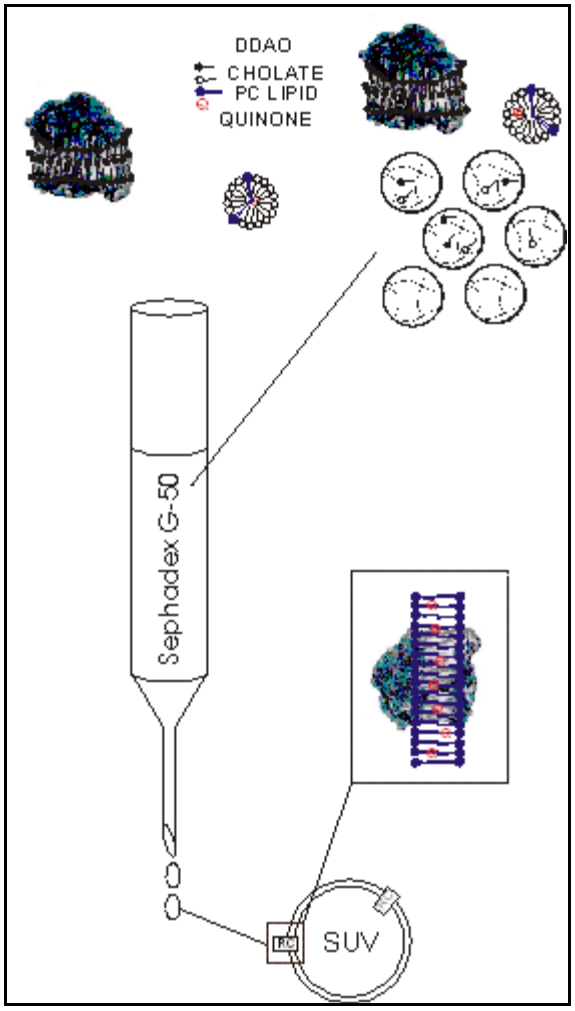

Figure 2.3.
Elution of phospholipid-cholate and Reaction Centre-DDAO mixed micelles through a Sephadex G-50 packed column giving rise finally to small unilamellar vesicles (SUVs). The molecules are so represented: black spheres with rods (DDAO), white-filled spheres with rods (cholate), blue sphres with rods (phosphatidylcholine, PC) and red Q letters (quinones).

This elution is a non-equilibrium, relatively fast process (~45 min) if compared with other detergent removal methods such as dialysis, which requires at least several hours[190].

In addition dynamic light scattering (DLS) measurements performed by us at various PC weights and cholate/PC molar ratios revealed very reproducible proteoliposome diameters (50÷100 nm,

according to starting conditions) and relatively low size polydispersity.

Regarding the RC orientation within the vesicles bilayer, it has to be said that this is purely statistical, with almost 50% of the RC facing the exterior of the liposomes with the docking site for the cytochrome c_2 while the other half oriented in the opposit way. This feature was checked on several samples of proteoliposomes by using citochrome *c* from horse heart (from Sigma) as electron donor to the photoxided bacteriochlorophyll dimer P^+, added to the suspension together with sodium ascorbate and the laser induced bleaching at 870 nm checked before and after the addition. In any tested circumstance the data showed that after the addition of the reducing agent for the P^+, the signal intensity reduced to half the original. This represents a clear indication that only half of the RC are present with the docking side for the cytochrome facing the exterior of the liposomes.

2.3. The photolysis technique.

2.3.1. Early photolysis and additional considerations.

Laser and flash photolysis - differing only in the excitation light used, laser or normal lamp respectively - have become since 1970's very useful tools for monitoring fast decaying metastable states[191], as the light-induced charge separated state $P^+Q_A^-$. A general discussion of the first and basic photolysis methods can be found in some old text[192], which nevertheless now remains interesting mainly on a “history of science” point of view.

Since at least thirty years the use of pulsed lasers has solved the problem of introducing a large number of photons into the sample in a small time range. Ruby or neodimium lasers with energies in the joule (J) range have been commonly used for excitation since then.

However in the late 1970's some experiments have been successfully performed also using less powerful exciting laser sources such as an N_2 gas laser with ~ 10^{-3} J photon emissions[193, 194]. At that times this source had the advantage of a much faster pulse rate, longer life and lower price[191]. In our first trials of building a new photolysis apparatus (extensively illustrated in par. 2.3.2 in its last and working version) such features suggested us to adopt a N_2 laser we already had (EMG 100-201 excimer laser, Lambda Physik, 337 nm, 2 mJ/pulse as single shot, 6 ns pulse width), though its lower energy output made alignment of exciting and monitoring beams a crucial step. The need of focusing the two beams in a small spot few square millimeters (mm^2) large has been already discussed in literature in reference to the signal to noise ratio[193] (S/N, whose values for our experimental traces will be mentioned in par. 2.3.2).

Really the alignment problem is critical also for more powerful light sources. In fact, the reason inducing us later to change idea about the N_2 laser and to choose other exciting lights such as a Xenon flash lamp (40 mJ/pulse) or a Nd:YAG laser (300 mJ/pulse) was not the energy delivered to the sample with each pulse (in our case increasing in the following order: N_2 laser < Xenon flash lamp < Nd:YAG laser) but rather the need to avoid excitation of the RC protein in the UV spectral region since it leads to

long-living charge separated states[195] (see par. 2.3.3 for further details).

At present, laser with a pulse duration as low as few nanosecond became relatively unexpensive (having prices in the order of 10^{+4} €) and moreover well affordable, so that nanosecond resolution in such modern apparatus - as that we built - has been routinely achieved.

2.3.2. Our photolysis apparatus

Before the beginning of every series of experiments an UV-Vis spectrum of the sample was always recorded in order to check both the RC concentration (eq. 1 in this chapter) and the integrity of cofactors.

Exponential recoveries of the initial non-excited state PQ_A from the charge separated state $P^+Q_A^-$ - that is the so-called "charge recombination kinetics" (par. 1.4.4) - were monitored at 870 nm (NIR region) by a home-built kinetic single beam spectrophotometer realized with orthogonal geometry between monitoring (or measuring) and exciting beams in order to minimize the interference between the two

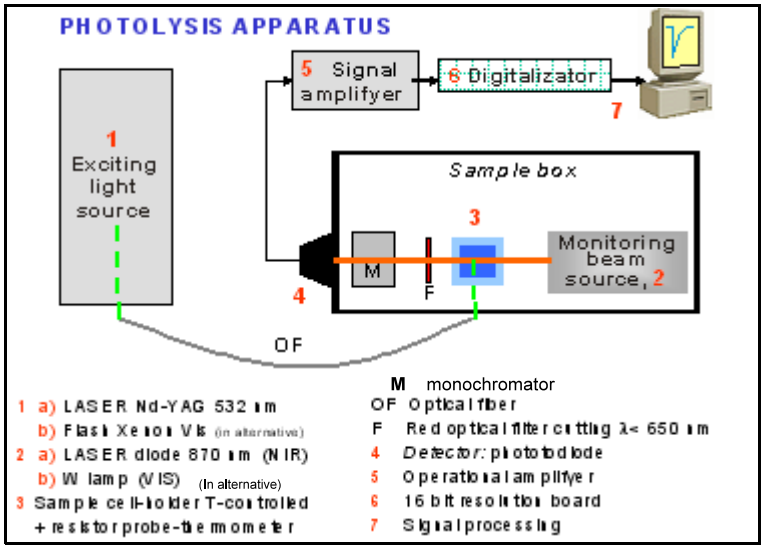

Scheme 2.2.
Laser photolysis apparatus built to perform our charge recombination measurements.

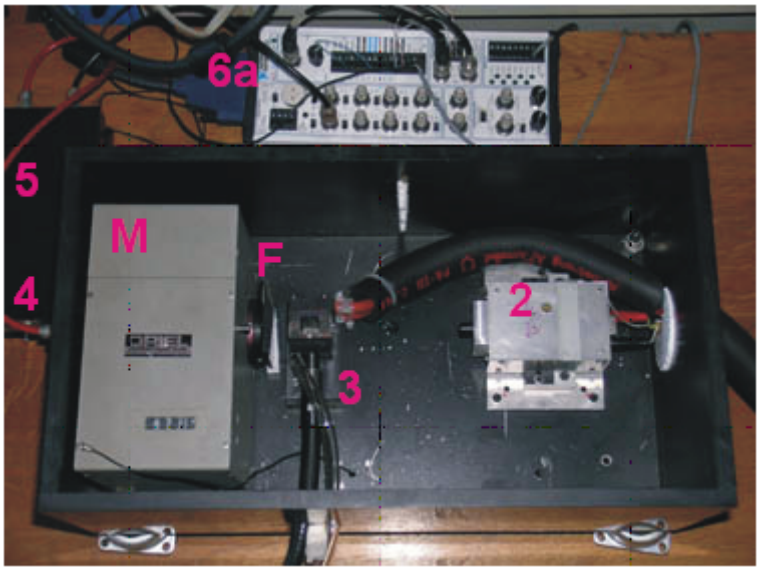

Figure 2.4 A.
Top view of the sample box: the labelling numbers are the same as in scheme 2.2.

light sources (scheme 2.2 and figures 2.4 A and 2.4 B). This geometry is the only allowed when the kinetic process to study is quite slow (as in our case) since it minimizes the attenuation of the signal due to the diffusion of the excited molecular species out from the region monitored by the measuring beam. Moreover this geometry quite semplifies the optical part of the apparatus because less focalization optics (lenses, filters, mirrors, etc.) are required.

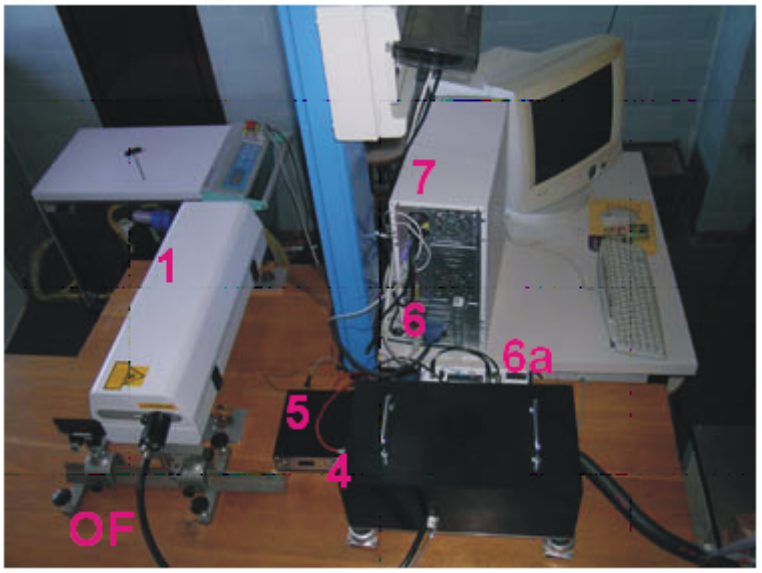

Figure 2.4 B.
Whole laser photolysis apparatus. The sample box of the scheme 2.2 is shown as closed (black). The label numbers used here are the same as in scheme 2.2.

The monitoring beam was provided by a laser diode (Roithner Lasertechnik, λ=870 nm, number 2 in scheme 2.2 and in fig. 2.4 B), operating at an average power of 2 mW, illuminating the sample cuvette through a 0.5 mm diameter pin-hole.

A silicon photodiode (UDT, 10D, nr. 4 in scheme 2.2 and in figures 2.4 A, B) working in photovoltaic mode thanks to the connection with a high speed di-fet operational amplifier (Texas Intruments, OPA637AP, nr. 5 in scheme 2.2 and in figures 2.4 A and B) has been used as detector. The time constant of the whole circuitry was kept to few microseconds (see par. 2.3.4 for details).

In order to avoid any interference from the exciting light - also through reflections internal to the cuvette - the measuring beam passed through a red glass filter cutting wavelengths below 650 nm (Corning, no. 2-64, labeled F in scheme 2.2 and fig. 2.4 A), placed in front of the 800 μm entry slit of a grating monochromator (Oriel, mod. 7240, labeled M in scheme 2.2 and fig. 2.4 A); this latter was located between the sample and the detector.

The exciting pulse was provided by a frequency doubled Nd:YAG solid state laser (Quanta System, Handy 710): its wavelength emission was λ= 532 nm, with 7 ns pulse width, 300 mJ/pulse (nr. 1 in scheme 2.2 and in fig. 2.4 B).

The light was focused on the sample cell holder by means of a liquid optical guide (Oriel, labeled OF in scheme 2.2 and in fig. 2.4 B): this guide was in direct contact with the cuvette front-surface in order to maximize the number of photons delivered to the sample with each laser pulse.

Also photographic and intense UV-Vis xenon flash lamps could be used as exciting light source, provided passing through suitable optical filters (par. 2.3.3): unfortunately however they generally have large pulse widths (up to 10 ms) which may affect the acquisition of the first data points. This feature will affect especially the study of photochemical processes characterized by fast kinetics. Therefore a short pulse width (high emission coherence) together with other well-known features - such as to have monochromatic, intense and stable emissions - made highly preferable the employment of the Nd:YAG laser (par. 2.3.3). Therefore in all our measures only this laser source was employed.

Data have been acquired by means of a 200 kS/s[47], 16-bit resolution acquisition card (National Instruments, PCI-6013, equipped with the BNC-2120 board, respectively nrs. 6 and 6a both in scheme 2.2 and in fig. 2.4 B) installed onto a PIII computer (nr. 7 in scheme 2.2 and in fig. 2.4 B). Paragraph 2.4.1 will illustrate further details about these components.

The acquisition of the data was driven by home-built acquisition software developed in the LabView 6.0 environment. By means of this acquisition software, before the kinetic traces were mathematically deconvoluted according to the procedure described in par. 2.4.2 (*fitting*), they were converted from voltage signals in absorbance changes (ΔAbs) through several operations. This was necessary mainly in order to compare traces from different samples; a comparison is instead meaningless in the voltage mode because not related to any quantity variable with sample concentration, (e.g. absorbance).

The acquisition software took care also of:

a) gating of the measuring light (turned on 5 s before starting each experiment and switched off immediately after the acquisition);
b) triggering of the exciting light source;
c) delay time among consecutive experiments (scans);
d) number of acquired data points (generally 4000) and acquisition time range.

Points (a) and (b) will be better examined in par. 2.4.1.

About (c) and (d): typically, 8-12 scans (depending on RC concentration) were averaged in each experiment, in order to have a S/N ratio of at least 20.

The time resolution of the apparatus was in the millisecond range: it increased increasing the number of acquired data points and, on the contrary, it decreased increasing the acquistion time range. In our measures the apparatus was not used at the maximum resolution, which may reach the microsecond range.

About the delay time, the RCs were left dark adapt between scans for at least 60 s in order to let any long-lived charge separated states (in case generated) to relax back to the ground state. It has to be said, in fact, that exposure to trains of single UV light pulses or exposure to continuous Visible illumination may lead to the formation of long-

47. 200 kS/s = 200 kSamples/second = 200,000 experimental points per second.

lived charge separated states, with lifetimes up to tens of seconds (see paragraphs 2.3.3 and 2.4.1 for further details).

Temperature of the cell holder (nr. 3 in scheme 2.2 and in fig. 2.4 A) was kept constant (± 0.2 K) using a thermocryostat (Julabo, mod. ED). The sample temperature was monitored by a Pt-100 ceramic resistor (Degussa, accuracy ± 0.2 K) immersed directly into the cuvette and connected to a digital thermometer (Italmec, mod. VMD1).

The quartz cuvette used was 1 cm optical path, with five transparent walls and with reduced thickness in order to be filled also by small volumes of sample (optimal volume 1 ml).

2.3.3. Excitation light sources.

It has been already mentioned (par. 2.3.1) the possibility to employ different excitation light sources, such as a Xenon flash lamp (filtered in order to emit in the Visible[48]) or a N_2 laser or rather a Nd:YAG frequency doubled laser. These latter respectively emit in the UV (337 nm) or in the Visible region (532 nm).

Although the N_2 laser has been of widespread use in several research fields its use in photolysis has been quite limited[191]. In our specific case very soon we discovered that our N_2 laser (EMG 100-201 excimer laser, Lambda Physik, 337 nm, 2 mJ/pulse as single shot, 6 ns pulse width), though employed in single shots, was not useful for our purposes. Our aim - just to remember - was to measure correct charge recombination kinetic traces (par. 1.4.4), which require correct baselines coincident with the value registered before the excitation (zero). This is especially important in view of the subsequent fitting operation (par. 2.4.2), which has to be performed on experimental data points.

The suitable experiment allowing us to rule out the N_2 laser as excitation light

48. In case of using a Xenon flash lamp for our measures (always possible) among the emission wavelengths in the visible only those between 400 and 600 nm have to be selected. Cutting below 400 nm (blue filter) has the reason to avoid UV radiations leading to long-term excitations; cutting above 600 nm (red filter) is in order to prevent interference of the excitation light with the monitoring beam (working in the NIR region).

consisted in a series of consecutive laser pulses (*train of pulses*) at time intervals of 8÷9 s between each other (for the purposes of the experiment to have exact intervals was not important): these were performed on dark adapted (i.e., relaxed) RCs reconstituted in vesicles. Charge recombination decay data were then corrected by keeping into account the corresponding baselines, in order to avoid absorbance drifts and artifacts (i.e., weak *bleaching*) caused by the measuring light and in order to compare results coming form different samples (see below). The resulting data were collected in the same plot showing photoinduced absorbance variations measured at 870 nm (Abs_{870}) versus time (par. 2.4.2).

By this way, after several N_2 laser pulses (frequency ~ 0.1 Hz) the baseline of data showed an evident shift toward negative values of $Abs_{870\ nm}$, just as some RCs were not able to recover the ground state PQ_A from the excited one $P^+Q_A^-$ (fig. 2.5). This behavior has been already attributed[195] to the formation of long-lived charge separated states $P^+Q_A^-$. It cannot be attributed instead to measuring beam effects just since these latter have been excluded by subtracting the relative baseline, which is sensitive only to the measuring light (obviously during baseline acquisition excitation light does not reach

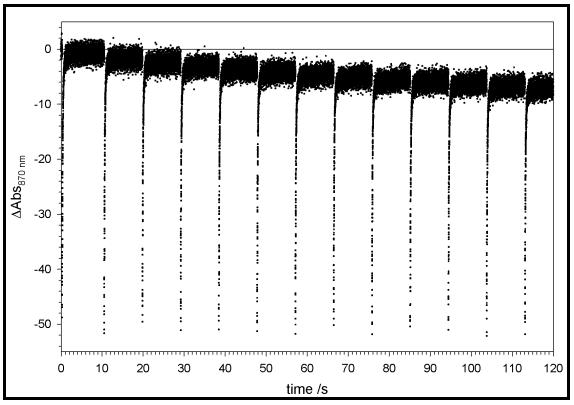

Figure 2.5.
UV (337 nm) laser N_2, 0.1 Hz pulse train effect on dark adapted Rcs in vesicles. Energy ~2 mJ/pulse. Corrected for the baseline.

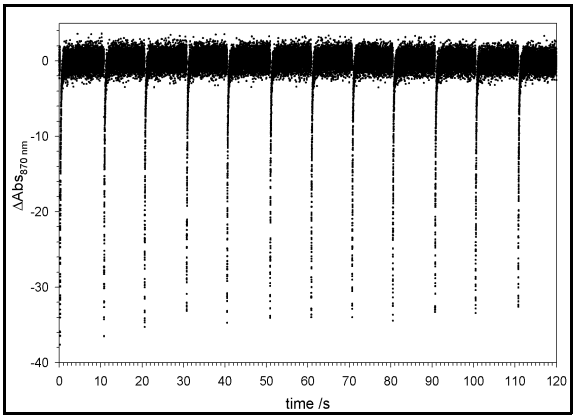

Figure 2.6.
Visible (400-600 nm) flash, 0.1 Hz pulse train effect on dark adapted Rcs in vesicles. Energy ~ 40 mJ/pulse. Corrected for the baseline.

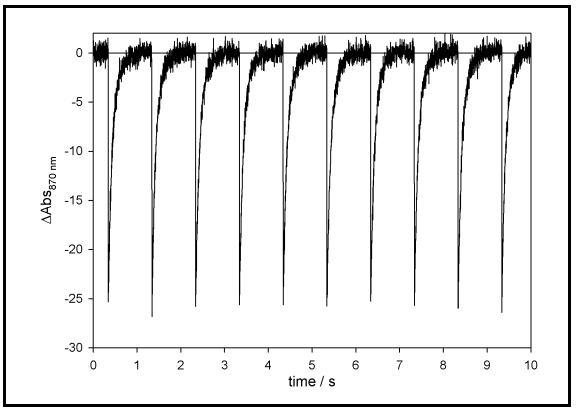

Figure 2.7.
Visible Nd:YAG laser (532 nm), 1 Hz pulse train effect on dark adapted RCs in vesicles. Energy ~ 300 mJ/pulse. Corrected for the baseline.

the sample).

Analogous experiments and the same data treatment were performed on similar RC samples, but by means of a Xenon visible flash lamp (frequency ~ 0.1 Hz) and of a Nd:YAG 532 nm laser (frequency ~ 1 Hz): results are reported respectively in figures 2.6 and 2.7.

The above figures clearly demonstrate that only these two latter light sources may be used without risking any long-lived charge separated state. The result of the Nd:YAG laser is however more significant: even at a ten times higher pulse frequency (10 Hz against ~ 0.1 Hz of both others) this light source does not induce any charge separation.

Also fig. 2.8 suggests such conclusions, showing the differences between absorbance variations after the i-th pulse (Abs_i) and after the starting pulse of the sequence (Abs_0). In addition fig. 2.8 shows that between flash lamp and Nd:YAG laser the latter should be preferred since it is the only having a well stable emission, with relative oscillations smaller than 4 %. The flash lamp instead - rather than leading to long-lived charge separated states (not evidenced in fig 2.6 since the baseline recovers always the initial zero value) - suffers an intrisic lack of stability, evident if the heights of the pulse peaks are compared. So for such reason, and also because of its monochromatic and short pulse emission, it has been established to use the Nd:YAG laser for all the measurements.

The fact that the least intense (~ 2 mJ/pulse emission) but UV exciting light was more effective than much more powerful visible light sources - such as Nd:YAG laser and flash lamp - in producing long-lived charge separated states is mainly a consequence of the RC absorption spectrum (fig. 1.33, par. 1.4.3.1). Here, in the UV region around 337 nm there is a sharp peak, with an absorbance values ~1.0, attributed to both the aromatic amino acids of the protein and the ubiquinone molecules. On the contrary, at 532 nm and

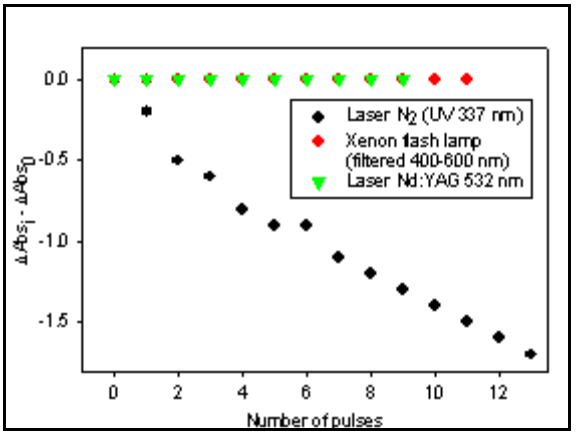

Figure 2.8.
Pulse train effect on the PQ_A state recovery for different excitation light sources (see text for details).

in the 400÷600 nm range absorbance is always lower than 0.35.

Moreover, the differences among light sources in generating long-lived charge separated states could be related also to their photon energies, at 337 and 532 nm. The variation between them is only by a factor of 1.6, which seems to be too small to determine such different consequences.

2.3.4. Electronic details about the apparatus.

2.3.4.1. Photodiodes.

The purpose of any photodetector is to convert electromagnetic radiation into an electronic signal, ideally one that is proportional to the incident light intensity.

Photodetectors can be either photomultipliers (PMT) or photodiodes (PD).

Since in our photolysis apparatus we employed a PD, this paragraph will be dedicated mainly to some features of PDs, though for the sake of comparison PMTs will be mentioned anyway.

It is worth noticing that because they are compact, versatile and can be produced economically in high volume, PDs have become the detector of choice in applications from biomedical instrumentation to telecommunications.

PDs are fabricated from semiconductor materials, among which the most popular choices are silicon (Si) or gallium arsenide (GaAs)[196].

When a photon of light is absorbed it excites an electron and produces a single pair of charge carriers in the semiconductor lattice, an electron and a hole (i.e., an electron vacancy). Current passes through a semiconductor when the charge carriers separate and move in opposite directions. The trick in a photodiode is to collect the photon-induced charge carriers as current or voltage at the electrodes, before they have a chance to recombine. This is achieved using a *pn* or *p*-*i*-*n* diode junction structure (hence the term *p*-*i*-*n* photodiode), in which *n* and *p*-type semiconductor materials are doped to produce respectively an excess or a deficiency of electrons.

At the *pn* junction, this disparity creates a concentration gradient which causes electrons to diffuse into the *p*-layer and holes to diffuse into the *n*-layer (*diffusive force*). This diffusion produces an opposing internal electrical field (and an electrical potential) across the junction, which attracts charge carriers in the direction opposite to that of the previous diffusive force (*drift force*, fig. 2.9). The resultant equilibrium condition is characterized by a small *internal bias* voltage (to whom an external one may be added), causing any charge carriers in the region spanning both sides of the junction - called also "depletion region" since charge carriers cannot reside there - to be rapidly swept to the appropriate original layer.

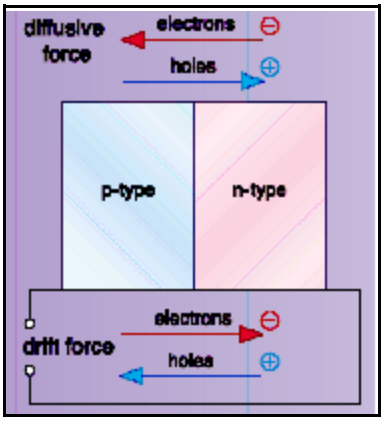

Figure 2.9.
Scheme illustrating how the internal bias voltage originates from the equilibrium between diffusive and drift forces acting on the charge carriers.

Hence, in a *p-i-n* photodiode, charge carriers produced by photon absorption are swept across the junction by the internal (and any external) voltage bias, which produces a small photocurrent at the electrodes (represented in fig. 2.9 as white little circles connected by wires to *p* and *n* semiconductor materials, see also fig. 2.10). In a generic *p-i-n* PD, light enters the device through the thin *p*-type layer.

The *quantum efficiency* of a PD is defined as the ratio of the photocurrent in electrons to incident light intensity in photons: this is a measure of the PD sensitivity.

The most important performance characteristics of PDs are response speed, quantum efficiency at the wavelength of interest, size and shape of the active area, response linearity, spatial uniformity of response, dark noise and other noise sources impacting sensitivity.

Our use of a silicon PD as a detector instead of a PMT was dictated by two main considerations: the low energy of the electromagnetic (EM) wave necessary to be monitored by the detector (high sensitivity in detecting) and the need of keeping instrumental costs as low as possible.

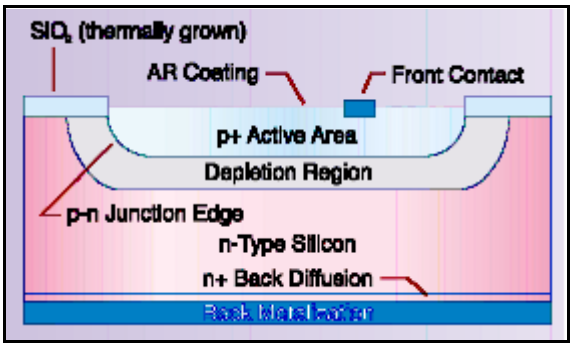

Figure 2.10.
Schematic representation of a photodiode.

Silicon PDs absorb light over the

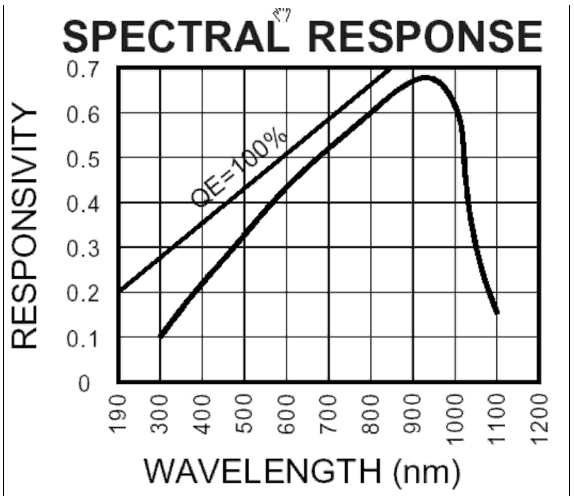

Figure 2.11.
Typical spectral response of a silicon photodiode.
QE = Quantum Efficiency.

range 250÷1100 nm (GaAs instead between 800 and 2000 nm). In this region the typical PMT sensitivity is not very high and this results in a poor S/N ratio unless one uses particularly designed PMT with enhanced response in the NIR range, which are usually extremely expensive and often require quite complicated experimental setup (for example, most of them need to be cooled in order to work properly). On the contrary, at least in the NIR region where our measuring light falls (870 nm), silicon PDs show a peak in their sensitivity (fig. 2.11), thus requiring for our purposes practically no amplification at all. Moreover the flat shape of our silicon PD was right in order to attach the device just on the outer slit of the monochromator, quite reducing complications in building the sample compartment of our instrument and, consequently, reducing also its cost.

The silicon PD selected by us, manufactured by UDT (now OSI Electronics), has an high active surface (10 mm^{+2}) and it is equipped with a BNC connector that eases its insertion in the circuitry. Since the kinetics of the photochemical event that we are interested to follow is of the order of seconds, the fact that the rising time of the selected PD is around 1 μs does not influence the reliability of the measurements[196].

2.3.4.2. Current-to-voltage conversion.

When in a PD the signal is detected as a current this is referred to as a *photoconductive operation*: in that case an external electrical bias (voltage) is applied to *p* and *n* layers, i.e., in order to expand the thickness of the junction region for several purposes. Conventional unbiased operation (without applying an external voltage) is instead referred to as *photovoltaic operation*, because signal is detected as a voltage.

This latter is preferable for applications requiring high linearity of response and/or low dark noise[196]: in our case the latter condition was especially important since light signals could be weak.

So, in order to monitor the low current induced by incoming photons in the circuitry where the PD is inserted, the most convenient way seems to convert this current into a voltage, by means of a high impedance *operational amplifier* (OPAmp). A high input impedance was necessary to avoid a high amount of current to be drained from the PD junction and so to generate an amplified voltage from a given input current.

According to the electrical scheme of fig. 2.12, we choose to have our PD operating in a photovoltaic mode since in our measurements the conditions of low level for light / low response speed are met. Detection of weak (or unfocused) light requires PDs with a large active area, which raises the capacitance of the PD circuitry (measured in faraday, F), slowing in turn the PD frequency response (low response speed).

Electrical characteristics of even a simple PD can be remarkably complex, so engineers usually represent PDs with *equivalent circuits*. These are virtual circuits consisting of multiple components whose overall behavior matches that of the PD[196].

The OPAmp used to convert current to voltage is a di-FET, high gain, high speed operational amplifier manufactured by Texas Instruments (OPA 637AP): it works with practically unitary gain and with a feedback capacitor of 10 pF in order to limit the frequency response and to avoid gain peaking. As a whole, the circuitry shown in fig. 2.12 led to a detector electronic dead time of the order of few microseconds, thus ensuring extremely reliable measurements with a time resolution of the order of hundreds of milliseconds.

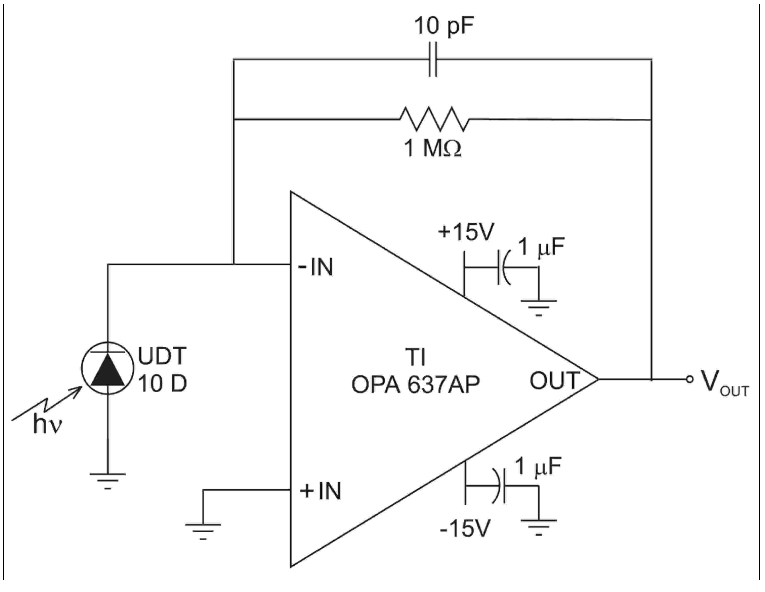

Figure 2.12.
Electrical scheme of the current to voltage converter used in the detector of the home-built single beam spectrophotometer.

2.4. Signal acquisition and data treatment.

2.4.1. Signal monitoring and processing.

In order to acquire and digitalize the signal coming from the photodiode (component nr. 4 in scheme 2.2 and in both figures 2.4 A and 2.4 B), a 16 bit resolution and 200 kS/s acquisition board PCI 6013 from National Instruments (nr. 6 in scheme 2.2 and in fig. 2.4 B) has been used in connection with the BNC 2120 multifunction board (device allowing to attach the suitable cables to the PC board).

To fully access the Data Acquisition (DAQ) features, a software working in the LabView 6.0 environment has been designed.

Though the PCI 6013 board can manage up to 16 not referenced[49] single ended analog input signals, for our purposes just one input has been used.

As a source of pulses, the PCI 6013 board can produce two distinct analog pulses (whose characteristic height, proportional to voltage, and width are software selectable) to be addressed to two independent BNC port onto the BNC-2120 board. It can also manage up to 8 independent digital I/O signals. These features have been fully used in order to drive our home built single beam photolysis apparatus (par. 2.3.2), according to the following description.

In order to avoid the sample from being illuminated by the actinic measuring light during periods other than the measuring time, the 870 nm laser diode (nr. 2 in scheme 2.2 and in fig. 2.4 A) has been gated. This has been accomplished by using one of the eight digital output port of the PCI 6013 board.

When in the logical status 1, the + 5V output voltage was used to drive a relay acting on the power supply of the measuring laser light source. To allow the damping of any drift in the light intensity, the turning on of the measuring light was performed 5s (this time is indicated as Δt_1 in fig. 2.13) before to start any measurement.

A 100 ns wide and 5 V high square pulse was then generated by the PCI 6013 board in order to be used as pre-trigger pulse for the acquisition (TRG_1 in fig. 2.13), which started as soon as a second 100 ns wide, 5 V high square pulse was generated

49. That is “whose potential is not referred to a common ground”.

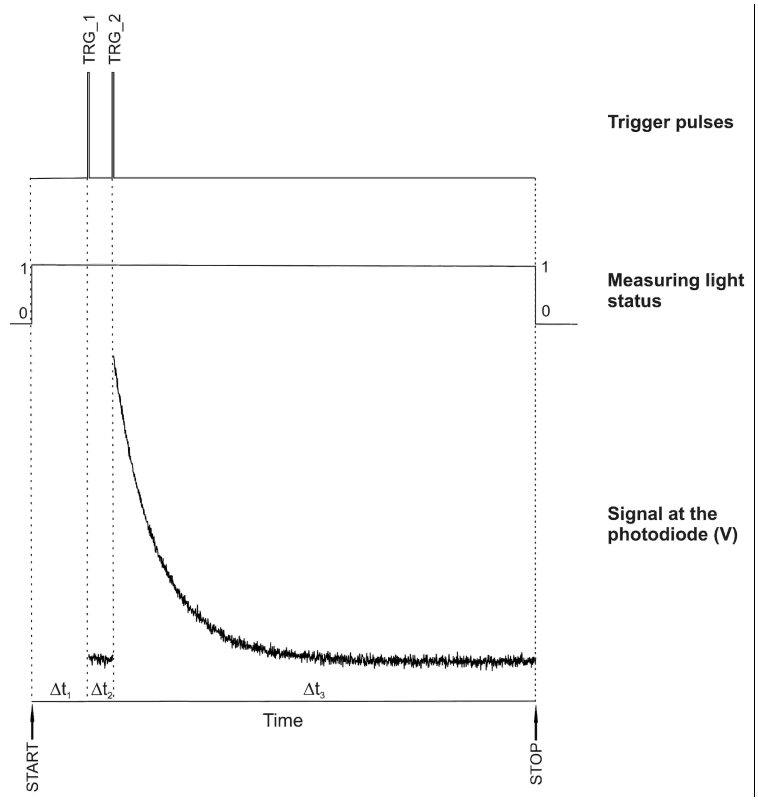

Figure 2.13.
Pulse sequence generated by the PCI 6013 acquisition board (see text for details). The time lengths indicated in the drawing are not in scale.

(TRG_2 in fig. 2.13). The number of points acquired as pre-trigger was software selectable, and the time required for their acquisition is indicated as Δt_2 in fig. 2.13. TRG_2 pulse was also used as external trigger source for the Nd:YAG excitation laser pulse.

The time required to acquire the charge recombination signal (also in this case software-selectable both as number of points and scan rate) is indicated as Δt_3 in fig. 2.13. Once the trace was acquired, the switching of the digital output to 0 logical condition (0 V) led to the turning off of the measuring light. The total light exposure of the sample to the actinic measuring beam results, therefore, from the sum of the three Δts.

Generally, several scans were acquired for each experiment (their numbers being also software selectable), and among consecutive scans a waiting time of at least 60s has been always used (as suggested by literature data[195] in order to prevent the formation of long-living charge separated states).

The averaging of the traces and the subsequent conversion of the variation in the sample transmittance (T, expressed as the difference $\Delta V = V_{(t)} - V_{(t=0)}$) into absorbance variation, ΔAbs, was also accomplished by the dedicated software, which made also possible the storage of the averaged trace as ASCII file.

2.4.2. Kinetic trace deconvolution.

Temperature-dependent measures on RC micelles and proteoliposomes have been performed by recording the charge recombination kinetics (par. 1.4.4) for every chosen temperature at 870 nm, in close proximity to the absorption peak of the bacteriochlorophyll dimer (P, 865 nm).

Photoexcitation leads to a decrease of the absorbance at 870 nm ($\Delta Abs_{870\ nm} < 0$, called *bleaching*) because of the P oxidation to P^+; subsequently there is an exponential decay of the absorbance variation until it reaches the pre-flash initial value of zero. Therefore kinetic traces $\Delta Abs_{870\ nm}$ versus time, made of thousands of experimental points, will have the form of negative exponential curves (fig. 2.14). In our case usually 4000 points*s^{-1} were acquired, but their number is software selectable and it has a direct proportionality with resolution during data acquisition (par. 2.3.2).

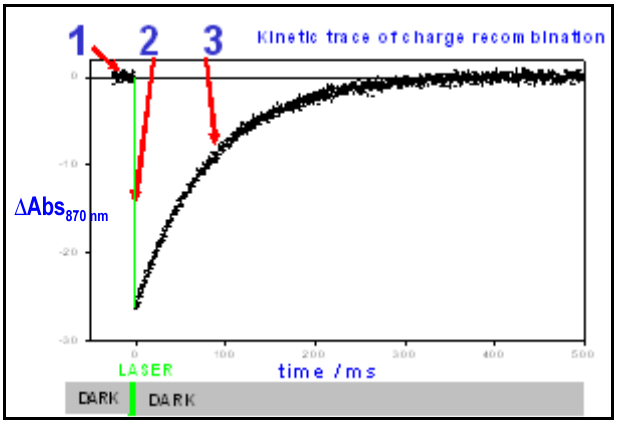

Figure 2.14.

Phase 1. Initial **baseline** points (RC dark adapted)

Phase 2. **Laser pulse** ⇒ photolysis ⇒ bleaching (Dabs < 0)

Phase 3. **Charge recombination**: exponential decay $P^+Q_A^- \rightarrow PQ_A$, intramolecular process, first order.

In detergent solution quinone-depleted RCs have showed only single-exponential $P^+Q_A^-$ recombination with k_{AP} as kinetic constant of the decay (par. 1.4.4), as follows:

$$\Delta Abs = \Delta Abs^\circ * [\exp(-k_{AP} * t)] \qquad \textbf{(2-2)}$$

Otherwise, when the same RCs are inserted in liposomes a small fraction of proteins undergoing $P^+Q_B^-$ charge recombination (with constant $k_{BP,}$ see par. 1.4.4) is detected, and the overall P^+ decay can be accounted for by two exponentials (eqn. 2-3):

$$\Delta Abs = [\Delta Abs_F * \exp(-k_{AP} * t)] + [\Delta Abs_S * \exp(-k_{BP} * t)] \qquad \textbf{(2-3)}$$

where ΔAbs_F, ΔAbs_S are the contribution to the total change in absorbance ΔAbs, respectively from “fast decay” (rate constant k_{AP}) and “slow decay” (rate constant k_{BP}).

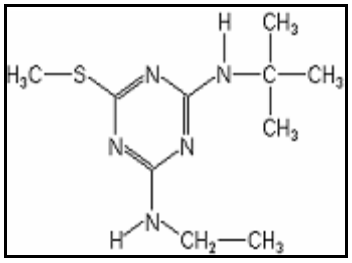

Figure 2.15.
Terbutryne structure.

This is due to the statistical distribution of quinones and RCs among vesicles[197]. Addition of terbutryn (a competitive inhibitor for the Q_B site whose structure is shown in fig. 2.15) restores the single exponential behavior of the $P^+Q_A^-$ decay. The amplitude of the bleaching at time=0 and the rate of $P^+Q_A^-$ recombination were found to be unaffected by the presence of the inhibitor (data not shown).

Experimental data were fitted to the relevant equations by a least square routine based on the Simplex[198, 199] algorithm implemented in the STEFIT software (Stelar s.n.c., for some details see par. 2.4.3.3). Given the cross-correlation between some best-fit parameters (par. 3.1 of the Third chapter), the error associated with the *i*-th fitting parameter was evaluated by means of a *Monte Carlo simulation*, as described in literature and in par. 2.4.3.2[200].

Moreover, to experimental data collected from proteoliposomes made of PC or CL (fig. 3.3) was applied an advanced calculation and fitting procedure, named *global analysis*[201](par. 2.4.3.3): the aim was to reduce the uncertainty associated to every fitted parameter.

2.4.3. Statistical analyses of data.

2.4.3.1. Krug's approach to the enthalpy-entropy compensation effect.

This paragraph would like to be an introduction to the statistical analysis carried out first by Krug and coworkers - and adopted by us in par. 3.1 - in order to "successfully manage" the frequent compensation effect found in enthalpy/entropy experimental data.

Measures of the photoinduced absorbance variations $\Delta Abs_{870\ nm}$ following temperature variations and subsequent fitting procedures (par. 2.4.2) allow to determine

enthalpy and entropy changes related to the ubiquinone binding process at the Q_A site. For this purpose it is necessary to perform a Van't Hoff analysis of thermodynamic data, as it will be shown in the Third Chapter, par 3.1.

In this view, it is worth noticing that plots of enthalpies vs. entropies often form straight lines. Several standard chemistry text treat these linear plots as authentic representation of an extrathermodynamic relationship (i.e., not related to thermodynamics), which is sometimes called *isokinetic effect* or *enthalpy-entropy compensation effect*. High values of the correlation coefficient in enthalpies vs. entropies plots are taken to imply chemical causation for the linear correlations: probably for this reason many researchers use to fill and publish such plots[202].

On the contrary, it has already been demonstrated[202] that when enthalpy and entropy data are plotted in the way above mentioned any true functional dependence (i.e., extrathermodynamic or chemical) - if exists - is usually masked by a dominant statistical compensation pattern which arises solely from experimental errors. That is, the observed distribution of data points along straight lines in these planes is more often due to the propagation of measurement errors rather than to a chemical origin. Statistical compensation has been often confounded with chemical questions, in the hypothesis that in these cases chemical variations were small compared to experimental errors. It has been also developed a hypothesis test for determining whether the observed compensation effect has a strong chemical contribution or whether the observed distribution of data in such plots is indistinguishable from a statistical pattern generated by random errors.

This analysis may be applied to the cases for which enthalpies, entropies and free energies are estimated from the variation of rate (*k*) or equilibrium constants (*K*) with temperature[202]. In fact both kinetic and equilibrium enthalpy and entropy determinations can be made similarly using plots of such constants vs. inverse temperatures (eqns 2-4a and 2-5a): enthalpies are obtained from the slopes of data on Arrhenius or van't Hoff plots and entropies are obtained from the respective intercepts.

ARRHENIUS EQUATION

$$k = A * \exp(-E_A/RT) \qquad \textbf{(2-4)}$$

VAN'T HOFF EQUATION

$$K = \exp\left(-\frac{\Delta G^\circ}{RT}\right) \qquad \textbf{(2-5)}$$

ARRHENIUS PLOT based on the equation:

$$\ln\left(\frac{k}{A}\right) = -E_A/RT \qquad \textbf{(2-4a)}$$

$$E_A = \Delta G^* = \Delta H^* - T\Delta S^* \qquad \textbf{(2-4b)}$$

$$\ln\left(\frac{k}{A}\right) = -\frac{\Delta H^*}{RT} + \frac{\Delta S^*}{R} \qquad \textbf{(2-4c)}$$

VAN'T HOFF PLOT based on the equation:

$$\ln K = -\frac{\Delta G^\circ}{RT} \qquad \textbf{(2-5a)}$$

$$\ln K = -\frac{\Delta H^\circ}{RT} + \frac{\Delta S^\circ}{R} \qquad \textbf{(2-5b)}$$

Note. Stars (*) indicate thermodynamical parameters of *activation*, that is referred to the transition state.

Errors associated with the measurements, $\ln k_i$ and $\ln K_i$, are assumed to be normally (i.e., according to a gaussian distribution) and indipendently distributed with zero mean and constant variance. In par. 3.1 of the next chapter we will meet only the van't Hoff equation 2-5a referred to the binding equilibrium of the ubiquinone Q_{10} at the Q_A site.

Data taken over narrow temperature ranges give relatively uncertain enthalpy and entropy estimates, together with ΔH - ΔS correlation coefficients approaching unity. So, if $\ln k_i$ or $\ln K_i$ data are plotted against inverse temperatures they show a strong dependence of the intercept estimate (proportional to ΔS of the examined process) on the slope estimate (proportional to $-\Delta H$) just because the data were taken over a very small temperature range far from the origin[202] (fig. 2.16).

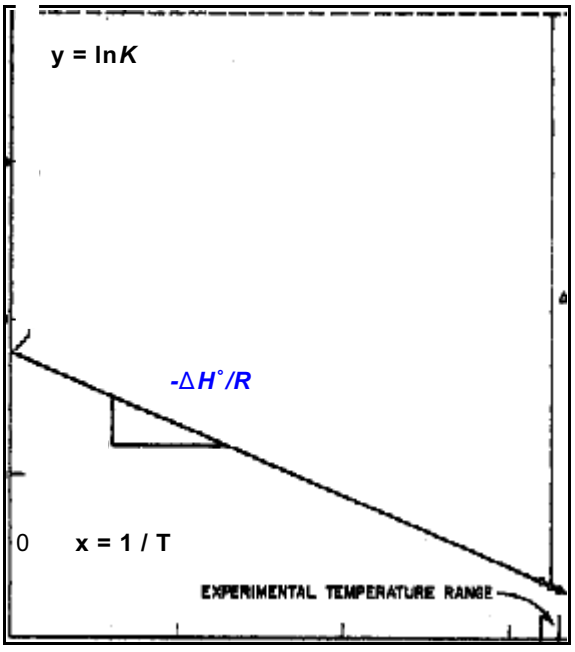

Figure 2.16.
Plot of *lnK* vs. 1/T (according to equation 5b).

In fact, whenever experimental errors are large compared to thermodynamic variations, the estimated correlation coefficient will be usually much larger than 0.95[202]. This will be just the case of our measures about quinone binding at the Q_A site (par. 3.1).

Correlated parameter estimates are

obtained in other chemical investigations as well. In enzyme studies, for example, the Michaelis-Menten parameter estimates corresponding to the maximum catalysis rate and to the substrate concentration determining half of the maximum rate[203] (called respectively v_{max} and K_m) are highly correlated if estimated from a Lineweaver-Burk plot when the range of inverse substrate concentration is small. The magnitude of this correlation can be found by an analysis parallel to the one given above[202].

A. The statistical compensation equation. To determine the distribution of enthalpy and entropy estimates in the ΔH - ΔS plane due to experimental or measurement errors it is necessary first to consider the shape of the relevant confidence region[204] (defined as the range in which with a x % probability the experimental values will fall, hence called "x % confidence limit", e.g. 68 % or 95 %[205]).

Since the form of the model to which data are fitted is linear (Arrhenius or van't Hoff plot), the confidence region at any level of significance (that "x %" above mentioned) is elliptical[202]. The extreme elongation of the ellipse gives it the appearance of a straight line. Moreover, canonical analysis of the elliptic equation shows that the major axis has a slope of $T_{hm} = < 1/T_i >^{-1}$, being T_{hm} the harmonic mean performed on the experimental temperatures T_i (see also definition at p. 209, eqn. 3-6). Thus enthalpy and entropy estimates will fall along a line with slope T_{hm} when the experimental errors are large compared to thermodynamic variations (temperature included). Thus data plotted in ΔH - ΔS coordinates with a high correlation coefficient and slope near T_{hm} must be suspect of having experimental errors masking (i.e., which can be confounded with) any chemical or physical effect that may be present[202].

B. Hypothesis test. A useful hypothesis test should discriminate between the statistical compensation pattern and any linear chemical compensation pattern.

Moreover, the elaboration of this test will allow to understand how tightly correlated thermodynamic parameters (e.g. H° and S°) can be substituted in a suitable way by uncorrelated ones (such as H° and $DG^\circ(T_{hm})$, the binding free energy measured at the harmonic temperature), as it will be done in the eqn. 3-7 (par. 3.1).

Since the statistical compensation pattern and any linear chemical compensation pattern between ΔH and ΔS have an identical linear dependence it is possible to start

expressing them in the same form, as[206, 207]

$$\Delta H = \beta * \Delta S + \Delta G(T_{hm}) \qquad \textbf{(2-6)}$$

As a matter of fact, the two linear compensation patterns differ only for the parameter β: hence in order to discriminate between them it is sufficient to test the value of this parameter.

The hypothesis is the following: if it is $\beta = T_{hm}$ then the origin of the correlation and of the compensation between Δ*H* and Δ*S* is mainly statistical, due to the propagation of experimental errors (as already mentioned before). Unless this hypothesis can be rejected there is no reason to suspect the existence of chemical or physical causation and therefore no reason to create theories in order to explain it (apart from purely statistical ones).

Many authors[206, 207, 208] have already warned that plots with slopes approximately equal to experimental temperatures (the average of the whose inverse values is defined as the harmonic temperature T_{hm}) may be simply manifestation of the propagation of experimental errors. A deep examination of literature data definitely confirmed this suspect[202].

An ordinary least-square analysis on Δ*H,* Δ*S* data is enough to reflect the statistical compensation effect that is always present between them. If the data are sufficiently far from the statistical compensation line, the estimate of the slope of the line fitting them (β) will be significantly different from T_{hm} and it would suggest the probable presence of a detectable chemical or physical compensation factors (thus the $\beta = T_{hm}$ hypothesis would be rejected).

The test just illustrated is based on the following analysis. The line describing the major axis of the ellipse composed by any single experimental data pair can be derived from a canonical analysis to be given by the equation[202]

$$(\Delta H - \Delta H(T_{hm})) = T_{hm} * (\Delta S - \Delta S(T_{hm})) \qquad \textbf{(2-7)}$$

that is equivalent to

$$\Delta H = T_{hm} * \Delta S + \Delta G(T_{hm}) \qquad \textbf{(2-8)}$$

This equation will be used in par. 3.1 (eqn. 3-7) in order to describe the dependence of the ubiquinone binding equilibrium on temperature in terms of two

parameters ($\Delta G^{\circ}(T_{hm})$ and ΔH°) whose estimates are statistically independent on one another, contrary to ΔH° and ΔS°.

Thus, under the assumption that a series of data pairs (ΔH, ΔS) vary only as a consequence of measurement errors from a single pair of fixed values of thermodynamical parameters ($\Delta H(T_{hm})$, $\Delta S(T_{hm})$) and that the resulting probability ellipse is very elongated (which is a good approximation for usual experimental temperature ranges), the data (ΔH, ΔS) will be distributed essentially along a line characterized by a known slope, T_{hm}, and unknown intercept $\Delta G(T_{hm})$. It has been demonstrated also that: deviations from that line in a perpendicular direction (approximately the direction of the ΔH or *y* axis) have the magnitude of the error on the free energy estimate $\Delta G(T_{hm})$; deviations have zero mean and constant variance; the spread of data along the statistical compensation line is generally much greater than that away from it, for usual experimental temperature ranges.

Finally, because of what is has been just examined, standard deviations (i.e., errors) of free energies estimated from the standard deviations of enthalpies and entropies must take into account the correlation between ΔH and ΔS[202].

2.4.3.2. Monte Carlo method.

Introduction. As well as the previous, also this paragraph would like to be an introduction to a quantitative analysis method which has been applied on many experimental data collected for the work represented by this Thesis.

As first point, quantitative analyses of experimental data generally involve some numerical processes in order to provide the best estimates for the parameters of the model employed to characterize observations (least-squares[209], method of moments[210], etc.).

Then, as second point, the derived parameter values are, in turn, interpreted to provide information about the observed properties of the experimental system being considered. This fundamental process applies either for the simplest of analyses or for the highly sophisticated modeling algorithms in use today for interpretation of a wide

range of complex biomolecular phenomena.

Anyway, the level of confidence one can have in the interpretation of derived parameter values depends strongly on the nature and magnitude of the confidence probability distribution of the same values about their most probable (or best-fit) estimates.

Determination of reliable estimates for confidence intervals associated with model parameters may be critical in discerning between alternative interpretation of some biomolecular phenomena (e.g. the statistical justification for existence of quaternary enhancement in human hemoglobin oxygen-binding behavior[211]). In other words, about the first point above mentioned, not only the most probable derived value (best estimate) is significant, but also the shape and breadth of the distribution of expected parameter values are also of critical importance with regard to arriving at a statistically significant conclusion. Knowledge of complete confidence probability distributions, as well as the possible correlation existing among parameters is also very useful for pointing out the relative behavior of parameters between different models used to interpret the same data (e.g. models that explicitly account for ligand cooperative binding versus those allowing nonintegral binding stoichiometries to accommodate effects arising from cooperativity).

Methods for estimation of parameter confidence intervals vary in the level of sophistication which has to be employed to obtain a certain level of reliability for estimates.

It is worth noticing that the great majority of parameter estimation procedures employed in the interpretation of biophysical data are cast in terms of complex mathematical expressions and processes that require evaluation of nonorthogonal, correlated model parameters.

Moreover, the numerical procedures that have been developed for estimating confidence intervals all involve some approximations, particularly about the shape of the confidence probability distributions[201]. Sometimes these approximations may produce grossly incorrect estimates, particularly with more simplistic methods applied to situations exhibiting correlation (also complex, nonlinear) among the parameters being estimated[212]. An example could be found in par. 3.1, dealing with the strongly correlated ΔH and ΔS parameters without using the Krug's approach illustrated in par.

2.4.3.1.

Monte Carlo method in details. The ultimate objective of a quantitative analysis method of experimental data is to have available the entire joint confidence probability distributions for each of the parameters being estimated in an analysis. The Monte Carlo (MC) approach is unique in the sense that it is capable of determining confidence intervals for probability distributions, in principle to any desired level of resolution and it is conceptually extremely easy to implement.

The necessary informations for the application of a MC method in order to estimate confidence intervals and probability distribution profiles of experimental data is twofold:

a) an accurate estimate of the distribution of experimental uncertainties associated with the data being analyzed (it corresponds approximately to the first point at the beginning of this paragraph;

b) a mathematical model capable of characterizing the experimental observations (it collects in some way both points at the beginning of this paragraph).

The MC method is then applied by means of (fig. 2.17):

1) a statistical analysis of the experimental data (*fitting*) in order to find the *most probable parameter values* - the so-called "*best estimates*" or "*best-fitting parameters*" - associated with the corresponding uncertainties, according a suitable mathematical model (i.e., one capable of reliably describing the data[50]);

2) a generation of a "perfect data set" ("noise-free" simulated data points, see below): the calculation is performed on the same equations of the model with the new available parameters, using also exactly the same indipendent variable

50. We will proceed further on under the assumption that the mathematical model being used to analyze the data is properly "valid" (i.e., absolutely exact, not under discussion) in terms of both statistical probability and theoretical predictions, not only following empirical fitting [201, 209].

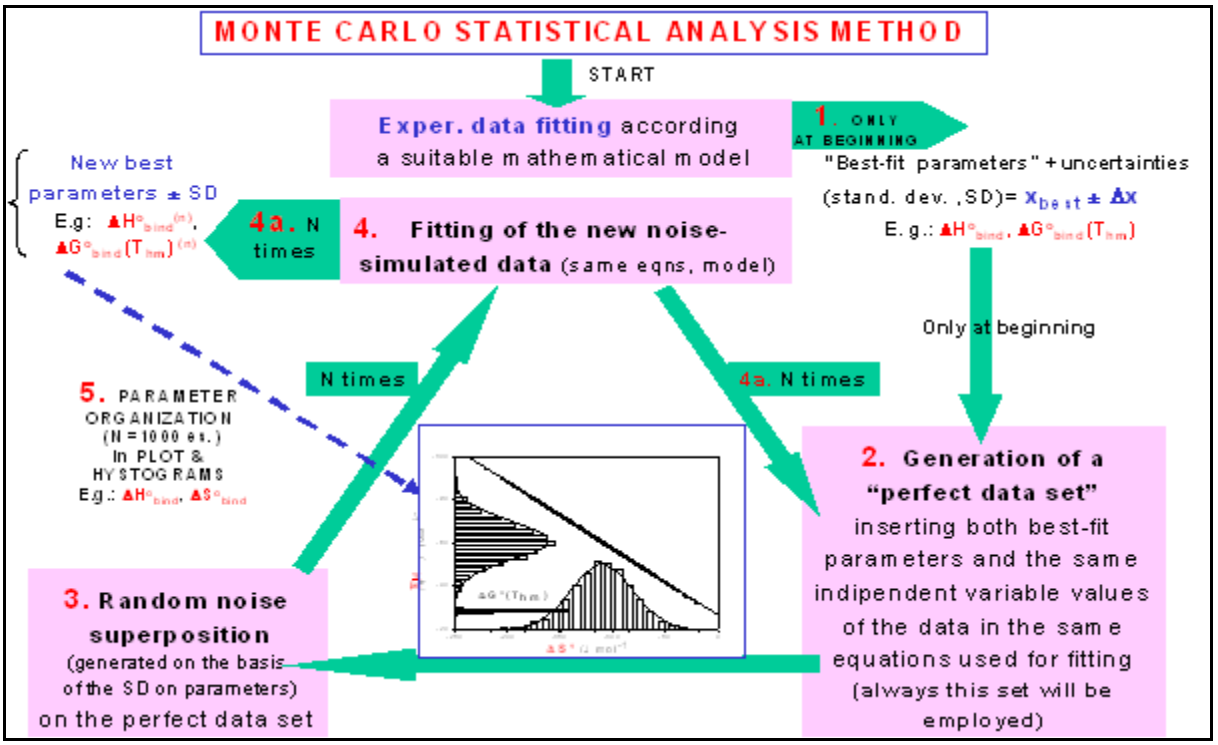

Figure 2.17.
Scheme illustrating the Monte Carlo statistical analysis method: numbers are the same as in the explanation at the previous page. Examples drawn from a thermodynamical application of this method are signed in red colour (see par. 3.1 for details).

values as those occurring in the original data;

3) a superposition of a few hundred sets (*n*) of simulated noise (evaluated on the basis of the experimental data uncertainties) on the “perfect” data;

4) another statistical analysis of each set of noise-containing data (e. g. nonlinear least squares fitting) according to the same model equation chosen for the initial fitting procedure, step 1); subsequent tabulation (*plot*) of each set of the new most probable parameter values;

5) a generation of hystograms on the basis of the tabulated sets of values.

The above mentioned hystograms represent discrete approximations of the model parameter confidence probability distributions, as derived from the original data set and from the distribution of experimental uncertainties contained therein.

The level of resolution attainable in determining confidence probability profiles by this method is dependent on the number of MC "cycles" performed (i.e., the number *n* of noise-containing, simulated data sets considered): the more cycles carried out, the more accurate will be the resolution of the probability distribution. Consequently, the amount of computer time needed to generate a probability distribution after 100÷1000 MC cycles will be of the order of 100÷1000 times that required for an individual parameter estimation (fitting procedure).

Though long time consuming, no other method is considered so easy in order to provide profiles of confidence probability distributions associated with estimated model parameters[212].

After some 100 to 1000 of such fits the estimated parameters are generally analyzed for the mean, standard deviation, skew and kurtosis of the distribution of values for each parameter. The skew and kurtosis are effectively the second and third moments of the distribution. To be statistically different from a Gaussian distribution the skew and kurtosis must be larger than the absolute value of $(6/n)^{1/2}$ and $(24/n)^{½}$, respectively, *n* being the number of cases (i.e., the number of data sets) in the obtained parameter value distribution[199].

The purpose of viewing these distributions is to investigate instrinsic biases inherent in the parameter estimation. For example, simulations by Straume and Johnson[211] demonstrated inherent skewing in estimates of intrinsic and cooperative free energy terms for models of oxygen binding to hemoglobin.

Biased distributions can also be generated by over- or underdetermined fitting problems or highly correlated parameters (par. 2.4.3.1). Fits are judged to be "good" if the variance of the fit is the same as the standard deviation of that noise set and if the residuals are random. Square correlation coefficients (R^2) vary from 0 to 1, with a value of 0 indicating a complete absence of correlation and 1 indicating perfect correlation[213].

2.3.4.3. Global analysis of biochemical and biophysical data.

Introduction. Global analysis of data represents the simultaneous analysis of multiple experiments in terms of internally consistent sets of fitting parameters. In other words, in these experiments parameters are assumed to be referred to the same equations or relations, so that reference parameters and equations are the same for many sets of experimental data (homogeneous data but obtained from different experiments).

Such an analysis has been applied to several samples of proteoliposomes made of CL or PC, separately for CL and PC (two and three, respectively).

This type of analysis has been previously introduced in many different fields and by many different groups. It is important here to give and explain a motivation for performing global statistical treatments and rigorous error analyses.

The goal of experimental science, biochemistry as well as other sciences, is to relate laboratory observations (i.e., data) into biological information (e. g. rate constants, binding constants, etc.). Regretfully, the laboratory techniques utilized in biochemistry and biophysics very rarely directly yield useful biological information: the researcher must instead analyze data in such a manner as to extract information from them.

The first analysis problem is generally to determine what class of mathematical and computer algorithms should be applied to model and fit the data. The relationship between experimental observables and biological informations in almost all of biochemistry and biophysics is nonlinear. In the majority of cases referred to these scientific fields (greater than 90 %[201]) the proper technique to analyze the data is nonlinear least-squares[214].

A typical mistake in such a work is attempting to transform data in a manner such that a nonlinear model is transformed into a linear one. Many transforms of this type have been utilized in biochemistry, as the Scatchard plot or general logarithmic transformations or the Lineweaver-Burke double-reciprocal plot (par. 2.4.3.1). Although using graphical transforms in order to obtain experimental parameters is still common practice, these methodologies should be avoided if at all possible. A general rule is then that data should not be transformed in any way (besides trivial linear operations such as multiply, divide or add a constant value) prior to performing a data analysis. In fact

graphical transformations still in use in biochemistry were developed prior to the existence of laboratory computers and good nonlinear analysis software. These conditions now no longer exist, so graphical methodologies should definitely not be considered viable techniques, but they have to be used only as simple representations of the data: statistical analysis should be performed in a nonlinear fashion on the "raw" data[201].

About this topic requirements of different laboratories in biochemistry and biophysics vary greatly.

When only small numbers of data points (e. g. 10 ÷ 500) have to be fitted to model equations which can be easily described analitically (e. g. sums of exponentials such as charge recombination decay kinetic traces mentioned in par. 1.4.4 and shown in par. 2.4.2, if considered individually, or simple binding isotherms) prepackaged nonlinear data analysis programs will probably be sufficient. An example of a general purpose software of this type would be SigmaPlot 9.0, that we used for quick initial fitting procedures on individual exponential decay curves (Systat Software, Inc., Point Richmond, CA, USA). Within this software one can specify model equations containing several fitting parameters as well as indipendent variables.

On the contrary, if a research laboratory routinely analyzes larger number of data points and/or multiple experiments (global analysis) with more complicated sets of fitting functions, it will be more advantageous to adopt a nonlinear statistical program which can be specifically modified and optimized for particular experimental configurations.

An example of this second type of software is STEFIT (already mentioned in par. 2.4.2). This is a versatile function fitting package running in DOS language. Its rather unique feature is the possibility to fit simultaneously several experimental curves with shared adjustable parameters. Worth mentioning is also the opportunity of defining User functions, choosing among several fitting algorithms[215].

Global analysis approach. Instead of graphical or similar mathematical transformations of experimental data, above mentioned as methodologies to avoid, it is important to consider that incorporating "scientific constraints" into the data analysis can lead to obtain useful biological informations from a whole set of experiments. In other words, "scientific constraints" denote direct application (into the statistical analysis

software and *a priori*) of the mathematical constraints imposed on the data through experimental conditions and design and accessory information[201].

An example may help to clarify this concept. For many classes of data, one is often interested in recovering closely spaced lifetimes (τ, or kinetic constants, *k*) from a sum-of-exponentials model equation. If one simply consults data analysts (or mathematicians) and describes that one needs to recover from data with noise multiple lifetimes which differ by as little as 5 ÷ 10 % of their values, they will say that it is impossible. Experimentally, on the contrary, one may be able to manipulate the system under investigation such that very closely spaced exponentials can be resolved. This is possible by constraining the data analysis referred to multiple experiments: in the field of time-resolved fluorescence spectroscopy, for instance, multiple data sets can be obtained which all have a common set of lifetimes but differing preexponential terms, by collecting individual kinetic measurements at multiple emission wavelengths. If one analyzes all the various data of these multiple experiments as if they were indipendent of one another, then the multiple closely spaced relaxation times cannot be recovered. If data analysis of all the experiments is instead carried out simultaneously, applying the scientific constraint that all the data sets have internally consistent sets of relaxation times (with varying amplitude terms), then the correct relaxation times may be recovered.

Moreover, to continue explaining the global analysis approach to experimental measurements it is necessary to introduce the concept of the "error surface" for a data set coming from several experiments, which contains all the statistical information available from the data[201]. The error surface referred to a series of experiments is represented as a plot of the χ^2 statistic along the *z* axis versus all the fitting parameters along the other axes. The χ^2 statistic (eqn. 2-9) is a single-valued function which approaches unity for properly weighted data and good fits, while it grows larger as the data fit worsens:

$$\chi^2 = \sum_{k=1}^{nexps} \sum_{i=1}^{ndata(k)} \frac{[data(i,k) - model(i,k)]^2}{\sigma^2(i,k)(N-m-1)} \qquad \textbf{(2-9)}$$

The experimental data and the proposed fit to the data are denoted by *data* and *model*, respectively. *N* is the number of data points in the data surface, $\sigma(i,k)$ is the

standard deviation in the *i*-th data point of the *k*-th experiment, while *m* is the number of total fitting parameters, *nexps* is the total number of experiments and *ndata* is the number of data points in the *k*-th experiment.

If one examines the error surface for a particular experiment and discovers that it is very "flat" (i.e., the χ^2 statistic does not significantly change as the values of the fitting parameters are altered), then it means that the experiment will be unable to properly resolve the fitting parameters of the model. In other words, the link between between experimental data and biological information is very weak[201].

Moreover, it should be mentioned that the error surafce results to be indipendent of the type of nonlinear least-squares methodology utilized to analyze the data. Hence, there is absolutely *nothing substantial* to gain by applying different types of data analysis routines on the same data set. For instance, the 67 % confidence region - generally chosen to represent the error surface as a whole of ridges, peaks, spikes and horseshoe-shaped zones - results not at all changed by the analysis routine method applied. Only through additional experimentation can one expect to better resolve similar experimental parameters (e. g. relaxation times).

Although this is not so encouraging for the experimentalists, it spontaneously gives rise to a question: what can be done to improve the quality of the data, that is to obtain a better *c* statistic and then a better error surface?

The answer to such a question takes two distinct pathways:

(1) to increase the signal-to-noise ratio of the experiment currently examined, but this is an experimental problem and thus it is beyond the purposes of this paragraph;

(2) to combine together multiple experimentswhich will better risolve the reference model. Although both pathways may be extremely interesting, particular emphasis is given here to global analysis techniques placed on combining together multiple experiments to better determine model fitting parameters.

It has to be remembered also that from the somewhat complex definition above mentioned, high dimensional error data surfaces can be reduced to only two dimensions

and then examined in more detail by a series of nonlinear analyses associated with any given fitting parameter (i.e., the *i*-th), systematically altering the *i*-th parameter over any range, while other fitting parameters are allowed to adjust to a fixed value so as to obtain the minimum possible χ^2 value. At the end of the χ^2 minimization, the value of each fixed parameter and the corresponding value of the χ^2 obtained for this fit condition are plotted, giving rise to a rigorous confidence interval on the *i*-th parameter. Every *i*-th parameter by this way can have its own bidimensional plot.

About the question raised before, important literature data reveal then that increasing the signal-to-noise ratio of a single experiment provides only very gradual changes in the shape of the associated error surface (once the signal-to-noise ratio reaches a particular value), compared to the dramatic change obtained on performing a global analysis of combined multiple experiments. This result holds in general.

Implementation of global analysis routines finally involves rather simple modifications of already existing nonlinear least-squares packages. The main change in the algorithm is providing an additional step whereby model-dependent summation of the normal nonlinear least-squares equations can be performed[201].

CHAPTER 3

RESULTS, DISCUSSION AND CONCLUSIONS

Aims of the experimental work.

Our experimental measures about charge recombination were addressed to the following two main goals.

1) To determine some thermodynamical parameters of binding (G_{bind}°, H_{bind}°, S_{bind}°) for the ubiquinone-10 (Q_{10}) to the Q_A site of RCs reconstituted in liposomes made of phosphatidylcholine (PC) and/or cardiolipin (CL).
This study led also to the evaluation of possible differences in the Q_{10} interaction specifically due to the CL presence.
The above mentioned parameters will be obtained through photoinduced absorbance variation (Abs) kinetic measures (*charge recombination*, par. 1.4.4) performed by means of a specific laser photolysis apparatus built by us (par. 2.3.2). The choice of this aim was suggested by the fact that experimentally measured binding parameters of the quinone to the Q_A site were yet not available in literature.

2) To evaluate the effects of the interaction CL-RC in CL-containing proteoliposomes (made of CL only or mixed PC/CL) and in RC-DDAO micelles (mixed micelles of protein and detergent DDAO) following progressive additions of CL.
Employing two different experimental systems allows to explore wider CL concentration ranges.
Results will be obtained by the same measures mentioned at the point (1) but taking into account the decay constants k_{AP} (instead of Abs values).
The choice of this aim was induced by the absence in literature of any detailed and quantitative development for such a subject.

3.1. Ubiquinone binding to the Q_A site.

In our experimental work we have probed the kinetics of P^+ decay in *Rb. sphaeroides* Reaction Centres (RCs) reconstituted into micelles and liposomes by following laser-induced absorbance changes recorded at 870 nm (ΔAbs_{870}). A representative trace is shown in fig. 3.1.

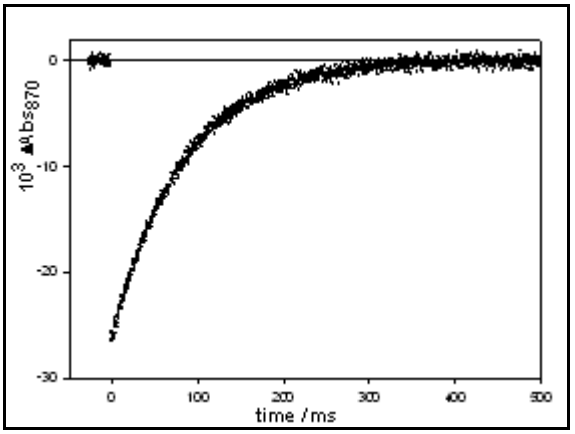

Figure 3.1.
Time course of the absorbance change after a laser pulse for RC in DDAO micelles doped with cardiolipin (CL, circles). Conditions: RC 2.3 mM; [CL]/[RC]=103. The absorbance variation is negative because of the absorbance decrease (*bleaching*) undergone by the protein at 870 nm following illumination (see RC spectrum in fig. 1.33).

In the hypothetical case of totally quinone-depleted RCs - it is experimentally impossible to remove all the ubiquinone from the RCs without denaturation - the charge separation would be limited to the bacteriopheophytin molecule (the intermediate electron acceptor) and the subsequent charge recombination (par. 1.4) would occur on a sub-microseconds time-scale (fig. 1.32). Therefore, with our experimental set-up, it would not be possible to detect any absorbance change.

In the presence of a pool of ubiquinone (Q_{10}) molecules, instead, the binding sites of the protein are occupied by quinones according to the following equilibrium binding scheme between the RC and Q_{10} (starting from hypothetical non-equilibrium concentrations in the absence of any quinone bound to the RC):

$$RC + Q_{10} \rightleftarrows RCQ_i \qquad \textbf{(3-1)}$$

	RC		Q_{10}		RCQ_i
STARTING CONCENTRATIONS	$[RC]$		$[Q]$		0
EQUILIBRIUM CONCENTRATIONS	$[RC] - [RCQ_i]$		$[Q] - [RCQ_i]$		$[RCQ_i]$

where $[RC]$, $[Q]$ and $[RCQ_i]$ indicate respectively: the total protein concentration ($[RC]=[RC]_{f\,(free)}+[RCQ_i]$), the total quinone concentration and the RC concentration with the Q_i-site occupied. Inserting the equilibrium concentrations into the dissociation

constant for the i-site $K_{D,Qi}$ the result[51]:

$$K_{D,Q_i} = \frac{([RC]-[RCQ_i])*([Q]-[RCQ_i])}{[RCQ_i]} = \frac{([RC]-[RCQ_i])*[Q]_f}{[RCQ_i]} \qquad \textbf{(3-1a)}$$

where $[Q]_f$ denotes the free quinone concentration.

The equation 3-1a can be further rearranged leading to:

$$[RCQ_i]*(K_{D,Q_i}+[Q]_f) = [RC]*[Q]_f \qquad \textbf{(3-1b)}$$

$$[RCQ_i] = \frac{[RC]*[Q]_f}{K_{D,Q_i}+[Q]_f} \cong \frac{[RC]*[Q]_f}{K_{D,Q_i}} \qquad \textbf{(3-2)}$$

where in the denominator of eqn. 3-2 $[Q]_f$ could be eliminated since below we will refer to the tight binding at the Q_A site, for which the concentration of free residual unbound quinone ($[Q]_f$) is negligible.

Since both the $P^+Q_A^-$ and the $P^+Q_AQ_B^-$ states are long-lived compared to the excitation light pulse, in the presence of ubiquinone bound to the RC it is possible to follow the time course of the charge recombination. Furthermore, since the photoinduced electron transfer up to Q_B can proceed only through Q_A, the proteins with the Q_B site occupied and the Q_A site empty will not contribute to the observed signal[52].

The decay of P^+ following a laser pulse was monitored at 870 nm at different temperatures and total quinone concentrations ([Q]).

The experimental traces were fitted to one or two exponentials (depending on their features, see par. 2.4), thus obtaining the amplitude of the bleaching at time t=0 ($\Delta Abs_{870}(0)$) and the kinetic constants of the decay k_{AP} (par. 3.2). $\Delta Abs_{870}(0)$ is proportional to the concentration of RCs having the Q_A site occupied according to:

$$\Delta Abs_{870}(0) = Z*[RCQ_A] \qquad \textbf{(3-3)}$$

---

51. We prefer to introduce now a dissociation constant instead of a binding constant because from that we will pass more easily to the thermodynamic binding parameters of the eq. 5.

52. This situation is however well unlikely because the Q_A site shows a much higher affinity for the ubiquinone than the Q_B site: in RC micelles $\Delta G^\circ_{bind}(Q_{10}, Q_A \text{ site}) = -21.4$ kJ*mol^{-1} versus $\Delta G^\circ_{bind}(Q_{10}, Q_B \text{ site}) = -11.4$ kJ*mol^{-1}[33].

where Z depends on the differences in the molar absorbance coefficients between P^+ and P and on the saturation degree of the light-pulse.

The contribution of the binding to the Q_B site can be neglected in the calculation of the $[Q]_{f,}$ since the RCs have been depleted of the majority of the ubiquinone content (only 40 % of the Q_{10} at the Q_A site is maintained, see par. 2.1) and since the binding to the Q_B site is much weaker than that to the Q_A site (foootnote nr. 52) . Accordingly, for an isothermal binding curve the following relationship holds:

$$[RCQ_A] = \frac{([RC] - [RCQ_A]) * ([Q] - [RCQ_A])}{K_{D,Q_A}} \qquad \textbf{(3-4)}$$

On this basis the temperature dependence of the quinone binding to the RC can be described taking into account the classical Van't Hoff relationship:

$$K_{D,Q_A} = \exp\left(\frac{+\Delta G^\circ}{RT}\right) = \exp\left(\frac{\Delta H^\circ}{RT} - \frac{\Delta S^\circ}{R}\right) \qquad \textbf{(3-5)}$$

where R is the gas constant, T is the thermodynamic temperature and ΔG°, ΔH°, ΔS° are the standard free energy, enthalpy and entropy changes associated to the quinone binding at the Q_A site. $K_{D',QA}$ is referred to the dissociation equilibrium, the reverse of the binding: this is the reason of the positive sign in the equation 3-5.

The above description implicitly assumes that the binding interaction between RCs and quinone molecules occurs in a homogeneous system. Experimentally such a situation is met in reverse micelles[216, 200] or, when dealing with highly hydrophilic quinones, in aqueous dispersion of direct micelles[217]. Proteoliposomes are more complicated: they are micro-heterogeneous systems composed of an ensemble of disconnected hydrophobic domains where both RCs and quinones are inserted and statistically distributed, resulting in two additional complications.

First, the quinone-binding should be handled in terms of the relevant distribution functions. For most of the purposes, however, equations from (3-1a) to (3-4) well describe the binding process in vesicles as long as one uses concentrations (of quinone and RC) evaluated with respect to the apolar volume only[53, [139]].

---

53. This is equivalent to expand $\Delta Abs(0)$ in Taylor series around the mean local concentration of RC and quinone and retaining only the first term.

The second point is the tuning of quinone concentration in vesicles. It is very difficult to modulate with accuracy the concentration of ubiquinone within the bilayers: it is not possible to simply add ubiquinone as ethanol or DMSO solution because a *quantitative* transfer into the vesicle's bilayer cannot be assumed. This is a crucial point when dealing with the high affinity Q_A site because one has to probe very low concentrations and the contribution of tightly bound quinone molecules cannot be neglected[54] (40% of RCs have the Q_A site still occupied in our preparations). It is clear that under these constraints, the determination of binding isotherms is not feasible.

To overcome this problem the binding at the Q_A site was studied at constant quinone concentration by varying the temperature. Light-induced absorbance changes were measured at different temperatures on the same sample.

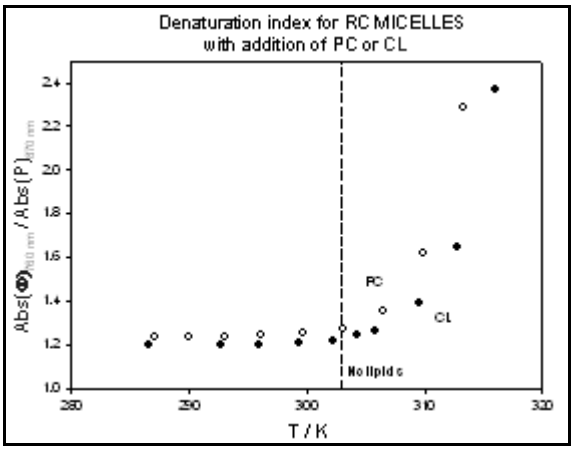

Figure 3.2.
Denaturation index for RCs in detergent micelles in the presence of phosphatidylcholine (PC, open circles) or cardiolipin (CL, black circles) added as ethanol solutions in a ratio lipid/RC= 40. The temperature of starting denaturation for RC micelles in the absence of added lipids is also reported as a dashed line. The index is calculated as ratio of the two minor peaks of the UV-NIR triplet in the RC spectrum (fig. 1.33): $Abs_{760\ nm}/Abs_{870\ nm}$.

The proteoliposome solution was first equilibrated at high temperature (~308 K) in the dark for 30 min: of course this temperature was below the starting temperature of thermal denaturation for RCs in the presence of small amount of lipids, identified to be 310 K or higher (fig. 3.2). Then the sample was cooled down by steps of 4 K. At each temperature the sample was incubated in the dark for 15 min before the measurement. At the end of the temperature scans the solution was warmed up to 298 K to check for thermal hysteresis

54. In *reverse micelles* the binding is complete already at a quinone concentration equal to 1 mM. In a *typical proteoliposome* preparation, this local (hydrophobic) concentration corresponds to few quinone molecules per RC molecule. Here the hydrophobic phase volume (V_h) is given by the number of lipid moles (n_L) multiplyed by the molar volume of the lipid ($V_{m(L)}$). Typically we have (par. 2.2): $V_h=n_L*V_{m(L)}= =(5*10^{-6}\ mol)*0.634\ l*mol^{-1} \approx 3*10^{-6}\ l$ versus a usual total volume of $1*10^{-3}$ l. It implies that in vesicles hydrophobic (local) concentrations, as that of quinone, result to be at least 300 times higher than those in aqueous buffers.
By this way, quinone 1 mM in lipidic phase corresponds to ~ 3 µM in water, while it has been used always RC ~2 µM: the ratio Q_{10} / RC is close to one.

(differences are below 5%).

Typical curves $\Delta Abs_{870}(t= 0)$ vs. T are shown in fig. 3.3 for proteoliposomes made of cardiolipin (panel A) and lecithin (panel B). For both the phospholipids the overall trend follows the dependence of $K_{D,QA}$ on the temperature observed in reverse micelles[216, 200]: the lower the temperature, the tighter the binding, thus resulting in an increase of $\Delta Abs_{870}(0)$.

In these experiments, the number of quinone molecules is fixed by the number of RCs and by the degree of occupancy of the Q_A site: this latter was measured to be the 40%, simply by saturating the site through addition of the water-soluble ubiquinone Q_0 (a molecule with the same head as the native ubiquinone Q_{10} but devoid of the hydrophobic tail).

However, we have still some limited degrees of freedom in tuning the local (or hydrophobic) quinone concentration by changing the phospholipid loading, and thus the volume of the hydrophobic domains.

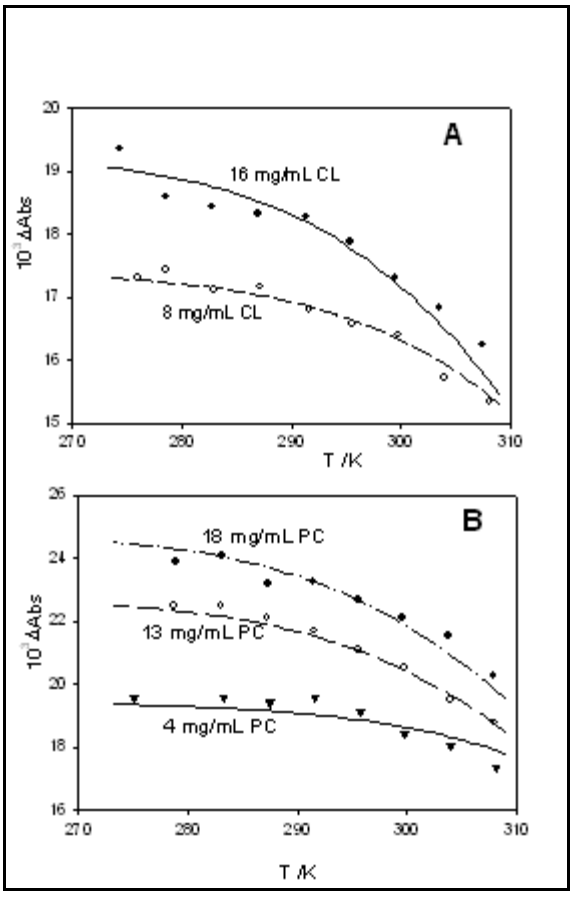

Figure 3.3.
Q_A site functionality as a function of the temperature for RCs reconstituted in vesicles made of cardiolipin (panel A) and phosphatidylcholine (panel B). Conditions: overall RC concentration= 2.3 μM; quinone/RC molar ratio= 0.4. The curves are the global best-fit according to the eqns. 2-4 and 8 (the values of $\Delta G^{\circ}(T_{hm})$ and ΔH° are listed in table 3.1). For the sake of readability the curves have been shifted vertically by adding a constant term.

As an example in fig. 3.3 are shown data collected at different phospholipid concentrations (reported as mg/ml; for every sample the overall RC concentration was 2.3 μM). A lower phospholipid loading results in a weaker temperature dependence. This is because at high quinone concentration (low phospholipid amount) the Q_A site is almost fully saturated, independently on the temperature.

It should be stressed that it is not possible to compare the $\Delta Abs_{870}(0)$ values of different samples because the parameter Z in the equation 3-3 depends on the degree of the light-pulse saturation and thus also on the scattering efficiency of liposome

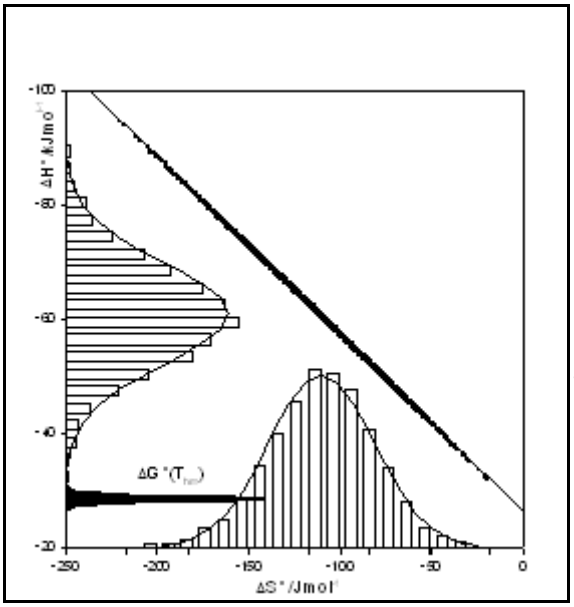

Figure 3.4.
Monte Carlo (MC) analysis of quinone binding to the Q_A site in CL vesicles. The simultaneous fit of the data shown in fig. 3.3 A was analyzed by means of a MC simulation as described in the text. The main graph shows the correlation plot ΔH° vs. ΔS°. It is evident that all the data follow a straight line with a correlation coefficient R^2= 0.9997. The slope coincides to the mean harmonic temperature T_{hm}; the intercept corresponds to the standard free energy of binding at T_{hm}. Histograms (open bars) representing the frequency of ΔH° and ΔS° are drawn on the ordinate and abscissa, respectively. On the ordinate are also drawn the frequencies for $\Delta G^\circ(T_{hm})$ according to the equation 3-8. Due to the large statistical enthalpy-entropy compensation, large spreads of ΔH° and ΔS° result in a moderate uncertainty on $\Delta G^\circ(T_{hm})$. Analysis of quinone binding in PC vesicles (i.e. data of the fig. 3.3 B) provides essentially the same results.

solutions. Actually the $\Delta Abs_{870}(0)$ values tend to the same value at low temperature: therefore, for the sake of clarity, the curves of fig. 3.3 have been arbitrarily shifted.

It appears that the RCs in vesicles made of both cardiolipin (CL) and PC follow qualitatively the predictions of eqns. (3-2)-(3-5).

For a given phospholipid it is possible to fit simultaneously all the data sets to eqns. 3-3, 3-4 and 3-5. In such a global analysis[201] for each sample, [*Q*] is a known quantity and *Z* an adjustable parameter. Of course all the samples share the same ΔH° and ΔS°.

Unfortunately, ΔH° and ΔS° are strongly correlated in the Van't Hoff relation (eq. 5) and the independent variables (*T* and [*Q*]) can be tuned only over limited ranges.

A Monte Carlo (MC, par. 2.4.3.2) simulation furnishes a straightforward evaluation of the significance of the values calculated under these conditions[212,213]. The distribution of $(\Delta H^\circ, \Delta S^\circ)$ value pairs on a straight line, obtained from MC analysis of the data (1000 runs in each case), is shown in fig. 3.4 in the case of CL vesicles and it clearly illustrates the large uncertainties associated with the best-fit parameters. The evident strong statistical correlation between enthalpy and entropy is an usual compensation between regression parameter estimates occurring when the range of variation of the independent variable (T^{-1}) is small (par. 2.4.3.1).

In these conditions the correlation is linear with a slope coincident to the harmonic mean temperature (T_{hm}), defined as

$$T_{hm} = \left(\frac{1}{n} \sum_{j=1}^{n} \frac{1}{T_j} \right)^{-1} = <1/T>^{-1} \qquad \textbf{(3-6)}$$

being *n* the number of experimental points.

This was predicted and demonstrated already thirty years ago by Krug and coworkers[202]. As shown in fig. 3.4, ΔH° follows the equation of a straight line if reported as a function of ΔS°. It was demonstrated also that the intercept of the line is a measure of the free energy change at T_{hm} (hereafter $\Delta G^\circ(T_{hm})$, par. 2.4.3.1)[202]. So in formulae it is possible to express ΔH° as

$$\Delta H^\circ = \Delta G^\circ(T_{hm}) + T_{hm} * \Delta S^\circ \qquad \textbf{(3-7)}$$

Using the above relation it is possible to easily rewrite the equation 3-5 as

$$K_{D,Q_A} = \exp\left(\frac{\Delta G^\circ(T_{hm}) - \Delta H^\circ}{RT_{hm}} + \frac{\Delta H^\circ}{RT} \right) \qquad \textbf{(3-8)}$$

By means of such a transformation we can describe the dependence of the binding equilibrium on temperature in terms of two parameters ($\Delta G^\circ(T_{hm})$ and ΔH°) whose estimates are statistically independent on one another[202]. A MC analysis on these uncorrelated parameters gives for $\Delta G^\circ(T_{hm})$ a confidence probability distribution much narrower than those of ΔH° and ΔS° previously (fig. 3.4, see also par. 2.3.4.2).

It is therefore possible to fit the experimental data to the eqns. 3-3, 3-4 and 3-8 and to quantify the affinity of the quinone for the primary acceptor binding site through the free energy change at T_{hm} = 291 K.

Eqns. 3-3, 3-4 and 8 nicely describe the experimental data (see curves in fig. 3.3). The best-fit parameters obtained by means of the above described procedure (listed in table 3.1) were independent on the class of phospholipid used. The quinone affinity for the Q_A site of RC is higher in vesicles than that previously found in reverse micelles (fourth column in table 3.1). A similar result was found for the binding of quinone at the Q_B site[139] (fifth and sixth columns in table 3.1).

According to the table, the main difference in quinone binding to the Q_A site between vesicles and reverse micelles is due to the entropic contribution.

Actually, the entropy cost to be paid upon binding is $\Delta S^\circ = (S^\circ)_{bound} - (S^\circ)_{unbound} =$

-180 J/mol in reverse micelles, but only -(110÷120) J/mol in vesicles. Likely this is due to the fact that the degrees of freedom associated to the unbound quinone are less in the bilayer (a crowded bidimensional environment) than in the large organic bulk surrounding the reverse micelles, resulting in a smaller negative ΔS° variation in vesicles. Only for the sake of comparison, in the same table also some values referred to the binding at the Q_B site have been reported.

More important, the quinone affinity at 291 K is the same for cardiolipin and lecithin (within 3%) and also the enthalpy and entropy changes determined in both CL and PC liposomes seem to be essentially the same. On these bases, it seems that the presence of high concentration of cardiolipin does not induce gross changes in the interactions taking place at the Q_A binding site, between the ubiquinone molecules and the protein. On the contrary, cardiolipin strongly affects the rate of charge recombination from the $P^+Q_A^-$ state, as detailed in the following section.

Table 3.1. Thermodynamical parameters for the ubiquinone binding to the Q_A site of the RC; the reference state is 1 M with respect to the apolar volume; T_{hm} = 291 K.

	Q_A site			Q_B site	
	CL vesicles	PC vesicles	Reverse micelles*	PC vesicles[33]	Rev. micelles[33]
ΔG° / kJ*mol^{-1}	- 29 ± 1	- 28 ± 1	- 22.3 ± 0.1	- 14.6 ± 0.6	- 11.4 ± 0.9
ΔH° / kJ*mol^{-1}	- 60 ± 10	-70 ± 15	- 75 ± 3	- 55 ± 4	- 51 ± 4
ΔS°/J*mol^{-1}*K^{-1}	- 110 ± 30	-120 ± 30	- 180 ± 10	- 140 ± 10	- 130 ± 15

* These data are from reference 200.

From a comparison between the data for the binding at the Q_A and Q_B sites it emerges that binding at the Q_A site is more exoergonic and exothermic than that at the Q_B site - as expected -, both in PC vesicles (data on both sites are available only for PC vesicles) and in reverse micelles. On the contrary, entropic contributions are relatively similar between the two sites in PC liposomes: the difference in the free energy values is a direct consequence of that between enthalpy values. Reverse micelles reveal instead a higher degree of order (then a more negative value of ΔS°) for the Q_A site binding of the ubiquinone than for the Q_B site: this is a consequence of the mobility

difference of the quinone cofactor between the two sites.

As well as the Q_A site, also the Q_B site affinity for the ubiquinone is higher in liposomes than in reverse micelles: lipid vesicles represent an environment mimicking certainly closer the bacterial cell membrane than reverse micelles. It further demonstrates - in relation to par. 1.5 - that lipid-protein interactions may play a prominent role in the RC functioning, as well as it happens for many other membrane proteins (par. 1.3).

3.2. $P^+Q_A^-$ → PQ_A electron transfer: effect of the cardiolipin binding.

The photo-induced charge separation and the subsequent charge recombination for RCs with only the Q_A site occupied is described by[218]

$$PQ_A \underset{k_{AP}}{\overset{h\nu}{\rightleftharpoons}} P^+Q_A^- \qquad \textbf{(3-9)}$$

These electron transfer processes, being intramolecular, obey first-order kinetics[141, 219]. The temperature dependence of $P^+Q_A^-$ recombination kinetics has been examined in liposomes made of PC and CL and in detergent micelles as well. The main results are presented in fig. 3.5: the charge recombination rate constants (k_{AP}), even if observed in different environments, are of the same order of magnitude, and speed up when cooling, as recognised by several authors in previous studies on detergent micelles[141, 220, 221, 222, 223].

However, since in the introduction it has been widely stressed that the lipid environment surrounding a membrane protein (in terms of composition and physico-chemical properties) strongly influences the behaviour of the embedded protein itself, it is expected that k_{AP} values obtained in proteoliposomes made of different phospholipids are clearly different. In fact at all the temperatures the charge recombination kinetics in CL proteoliposomes are systematically faster than those observed in PC proteoliposomes.

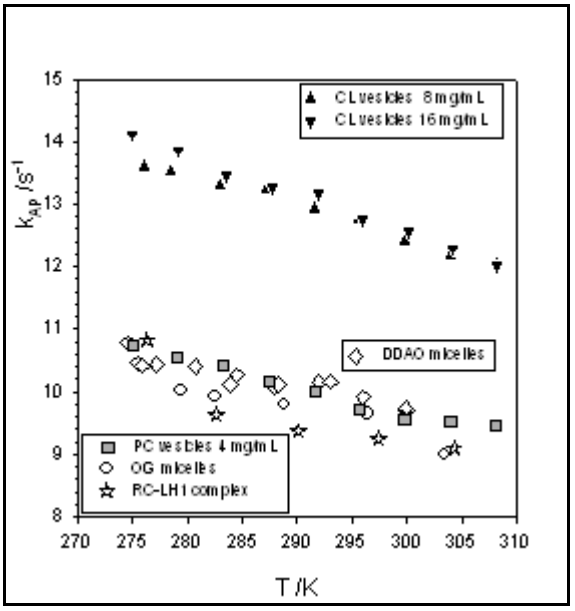

Figure 3.5.
Rate constant of $P^+Q_A^-$ recombination as a function of the temperature for reaction centers in different systems: CL vesicles (closed triangles); PC vesicles (gray squares); detergent micelles (open symbols); core complex (stars). Data in micelles of octylglucoside (OG) and core complex (RC-LH1) are from reference 224, for other assays the RC concentration was 2.3 M.

For the sake of comparison in fig. 3.5 are also reported results obtained for RCs suspended in DDAO and octylglucoside

(OG) micelles and for RCs reconstituted in core complexes[224] (the light-harvesting antenna complex, LH-I, shows a circular arrangement that allows the LH-I to locate inside the RC, forming the so-called core complex, see par.1.4)[5, 88].

Quite surprisingly, CL vesicles represent the notable exception of a general trend. Fig. 3.5 shows that PC vesicles, direct micelles made of two different detergents, and core complexes share essentially the same behavior with respect to the backward electron transfer. This finding suggests that the increase (30%) in the rate of $P^+Q_A^-$ recombination observed for RCs embedded in CL vesicles is unrelated to the physical assembly of RC within the bilayer but is likely to be dependent on the binding of cardiolipin molecules to the protein.

Accordingly, the investigation was extended to RCs solubilized in detergent (DDAO) micelles loaded with CL (fig. 3.6): for all the tested temperatures, k_{AP} increases upon CL loading. On the contrary, addition of lecithin to RCs in DDAO solution does not change the rate of charge recombination. Interestingly, k_{AP} for RCs embedded in liposomes made of both the phospholipids (CL 50 mole%) is lower than that measured in liposomes made of pure CL. As a whole, the results of fig. 3.6 strengthen the hypothesis of some specific interaction (binding) between cardiolipin and RC.

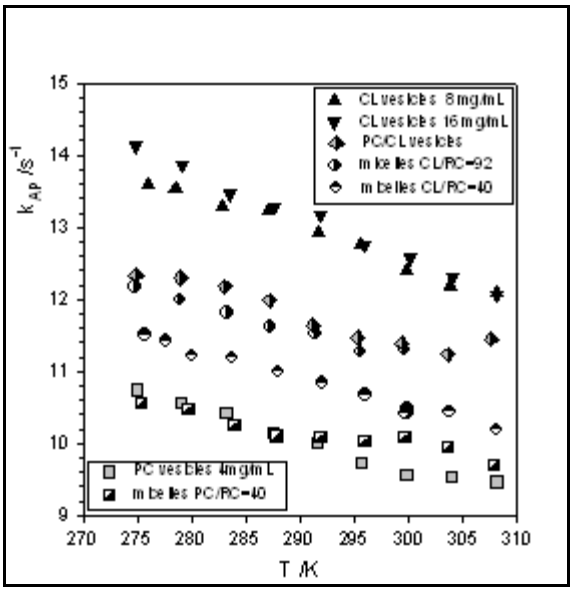

Figure 3.6.
Rate constant of $P^+Q_A^-$ recombination as a function of the temperature for reaction centers solubilized in DDAO micelles doped with different amounts of CL (semi-filled circles). Also shown are the results found for DDAO micelles doped with PC (semi-filled squares) and for vesicles made of a mixture of CL and PC (50 mole % in CL; 15 mg/mL of total lipids – semi-filled diamonds). In the case of micelles, the CL or PC loading is expressed as lipid/RC mole ratio. For purpose of comparison are shown data for vesicles made of pure CL and PC (same symbols as in fig. 3.5).

This point was further afforded in the case of RCs solubilized by DDAO micelles. In such a system the ratio CL/RC is easily tuned by adding cardiolipin as concentrated ethanol solution[163]. The results of this isothermal (T=299 K) titration are shown in fig. 3.7. For the sake of comparison, in the same figure are also shown the relevant data of fig. 3.6.

The ordinate of fig. 3.7 represents the ratio k_{AP}/k_{AP}°, being k_{AP}° the rate

constant observed in DDAO micelles without cardiolipin. The abscissa of fig. 3.7 represents the cardiolipin concentration evaluated with respect to the apolar volume of the aggregates. This choice should be the relevant parameter for the binding process (because RC and CL are both water insoluble) and allows a consistent treatment of data collected in micelles and liposomes. The cardiolipin concentration in the apolar phase was evaluated according to:

$$[CL]_{apolar} = \frac{n_{CL}}{V_{apolar}} = \frac{n_{CL}}{n_{CL}v_{CL} + n_A v_A} \qquad \textbf{(3-10)}$$

where n_{CL}= moles of cardiolipin; n_A= moles of the other amphiphile (PC or DDAO); v_{CL} and v_A are the molar volumes of cardiolipin and amphiphile evaluated taking into account only the apolar moiety (tail); v_{CL} and v_A have been given in the par. 2.2. In the case of DDAO n_A was evaluated by assuming 250 DDAO molecules per RC[225].

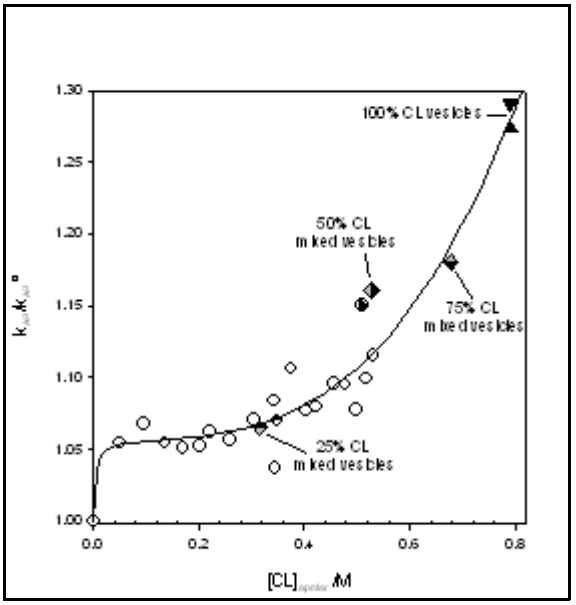

Figure 3.7.
Isothermal (T=299 K) CL titration of RC. The abscissa is the cardiolipin concentration evaluated with respect to the apolar volume (eq. 10); the ordinate is the rate constant of $P^+Q_A^-$ recombination normalised to the rate found in DDAO micelles ($[CL]_{apolar}$=0). Circles denote experiments in micelles (the two semi-filled circles are from fig. 3.6). Results obtained in liposomes made of pure CL (closed triangles) and of CL-PC mixtures (semi-filled diamonds) are also shown (the vesicles composition is expressed as CL mole%). The solid curve is the best-fit of the data to equation 19; best fit parameters are Y^1=1.06 ± 0.02; Y*= 6 ± 2; n= 4 ± 1; K^1= 4 ± 3 mM; $K_0=(K^*)^{1/n}$= 0.46 ± 0.07 M (table 3.2).

As a whole, the data presented in fig. 3.7 suggest a mechanism of binding of CL to RC substantially independent of the system where the interaction has been evaluated. It has to be noted, in fact, that the experimental points of fig. 3.7 refer to samples of different nature: RC in DDAO micelles with additions of CL (resulting in solutions having different ethanol content, but always lower than 5 % V/V); RC in mixed PC/CL vesicles; RC in pure CL vesicles.

The presence of trace amount of CL induces a small (5%) but highly reproducible jump in the k_{AP}/k_{AP}° value (remember that in the absence of added cardiolipin k_{AP}° is the about the same for RCs in different environments, depending only on temperature, see

figures 3.5 and 3.6). Then the rate constant of the decay from $P^+Q_A^-$ remains almost unchanged upon CL loading until a sudden increase in the k_{AP}/k_{AP}° value is observed for $[CL]_{apolar}$~ 0.5 M.

Assuming that the binding of cardiolipin influences somehow the rate of the electron transfer between Q_A^- and P^+, the evolution of the quantity k_{AP}/k_{AP}° upon CL loading suggests the existence of two classes of binding sites for CL, as found in the case of bovine heart cytochrome oxidase[226] and as recently supposed also for the Reaction Centre on the basis of experimental evidences[12, 163] (see discussion of the results for details). Thus, we have tentatively described the P^+ decay following the laser-induced charge separation according to the scheme below:

$$\begin{array}{ccc} P^+Q_A^- \cdot CL & \xrightarrow{k_{AP}^1} & PQ_A \cdot CL \\ K^1 \quad \updownarrow & & \\ P^+Q_A^- & \xrightarrow{k_{AP}^\circ} & PQ_A \\ K^* \quad \updownarrow & & \\ P^+Q_A^- \cdot (CL)_n & \xrightarrow{k_{AP}^*} & PQ_A \cdot (CL)_n \end{array} \qquad \textbf{(3-11)}$$

where $P^+Q_A^-$ represents the charge-separated state of the native RCs (without bound CL), while $P^+Q_A^- \cdot CL$ and $P^+Q_A^- \cdot (CL)_n$ represent RCs with cardiolipin molecules bounded to two different classes of binding sites. According to the scheme these different RC-CL complexes relax to the neutral state with different rate constants, being respectively k_{AP}°, k_{AP}^1, k_{AP}^*. In addition K^1 is the dissociation constant for the first binding site

$$K^1 = \frac{\left[P^+Q_A^-\right]\left[CL\right]}{\left[P^+Q_A^- \cdot CL\right]} \qquad \textbf{(3-12)}$$

while K^* describes the cooperative binding of cardiolipin to the n sites of the RC, according to the Hill equation (then n is called also “Hill coefficient”)[227]

$$K^* = K_0^n = \frac{\left[P^+Q_A^-\right]\left[CL\right]^n}{\left[P^+Q_A^- \cdot (CL)_n\right]} \qquad \textbf{(3-13)}$$

In the above equation K_0 is the dissociation constant of the elementary step of the cooperative process. Therefore the time course of the observed P^+ decay depends on the rates of the CL binding/release and of the charge recombination processes.

Any time a dynamic phenomenon such as a ligand binding to a protein is considered, the time scale of both the probing technique and that of the binding/dissociation equilibrium has to be taken into consideration. In our case, what is considered are the effects of CL on the $P^+Q_A^-$ charge recombination process, which in the same time is also the probing means necessary to detect such effects.

In the analysis of our experimental data two limiting cases can be evidenced: the binding exchange of CL with the RC in DDAO micelles as well as in liposomes can be *fast* or *slow* compared to the charge recombination process itself. Since data treatment is quite different in the two cases, these will be dealt separately in next sections.

***Fast* exchange case.**

In the following analysis we will assume that for RCs reconstituted in detergent micelles or in liposomes made of CL - either pure or mixed with PC - the CL exchange to its binding sites is fast compared to the charge recombination from the generic $P^+Q_A^-\cdot(CL)_x$ state ($0 \le x \le n$). This latter process is associated with a kinetic constant k_{AP} variable around 10 s^{-1} with temperature and according to the environment in which the RC is reconstituted (e.g. micelles, PC, CL or mixed PC/CL liposomes, see fig. 3.5 and 3.6). It means that to the total process will contribute not singularly distinguishable recombinations from all the three charge separated states reported in the scheme 3-11.

Assuming then a fast exchange, the decay rate of P^+ after the light pulse is

$$\frac{d\left[P^+\right]}{dt} = -k_{AP}^{\circ}\left[P^+Q_A^-\right] - k_{AP}^{1}\left[P^+Q_A^- \cdot CL\right] - k_{AP}^{*}\left[P^+Q_A^- \cdot (CL)_n\right] \qquad \textbf{(3-14)}$$

where $[P^+]$ is the concentration of all the charge separated states ($[P^+]=[P^+Q_A^-]+[P^+Q_A^-\cdot CL]+[P^+Q_A^-\cdot(CL)_n]$).

Introducing the fractions $\alpha = [P^+Q_A^-\cdot CL]/[P^+]$ and $\beta = [P^+Q_A^-\cdot(CL)_n]/[P^+]$ the equation 3-14 can be rewritten as

$$\frac{d[P^+]}{dt} = -\left\{k_{AP}^{o}(1-\alpha-\beta) + k_{AP}^{1}\alpha + k_{AP}^{*}\beta\right\}[P^+] \qquad \textbf{(3-15)}$$

In other words, assuming a fast exchange the scheme 3-11 predicts a single exponential decay of the radical cation P^+ with an observed rate constant k_{AP} resulting from the sum of different contributions and given by the equation 3-16

$$k_{AP} = k_{AP}^{o}(1-\alpha-\beta) + k_{AP}^{1}\alpha + k_{AP}^{*}\beta \qquad \textbf{(3-16)}$$

Then, since equations 3-12 and 3-13 can be rewritten in terms of α and β,

$$K^1 = \frac{[P^+Q_A^-]}{[P^+]} * \frac{[P^+]}{[P^+Q_A^-\cdot CL]} * [CL] = \frac{(1-\alpha-\beta)[CL]}{\alpha} \qquad \textbf{(3-17)}$$

$$K^* = \frac{[P^+Q_A^-]}{[P^+]} * \frac{[P^+]}{[P^+Q_A^-\cdot (CL)_n]} * [CL]^n = \frac{(1-\alpha-\beta)[CL]^n}{\beta}$$

obtaining α and β from equations 3-17 and inserting them into the equation 3-16, the experimentally observed k_{AP} is expressed as a function of the binding constants 3-12, 3-13, according to

$$k_{AP} = \frac{k_{AP}^{o}K^1K^* + k_{AP}^{1}K^*[CL] + k_{AP}^{*}K^1[CL]^n}{K^*(K^1+[CL]) + K^1[CL]^n} \qquad \textbf{(3-18)}$$

and therefore the data of fig. 3.7 should be described by the following equation

$$\frac{k_{AP}}{k_{AP}^{o}} = \frac{K^1K^* + Y^1K^*[CL] + Y^*K^1[CL]^n}{K^*(K^1+[CL]) + K^1[CL]^n} \qquad \textbf{(3-19)}$$

where Y^1 and Y* are the ratios $k_{AP}{}^1/k_{AP}{}^\circ$ and $k_{AP}{}^*/k_{AP}{}^\circ$, respectively. The cardiolipin concentration is evaluated with respect to the apolar volume ($[CL]=[CL]_{apolar}$). The equation 3-19 well describes the experimental data (the fit is in fig. 3.7). The best fit parameters are reported in the following table.

Table 3.2. Best fit parameters for the experimental data reported in fig. 3.7, according to eqn. 3-19.

Y^1	Y*	n	$K_0 = (K^*)^{1/n}$	K^1
1.06 ± 0.02	**6 ± 2**	**4 ± 1**	**0.46 ± 0.07 M**	**4 ± 3 mM**

***Slow* exchange case**.

We start by assuming that the rates of binding and release (i.e. exchange) of cardiolipin to the RC-lipid complexes of scheme 3-11 are slow compared to the rate of charge recombination from $P^+Q_A^-$. Under this condition, each light-induced species undergoes independently to exponential charge recombination

$$\frac{\left[P^+\right]_t}{\left[P^+\right]_{t=0}} = F^\circ \exp\left(-k_{AP}^0 t\right) + F^1 \exp\left(-k_{AP}^1 t\right) + F^* \exp\left(-k_{AP}^* t\right) \qquad \textbf{(3-20)}$$

where the fractions

$$F^{\circ} = \frac{\left[P^{+}Q_A^{-}\right]_t}{\left[P^{+}\right]_{t=0}} = \frac{\left[PQ_A\right]}{\left[RC\right]_{tot}} = \frac{\left[PQ_A\right]}{\left(\left[PQ_A\right]+\left[PQ_A \cdot CL\right]+\left[PQ_A \cdot (CL)_n\right]\right)}$$

$$F^{1} = \frac{\left[P^{+}Q_A^{-} \cdot CL\right]_t}{\left[P^{+}\right]_{t=0}} = \frac{\left[PQ_A \cdot CL\right]}{\left[RC\right]_{tot}} = \frac{\left[PQ_A \cdot CL\right]}{\left(\left[PQ_A\right]+\left[PQ_A \cdot CL\right]+\left[PQ_A \cdot (CL)_n\right]\right)} \qquad \textbf{(3-21)}$$

$$F^{*} = \frac{\left[P^{+}Q_A^{-} \cdot (CL)_n\right]_t}{\left[P^{+}\right]_{t=0}} = \frac{\left[PQ_A \cdot (CL)_n\right]}{\left[RC\right]_{tot}} = \frac{\left[PQ_A \cdot (CL)_n\right]}{\left(\left[PQ_A\right]+\left[PQ_A \cdot CL\right]+\left[PQ_A \cdot (CL)_n\right]\right)}$$

reflect the dissociation equilibria taking place *befor*e the saturating flash: in fact light excitation and subsequent charge recombination, as fast processes, let unalterate the relative distribution of indipendent states PQ_A, $PQ_A \cdot CL$, $PQ_A \cdot (CL)_n$ existing before they occur.

$$R^{1} = \frac{\left[PQ_A\right]\left[CL\right]}{\left[PQ_A \cdot CL\right]}$$

$$R^{*} = \frac{\left[PQ_A\right]\left[CL\right]^{n}}{\left[PQ_A \cdot (CL)_n\right]} \qquad \textbf{(3-22)}$$

Then, from the equation 3-22 it is possible to draw

$$\frac{[CL]}{R^1} = \frac{[PQ_A \cdot CL]}{[PQ_A]}$$

$$\frac{[CL]^n}{R^*} = \frac{[PQ_A \cdot (CL)_n]}{[PQ_A]} \qquad \textbf{(3-22a)}$$

$$1 + \frac{[CL]}{R^1} + \frac{[CL]^n}{R^*} = \frac{[PQ_A] + [PQ_A \cdot CL] + [PQ_A \cdot (CL)_n]}{[PQ_A]}$$

By this way *F°, F¹ and F** can be expressed as a function of the dissociation constant R^1 and R* and of the cardiolipin concentration according to

$$F^\circ = \frac{1}{1 + \frac{[CL]}{R^1} + \frac{[CL]^n}{R^*}}$$

$$F^1 = \frac{[CL]}{R^1} \frac{1}{1 + \frac{[CL]}{R^1} + \frac{[CL]^n}{R^*}} \qquad \textbf{(3-23)}$$

$$F^* = \frac{[CL]^n}{R^*} \frac{1}{1 + \frac{[CL]}{R^1} + \frac{[CL]^n}{R^*}}$$

The rate constants are expected to have similar values and in presence of experimental noise a safe deconvolution of P^+ time course into three exponentials, according to the equation 3-20, is not feasible. Instead, one can describe the multi-exponential behavior by a cumulant expansion (to the second order) obtaining[139]

$$\frac{[P^+]_t}{[P^+]_{t=0}} = \exp\left(- < k_{AP} > t + \frac{\sigma^2}{2} t^2\right) \qquad \textbf{(3-24)}$$

where $<k_{AP}>$ and σ^2 are the mean and the variance of the charge recombination rate

$$< k_{AP} >= F^\circ k^\circ_{AP} + F^1 k^1_{AP} + F^* k^*_{AP} \qquad \textbf{(3-25)}$$

$$\sigma^2 = F^\circ\left(k^\circ_{AP} - < k_{AP} >\right)^2 + F^1\left(k^1_{AP} - < k_{AP} >\right)^2 + F^*\left(k^*_{AP} - < k_{AP} >\right)^2 \qquad \textbf{(3-26)}$$

Using equations 3-23, dividing equation 3-25 by k_{AP}° and remembering that Y^1 and Y* denote the ratios $k_{AP}{}^1/k_{AP}^\circ$ and $k_{AP}{}^*/k_{AP}^\circ$ one obtains

$$\frac{< k_{AP} >}{k^\circ_{AP}} = \frac{1 + \frac{Y^1}{R^1}[CL] + \frac{Y^*}{R^*}[CL]^n}{1 + \frac{[CL]}{R^1} + \frac{[CL]^n}{R^*}} \qquad \textbf{(3-27)}$$

The above equation can be rearranged multiplying and dividing the right-hand term by R^*R^1 obtaining

$$\frac{< k_{AP} >}{k^\circ_{AP}} = \frac{R^1R^* + Y^1R^*[CL] + Y^*R^1[CL]^n}{R^1R^* + R^*[CL] + R^1[CL]^n} \qquad \textbf{(3-28)}$$

that is an expression formally equivalent to the equation 3-19. The only difference is the meaning of the dissociation constants R^1, R^* (eqn. 3-22) that in the above equation refer to the dark equilibria. These latter remain unaltered by light excitation and subsequent charge recombination, which are assumed to be much faster events than every kind of exchange of CL to its binding sites.

Note that for high recombination rates $<k_{AP}>$ and small σ^2 (i.e. $\sigma/<k_{AP}> <1$) equation 3-24 is approximately mono-exponential with a decay constant $<k_{AP}>$. This point and the equivalence of eqns. 3-19 and 3-28 indicate that the results of fig. 3.7 do not permit to discriminate between fast and slow CL-exchange. However, the features of the charge recombination kinetics registered by us are inconsistent with the hypothesis of slow cardiolipin exchange as detailed in the following.

According to eqns. 3-25 and 3-26 the dependence of $<k_{AP}>$ and σ on CL concentration are correlated. In particular, according to eqns. 3-23, 3-25 and 3-26 the ratio $\sigma/<k_{AP}>$ is expected to increase upon CL loading. The experimental charge recombination kinetics, however, do not follow such a prediction.

A typical result is shown in fig. 3.8. The experimental trace (circles) recorded for RC in DDAO micelles (RC 2.3 μM) doped with cardiolipin ([CL]/[RC] molar ratio=103, $[CL]_{tot}$ ~230 μM corresponding to $[CL]_{apolar}$=0.53 M) is compared with the predictions for fast and slow CL exchange.

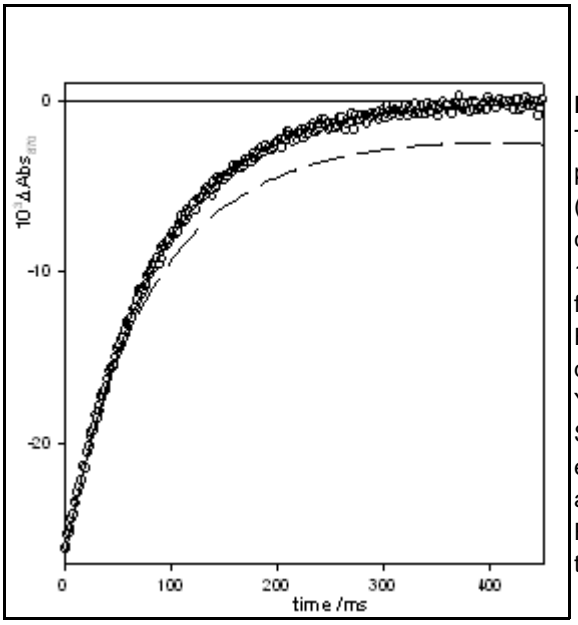

Figure 3.8.
Time course of the absorbance change after a laser pulse for RCs in DDAO micelles doped with CL (circles). Conditions: RC 2.3 M; [CL]/[RC]=103; the cardiolipin concentration in the apolar phase (eqn. 3-10) is $[CL]_{apolar}$=0.53 M. Also shown are the predictions for fast and slow CL exchange.
Fast exchange (solid curve): single exponential with decay rate given by eqn. 3-19 and the parameters Y^1=1.06; Y*=6; n=4; K^1=4 mM; $K_0=(K^*)^{1/n}$= 0.46 M.
Slow exchange (dashed curve): the decay follows eqn. 3-24 with the parameters $<k_{AP}>$ and σ calculated according to eqns. 3-23, 3-25 and 3-26 inserting in R^1, R* the values found for K^1, K* respectively (by fitting the experimental points in fig. 3.7 with the eqn. 3-19).

For fast exchange a single exponential with k_{AP} given by eqn. 3-19 is expected (solid line). Differently, in the case of slow exchange the P^+ decay is expected to follow eqn. 3-24 with $<k_{AP}>$ and σ given by eqns. 3-28 and 3-26, respectively (dashed line).

At short times the two predictions coincide because eqns. 3-19 and 3-28 are undistinguishable: to describe equation 3-28 is sufficient the first order of the cumulant analysis. However at this high cardiolipin loading ([CL]/[RC]=103) eqns. 3-25 and 3-26 by calculations predict $\sigma/<k_{AP}>$=0.46, resulting in a clear deviation of the slow-exchange prediction from the experimental data.

The hypothesis of slow exchange clearly resulted incorrect; however it may be yet interesting to examine how we approached the initial assumption of a fast exchange.

This was suggested and justified by two experimental considerations.

a) Excluding the non-annular cardiolipin found in many RC crystal structures, (strongly bound to the protein surface, thus not interested to exchange phenomena with identical molecules contained in the vesicle bilayer), other possible surface-interacting CLs in proteoliposomes should be significantly restricted in motion and slowed in the exchange rate within a common "pool of CL molecules". The lowest limit for the exchange rate, though not precise ($\sim 10^{+6}$ s^{-1} [41]), is much larger than the recombination constant k_{AP} ($\sim 10\ s^{-1}$). In detergent-RC micelles also, CL exchange between "detergent phase" and its binding site (within the same RC micelle) should be much faster than recombination from $P^+Q_A^-$ ($\sim$0.1 s), if analogy of CL with Q_B ubiquinone - both highly hydrophobic - is accepted (intermicellar exchange could be much slower)[228].

b) About binding/dissociation of ubiquinone-10 (Q_{10}) molecules at the Q_B site of RCs reconstituted in PC liposomes, recent studies[4] demonstrated that if the quinone concentration is at least five times higher than that of RC ($[Q_{10}] > 5*[RC]$) the Q_{10} exchange results to be faster than charge recombination from $P^+Q_A^-$. Since CL is hydrophobic as well as Q_{10} and since the CL/RC molar ratio we used in RC micelles and proteoliposomes was always higher than five, this result could be legitimately employed as a starting hypothesis for our data analysis.

3.3. Discussion of the results.

According to the results of section 3.1 the binding affinity of the quinone for the Q_A site of RCs embedded in vesicles made of lecithin and cardiolipin is the same. This evidence allows to rule out every hypothesis dealing with changes in the number of hydrogen bonds between the quinone molecule and the protein environment. In addition, drastic changes in the protein-quinone mutual orientation are unlikely because a prominent variation in the intensity of quinone-protein interactions is expected in such a case.

The rate of charge recombination from $P^+Q_A^-$ is essentially the same in the case of RCs in detergent micelles (made of DDAO or OG) and lecithin vesicles.

On the contrary, in the presence of cardiolipin the light-induced $P^+Q_A^-$ state recombines faster (k_{AP} higher) in the following order: RC micelles < PC/CL vesicles < CL vesicles (par. 3.2).

It clearly indicates that the state $P^+Q_A^-$ is progressively destabilized by the CL addition, increasing its free energy content (fig. 3.9). Such an effect is easily discernible in different self-assembled amphiphile aggregates containing CL, both micelles and vesicles (figures 3.5-3.7).

In fact electron transfer reactions, differently from most of the chemical reactions, show correlations between kinetics and thermodynamics: to a larger free energy difference between initial and final states of the reaction corresponds an higher rate constant, as it is described by the relevant Marcus theory[142] (to whom we will refer later in this paragraph and in Appendix A).

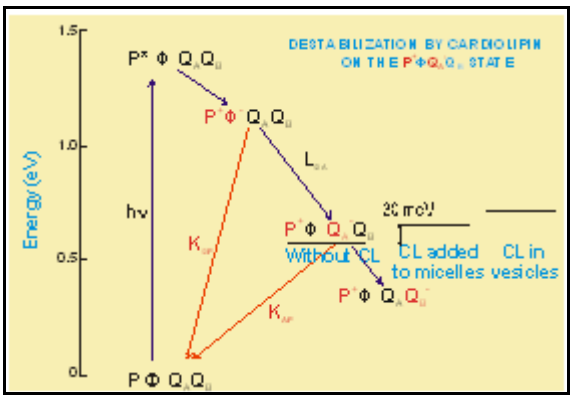

Figure 3.9.
Energy diagram of the RC cofactors involved in the electron transfer. The slight increases in the free energy states caused by the presence of CL have been exaggerated for the sake of clarity. The diagram is drawn from the fig 1.33.

A similar effect of destabilization of $P^+Q_A^-$ was qualitatively described - for RCs in DDAO micelles - in a recent paper by Rinyu and coworkers[163] but the lack of quantitative data precludes an accurate

comparison.

Here two RCs were alternatively mutated at the level of the Q_A pocket (fig. 1.34): methionine M218 were changed in alanine (M218MA) or glycine (M218MG) obtaining faster back reactions from $P^+Q_A^-$ by a factor of three and four, respectively (the recombinations from $P^+Q_B^-$ were instead slowed approximately for the same factor). These mutations altered the environment of the Q_A site, making it less favourable towards the quinone reduction, then lowering the redox potential $E_m(Q_A/Q_A^-)$ and increasing the free energy level of the $P^+Q_A^-$ state . So, interestingly, a qualitatively similar acceleration of the back reaction from $P^+Q_A^-$ occurs in the case of mutations at the Q_A site as well as when CL is added on samples (this latter effect is always much smaller than the other).

Still more interesting is the explanation provided by the authors. Besides the recombination process from $P^+Q_A^-$ to PQ_A proceeding by direct tunneling (par. 1.4.4), the Q_A site mutations made accessible an alternative thermally activated route via $P^+\Phi_A^-$ (where Φ_A is the active bacteriopheophytin cofactor): increasing contributions from this additional route result in an acceleration of the overall rate of recombination k_{AP} (see the scheme below and fig. 3.9).

$$P\Phi_A Q_A \underset{k_{\Phi P}}{\overset{h\nu}{\rightleftharpoons}} P^+\Phi_A^- Q_A \xleftrightarrow{L_{\Phi A}} P^+\Phi_A Q_A^- \qquad \textbf{(3-29)}$$

$$\xleftarrow[\qquad\qquad k_{AP} \qquad\qquad]{}$$

where $k_{\Phi P}$ and k_{AP} are kinetic constants for the recombination from $P^+\Phi_A^-Q_A$ and $P^+\Phi_A Q_A^-$ respectively, while $L_{\Phi A}$ is the equilibrium constant for the electron transfer between $P^+\Phi_A^-Q_A$ and $P^+\Phi_A Q_A^-$.

Moreover, in the above mentioned paper Rinyu and coworkers report also detailed measurements carried out on wild-type RCs after addition of cardiolipin and involving two different phenomena: the delayed fluorescence from the primary donor accompanying the $P^+Q_A^-$ charge recombination and the back reaction from $P^+Q_AQ_B^-$.

Upon cardiolipin loading the authors found a sharp increase in the emission yield of delayed fluorescence, deducing an appreciable decrease in the free energy drop from the excited state $P^*\Phi Q_AQ_B$ to the charge separated state $P^+\Phi Q_A^-Q_B$ (with the indication of all the cofactors, even those unaltered in the specific energy transition, as

in fig. 3.9). The slowing of the recombination from $P^+\Phi Q_A Q_B^-$, measured on the same samples, was accounted for by a 30 meV increase in the free energy drop from $P^+\Phi Q_A^- Q_B$ to $P^+\Phi Q_A Q_B^-$ (fig. 3.9). The energy level of $P^+\Phi Q_A Q_B^-$ instead may be assumed to be practically unchanged even after CL additions: cardiolipin indirectly leads to variations on the rate and relative amount of the back reaction from Q_B ubiquinone - through the mediation of the Q_A ubiquinone -, but not directly on the thermodynamic stability of the $P^+\Phi Q_A Q_B^-$ state[163] (par. 1.5.2).

Thus, as a whole the results by Rinyu suggested the same conclusion as that we just showed: cardiolipin induces an increase in the free energy level of the $P^+Q_A^-$ - that is destabilization - with respect to the neutral state PQ_A.

Around room temperature - or, in other words, at temperatures far from cryogenic ones - electron transfer theories are well approximated by the well known Marcus expression[142]:

$$k = \frac{2\pi}{\hbar} V^2 \frac{1}{\sqrt{4\pi\lambda KT}} \exp\left[-\frac{(\varepsilon-\lambda)^2}{4\lambda KT}\right] \qquad \textbf{(3-30)}$$

The expression describes the dependence of the electron transfer rate constant (*k*) on the reorganization energy λ, the driving force ε and the electron coupling matrix element V between initial and final states. ε is defined here as (-ΔG) of the electron transfer reaction, so as for a spontaneous process (ΔG < 0), like the recombination from $P^+\Phi Q_A^- Q_B$ to $P\Phi Q_A Q_B$ (fig. 3.9), its sign has to be positive. Other symbols in eqn. 3-30 as ħ, *K*, *T* have their usual meaning of the Planck constant *h* divided by 2π, the Boltzmann constant and the temperature, respectively.

At room temperature the effect of cardiolipin can be easily handled on the basis of the Marcus model by assuming that, upon CL loading, the driving force for the reverse electron transfer $P^+Q_A^- \rightarrow PQ_A$ increases because of the CL induced $P^+Q_A^-$ destabilization, leaving essentially unchanged λ and V. This latter is a long-range coupling since the spatial separation between P^+ and Q_A^- is very large in relation to electron trasfer distances (25 Å)[141] (this is the main reason of the long time scale of the $P^+ \rightarrow Q_A^-$ electron transfer if compared with many others).

Under these conditions the ratio between the rate constants in the presence (k_{AP}) and in the absence (k_{AP}°) of cardiolipin is

$$\frac{k_{AP}}{k_{AP}^{o}} = \exp\left[\frac{-\left(\varepsilon^{CL}-\lambda\right)^{2}+\left(\varepsilon^{\circ}-\lambda\right)^{2}}{4\lambda KT}\right] \qquad \textbf{(3-31)}$$

where ε^{CL} and ε° are the driving forces for charge recombination in presence and absence of cardiolipin, respectively. For RCs from *Rb. sphaeroides* the value of ε° is estimated to be 0.52 eV[229]: as above discussed, since the bound CL induces only a moderate change in the driving force of charge recombination in comparison to the absolute values ($\Delta\varepsilon = \varepsilon^{CL} - \varepsilon^{\circ} = +30$ meV), it is possible to express in a simpler way the difference between square quantities at the numerator of the eqn. 3-31, at constant λ:

$$-\left(\varepsilon^{CL}-\lambda\right)^{2}+\left(\varepsilon^{\circ}-\lambda\right)^{2} = \left(\varepsilon^{\circ}\right)^{2}-\left(\varepsilon^{CL}\right)^{2}+2\lambda^{*}\left(\varepsilon^{CL}-\varepsilon^{\circ}\right) \qquad \textbf{(3-31a)}$$

Decomposing the difference between two square quantities it continues:

$$\left(\varepsilon^{\circ}\right)^{2}-\left(\varepsilon^{CL}\right)^{2}+2\lambda^{*}\left(\varepsilon^{CL}-\varepsilon^{\circ}\right) = \left(\varepsilon^{\circ}-\varepsilon^{CL}\right)\left(\varepsilon^{\circ}+\varepsilon^{CL}\right)+2\lambda^{*}\Delta\varepsilon =$$
$$= -\Delta\varepsilon^{*}\left(\varepsilon^{\circ}+\varepsilon^{CL}\right)+2\lambda^{*}\Delta\varepsilon = -2\Delta\varepsilon^{*}\left(\frac{\varepsilon^{\circ}+\varepsilon^{CL}}{2}-\lambda\right) \qquad \textbf{(3-31b)}$$

Finally, since Δε is negligible with respect to ε^{CL} and ε°, it is possible to approximate $\varepsilon^{\circ} + \varepsilon^{CL} \approx 2\,\varepsilon^{\circ}$ (being ε° the best estimated value between the two), thus:

$$-2\Delta\varepsilon^{*}\left(\frac{\varepsilon^{\circ}+\varepsilon^{CL}}{2}-\lambda\right) = -2\Delta\varepsilon^{*}\left(\varepsilon^{\circ}-\lambda\right) \qquad \textbf{(3-31c)}$$

Inserting the result in the previous equation 3-31 one obtains:

$$\frac{k_{AP}}{k_{AP}^{o}} = \exp\left[\frac{-2\Delta\varepsilon^{*}\left(\varepsilon^{\circ}-\lambda\right)}{4\lambda KT}\right] \qquad \textbf{(3-32)}$$

The value of reorganisation energy λ for the $P^{+}Q_{A}^{-}$ recombination has been obtained in several investigations by varying the driving force (via substitution of the native ubiquinone with other types of quinones[230] or through site-directed mutants[231]) and/or by varying the temperature[141, 222, 232] .

The resulting estimates for λ reveal a spread of values, ranging from 0.667[141] to 0.93 eV[222] . However, such a distribution of values has little effect on the outcome of the above equation because λ appears both on the numerator and denominator of the exponential argument. Indeed, the ratio k_{AP}/k_{AP}°, evaluated according to equation 32 and using the above λ values, ranges from 1.15 to 1.30, in remarkable agreement with the independent experimental results summarised in fig. 3.7.

It seems therefore that the peculiar dependence of the rate of $P^{+}Q_{A}^{-}$ recombination upon CL binding could mainly be ascribed - without further examination - to the increase, induced by cardiolipin, in the free energy drop associated to the $P^{+}Q_{A}^{-} \rightarrow PQ_{A}$ electron transfer (previously inferred from fluorescence experiments[163]). The interpretation on molecular terms is, however, very delicate and deserves a necessary refinement for this explanation, well true even though too poor.

It is useful to remember that in their functioning proteins undergo a variety of (fast) vibrations and (slower) structural rearrangements, these latter called protein-specific motions. Consequently during their motions they assume a large number of different conformations (or substates) instead of a unique state of minimum free energy, giving rise - from a thermodynamic point of view - to a complex energy landscape. The substates, usually represented as valleys, are separated by free energy barriers that have to be surmounted during conformational changes. The different height of these activation barriers explains the wide variety of time scales involved in protein motions (from femtoseconds to milliseconds).

The main point is that conformational dynamics is intimately connected to protein functions (i.e. electron transfer). At lower temperatures - such as cryogenic ones - large distributions of reaction rates are usually found, reflecting the heterogeneity of protein molecules frozen in different substates, On the contrary, at sufficiently high temperatures free fluctuation among substates leads to an averaging of the kinetic coefficients. At intermediate temperatures conformational transitions occur on the time scale of the reaction, allowing to investigate protein motions through temperature-dependent studies of reaction rates, as it could reveal our case, though not specifically planned for this purpose[141].

Back about the RC, following light absorption the sudden appearance of

separated charges inside the RC is an abrupt perturbation of its dark-adapted equilibrium state (even quantifiable as a high pressure existing inside the protein[195]), and adjustment of protein conformation begins immediately, to accommodate the *de novo* charges of P^+ and Q_A^- [141]. The negative charge primarily appears on the Φ_A cofactor, then fast electron transfer shifts it to Q_A^- (par. 1.4.2).

At room temperature the formation of the light-induced charge separated state $P^+Q_A^-$ (~200 ps, vertical up-directed transition in fig. 3.10) is faster than the protein transition from a dark-adapted to light-adapted conformation, named relaxation and defined as an internal motion tending to a minimum on a conformational free energy surface. Therefore the rise of $P^+Q_A^-$ takes place in a conformational substate still dark-adapted.

By this way, in RCs depleted of the Q_B quinone, the reduction of Q_A was observed to lead to rapid relaxation of the protein (D →L upper, non-vertical transition in fig. 3.10) during the "long" lifetime of the charge separated state (decay time constant ≈ 100 ms): this process was suggested to involve several conformational substates, represented in fig. 3.10 as "noise" in a rugged energy surface. This relaxation - which at 300 K was calculated to occur in 1 ps to few ms - occurs just because it leads to a decrease in both the driving force ε and the electronic coupling V between acceptor and donor states[141].

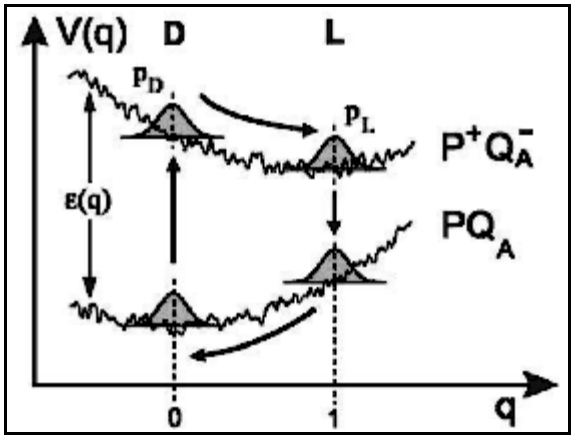

Figure 3.10.
Schematic depiction of the rugged energy surfaces in the neutral (PQ_A) and charge-separated (P^+Q_A) states of RCs. The energy gap, ε, which controls the electron transfer rates, varies as a function of the conformational coordinate q (it is generically defined V(q)). D(0) and L(1) refer to dark- and light-adapted conformations; the probability distributions p_D and p_L represent structural heterogeneity within these states.

After the relaxation, stabilizing the light-adapted state, the back reaction $P^+Q_A^-$ → PQ_A takes place (represented by the vertical arrow bottom-directed), followed by a "back" transition light- to dark-adapted in order to reduce the free energy content (fig. 3.10). In the diagram shown both the charge separation and recombination are represented as vertical transitions between electronic states, since they are usually faster then conformational fluctuations involving also the atom nuclei (Franck-Condon approximation)[233].

Differently, upon cooling the RC

relaxation from dark-adapted to light-adapted conformation is progressively hindered, thus charge recombination is forced to start from the higher energy dark-adapted conformation. This accounts for the striking increase in k_{AP}[141, 233] (related to the free energy difference of the process by eqn. 3-21).

Parallel studies[234] performed *at room temperature* by embedding the protein within a solid sugar matrix fully confirm such a description of the interplay between protein dynamics and electron transfer rate.

On these bases, the CL induced increase in the free energy drop associated to the $P^+Q_A^- \rightarrow PQ_A$ electron transfer could reflect the hampering of relevant conformational motion by the lipid, in a way similar to a sharp decrease of temperature (down to cryogenic values[141]) or to the effect of a viscous matrix surrounding the protein (e.g. made of sugars glasses or polymer films[234]).

Two additional evidences support this point of view.

First, the same increase in k_{AP} was found, in the absence of cardiolipin, in liquid solutions of trehalose where the internal dynamics of RC is moderately slowed down[219].

Second, it has been previously reported by our own experiments and by literature data respectively that:

a) addition of cardiolipin to RC micelles improves the RC thermal stability (fig. 3.2);

b) similarly, disruption by site-directed mutagenesis of the specific molecular interaction between RC and the “famous” crystal-bound cardiolipin strongly affects the thermal stability of the RC[56] (see par. 1.5.1.1 for details).

Both these latter observations suggest some cardiolipin-induced hampering of the unfolding conformational dynamics.

In this view, even the effect of site-specific mutations within the Q_A pocket, previously illustrated (equation scheme 3-29), could be interpreted in terms of hindrance of structural rearrangements leading to an acceleration of the recombination from Q_A. In this case the effect is much larger (k_{AP} is sped up 3÷4 times in comparison with wild-type non-mutated RCs) than the maximum induced by CL: this latter corresponds to CL pure proteoliposomes, where the increase of k_{AP} with respect to CL lacking samples (RC micelles and PC proteoliposomes) reaches almost the 30 %[163].

The temperature range we explored by our experiments (275÷310 K) would be

just intermediate between lower-cryogenic temparatures - completely freezing most of the RC molecular motions - and room temperatures - generally high enough to average most of the fluctuatons and so limiting the possibility of studies about protein-specific motions.

Cardiolipin is a unique dianionic phospholipid with four acyl chains that could exert its effect directly on the electron acceptor cofactors or indirectly via specific lipid-protein interactions. Presently the only known interaction between cardiolipin and the Reaction Centre from *Rb. sphaeroides* is that revealed by the high-resolution X-ray crystal structure published in 1999 by McAuley et al.[15], followed few years later by the discovery of further two lipids, phosphatidyl choline (PC) and a glycolipid, bound to the protein surface in another diffraction structure[60] (see par. 1.5.1 for details).

In addition very recent and important papers published in 2004-2005 are more and more supporting the hypothesis that on the RC there should be other binding sites for cardiolipin molecules, probably weaker than that already found and therefore still not identified. Their main conclusions will be summarized below.

Rinyu and coworkers[163] consider unlikely that the effects observed for the CL, many of them characterized by a small magnitude, are related only to the crystal bound CL molecule: such effects could well involve a tight binding site but rather indicating a partial occupancy of the site by endogenous lipid. In addition, all experimental data available about the crystal-bound cardiolipin describe it as a non-annular lipid located on the RC surface (par. 1.5.1), close to the membrane-water interphase where the dielectric constant should be intermediate between that of water (80) and that of the membrane (~2, par. 1.2.3), then not so small. Such an environment could moderately stabilize the negative net charges of CL - differently from highly apolar regions where free charges are “forbidden” for energy reasons[41] -. This makes less reasonable that CL influence on the Q_A site may be electrostatic - as easily expected -, receiving also confirmation by the lack of any effects on Q_B over an essentially equal distance (~15 Å).

Moreover, since other results clearly indicated that the cardiolipin effect on electron transfer properties of the RC is very similar between wild-type proteins and proteins specifically mutated at the CL binding pocket, it further suggests that CL may exert its direct influence on the Q_A site by alternative means, such as interactions at

other specific, but weaker, binding sites.

Similarly, another recent publication[12] underlines the potential and "dangerous" temptation, after having identified a binding site for a particular lipid, of trying to assign every known functional effect on the interacting protein (e.g. the increase in the energy of $P^+Q_A^-$) to the last identified lipid of that class (the "usual suspect"). This is a general concept for many membrane proteins and bound lipids. Moreover, besides the crystallographically detected cardiolipin-site, the authors propose one or more additional CL bound at other surface locations near the Q_A site.

As a last literature example, a paper dedicated to calorimetric measures on the RC[56] (par. 1.5.1.1) attributes the presence of two separate peaks in DSC traces of wild-type RCs - after having ruled out other hypotheses - to two populations undergoing the same thermal denaturation but differing in the occupancy of many cardiolipin binding sites (CL protects the RC from denaturation). The existence of many binding sites rather than only one has been supposed just because a unique tight binding could not explain such an experimental heterogeneity.

The functional study presented in this thesis is well in line with these evidence-based opinions and it points to the existence of more than one site of binding for CL on the RC (fig. 3.7), at difference with the unique site observed in the X-ray structures.

The cardiolipin observed in RC crystals is tightly bound. This can be inferred first from its location, adherent to the protein surface (see par. 1.5.1 for details), with the polar groups rigidly involved in several electrostatic and hydrogen bonding interactions while the farthest acyl chains are located in grooves and cavities on the RC surface[15, 56, 60, 235]. This is a typical arrangement for non-annular lipids (par. 1.3), suggesting that CL - as well as PC and the glycolipid bound to the RC surface - belongs to this class of membrane protein-interacting lipids. The tight binding cardiolipin-RC can be inferred also by the presence of CL in RCs embedded in lipidic cubic phases[31] (where the bicontinuous apolar domain furnishes a large solvent pool for CL).

We expect, therefore, that a large fraction of our RCs retain that endogenous cardiolipin molecule. One can speculate that the high affinity binding site (K^1=4 mM) seen in the CL titration of RC (fig. 3.7) corresponds to tightly bound cardiolipin molecule seen in several RC crystal structures. According to such a hypothesis the initial and very

small increase on the k_{AP} (5 %) could be explained by a limited effect due to partial occupancy of the site by endogenous cardiolipin. The location of this lipid and its proved role as protector from protein unfolding and thermal denaturation (see above) allow to define CL as a non-annular surface lipid in the bound lipid classification of par. 1.3.

At variance, the following two features related to the second class of binding sites (found by us referring to eqn. 3-19) permit to exclude any relation with the CL pocket recognized in X-ray structures.

1) These secondary sites are characterized by *low affinity binding.* From the eqn. 3-10 a local (i.e. hydrophobic) concentration of cardiolipin of about 0.5 M corresponds in RC micelles with RC about 2 μM - as in every our sample - to an overall CL concentration of ~200 μM, that is close to the maximal admitted loading of CL in aqueous DDAO solutions without causing significant changes in the solvent polarity (par. 2.2). This value only slightly saturates the RC (fig. 3.7).

Furthermore even in pure CL vesicles, when the hydrophobic concentration of the lipid is about 0.8 M (corresponding for 100 % CL liposomes of fig. 3.7 to an overall concentration of ~ 5 mM) the CL binding appears to be incomplete because it maintains still an incresing trends. Thus we can certainly exclude that in RC crystals (without addition of exogenous CL) such sites are occupied.

2) The binding of cardiolipin is *cooperative*. This means that several CL molecules bind the RC. A rough estimate of the number of ligands involved in cooperative binding is given by the Hill coefficient (*n* in equation 3-13). According to the data of fig. 3.7 the RC accommodates about four molecules of cardiolipin (*n*=4), while in the RC structures only one CL molecule is observed.

Presently, we have indications neither on the location of these low-affinity binding sites nor on the mechanism of cardiolipin-induced destabilization of the $P^+Q_A^-$ state.

From literature data comparisons it has been found that in relation to the faster recombination from $P^+Q_A^-$ (with respect to the same state without CL) and to the induced destabilization CL acts in the same way as a mutation within the Q_A pocket[163] (see

above), confirming that direct perturbative effects of CL on cofactor energy levels occur entirely on the Q_A site. In par. 1.5.3 in fact the effects of CL on Q_B site were explained as indirect.

The effect is however specific for cardiolipin and is not shared by lecithin. In addition, in the future it would be interesting to study the effects on the RC of other anionic phospholipids physiologically significant present in the cell membranes from *Rb. sphaeroides,* such as phosphatidyl glycerol.

By definition, a cooperative binding involves some conformational changes of the protein. The fit of the titration curve of Fig. 3.7 to equation 3-19 gives $Y^* = 6 \pm 2$: in RCs fully satured with CL this corresponds to a rate constant for the $P^+Q_A^-$ recombination equal to $k_{AP}^* = 50 \pm 20\ s^{-1}$ (if k_{AP}° is $8.3\ s^{-1}$). This is close to the rate constant for $P^+Q_A^-$ decay found at room temperature for RC entrapped in very rigid trehalose matrix ($k_{AP} = 35\ s^{-1}$), where conformational relaxation is severely inhibited[234, 236]. This is consistent with the hypothesis that cardiolipin causes hindrance of the protein relaxation leading to an energy decrease for the $P^+Q_A^-$ state (fig. 3.10): by this way CL makes possible faster charge recombinations.

3.4. **Conclusions**.

In recent years numerous structural studies have demonstrated that one molecule of cardiolipin tightly binds the photosynthetic reaction center from *Rb. sphaeroides*. The cardiolipin binding site seems to be highly preserved over different photosynthetic bacteria (see par. 1.5.1 for details).

In the present functional study, we showed that the addition of cardiolipin does not affect the affinity of the Q_A site for the ubiquinone, but has a relevant influence on the rate of $P^+Q_A^-$ recombination.

The rate constant for the $P^+Q_A^- \rightarrow PQ_A$ electron transfer obtained in micelles and vesicles both containing CL follows the same trend when cardiolipin concentration evaluated with respect to the apolar phase is used as relevant variable. Moreover, our results reveal that there are two classes of binding sites for cardiolipin.

The high-affinity site is compatible with the binding site observed in crystallographic studies. On the contrary, a cooperative binding involving about four CL molecules and taking place at high cardiolipin loading is a feature previously unreported.

It appears that the main effect of cardiolipin on the electron transfer can be ascribed to a destabilization of the $P^+Q_A^-$ charge separated state. On the basis of previous studies we propose that such an effect is likely due to CL induced inhibition of protein conformational relaxation that stabilizes the light-induced $P^+Q_A^-$ state.

References.

1. L . Stryer, “The photosynthesis” in *Biochemistry*, chapt. 26, 4th ed. (1995), W. H. Freeman and Company, New York and Basingstoke.

2. J. Nagyvary, J. Bechert, *Biochem. Edu.* 27 (1999), 193.

3. J. D. Rawn, “The photosynthesis” in *Biochemistry*, vol. I, chapt. 18 (1988), p. 489, McGraw-Hill.

4. “The photobiology” (G. Forti Ed.), *Le Scienze* (italian edition of *Scientific American)*, vol. 46 (1989).

5. X. Hu, A. Damjanovic, T. Ritz and K. Schulten, *Proc. Natl. Acad. Sci. USA* 95 (1998), 5935.

6. R. Cogdell, P. Fyfe, S. Barrett, S. Prince, A. Freer, N. Isaacs, P. McGlynn and C. Hunter, *Photosynth. Res*. 48 (1996), 55.

7. Govindjee, “Purple bacteria” in *Photosynthesis energy conversion by plants and bacteria* (Govindjee Ed.), chapt. 4 (1982), p.81, Academic Press, New York.

8. G. Cevc and D. Marsh, “Self-assembly” in *Phospholipid Bilayers: Physical Principles and Models,* chapt. 2 (1987), John Wiley & Sons, New York.

9. C. Tanford, “*The Hydrophobic Effect”* (1980), Wiley, New York.

10. W. Dowhan, *Annu. Rev. Biochem.* 66 (1997), 199.

11. G. Cevc and D. Marsh, “Bilayer properties” in *Phospholipid Bilayers: Physical Principles and Models,* chapt. 1 (1987), John Wiley & Sons, New York.

12. P. K. Fyfe, A. V. Hughes, P. Heathcote and M. R. Jones, *Trends in Plant Science* 10(6) (2005), 275.

13. L . Stryer, “Structure and dynamics of membranes” in *Biochemistry*, chapt. 11, 4th ed. (1995), W. H. Freeman and Company, New York and Basingstoke.

14. F. L. Hoch, *Biochim. Biophys. Acta* 1113 (1992), 71.

15. K. E. McAuley, P. K. Fyfe, J. P. Ridge, N. W. Isaacs, R. J. Cogdell and M. R. Jones, *Proc. Natl. Acad. Sci. USA* , 96 (1999), 14706.

16. R. E. Overfield, C. A. Wraight, *Biochemistry* 19 (1980), 3328.

17. L. Nagy, E. Fodor, J. Tandori, L. Rinyu and T. Farkas*, Aust. J. Plant Physiol.* 26 (1999), 1.

18. A. Corcelli, M. Colella, G. Mascolo, F. P. Panizzi, M. Kates, *Biochemistry* 39 (2000), 3318.

19. S. Nubberger *et al.*, *J. Mol. Biol.* 234 (1993), 347.

20. T. Tsukihara *et al.*, *Proc. Natl. Acad. Sci. USA* 100 (2003), 15304.

21. M. Jormakka *et al.*, *Science* 295 (2002), 1863.

22. N. C. Robinson, *Biochemistry* 21 (1982), 184.

23. T. Mizushima, M. Yao, N. Inoue, H. Aoyama, E. Yamashita, H. Yamaguchi, T. Tsukihara, R. Nakashima, K. Shinzawa-Itoh, R. Yaono and S. Yoshikawa, *Acta Crystallogr. A55 Supplement* (1999), Abstr. P06.04.069.

24. W. Welte, W. Kreutz, *Biochim. Biophys. Acta* 692 (1982), 479.

25. T. H. Haines, *Proc. Natl. Acad. Sci. USA* 80 (1983), 160.

26. G. Fritzsh, L. Kampmann, G. Kapaun, H. Michel, *Photosynth. Res.* 55 (1998), 127.

27. E. C. Abresch, M. L. Paddock, M. H. B. Stowell, T. M. McPhillips, H. L. Axelrod, S.M. Soltis, D. C. Rees, M. Y. Okamura, G. Feher, *Photosynth. Res.* 55 (1998), 119.

28. M. Ollivon, S. Lesieur, C. Grabielle-Madelmont, M. Paternostre, *Biochim. Biophys. Acta* 1508 (2000), 34.

29. R. R. C. New, "Preparation of liposomes" in *Liposomes, a practical approach*, chapt. 3 (1994), IRL Press.

30. G. Cevc and D. Marsh, "Non-bilayer phases" in *Phospholipid Bilayers: Physical Principles and Models,* chapt. 14 (1987), John Wiley & Sons, New York.

31. G. Katona, U. Andreasson, E. M. Landau, L. E. Andreasson, R. Neutze, *J. Mol. Biol.* 331 (2003), 681.

32. R. M. Epand, *Biochim. Biophys. Acta* 1376 (1998), 353.

33. A. Mallardi, M. Giustini and G. Palazzo, *Recent Res. Devel. Physical Chem.* 6 (2002), 371.

34. E. Rivas, B. Costa, T. Gulik-Krzywicki and F. Reiss-Husson, *Biochim. Biophys. Acta* 904 (1987), 290.

35. L. Baciou, T. Gulik-Krzywicki and P. Sebban, *Biochemistry* 30 (1991), 1298.

36. P. Sebban, P.Parot, L. Baciou, P. Mathis, A. Verméglio, *Biochim. Biophys. Acta* 1057(1991), 109.

37. A. Taly, L. Baciou, P. Sebban, *FEBS Letters* 532 (2002), 91.

38. M. P. Heyn, R. J. Cherry and N. A. Dencher, *Biochemistry* 20 (1981), 840.

39. S. A. Simon and T. J. McIntosh, *Methods Enzymol.* 127(1986), 511.

40. P. V. Ioannou, B. T. Golding, *Prog. Lip. Res.*17 (1979), 279.

41. A. G. Lee, *Biochim. Biophys. Acta* 1612 (2003), 1.
A. G. Lee, *Biochim. Biophys. Acta* 1666 (2004), 62.

42. A. Berkaloff, J. Bourguet, P. Favard, M. Guinnebault "La membrana plasmatica", *La cellula, fisiologia*, chapt. 1(1974), Mondadori ed..

43. S. Singer, G.L. Nicholson, *Science* 172 (1972), 720.

44. S. Manno, Y. Takakuwa and N. Mohandas, *Proc. Natl. Acad. Sci. USA* 99 (4) (2002), 1943.

45. A. Watts, *Biochim. Biophys. Acta* 1376 (1998), 297.

46. M. Ø. Jensen, O. G. Mouritsen, *Biochim. Biophys. Acta* 1666 (2004), 205.

47. D. A. Brown, *Proc. Natl. Acad. Sci. USA* 98 (19) (2001), 10517.

48. Y. Barenholz, *Progress in Lipid Research* 41 (2002),1.

49. T. J. Stevens, I. T. Arkin, *Proteins* 39 (4) (2000), 417.
E. Wallin, G. von Heijne, *Protein Sci.* 7 (1998), 1029.

50. For an up-to-date list of the membrane protein structures see:
http://blanco.biomol.uci.edu/Membrane_Proteins_xtal.html
http://www.mpibp-frankfurt.mpg.de/michel/public/memprotstruct.html

51. P. K. Fyfe, K. E. McAuley, A. W. Roszak, N. W. Isaacs, R. J. Codgell and M. R. Jones, *Trends in Biochemical Sciences* 26 (2) (2001), 106.

52. T. O. Yeates, H. Komiya, D. C. Rees, J. P. Allen and G. Feher, *Proc. Natl. Acad. Sci. USA* 84 (1987), 6438.

53. H. Michel, *Crystallization of Membrane Proteins* (1991), CRC Press, Boca Raton, FL, USA.

54. R. Grisshammer, C. G. Tate, *Q. Rev. Biophys.*, 28 (1995), 315.

55. R. M. Garavito, S. Ferguson-Miller, *J. Biol. Chem*. 276 (2001), 32403.

56. P. K. Fyfe, N. W. Isaacs, R. J. Codgell, M. R. Jones, *Biochim. Biophys. Acta* 1608 (2004), 11.

57. P. J. Loll, J. Struct. Biol. 142 (2003), 144.

58. C. Benning in *Lipids in Photosynthesis: Structure, Function and Genetics*, Siegenthaler eds.(1998), p. 83, P.A. & N. Murata, Kluwer, Dordrecht, The Netherlands.

59. J. F. Imhoff and U. Bias-Imhoff, "Lipid, quinones and fatty acids of anoxygenic phototropic bacteria" in *Anoxygenic photosynthetic bacteria* (1995), p. 179, R. E. Blankenship, M. T. Madigan, and C. Bauer editors. Kluwer Academic Publishers, Dordrecht, The Netherlands.

60. A. Camara-Artigas, D. Brune and J. P. Allen, *Proc. Natl. Acad. Sci. USA* 99 (17)(2002), 11055.

61. J. Oelze and G. Drews, *Biochim. Biophys. Acta* 265 (1972), 209.

62. J. L. Rigaud, B. Pitard and D. Levy, *Biochim. Biophys. Acta* 1231 (1995), 223.

63. J. L. Rigaud and B. Pitard, "Liposomes as tools for the reconstitution of biological systems" in *Liposomes as tools in basic research and industry*, J. R. Philippot, F. Schuber eds., chapt. 5 (1995), CRC Press, Boca Raton, FL, USA.

64. G. Cevc, D. Marsh, "Lipid hydration" in *Phospholipid Bilayers: Physical Principles and Models,* chapt. 3 (1987), John Wiley & Sons, New York.

65. G. V. Betageri, S. B. Kulkarni, "Preparation of liposomes" in *MML Series*, Volume I, chapt. 18 (1999), 491.

66. A. Darszon, C. A. Vanderberg, M. Schonfeld, M. H. Ellisman, N. C. Spitzer and M. Montal, *Proc. Natl. Acad. Sci. U.S.A.* 77 (1980), 239.

67. A. Darszon, C. A. Vanderberg, M. H. Ellisman and M. Montal, *J. Cell. Biol.* 81 (1979), 446.

68. J. L. Rigaud, A. Bluzat and S. Buschlen, *Biochem. Biophys. Res. Commun.* 111 (1983), 373.

69. D. D. Lasic, *Biochem. J.* 256 (1988), 1.

70. P. K. Vinson, Y. Talmon and A. Walter, *Biophys. J.* 56 (1989), 669.

71. G. D. Eytan, *Biochim. Biophys. Acta* 694 (1982), 185.

72. M. Paternostre, M. Roux, J. L. Rigaud, *Biochemistry* 27 (1988), 2668.

73. M. L. Jackson and B. J. Litman, *Biochemistry* 21 (1982), 5601.

74. J. Cladera, J. L. Rigaud, H. Bottin, M. Dunach, *J. Bioenerg. Biomembr.* 28 (1996), 503.

75. B. de Kruijff, Editorial, *Biochim. Biophys. Acta* 1376 (1998), 243.

76. J.N. Israelachvili, *Biochim. Biophys. Acta* 469 (1977), 221.

77. E. Sackmann, "Physical basis for trigger processes and membrane structures", in *Biological Membranes*, vol. 5, 1984, D. Chapman Ed., Academic Press, London, p. 105.

78. T. Gil, J. H. Ipsen, O. G. Mouritsen, M. C. Sabra, M. M. Sperotto, M. J. Zuckermann, *Biochim. Biophys. Acta* 1376 (1998), 245.

79. H. Palsdottir, C. Hunte, *Biochim. Biophys. Acta* 1666 (2004), 2.

80. W. van Klompenburg, I. Nilsson, G. von Heijne, B. de Kruijff, *EMBO J.* 16 (14) (1997) 4261– 4266.

81. M. Bogdanov,W. Dowhan, *J. Biol. Chem*. 270 (2) (1995) 732-739.

82. M. R. Jones, P. K. Fyfe, A. W. Roszak, N. W. Isaacs, R. J. Codgell, *Biochim. Biophys. Acta* 1565 (2002), 206.

83. P. Fromme, P. Jordan, N. Krauß, *Biochim. Biophys. Acta* 1507 (2001), 5.

84. K. Beyer, M. Klingenberg, *Biochemistry* 24 (1985), 3821.

85. G. B. Birrell, W. R. Sistrom, O. H. Griffith, *Biochemistry* 17 (1978), 3768.

86. G. Paradies, F. M. Ruggiero, P. Dinoi, G. Petrosillo, E. Quagliariello, *Arch. Biochem. Biophys.* 397 (1993), 91.

87. J. A. Killian, *Biochim. Biophys. Acta* 1376 (1998), 401.

88. T. Walz, S. J. Jamieson, C. M. Bowers, P. A. Bullough, C. N. Hunter, *J. Mol. Biol.* 282 (1998), 833; *see references therein*

89. D. Marsh, L. I. Horvàth, *Biochim. Biophys. Acta* 1376 (1998), 267.

90. J. R. Lakowicz, *Principles of Fluorescence Spectroscopy*, 1983, Plenum Press, New York.

91. E. Perochon, A. Lopez and J. F. Tocanne, *Biochemistry* 31 (1992), 7672.

92. W. L. Ash, M. R. Zlomislic, E. O. Oloo, D. P. Tieleman, *Biochim. Biophys. Acta* 1666 (2004) 158.

93. P. W. Atkins, "Physical chemistry" (1995), 3rd ed., Zanichelli, Bologna, Italy.

94. A. G. Lee, *Biochim. Biophys. Acta* 1376 (1998), 381.

95. M. Roth, A. Lewit-Bentley, H. Michel, J. Deisenhofer, R. Huber, D. Oesterhelt, *Nature* 340 (1989), 659.

96. D.M. Engelman , T.A. Steitz, A. Goldman, *Annu. Rev. Biophys. Biophys. Chem.* 15 (1986), 321.

97. R. Henderson and P. N. Unwin, *Nature* 257 (1975), 28.

98. U. Ermler, G. Fritzsch, S. K. Buchanan and H. Michel, *Structure* 2 (1994), 925.

99. J. Deisenhofer, O. Epp., K. Miki, R. Huber , H. Michel*, Nature (London)*, 318 (1985), 618.

100. A. Verméglio, P. Joliot, *Trends in microbiology* 7(11) (1999), 435.

101. C. Jungas, J. L. Ranck, J. L. Rigaud, P. Joliot, A. Verméglio, *EMBO J.* 18(3) (1999), 534.

102. G. McDermott, S. M. Prince, A. A. Freer, A. Hawthornthwaite-Lawless, M. Z. Papiz, R. J. Cogdell, N. W. Isaacs, *Nature* 374 (1995), 517.

103. N. Adir, H. L. Axelrod, P. Beroza, R. A. Isaacson, S. H. Rongey, M. Y. Okamura, G. Feher, *Biochemistry* 35 (1996), 2535.

104. C. Roy, D. Lancaster and H. Michel, "Photosynthetic Reaction Centres of purple bacteria" in *Handbook of metalloproteins* (2001), edited by A. Messerschmidt, R. Huber, T. Poulos and K. Wieghardt, John Wiley and Sons, Ltd, Chichester.

105. J. Deisenhofer, O. Epp, K. Miki, R. Huber , H. Michel, *J. Mol. Biol.*180 (1984), 385.

106. J. P. Allen, G. Feher, T. O. Yeates, H. Komiya, D. C. Rees,, *Proc. Natl. Acad. Sci. U.S.A.* 84 (1987), 5730.

107. J. P. Allen, G. Feher, T. O. Yeates, H. Komiya, D. C. Rees, *Proc. Natl. Acad. Sci. U.S.A.* 84 (1987), 6162.

108. H. L. Axelrod, E. C. Abresch, M. Y. Okamura, A. P. Yeh, D. C. Rees and G. Feher, *J. Mol. Biol.* 319 (2002), 501.

109. G. Fritzsch, J. Koepke, R Diem, A. Kuglstatter and L. Baciou, *Acta Cryst. D* 58 (2002), 1660.

110. W. W. Parson, in DS bendall (ed.), *Protein electron transfer* (1996), BIOS Scientific Publishers, Oxford, 125.

111. G. Feher, *Photosynth. Res.* 55 (1998), 1.

112. A. J. Hoff, J. Deisenhofer, *Phys. Rep.* 287 (1997), 1.

113. J. P. Allen, G. Feher, T. O. Yeates, D. C. Rees, J. Deisenhofer, H. Michel, R. Huber, *Proc. Natl. Acad. Sci. U. S. A.* 83 (1986), 8589.

114. O. El Kabbani, C. H. Chang , D. Tiede, J. Norris, M. Schiffer, *Biochemistry* 30 (1991), 5361.

115. A. Zouni *et al.*, *Nature* 409 (2001), 739.

116. N. Kamiya and J. R. Shen, *Proc. Natl. Acad. Sci. U.S.A.* 100 (2003), 98.

117. W. Kuhlbrandt, *Nature* 411 (2001), 896.

118. T. A. Ceska, R. Henderson, *J. Molec. Biol.* 213 (3) (1990), 539.

119. H. Komiya, T. O. Yeates, D. C. Rees, J. P. Allen, and G. Feher, *Proc. Natl. Acad. Sci. U. S. A.* 85 (1988), 9012.

120. M. R. Gunner, A. Nicholls and B. Honig,, *J. Phys. Chem.* 100 (1996), 4277.

121. J. Barber, *Q. Rev. Biophys.* 36 (2003), 71.

122. R. J. Debus, G. Feher and M. Y. Okamura, *Biochemistry* 25 (1986), 2276.

123. H. L. Axelrod, E. C. Abresch, M. L. Paddock, G. Feher, M. Y. Okamura, *Proc. Natl. Acad. Sci. U. S. A.* 97 (2000), 1542.

124. M. H. B. Stowell, T. M. McPhillips, D. C. Rees, S. M. Soltis, E. Abresch, G. Feher, *Science* 276 (1997), 812.

125. L. M. Utschig, O. Poluektov, S. L. Schlesselman, M. C. Thurnaer, D. M. Tiede, *Biochemistry* 40 (2001), 6132.

126. M. Y. Okamura, M. L. Paddock, M. S. Graige, G. Feher, *Biochim. Biophys. Acta* 1458 (2000), 148.

127. P. Maróti, *Journal of Photochemistry and Photobiology B: Biology* 8 (1991), 263.

128. R. A. Friesner, Y. Won, *Biochim. Biophys. Acta* 977 (1989), 99.

129. A. Kuglstatter, U. Ermler, H. Michel, L. Baciou & G. Fritzsch, *Biochemistry* 40 (2001), 4253.

130. A. R. Crofts, C. A. Wraight, *Biochim. Biophys. Acta* 726 (1983), 149.

131. P. L. Dutton, J. S. Leigh, C. A. Wraight, *FEBS Lett.* 36 (1973), 169.

132. A. W. Rutherford and M. C. W. Evans, *FEBS Lett.* 110 (1980), 257.

133. E. G. Alexov, M. R. Gunner, *Biochemistry* 38 (1999), 8253.

134. M. S. Graige, G. Feher, M. Y. Okamura, *Proc. Natl. Acad. Sci. U. S. A.* 95 (1998), 11679.

135. D. Kleinfeld, M. Y. Okamura and G. Feher*, Biochim. Biophys. Acta* 766 (1984), 126.

136. R. Brudler, K. Gerwert, *Photosynt. Res.* 55 (1998), 261.

137. C. R. D. Lancaster, *Biochim. Biophys. Acta* 1365 (1998), 143.

138. M. Giustini, F. Castelli, I. Husu, M. Giomini, A. Mallardi, G. Palazzo, *J. Phys. Chem. B,* 109 (2005), 21187.

139. G. Palazzo, A. Mallardi, M. Giustini, D. Berti and G. Venturoli, *Biophys. J.* 79 (2000), 1171.

140. D. Kleinfeld, M. Y. Okamura and G. Feher, *Biochemistry* 23 (1984), 5780.

141. B. H. McMahon, J. D. Müller, C. A. Wraight and G. U. Nienhaus, *Biophys. J.* 74 (1998), 2567.

142. R. A. Marcus, N. Sutin, *Biochim. Biophys. Acta* 811 (1985), 265.

143. L. E. Morrison, J. E. Schelhorn, Th. M. Cotton, Ch. L. Bering, P. A. Loach, “Electrochemical and spectral properties of ubiquinones and synthetic analogs: Relevance to bacterial photosynthesis”, *Function of Quinones in Energy Conserving Systems* (1982), B. L. Trumpower ed, p. 35-58, Academic Press, New York.

144. J. Tandori, L. Nagy, A. Puskàs, M. Droppa, G. Horvàth and P.Maròti, *Photosynthesis Research* 45 (1995),135.

145. P. Maròti, D. K. Hanson, M. Schiffer and P. Sebban, *Nature* 2 (1995), 1057.

146. P. K. Fyfe, K. E. McAuley, J. P. Ridge, S. M. Prince, G. Fritzsch, N. W. Isaacs, R. J. Codgell and M. R. Jones, *Photosynth. Res.* 55 (1998), 133.

147. J. Deisenhofer, O. Epp, I. Sinning, H. Michel, *J. Mol. Biol.* 246 (1995) , 429.

148. J. Deisenhofer and H. Michel, *EMBO J.* 8 (1989), 2149.

149. C. R. D. Lancaster and H. Michel, *J. Mol. Biol.* 286 (1999), 883.

150. M. C. Wakeham, M. R. Jones, R. B. Sessions, P. K. Fyfe, *Biophys. J.* 80 (2001),1395.

151. N. J. Russell, J. L. Harwood, *Biochem J.* 181 (1979), 339.

152. A. Camara-Artigas, C. L. Magee, J. C. Williams, J. P. Allen, *Acta Crystallogr.*, D 57 (2001), 1281.

153. C. R. D. Lancaster, H. Michel, B. Honig, M. R. Gunner, *Biophys. J.* 70 (1996), 2469.

154. I. Fathir, T. Mori, T. Nogi, M. Kobayashi, K. Miki, T. Nozawa, *Eur. J. Biochem.* 268 (2001), 2652.

155. T. Nogi, I. Fathir, M. Kobayashi, T. Nozawa, K. Miki, *Proc. Natl. Acad. Sci. U. S. A.* 97 (2000), 13561.

156. D. Marsh, T. Pàli, *Biochim. Biophys. Acta* 1666 (2004), 118.

157. T. Haltia, E. Friere, *Biochim. Biophys. Acta* 1228 (1995), 1.

158. E. Katilius, Z. Katiliene, S. Lin, A. K. W. Taguchi and N. W. Woodbury, *J. Phys. Chem. B* 1063 (2002), 11471.

159. N. W. Woodbury and J. P. Allen in *Anoxygenic Photosynthetic Bacteria*, p. 527, eds. R. E. Blankenship, M. T. Madigan and C. E. Bauer (Kluwer, Dordrecht, The Netherlands)

160. T. A. Wells, E. Takahashi, C. A. Wraight, *Biochemistry* 42 (2003), 4064.

161. C. A. Wraight, *Israel Journal of Chemistry* 21 (1981), 348.

162. P. H. McPherson, M. Y. Okamura and G. Feher, *Biochim. Biophys. Acta* 934 (1988), 348.

163. L. Rinyu, E. W. Martin, E. Takahashi, P. Maròti, C. A. Wraight, *Biochim. Biophys. Acta* 1655 (2004), 93.

164. C.A. Wraight, “Functional linkage between the Q_A and Q_B sites of photosynthetic reaction centers, in: G. Garab (Ed.), Photosynthesis: Mechanisms and Effects, vol. II, Kluwer Academic Publishing, Dordrecht, 1998, pp. 693– 698.

165. L. Nagy, F. Milano, M. Dorogi, A. Agostiano, G. Laczkò, K. Szebényi, G. Vàrò, M. Trotta and P. Maròti, *Biochemistry* 43 (2004), 12913.

166. S. M. Barnett, S. Dracheva, R. W. Hendler and I. W. Lewin, *Biochemistry* 35 (1996), 4558.

167. H. Michel and D. Oesterhelt, *Proc. Natl. Acad. Sci. U. S. A.* 77 (1980), 1283.

168. E. M. Landau, J. P. Rosenbusch, *Proc. Natl. Acad. Sci. U. S. A.* 93 (1996), 14532.

169. P. Nollert, H. Qiu, M. Caffrey, J. P. Rosenbusch and E. M. Landau, *FEBS Letters* 504 (2001), 179.

170. M. L. Chiu, P. Nollert, M. C. Loewen, H. Belrhali, E. Pebay-Peyroula, J. P. Rosenbush and E. M. Landau, *Acta Crystallog. sect. D* 56 (2000), 781.

171. E. H. Pape, W. Menke, D. Weick and R. Hosermann, *Biophys. J.* 14 (1974), 221.

172. G. V. Marinetti and K. Cattieu, *Chem Phys. Lipids* 28 (1981), 241.

173. F. Francia, J. Wang, G. Venturoli, B. A. Melandri, W. P. Barz and D. Oesterhelt, *Biochemistry* 38 (1999), 6834.

174. A. Vermeglio, P. Joliot and A. Joliot, *Biochim. Biophys. Acta* 1183 (1993), 352.

175. P. A. Loach, *Proc. Natl. Acad. Sci. U. S. A.* 97 (2000), 5016.

176. L . Stryer, "Description of an allosteric protein" in *Biochemistry*, chapt. 7, 4th ed. (1995), W. H. Freeman and Company, New York and Basingstoke.

177. H. Luecke, B. Schobert, H. T. Richter, J. P. Cartailler, and J. K. Lanyi, *J. Mol. Biol*. 291 (1999), 899.

178. P. Facci, V. Erokhin, S. Paddeu and C. Nicolini, *Langmuir* 14 (1998), 193.

179. V. Erokhin, P. Facci, A. Kononenko, G. Radicchi and C. Nicolini, *Thin Solid Films* 285 (1996), 805.

180. H. De Lima Santos, P. Ciancaglini, *Biochem. Edu.* 28 (2000), 178.

181. K. A. Gray, J. Wachtveitl, J. Breton, D. Oestherhelt, *EMBO J.* 9 (1990), 2061.

182. M. Y. Okamura, R. A. Isaacson, G. Feher, *Proc. Nat. Acad.. Sci.* U.S.A. 72 (1975), 3491.

183. M. Y. Okamura, "On the herbicide binding site in bacterial reaction centres", *Biosynthesis of the photosynthetic apparatus: molecular biology, development and regulation* (1984), 381.

184. L . Stryer, "Exploring the proteins" in *Biochemistry*, chapt. 3, 4th ed. (1995), W. H. Freeman and Company, New York and Basingstoke.

185. R. Angelico, A. Ceglie, U. Olsson, G. Palazzo, *Langmuir* 16 (2000), 2124.

186. S. Milioto, D. Romancini, R. De Lisi, *J. Solution Chem.* 16 (1987), 943.

187. O. Zumbuehl and H. G. Weder, *Biochim. Biophys. Acta* 640 (1981), 252.

188. W. Shankland, *Chem. Phys. Lipids* 4 (1970), 109.

189. G. Venturoli, A. Mallardi, P. Mathis, *Biochemistry* 32 (1993), 13245.

190. T. M. Allen, A. Y. Romans, H. Kercret, J. P. Segrest,, *Biochim. Biophys. Acta* 601 (1980), 328.

191. F. Castelli, *Chem. Phys. Lett.* 38 (3) (1976), 528.

192. G. Porter and M. A. West in *Techniques of chemistry*, vol. VI, part II, 3rd Ed., eds. A. Weissberger and G. G. Hammes (Wiley- Interscience, New York, 1974).

193. C. R. Goldschmidt, M. Ottolenghi and C. Stein, *Israel J. Chem.* 8 (1970), 29.

194. H. Schomburg, H. Staerk and A. Weller, *Chem. Phys. Letters* 21 (1973), 433.

195. F. van Mourik, M. Reus, A. R. Holzwarth, *Biochim. Biophys. Acta* 1504 (2001), 311.

196. B. Koren, *Spie's* ***optical electronics*** magazine (2001, august), 34.

197. L. Ambrosone, A. Mallardi, G. Palazzo, G. Venturoli, *Phys. Chem. Chem. Phys.* 4 (2002), 3071.

198. J. A. Nelder, R. Mead, *Comp. J.* 7 (1965), 308.

199. W.H. Press, B.P. Flannery, S.A. Teulkolsky, W.T. Vetterling, *Numerical Recipes*, Cambridge University Press: Cambridge, 1986 and references therein.

200. A. Mallardi, G. Palazzo, G. Venturoli, *J. Phys. Chem. B* 102 (1998), 9168.

201. J. M. Beechem, *Methods Enzymol.* 210 (1992), 37.

202. R. R. Krug, W. G. Hunter, R. A. Grieger, *J. Phys. Chem.* 80 (1976), 2335.
R. R. Krug, W. G. Hunter, R. A. Grieger, *J. Phys. Chem.* 80 (1976), 2341.
R. R. Krug, W. G. Hunter, R. A. Grieger, *Nature* 261 (1976), 566.

203. L. Stryer, "Introduction to enzymes" in *Biochemistry*, chapt. 8, 3th ed. (1989), W. H. Freeman and Company, New York and Basingstoke.

204. J. Mandel and F. J. Linning, *Anal. Chem.* 29 (1957), 743.

205. J. R. Taylor, "Introduzione all'analisi degli errori" (1986), par. 5.8, ed. Zanichelli, Bologna.

206. J. E. Leffler, *J. Org. Chem.* 20 (1955), 1202.

207. R. F. Brown and H. C. Newsom, *J. Org. Chem.* 27 (1962), 3010.

208. J. E. Leffler, *J. Org. Chem.* 31 (1968), 533.

209. M. L. Johnson and L. M. Faunt, *Methods Enzymol.* 210 (1992).

210. E. W. Small, *Methods Enzymol.* 210 (1992).

211. M. Straume and M. L. Johnson, *Biophys. J.* 56 (1989), 15.

212. M. Straume and M. L. Johnson, *Methods Enzymol.* 210 (1992), 117 and references therein.

213. J. J. Correia and J. B. Chaires, *Methods Enzymol.* 240 (1994), 593 and references therein.

214. M. L. Johnson and S. G. Frasier, *Methods Enzymol.* 117, 301.

215. www.stelar.it.

216. A. Mallardi, M. Giustini, G. Palazzo, *J. Phys. Chem. B* 101 (1997), 7850.

217. J. C. McComb, R. R. Stein, C. A. Wraight, *Biochim. Biophys. Acta* 1015 (1990), 156.

218. G. Feher, J. P. Allen, M. Y. Okamura, D. C. Rees, *Nature* 33 (1989), 111.

219. G. Palazzo, A. Mallardi, A. Hochkoeppler, L. Cordone, G. Venturoli, *Biophys. J.* 82 (2002), 558.

220. E. S. P. Hsi, J. R. Bolton, *Biochim. Biophys. Acta* 347 (1974), 126.

221. B. J. Hales, *Biophys. J.* 14 (1976), 471.

222. J. M. Ortega, P. Mathis, J. C. Willliams, J. P. Allen, *Biochemistry* 35 (1996), 3354.

223. G. Feher, M.Y. Okamura, D. Kleinfeld in *Protein structure: Molecular and Electronic Reactivity*; R. Austin, E. Buhks, B. Chance, D. De Vault, P.L. Dutton, H. Fraunfelder, V.I. Goldanskii Eds., Springer Verlag: New York , 1987, p 399.

224. F. Francia, M. Dezi, A. Rebecchi, A. Mallardi, G. Palazzo, B.A. Melandri, G. Venturoli, *Biochemistry* 43 (2004), 14199.

225. G. Feher, M.Y. Okamura in *The Photosynthetic Bacteria*, R.K. Clayton, W.R. Sistrom Eds., Plenum Press: New York, 1978, p 349.
P. Gast, P. Hemerlijk, A.J. Hoff, *FEBS Lett.* **1994**, *337*, 39.

226. N. C. Robinson, J. Zborowski, L.H. Talbert, *Biochemistry* 29 (1990), 8962.

227. L . Stryer, "Proteins transporting oxygen: myoglobin and hemoglobin" in *Biochemistry*, chapt. 7, 4th ed. (1995), W. H. Freeman and Company, New York and Basingstoke.

228. V. P. Shinkarev and C. A. Wraight, *Biophys. J.* 72 (1997), 2304.

229. H. Arata, W. W. Parson, *Biochim. Biophys. Acta* 638 (1981), 201.

230. M. R. Gunner, D.E. Robertson, P.L. Dutton, *J. Phys. Chem.* 90 (1986), 3783.

231. X. Lin, H. A. Murchison, V. Nagarajan; W. W. Parson, J. P. Allen, J. C. Williams, *Proc. Natl. Acad. Sci. U.S.A.* 91 (1994), 10265.

232. J. P Allen., J. C Williams., M.S. Graige, M. L. Paddock, A. Labahn, G. Feher, M.Y. Okamura, *Photosynthesis Research* 55 (1998), 22.

233. J.M. Kriegl, G.U. Nienhaus, *Proc. Nat. Acad.. Sci. U.S.A.* 101 (2004), 123.

234. L. Cordone, G. Cottone, S. Giuffrida, G. Palazzo, G. Venturoli, C. Viappiani, *Biochim. Biophys. Acta, Proteins and Proteomics* 1749 (2005), 252.

235. K. E. McAuley, P. K. Fyfe, R.J. Codgell, N.W. Isaacs, M.R. Jones, *FEBS Lett.* 467 (2000), 285.

236. F. Francia, G. Palazzo, A. Mallardi, L. Cordone, G. Venturoli, *Biochim. Biophys. Acta Bioenergetics* 1658 (2004), 50.